

**UCSF**

**UC San Francisco Electronic Theses and Dissertations**

**Title**

Structure and Function of the Mitochondrial Hsp90, TRAP1

**Permalink**

<https://escholarship.org/uc/item/8859n3c0>

**Author**

Lavery, Laura

**Publication Date**

2013

Peer reviewed|Thesis/dissertation

Structure and Function of the Mitochondrial Hsp90, TRAP1

by

Laura Adele Lavery

DISSERTATION

Submitted in partial satisfaction of the requirements for the degree of

DOCTOR OF PHILOSOPHY

in

Biophysics

in the

GRADUATE DIVISION

of the

UNIVERSITY OF CALIFORNIA, SAN FRANCISCO



Copyright 2013  
By  
Laura Adele Lavery

This dissertation is dedicated to  
Michelle, Richard and Madeline Lavery, and Jeffrey Tabor for everything.

## **Acknowledgments**

The work presented here would not have been possible or as great of an experience if it weren't for several mentors, colleagues, family and friends.

First and foremost I would like to thank David Agard for his guidance and mentorship throughout my years at UCSF and towards future goals. As well as for always encouraging and inspiring new creative ideas.

For my thesis committee Carol Gross and Geeta Narlikar I would like to express my deepest gratitude for support and fun times spent discussing science over the years.

My undergraduate research advisor, Andrew Ellington and adjunct advisor Christopher Voigt were both instrumental in my progression to UCSF and taught me the value of interdisciplinary research and teamwork in science.

My initial years in the Agard lab were met with great mentors and friends in Daniel Southworth, Justin Kollman, Kristin Krukenberg, and Ulrike Boettcher. I would like to particularly thank Timothy Street for always taking the time to talk and build models together. The initial collaborative work that we did (chapters 4 and 5) helped me tremendously in my science pursuits that followed.

I would like to thank my classmates of 2006 for support and encouragement throughout the years and for some fun times- especially creating some awesome skits!

To Nariman Naber (Nariperson) for a warm smile, a warm meal, and continued excitement about scientific pursuits I express my thanks.

I would also like to thank James Partridge (of team shake and bake) for taking the time to teach me crystallography and for being excited to accomplish the work presented in chapters 1 and 2 together.

For a wonderful environment and support in science and beyond I thank all the members of the Agard lab, past and present. To James Kraemer a special thank you for friendship and companionship in musical hiatuses between times of science. To my friends Klim Verba and Daniel Elnatan I express my thanks for fun discussions both Hsp90 and other fun topics. And further to Daniel express my thank you for intellectual and experimental contributions to the work that follows.

To my friends and fellow ladies Elaine Kirschke, Rebeca Choy and Elizabeth Montabana- thank you for being a friend (Golden Girls ref.) and for always having my back. With these ladies, I express my gratitude for immeasurable friendship to David Booth, Laura Franek, Shannon Vestal, Samuel Pfaff, Angela (Hezi) Mitchell, Stephen Floor, Matt Eames, Elizabeth Clarke, Bethany Simmons, Elizabeth (Hesper) Rego, Molly Darragh, Mariano Tabios, Karen Fenn, Daniele Canzio, John Bruning, Matt Davidson, Eric Davidson, Karen Davidson, Mark Davidson, Lisa and Josh Ecroyd, Lori Dixon, Gil Dixon, and Adam Tabor.

To my family- especially my mom, dad and sister whose names appear on the dedication page- I express my thanks for unwavering love and support.

Finally to Jeffrey Tabor- I am grateful for love and encouragement beyond what I can express. And- sometimes you make me laugh, so that's pretty cool.

## Structure and Function of the Mitochondrial Hsp90 (TRAP1)

Laura Adele Lavery

Laboratory of Dr. David A. Agard

Heat Shock Protein 90 (Hsp90) is a highly conserved molecular chaperone necessary for eukaryotic life. This member of the cellular folding machinery has been extensively studied in recent years due to its intimate link to fundamental biological pathways that govern cellular homeostasis and disease [1-3].

Hsp90 undergoes large ATP dependant conformational changes that are necessary for client maturation *in vivo* [4]. Though much progress had been made in building a model for a functional cycle of Hsp90 (Figure 1), the fundamental question of how Hsp90 functions to re-model clients remained unclear.

Several forms of Hsp90 can be found throughout evolution with most higher eukaryotes having four homologs: two in the cytosol (Hsp90 $\alpha$ , Hsp90 $\beta$ ), one in the endoplasmic reticulum (GRP94) and one in the mitochondria (TRAP1) [5].

Though not extensively studied at the time, I set out to investigate the structure and function of TRAP1, originally inspired by the balance between a higher eukaryotic Hsp90 and a simplified Hsp90 being most similar to the bacterial Hsp90 (bHsp90). With the latter comes the advantage of a more simple system where the large number of cochaperones identified for Hsp90 $\alpha/\beta$  are not known to be required for client interactions with TRAP. Further, unique biology and disease links of TRAP1 were emerging with *in vivo* data showing that TRAP1 had unique ties to cellular homeostasis

through interactions with client protein cyclophilin D (CypD), the master regulator of the mitochondrial permeability transition pore (mtPTP) and thus necrotic cell death[6].

Through this work I developed several biochemical/biophysical assays and strategies for working with TRAP1 *in vitro*, and through collaboration elucidated both shared and unique aspects of Hsp90 mechanism. Importantly, this work has provided a new hypothesis for Hsp90 mechanism of action with client proteins, which contributes a new model for the productive use of ATP hydrolysis for client re-modeling.

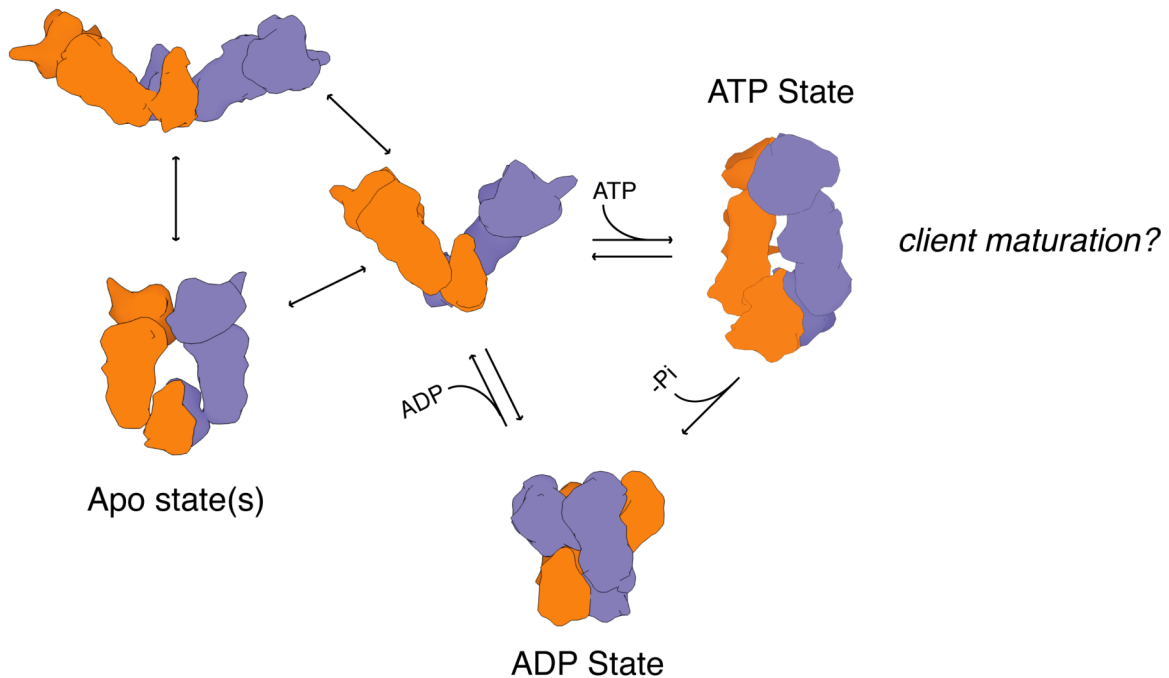


**Figure 1. Previous model for a functional Hsp90 chaperone cycle.** Hsp90 conformational states and putative apo->ATP->ADP cycle, showing equilibration between multiple apo states in solution. Upon ATP binding the chaperone closes to form a NTD dimerized state. Upon hydrolysis the ADP state is sampled before re-opening to the apo state equilibrium. The closed state is hypothesized to be the active chaperoning state and is modeled here by the yeast Hsp90 crystal structure. Not shown for clarity are two copies of the cochaperone p23, which are symmetrically deposited on either side of the N-terminal domains in this closed state model.

## References:

1. Taipale, M., D.F. Jarosz, and S. Lindquist, *HSP90 at the hub of protein homeostasis: emerging mechanistic insights*. Nat Rev Mol Cell Biol, 2010. 11(7): p. 515-28.
2. Trepel, J., et al., *Targeting the dynamic HSP90 complex in cancer*. Nat Rev Cancer, 2010. 10(8): p. 537-49.
3. Luo, W., et al., *Heat shock protein 90 in neurodegenerative diseases*. Mol Neurodegener, 2010. 5: p. 24.
4. Panaretou, B., et al., *ATP binding and hydrolysis are essential to the function of the Hsp90 molecular chaperone in vivo*. The EMBO journal, 1998. 17(16): p. 4829-36.
5. Johnson, J.L., *Evolution and function of diverse Hsp90 homologs and cochaperone proteins*. Biochim Biophys Acta, 2012. 1823(3): p. 607-13.
6. Kang, B.H., et al., *Regulation of tumor cell mitochondrial homeostasis by an organelle-specific Hsp90 chaperone network*. Cell, 2007. 131(2): p. 257-70.

## Table of Contents

<b>Chapter 1</b> .....	1
Structural asymmetry in the closed state of mitochondrial Hsp90 (TRAP1) supports a two-step ATP hydrolysis mechanism	
<b>Chapter 2</b> .....	79
A novel N-terminal extension in mitochondrial Hsp90 (TRAP1) serves as a kinetic regulator of chaperone activity	
<b>Chapter 3</b> .....	125
The role of the mitochondrial Hsp90 molecular chaperone (TRAP1) in Parkinson's disease	
<b>Chapter 4</b> .....	178
Substrate binding drives large-scale conformational changes in the Hsp90 molecular chaperone	
<b>Chapter 5</b> .....	219
Cross monomer substrate contacts reposition the Hsp90 N-terminal domain and prime the chaperone activity	
<b>Appendix:</b>	
Select Protocols.....	258-290



## List of Tables

### Abstract

**Figure 1.** Previous model for a functional Hsp90 chaperone cycle ..... vii

### Chapter 1:

**Table S1.** Crystallographic Data Table .....43-44

**Table S2:** R values for closed state model fitting of SAXS data .....45

**Table S3:** Steady-state kinetic values.....45

**Table S4:** Table of promising crystal results .....54-55

### Chapter 2:

**Table S1:** Percent closed state for TRAP1 homologs at varying temperatures ..... 112

**Table S2:** ATPase rates for WT and strap mutants ..... 112

**Table S3:** FRET closure rates for main text experiments.....112

**Table S4:** FRET closure rates for supplemental experiments ..... 113

### Chapter 4:

**Table S1:** Conformational equilibrium of HtpG while bound to  $\Delta 131\Delta$ .....210

## List of Figures

### Chapter 1:

<b>Figure 1:</b> Crystal structure of full-length TRAP1 in an asymmetric closed state.....	9
<b>Figure 2:</b> N-terminal strand extension regulates TRAP1 activity .....	13
<b>Figure 3:</b> Novel asymmetry revealed in the TRAP1 dimer .....	16
<b>Figure 4:</b> Solution methods support a conserved asymmetric closed state.....	20
<b>Figure 5:</b> Structure based MD:CTD interface mutations severely impair ATPase activity .....	23
<b>Figure 6:</b> NTD:MD crystal structure and implications for a strained closed state.....	25
<b>Figure 7:</b> New model for the conformational cycle of Hsp90.....	32
<b>Figure S1.</b> Theoretical SAXS curves for closed state models.....	36
<b>Figure S2.</b> DEER probe is labeled, active and forms an asymmetric closed state.....	37
<b>Figure S3.</b> MD:CTD Interface mutations do not prevent TRAP1 from reaching a closed state or effect overall fold.....	38
<b>Figure S4.</b> MD:CTD interface mutants destabilize the closed state. ....	39
<b>Figure S5.</b> NTD:MD crystal is formed after cleavage of full-length TRAP1 at a destabilized MC interface.....	40
<b>Figure S6.</b> NTD alignment of Full-length and NTD:MD TRAP1.....	40
<b>Figure S7.</b> Alternative Model for the chaperone cycle of Hsp90 .....	41
<b>Figure S8.</b> Heterodimers of MD:CTD interface mutants do not rescue ATPase.....	41
<b>Figure S9.</b> MD:CTD interface mutants have altered interaction with $\Delta 131\Delta$ .....	42
<b>Figure S10.</b> Crystal trials with hTRAP1 .....	48
<b>Figure S11.</b> Species screening produces better crystals .....	50
<b>Figure S12.</b> Se-Met Crystals require alternative ATP analogs to produce experimental maps...	

..... 52

## **Chapter 2:**

<b>Figure 1:</b> A temperature dependent kinetic barrier separates the apo to closed state transition of TRAP1 .....	87
<b>Figure 2:</b> Kinetic barrier to closed state is modulated by the NTD-strap .....	89
<b>Figure 3:</b> NTD-strap regulates the ATPase of Hsp90 homologs .....	91
<b>Figure 4:</b> The NTD-strap regulates closure rate of TRAP1 .....	93
<b>Figure 5:</b> Lid Closure rate is regulated by the NTD-strap.....	97
<b>Figure 6.</b> Model for the conformational cycle and unique energy landscape of TRAP1.....	102
<b>Figure S1.</b> The closed conformation of TRAP1 is stable post temperature induced closure	108
<b>Figure S2.</b> WT and strap mutants for hHsp90 .....	109
<b>Figure S3.</b> Alternative Model for the chaperone cycle .....	110
<b>Figure S4.</b> The closed state of TRAP1 is a stabilized state .....	110
<b>Figure S5.</b> Previous FRET measurements for the NTD:MD Intra-FRET pair .....	111

## **Chapter 3:**

<b>Figure 1.</b> TRAP1 is required for Parkin-dependent mitophagy .....	141
<b>Figure 2.</b> Metabolic defects in TRAP1 KO cells .....	143
<b>Figure 3.</b> MS/MS spectra identifying the three primary PINK1-derived phosphopeptides within hTRAP1 .....	144
<b>Figure 4.</b> PINK1 specific phosphorylation sites identified for hTRAP1 .....	145
<b>Figure 5.</b> Phosphomimetic hTRAP1 shows a 2-fold enhancement of ATPase.....	146
<b>Figure 6.</b> hTRAP1 interacts with human CypD in vitro.....	151

<b>Figure 7.</b> $^{13}\text{C}$ -NMR of full-length hTRAP1 .....	153
---	-----

#### **Chapter 4:**

<b>Figure 1.</b> Conformational flexibility of the Hsp90 molecular chaperone.....	184
---	-----

<b>Figure 2.</b> HtpG binds $\Delta 131\Delta$ , resulting in a conformational change .....	188
---	-----

<b>Figure 3.</b> Contraction of HtpG upon binding $\Delta 131\Delta$ .....	190
--	-----

<b>Figure 4.</b> Nucleotide dependence of $\Delta 131\Delta$ binding .....	195
--	-----

<b>Figure 5.</b> Substrate binding accelerates nucleotide-driven closure .....	197
--	-----

<b>Figure 6.</b> HtpG binds a specific region on $\Delta 131\Delta$ .....	199
---	-----

<b>Figure 7.</b> Hsp90 chaperone cycle for $\Delta 131\Delta$ .....	200
---	-----

<b>Figure S1.</b> Binding saturation measurements.....	205
--	-----

<b>Figure S2.</b> Substrate-induced conformational changes in the yeast and human Hsp90 homologs .....	205
---	-----

<b>Figure S3.</b> The Hsp90 conformational changes are specific to unfolded SN.....	205
---	-----

<b>Figure S4.</b> DAMMIN and MONSA reconstructions with the NM domain and $\Delta 131\Delta$ . .....	207
--	-----

<b>Figure S5.</b> Structure-based fitting of SAXS data.....	208
---	-----

<b>Figure S6.</b> Salt-dependent binding affinity.....	209
--	-----

<b>Figure S7.</b> $\Delta 131\Delta$ does not affect the reopening rate from the ATP state .....	210
--	-----

#### **Chapter 5:**

<b>Figure 1.</b> Hsp90 conformational flexibility .....	225
---	-----

<b>Figure 2.</b> Substrate binding affects an intrinsically unfavorable NTD rotation required for closure .....	227
--	-----

<b>Figure 3.</b> Substrate binding affects hydrogen-exchange patterns across the HtpG structure.....	231
--	-----

<b>Figure 4.</b> Mapping a substrate binding location on the HtpG middle domain .....	233
<b>Figure 5.</b> Cross-monomer substrate contacts are coupled to HtpG conformational changes	235
<b>Figure 6.</b> Model of NTD rotation in substrate activation of Hsp90 ATP hydrolysis cycle.....	240
<b>Figure S1.</b> Control FRET pair on the middle domain .....	243
<b>Figure S2.</b> .....	243
<b>Figure S3.</b> Selective amino-acid labeling of the middle domain to determine a $\Delta 131\Delta$ binding region on the HtpG MD .....	244
<b>Figure S4</b> .....	245
<b>Figure S5.</b> The 30 residue peptide from $\Delta 131\Delta$ has significant structure .....	246

# Chapter 1

Structural asymmetry in the closed state of mitochondrial  
Hsp90 (TRAP1) supports a two-step ATP hydrolysis  
mechanism

**Contributing Authors:** James R. Partridge, Theresa A. Ramelot, Daniel Elnatan,  
Michael A. Kennedy, and David A. Agard.

## Preface

Hsp90 is a highly conserved and critical molecular chaperone that is integrated in several aspects of biology through functional interactions with its select, yet large list of client proteins. Hsp90 clients are diverse and interactions with the chaperone are intimately linked to the ATP dependent conformational cycle outlined in figure 1 of the abstract to my thesis (page vii). From early studies, it was clear that nucleotide binding and hydrolysis are necessary to produce functional clients *in vivo* [1], where the closed state conformation is hypothesized to be the active chaperoning state for the Hsp90 family of chaperones. For many years, the biggest question in the Hsp90 field has been: how does Hsp90 utilize ATP to remodel a client proteins structure (from near-native to native/active client)? One hypothesis was that ATP binding alone could shift the conformational cycle of Hsp90 towards the closed state and that this was the active folding step. Then ATP hydrolysis would function to “kick-off” the client. Confounding this hypothesis is that nucleotide binding is not strictly necessary to sample the closed state and is observed (to varying degrees) under apo conditions [2]. Further, client affinities are weak (1-100 $\mu$ M range), in which case the client protein is predicted to fall off more than once during the slow closure transition of the chaperone. This observation made it difficult to understand why the energy of hydrolysis would be useful for client release.

The work presented in this chapter of my thesis, describes the discovery of a novel asymmetric closed conformation of the chaperone, revealed in our crystal structure of the mitochondrial Hsp90 (TRAP1) in an active closed state. Integrated with

recent studies that have elucidated client-binding site residues, this work provides a new hypothesis for Hsp90 mechanism of action with client proteins, contributing a much needed rationalization for how the energy of ATP hydrolysis can be effectively used to remodel client proteins.

A manuscript describing this study is currently in revision at Molecular Cell. James Partridge (post-doc) and I worked together to accomplish this work and are listed as co-first authors where my name appears first. Both James and I worked to obtain high-quality diffracting crystals. James is responsible for the solution of full-length TRAP1 and final refinements for all structures presented, as well as structural comparisons, CD and the ATPase measurements for the “strap” mutations (see below). I am responsible for all solution based data (SAXS, DEER assay development), EM, the NTD:MD crystal structure, and MD:CTD interface mutant ATPases. In-house SAXS analysis software was written and optimized for this study by David Agard. Also listed as authors is Daniel Elnatan (graduate student- Agard lab) who was instrumental in intellectual contributions and assistance with DEER experiments, as well as our collaborators Theresa Ramelot and Michael Kennedy (Kennedy lab- Miami University, Ohio) who are responsible for DEER data collection and analysis.

Finally, on the path to the findings described below there were several key mechanistic insights and developed strategies for working with TRAP1 as a model system, as well as crystallography progress on different TRAP1 homologs. To this end, I have written a section in the supplemental information (Supplemental crystal trial



information) describing this work, and included the progress with the other homologs in an effort to facilitate future work with the system.

## **Summary**

While structural symmetry is a prevailing feature of homo-oligomeric proteins, asymmetry provides unique mechanistic opportunities. We present the 2.3 Å crystal structure of full-length TRAP1, the mitochondrial Hsp90 molecular chaperone, in a catalytically active closed state. The TRAP1 homodimer adopts a novel, asymmetric closed conformation, where one protomer is reconfigured via a helix swap at the Middle:C-terminal Domain (MD:CTD) interface to form a previously unknown conformation. Importantly, this interface plays a critical role in client binding. Solution-based methods (SAXS and DEER) validate the asymmetry and point mutations aimed to disrupt unique contacts at each MD:CTD interface reduce catalytic activity across TRAP1 homologs. We further demonstrate the asymmetric state extends beyond TRAP1 to other Hsp90 systems. As shown crystallographically, absence of the CTD in the closed state restores perfect symmetry, indicating the presence of substantial strain that is only partially relieved by the asymmetric arrangement. Together, this leads to a new model in which formation and relief of asymmetry driven by ATP binding and hydrolysis is directly coupled to client remodeling.

## **Introduction**

Protein folding is a fundamental biological process and protein misfolding can have a dramatic impact on both cellular and organismal fitness. To ensure proper

folding and function, cells have evolved a class of proteins known as molecular chaperones to maintain cellular homeostasis. These molecular chaperones interact with substrate proteins at different folding stages and act in concert throughout the maturation process [3].

Heat shock protein 90 (Hsp90) is a highly conserved ATP-dependent chaperone essential to facilitate the folding and activation of nearly 10% of the proteome [4]. Unlike other chaperones, Hsp90 preferentially interacts with partially folded substrate “client” proteins [5] and primes them for downstream protein-protein or protein-ligand interactions [6]. Thus, beyond initial folding Hsp90 plays an important role throughout the functional lifetime for many clients. Known client proteins vary widely in sequence, structure, size and function, and for this reason client recognition and specificity are not well understood [7]. Disruption of Hsp90 activity can affect evolutionary outcomes [8, 9] and has been linked to human diseases including cancer [10], vascular disease [11], and neurodegeneration [12].

Hsp90 functions as a homodimer with each protomer consisting of three major domains: the N-terminal domain (NTD), responsible for ATP binding and hydrolysis, the middle domain (MD) that aids in hydrolysis, and the C-terminal dimerization domain (CTD) (Figures 1A and 1B). Crystal structures electron microscopy (EM) and small angle X-ray scattering (SAXS) of Hsp90 in the presence or absence of nucleotide have revealed large conformational changes between the major domain boundaries. In the absence of nucleotide a variety of structurally-distinct open states are populated in solution that are thought to aid in binding a diverse set of clients [13, 14]. The crystal

structure of yeast Hsp90 (yHsp90) [15] along with biochemical studies [16, 17] demonstrate that dimerization of the NTD between protomers mediates ATP hydrolysis and is essential for Hsp90 function. Following ATP hydrolysis, Hsp90 transiently adopts a compact ADP-bound conformation initially observed in the bacterial Hsp90 (bHsp90) [18] and later trapped in yHsp90 and human Hsp90 (hHsp90) [2]. Together, these data establish a model for the conformational cycle of Hsp90 whereby the protomer arms undergo concerted conformational changes through rounds of ATP binding, hydrolysis, and release [19]. Though hydrolysis is essential for *in vivo* function across Hsp90 homologs [1], it remains unclear how hydrolysis is used for client maturation.

Most eukaryotic cells contain four Hsp90 homologs: two in the cytosol (Hsp90 $\alpha/\beta$ ), and one in both the endoplasmic reticulum (ER, GRP94) and mitochondria (TRAP1) [20]. *In vitro* experiments have demonstrated that although the fundamental conformational states are well conserved, equilibria and kinetics are unique for every Hsp90 homolog [2], suggesting adaptation to the specific needs of clients in each cellular compartment and species. Within the eukaryotic cytosol Hsp90 function is aided by numerous Hsp90-specific co-chaperones, however, only one has been identified for the prokaryotic or organellar Hsp90s [20, 21].

TRAP1 is encoded in the nucleus and was originally identified as a binding partner of tumor necrosis factor receptor 1 [22]. TRAP1 has since been shown to localize primarily to the mitochondria [23] and most abundantly in the mitochondrial matrix [24]. Although few TRAP1 clients have been identified, there is an emerging appreciation for the role of TRAP1 in regulating mitochondrial protein homeostasis [25].

Specifically, TRAP1 has been implicated in critical pathways including mitochondrial fission/fusion [26], mitophagy [27, 28], and the necrotic form of cell death through regulating cyclophilin D [29]. TRAP1 appears closely linked to cancer progression [30, 31], and relevant for both familial and idiopathic forms of Parkinson's disease [27, 28, 32]. These characteristics highlight a growing understanding of TRAP1's biological role and underscore its potential as a unique therapeutic target.

To better understand both shared and unique aspects of TRAP1 mechanism, we determined the crystal structure of TRAP1 at 2.3 Å resolution. The full-length mature protein was crystallized as a dimer in a closed conformation with AMPPNP, ADP-AIF<sub>4</sub><sup>-</sup>, or ADP-BeF<sub>3</sub><sup>-</sup>. In the absence of client or co-chaperones, TRAP1 adopts an unexpected asymmetric conformation with the largest deviations at the MD:CTD interface. Complementary solution-based methods (SAXS and DEER) confirm that this asymmetric state is populated in solution and structure-based point mutations demonstrate the functional relevance of contacts at the two different MD:CTD interfaces. Further, *in vitro* experiments show conservation of asymmetry between TRAP1 homologs as well as in bHsp90. Additionally, we crystallized a truncated version of a TRAP1 dimer bound to AMPPNP but lacking the CTD. This 1.7 Å NTD:MD structure is perfectly symmetric and has implications for understanding how asymmetry is formed in the full-length dimer. Both sets of structures display a previously unknown N-terminal extension that we show serves a regulatory role for ATPase activity. Finally, we propose that our TRAP1 structure depicts an important functional state with significant implications for the utilization of energy from ATP hydrolysis during client remodeling.

## Results

### Structure of Full-length TRAP1 in an active closed state

High-quality diffracting crystals of the mature form of TRAP1 from zebrafish-zTRAP1 (84% similar to human TRAP1-hTRAP1), diffracted to 2.3 Å, however initial attempts at molecular replacement with previously solved models (full-length(FL) and NTD, MD, or CTD domains) of Hsp90 proved unsuccessful. Instead, the structure was experimentally phased using selenomethionine and SAD to 3.0 Å and native structures of TRAP1 bound to all three nucleotide analogs (AMPPNP, ADP-BeF<sub>3</sub><sup>-</sup>/AlF<sub>4</sub><sup>-</sup>) were refined at a maximum resolution of 2.3 Å (Table S1). No significant differences between the nucleotide analogs were observed.

The asymmetric unit contains a single closed-state dimer, with dimerization interfaces at both the CTD and the NTD (Figure 1A and Movie S1).

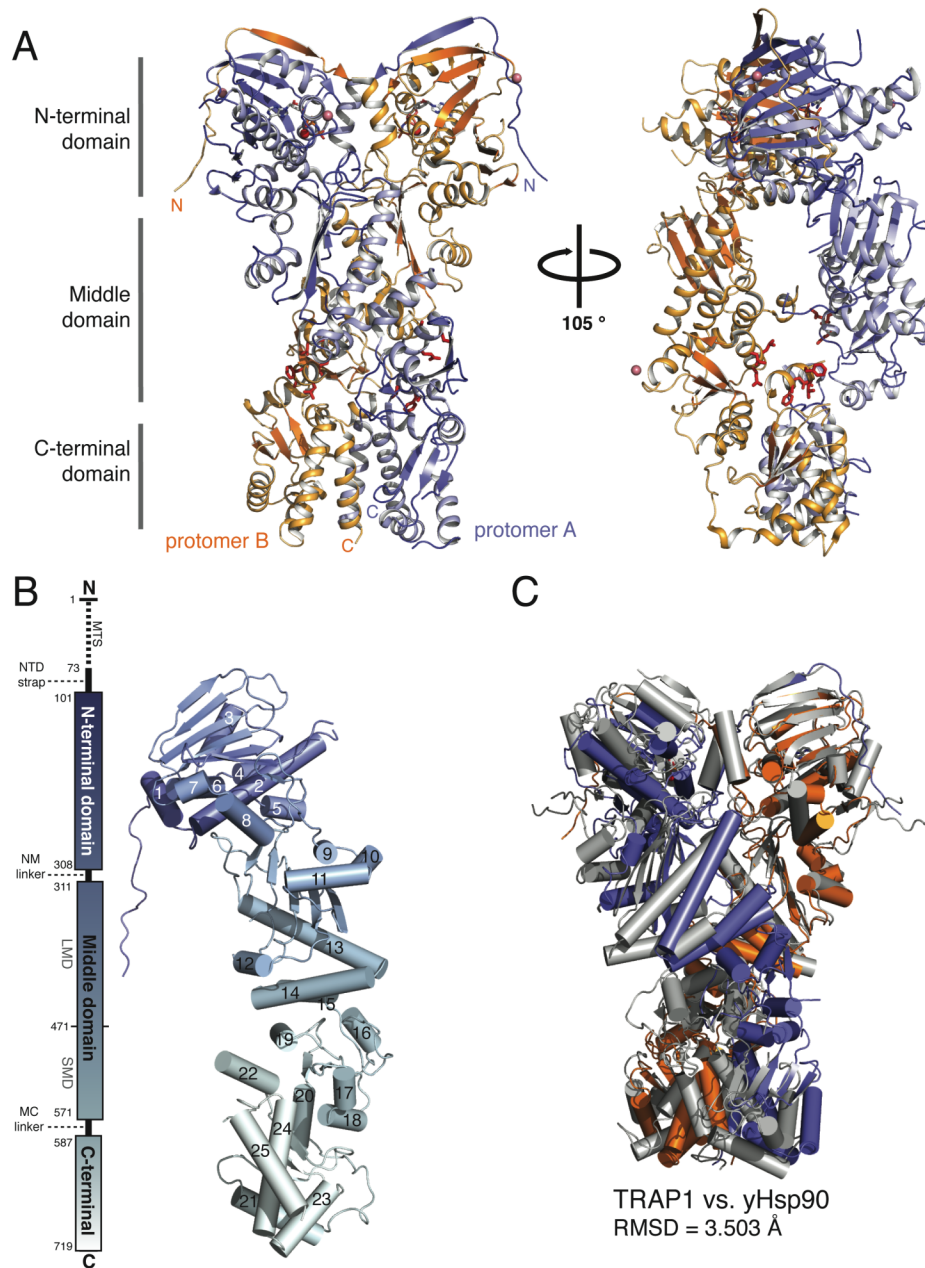


**Figure 1. Crystal structure of full-length TRAP1 in an asymmetric closed state.** A) Ribbon representation full-length TRAP1 from *D. rerio*. The homodimer has been crystallized in an asymmetric state, with each protomer forming a unique MD:CTD interface. Protomer B (orange) is similar to previously solved Hsp90 structures, while protomer A (blue) makes a novel contacts between the MD and CTD. Residues known to bind with clients in this region are differential presented and shown in red. Also visible is an N-terminal extension that exchanges between protomers to envelope the neighboring N-terminal domain. B) Map of domain boundaries in TRAP1 highlighting the mitochondrial targeting sequence and extended N-terminal strand swap (“strap”) (left). Cartoon representation to map the helical positions of a single protomer from TRAP1 (right). Progression from N to C-terminus is indicated with a transition from blue to gray. D) Comparison of TRAP1 structure (colors above) to the closed state of yHsp90 (gray). Overall RMSD value in comparison to TRAP1 is listed below.

At 2.3 Å resolution our model presents the highest resolution picture of FL-Hsp90 catalytic machinery, showing that the nucleotide coordinating residues and catalytic water necessary for hydrolysis [15] are positioned in a manner consistent with this being a catalytically active state. Distinguishing TRAP1 features are also visible, including the characteristic “LXCXE” motif in the MD [33], which we observe to form a disulfide bond between Cys516 and Cys542. From sequence alignments and in comparison to other Hsp90 homologs, vertebrate TRAP1 proteins have an inserted 8-residue motif that is part of H19.

Comparing the TRAP1 structure to the previously solved closed state of yHsp90 (stabilized by the co-chaperone p23) [15] it is clear that while the general architecture of the Hsp90 dimer is conserved there are striking differences in the overall conformation (Figure 1C). This is best illustrated with a morph between the two structures starting with TRAP1 and transitioning to the yHsp90 structure (Movie S2). In addition a unique 14-residue extension of the N-terminus as part of an extended β-strand swap is immediately apparent (Figures 1A, 1B and 2). In general, TRAP1 adopts a more compact conformation, shrinking the overall dimer height by ~4 Å and rotating clockwise by ~20° to constrict the cleft between protomers. Importantly, the major differences between the yHsp90 and TRAP1 structures arise from the non-equivalent conformations of protomers in TRAP1, illustrating a striking asymmetry of the closed TRAP1 structure (discussed in detail below). The asymmetry is unlikely to be a consequence of crystal contacts as protomer B has more substantial contacts but is most similar in conformation to the protomers in yHsp90 structure. Motivated by the unique features of

our TRAP1 structure we investigated the functional relevance of these novel structural elements.

### **The NTD-strand swap extension (“Strap”) and regulation of ATP turnover**

Previous studies with truncation mutants have implicated the N-terminus of yHsp90 in regulating ATPase activity, with truncations accelerating ATPase activity [34, 35]. These residues are notable as they encompass an initial  $\beta$ -strand and helix 1 (H1), both coupled to nucleotide binding and subsequent lid closure prior to hydrolysis. In isolated NTD structures both with and without nucleotide [18, 36-38] and an apo-NTD:MD structure [39], the first 7 residues form cis-protomer  $\beta$ -strand interactions to the NTD, while in the yHsp90 AMPPNP-bound closed state, these elements cross over to form analogous  $\beta$ -strand contacts with the trans-protomer. TRAP1, GRP94, and cytosolic hHsp90 $\alpha/\beta$  all contain an extension of the N-terminal strand between 10-50 residues long. Surprisingly this extension is not conserved in yHsp90 or bHsp90 to which TRAP1 is most closely related [33]. Our TRAP1 structure reveals that 14 additional ordered residues form extensive trans-protomer interactions to fully envelope the neighboring NTD, adding an additional 771 Å<sup>2</sup> of surface area to the N-terminal strand swap (Figure 1A and 2A). This extension of the N-terminal strand seems to act as a “strap” to further stabilize the closed state. Notably, the crystal structure of Grp94 was truncated to exclude this extension of the N-terminal strand [39].

To test the relevance of our observed strap, we truncated the extension to match yHsp90 ( $\Delta$ strap), and saw a 4-fold increase in ATPase activity relative to WT (Figure 2). As a more conservative test we made point mutations aimed at disrupting a salt bridge



(His87:Glu157) located at the extreme N-terminus of the strap (Figure 2A and 2B). Notably in hHsp90 the His and Glu residues are swapped preserving the salt-bridge in cytosolic hHsp90s. Mutating either His87 or Glu157 to Ala in zTRAP1 resulted in an ~3-fold increase in ATPase activity over WT (Figure 2C). These data support a role for the strap in regulating the Hsp90 ATPase cycle and suggest that elaborations at the N-terminus may serve to further tune the ATPase cycle for the particular demands of each Hsp90 homolog.

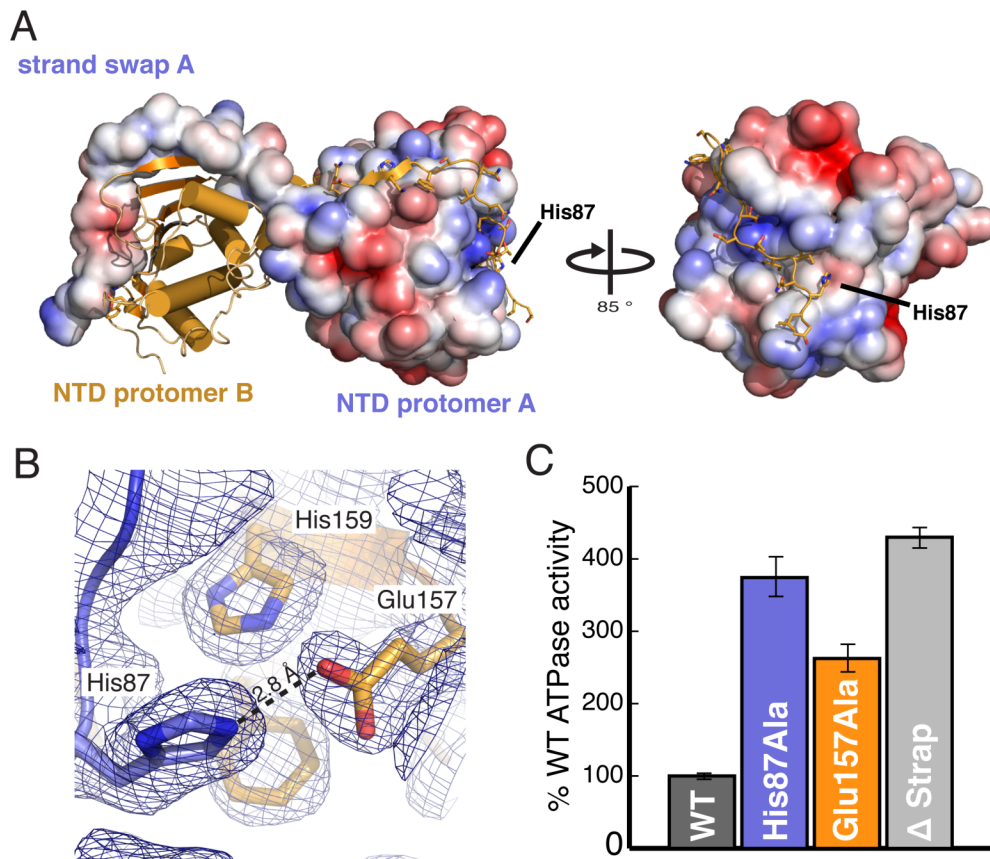


**Figure 2. N-terminal strand extension regulates TRAP1 activity.** A) Graphical representation of the NTD dimerization interface between protomers of TRAP1. A surface representation of protomer A highlights the electrostatic charge distribution of the NTD. Protomer B (orange) is depicted as a cartoon to highlight secondary structure. Clearly evident is the extensive contact,  $\sim 1,484 \text{ \AA}^2$ , that each NTD-strand swap makes with the neighboring protomer. B) The salt bridge between His87 and Glu157 is displayed with the  $2F_o - F_c$  electron density map. C) ATPase activity of WT TRAP1,  $\Delta$ strap, and point mutations to either His87 or Glu157, indicate that disruption of the salt-bridge via point mutation or removal of the strap leads to a significant acceleration of TRAP1 ATPase activity.

### Novel asymmetry in the closed state dimer

Unexpectedly, the two protomers from the TRAP1 homodimer have significantly different conformations resulting in a novel closed state. Although the differences are most pronounced at the domain interfaces, asymmetry pervades the entire structure (Figure 3). To accomplish the significant global changes between TRAP1 protomers,

hinge points between domains allow for flexibility and movement. Figure 3A illustrates the differences in protomer domain orientation within the TRAP1 dimer and is compared to yHsp90 [15]. Alignments between each individual domain illustrates the large changes in domain orientation relative to the overall dimer arrangement, and highlights a pronounced difference at a hinge point between the large-middle-domain (LMD) and small-middle-domain (SMD) between, helices 14 and 15 (Figure 1B) near residue 471. To compensate the NTD and CTD counter-rotate to maintain functional NTD and CTD interfaces (Figure 3A, inset). The separation of the MD into LMD/SMD sub-domains is consistent with previous studies predicting nucleotide dependent flexing [40, 41] and likely caused the difficulty in using molecular replacement to phase our initial diffraction data. Interestingly, the identified break point is where Hsp90 and other GHKL family member proteins significantly diverge, suggesting unique functions of the SMD and CTD in Hsp90 systems [42].

By aligning domains individually and mapping inter-protomer RMSDs back onto the structure of protomer B, it is evident that the individual NTDs and CTDs are similar and the largest deviations occur at the NTD:MD and MD:CTD domain interfaces (Figure 3B). At the NTD:MD interface, the loss of hydrogen bonds between Asp407:Lys384 and Glu409:Arg383 in protomer B lead to a shift of 4.4 Å and a deviation from protomer symmetry at Glu409 (Figure 3C). Notably, this shift occurs in a loop within the LMD (residues 411-422), which contains residues necessary to stabilize an active closed state [15, 43]. Here protomers A and B display significantly different B-factors (~40 and

60, respectively) suggesting differences in the energetics of the ATP  $\gamma$ -phosphate coordination by Arg417 within the LMD.

The largest deviations occur at the MD:CTD interface where the CTD amphipathic helix (H22) interacts with either H17 of protomer A (H17A) or H19 of protomer B (H19B) (Figure 3D). The different helices in contact with H22 alter which face of H22 is exposed to the dimer cleft by inducing an 8 Å translation and 87° rotation towards the MD when exchanging from H17A to H19B. Most importantly, this motion significantly changes the spatial arrangement of residues directly implicated in substrate binding in bHsp90 and yHsp90 (Figure 1A) [44]. As illustrated in Movie S3, H22 rotates and the substrate binding residues exchange between exposed and buried positions in the TRAP1 structure. These conformational changes suggest a potential use of asymmetry to influence client interactions and structure when bound to this region.

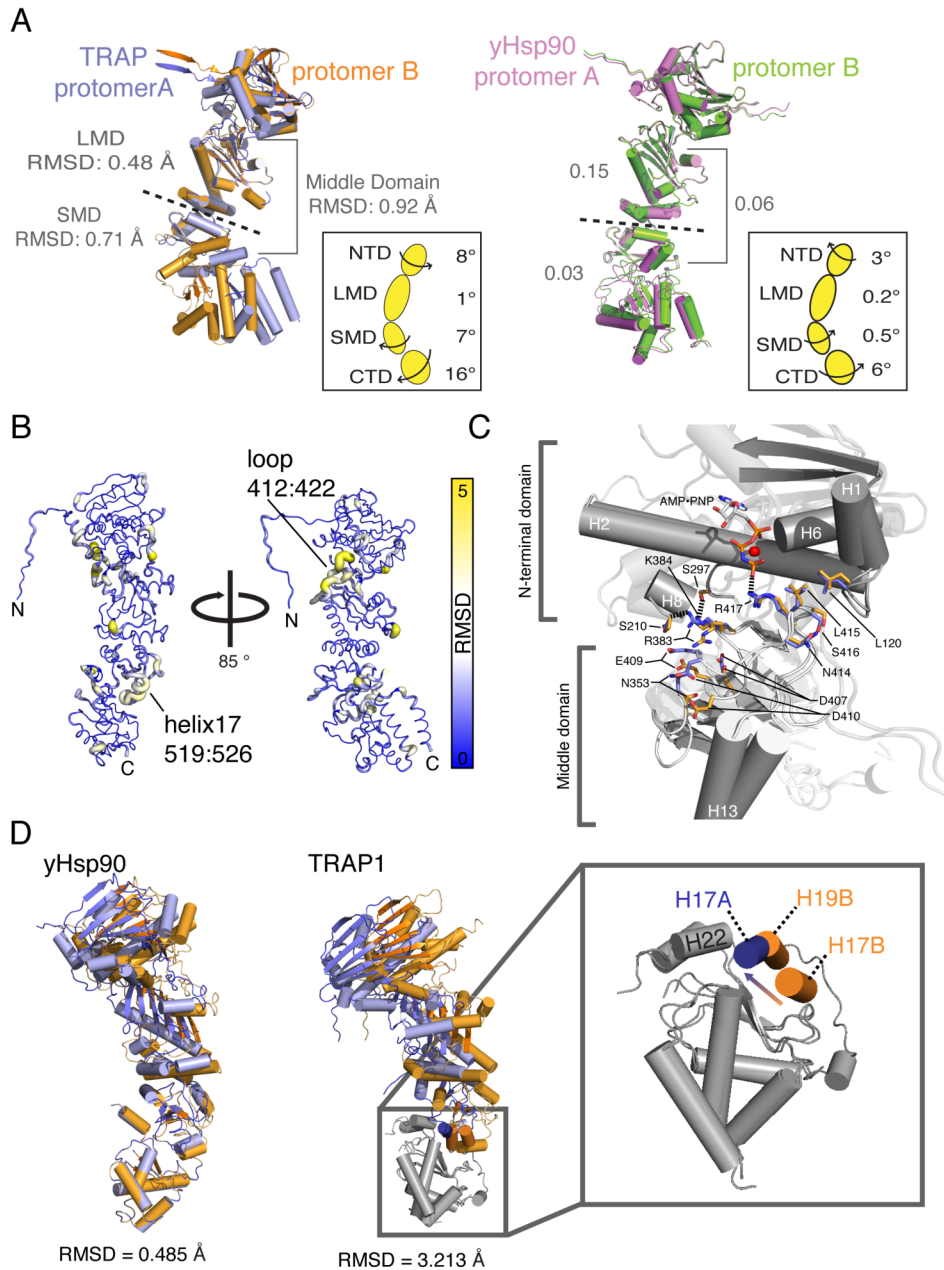


**Figure 3. Novel asymmetry revealed in the TRAP1 dimer.** A) Protomers from TRAP1 and yHsp90 full-length structures are aligned at the LMD to highlight asymmetry, particularly between domains from the TRAP1 structure. RMSD values are calculated to highlight differences between the LMD and SMD versus the entire middle domain. To more clearly depict these differences we calculated the direction and degree of rotation between sub-domains as highlighted in the inset panel. TRAP1 protomers have drastic differences between domains while yHsp90 protomers are similar. B) Graphical representation of the domain differences between protomers of TRAP1. Regions of high variability have higher RMSD values, illustrated with a thicker diameter and the color yellow. C) Close-up view of the NTD and MD illustrate the changes at the NTD:MD interface between protomers aligned at the NTD starts near Arg417. D) Alignment of the protomers from both yHsp90 and TRAP1 with overall RMSD values listed below. The zoomed panel illustrates the unique interface formed between the MD and CTD at the MD:CTD interface.

## **Solution based measurements support an asymmetric closed state**

To confirm the asymmetry seen in the crystal structure we sought methods that could probe the existence of an asymmetric closed conformation in solution. Small angle X-ray scattering (SAXS) has a proven ability to both determine novel solution conformations for Hsp90s and to allow for deconvolution of conformational states within a mixed population [13, 14, 45]. To confirm that the observed differences could be distinguished, theoretical  $P(r)$  curves were calculated for the asymmetric TRAP1 structure, the  $\gamma$ Hsp90 crystal structure, a model of TRAP1 in the  $\gamma$ Hsp90 conformation, and two symmetric models based on our asymmetric structure (homodimers of protomer A or protomer B; Figure S1). As expected, SAXS shows that the addition of AMPPNP or ADP-BeF<sub>3</sub><sup>-</sup> converts both hTRAP1 and zTRAP1 from an open state with broad  $P(r)$  distribution and a maximum distance of  $\sim 200$  Å to a more compact closed state with a more narrow  $P(r)$  distribution and a maximum distance of  $\sim 130$  Å (Figure 4A). At this resolution the structural transitions are essentially the same for both species and ATP analogs, suggesting a well-conserved closed state.

Previous work has demonstrated that while nucleotide stabilizes the closed state, a fraction of the population often remains in equilibrium with the apo state, despite saturating nucleotide concentrations [2, 13]. Additionally, the equilibrium constant between open and closed conformations is unique to each Hsp90 homolog. To quantitatively compare the calculated  $P(r)$  curves from our models with those obtained from experimental data, we accounted for the fraction of the population that remained in the apo state. To avoid potential errors in modeling the apo state, the  $P(r)$  from

corresponding apo data was used in a linear combination with each closed state model for fitting. Fit quality was gauged using a residual R, analogous to the crystallographic R-factor (Methods). Both qualitatively and quantitatively, the asymmetric conformation is a much better fit to the experimental data of TRAP1 in solution (Figure 4B and Table S2). Additionally, fits of the experimental data using a sum of symmetric models (homodimers of protomer A or protomer B) results in worse R-values (Table S2), supporting the existence of closed asymmetric homodimers in solution.

Double electron-electron resonance (DEER) was used as a complementary and higher resolution measure of asymmetry in solution. DEER is capable of measuring distances between two paramagnetic centers at a range of 18-80 Å. Although an ensemble technique, DEER measurements produce a distance distribution that resolves simultaneous states within the sample [46]. DEER probe positions were made within one protomer, based on solvent accessibility and to best distinguish the distance differences for the asymmetric protomer conformations. From simulations of spin labels at various candidate positions on the TRAP1 structure we chose a pair spanning the MD:CTD interface, Lys439 and Asp684 (hTRAP1), with a predicted distance change of ~14 Å (Figure 4C). Native cysteine residues were removed to facilitate site-specific labeling, which did not negatively affect ATPase activity and displayed a closed state distribution by SAXS that was indistinguishable from WT (Figure S2). After spin-labeling at encoded cysteine positions, heterodimers were formed after incubation with 10-fold excess cysteine-free TRAP1 and the population was closed with ADP-BeF<sub>3</sub><sup>-</sup>. The

resulting DEER distribution clearly shows two distinct peaks confirming the existence of two conformations in the closed state population (Figure 4D).

To further assess the pervasiveness of the TRAP1 asymmetric state we evaluated solution scattering for the closely related bHsp90. Using previously reported SAXS data that consists of ~100% closed state bHsp90 [14] we find that our asymmetric conformation is a much better fit than the previous closed state model (Figure 4B). This analysis extends our observation of an asymmetric closed state to other Hsp90 systems. Taken together, this data supports the existence of an asymmetric closed conformation in solution that is evolutionarily conserved between bacteria and humans.



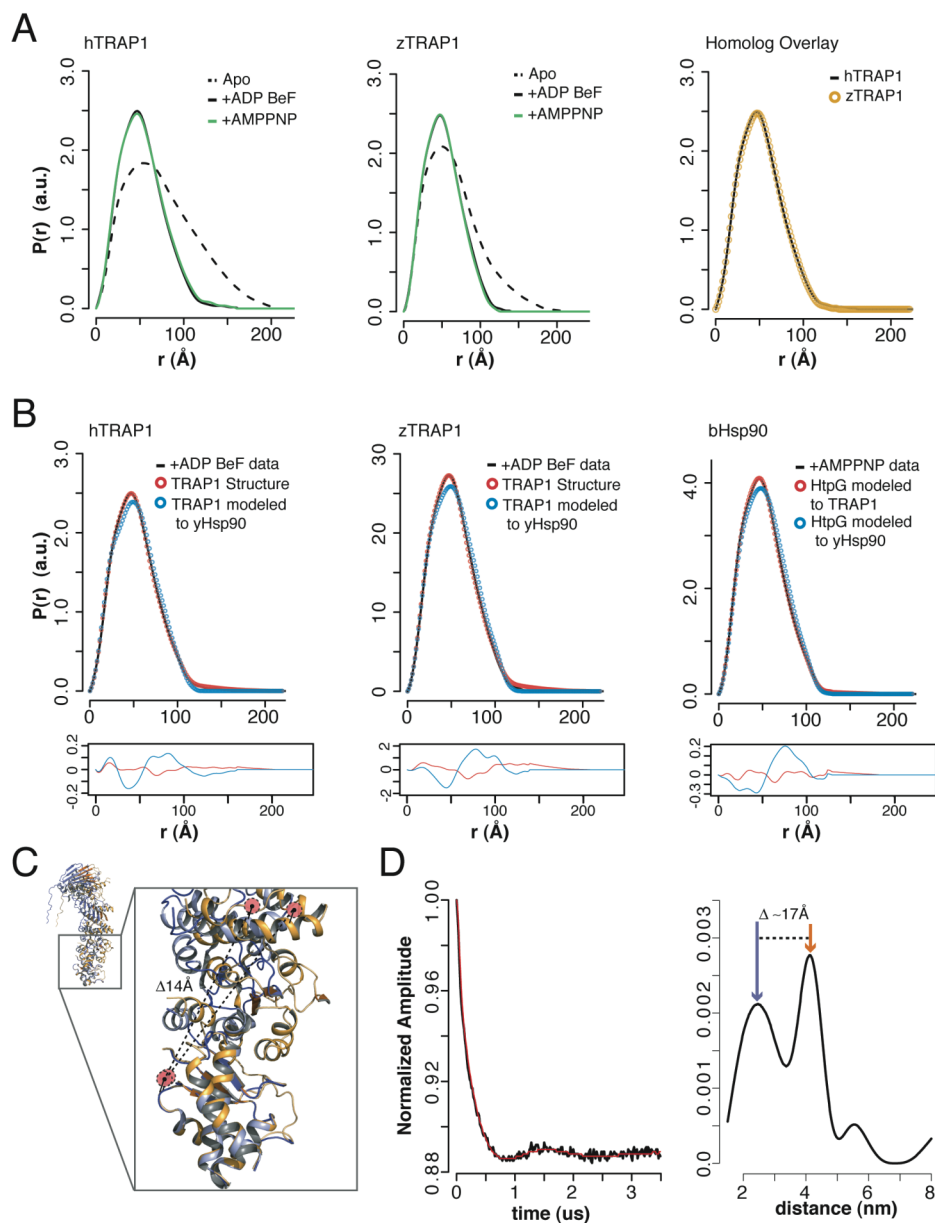


**Figure 4. Solution methods support a conserved asymmetric closed state.** A) SAXS curves of TRAP1 homologs in the apo and nucleotide bound states. Addition of ATP analogs result in a characteristic shift towards a more compact conformation. Overlaying the nucleotide bound SAXS curves from both homologs reveals little difference in the closed state conformation. B) SAXS curves of closed state hTRAP1, zTRAP1 from panel A, and bHsp90 from Krukenberg et al. overlaid against a least squares fit using apo data and theoretical scattering for the TRAP1 crystal structure, or a closed state model of each homolog in the yHsp90 conformation. Residuals are shown below each fit. C) DEER probe design shown on protomers A and B aligned at the CTD with a predicted change in distance of 14 Å at the chosen positions. D) Background corrected and normalized time-domain DEER data (black) fit by Tikhonov regularization (red) are shown on the left. Normalized frequency domain DEER distributions for closed state hTRAP1 (right) obtained after Tikhonov regularization. Two major peaks are observed in the presence of ADP-BeF supporting an asymmetric closed state in solution. Arrows are colored coded to designate either protomer A (blue) or B (orange).

### **Structure-based MD:CTD interface mutations severely impair ATPase activity.**

Having validated our crystallographic observations, we aimed to test the functional relevance of the asymmetric closed state that either exposes or buries distinct surfaces at the MD:CTD interfaces of chemically identical protomers. These interfaces vary significantly in buried surface area (A:410 Å<sup>2</sup>, B:1057 Å<sup>2</sup>) and hydrogen bonding networks. Notably, MD:CTD interface residues Asn519, His521, and Leu522 from H17 are buried, making hydrophobic and polar interactions in protomer A yet are fully exposed in protomer B (calculated using PISA) [47]. Conversely, residues Glu566 and Ile569 make interactions in protomer B and are exposed in protomer A (Figure 5A). To test the functionality of each MD:CTD interface, we mutated these residues and first confirmed their overall physical behavior was unperturbed. Circular dichroism spectroscopy of WT and mutant proteins demonstrated that secondary structure and thermal stability was unperturbed by even the most severe mutations (Figure S3A/B). Electron microscopy confirmed that the mutants could reach a closed state following incubation with nucleotide (Figure S3C).

To assess function, ATPase activities were measured using an enzyme-coupled assay [48]. The protomer A triple mutant (Asp519Ala.His520Ala.Leu522Lys) and protomer B double mutant (Glu566Ala.Ile569Lys) show a ~80% and 75% decrease in respective activity. Single mutations (protomer A:Leu522Lys and protomer B:Glu566Ala) were additionally tested and demonstrate significantly decreased activity (70% and 60%, respectively) (Figure 5B and Table S3). Having confirmed the relevance of our asymmetric MD:CTD interfaces from the zTRAP1 structure, we wanted to extend these

observations to hTRAP1. Mature hTRAP1 was purified in a similar fashion to zTRAP1 and produced hydrolysis rates and  $K_m$  values consistent with previous reports (Table S3) [48]. Mapping single point mutants from zTRAP1 to hTRAP1 (Leu507Lys and Glu551Ala), we observed an equivalent drop in ATPase activity (Figure 5B and Table S3). Moreover, the less severe Leu507Ser mutation had a predicted intermediate effect, and again supported the conserved function of protomer asymmetry (Table S3). The mutant data supports our structural observations and demonstrates the significance of both of the observed MD:CTD interfaces in regulating ATPase activity.

To better understand the physical origins of the decreased ATPase rates, we measured the steady-state rate at which the closed state accumulates for WT zTRAP1 and two different point mutants (Glu566Ala and Leu522Lys). Using SAXS, closure was initiated with ADP-BeF<sub>3</sub><sup>-</sup>, time points were recorded over the course of ~1 hr and scattering curves were processed as described above. While EM and ATPase activities indicated that the mutants could close, SAXS made it clear that the mutants showed less accumulation of closed state than WT suggesting that both sets of mutations destabilize the closed state (Figure S4). Together these data establish the conservation of structural, and functional importance of two distinct protomer conformations within a closed state.

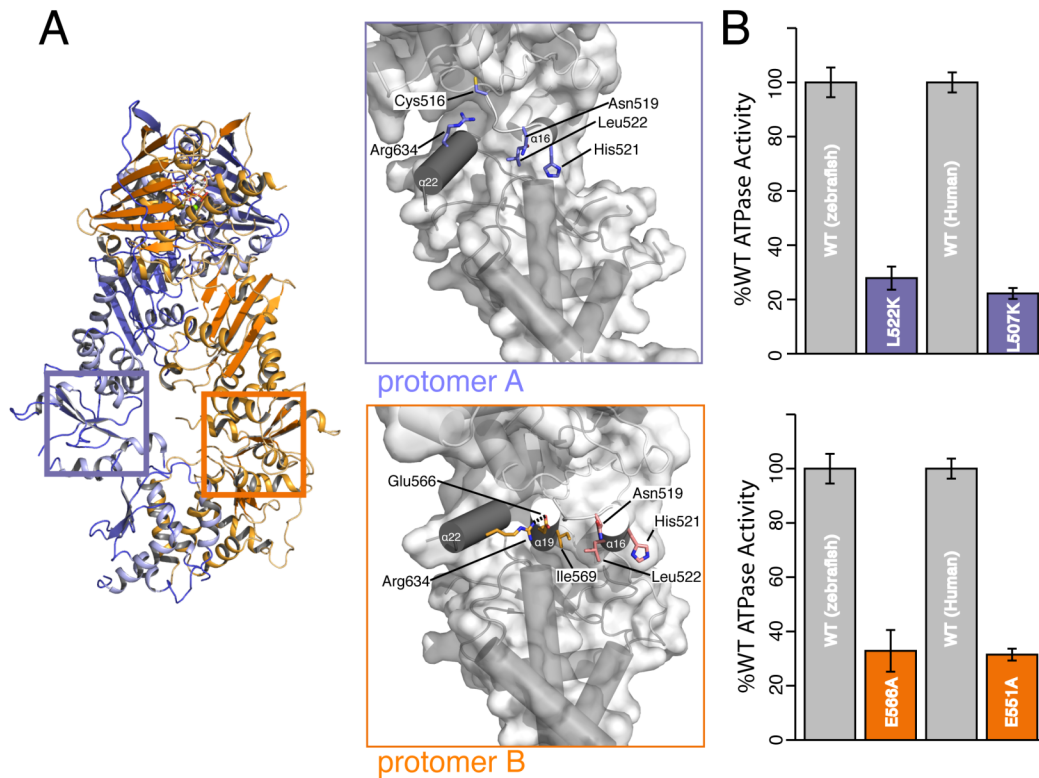


**Figure 5. Structure based MD:CTD interface mutations severely impair ATPase activity.** A) Crystal structure of TRAP1 rotated 75° from view in figure 1A. Highlighted regions are the distinct MD:CTD interfaces generated by the helix swap of protomers A and B highlighted in Figure 3. B) Relative  $k_{obs}$  (30 °C) of zTRAP1 and hTRAP1 with single point mutations designed to disrupt unique contacts at the MD:CTD interfaces. The equivalent drop in activity establishes conservation of asymmetric interfaces between homologs.

### Loss of CTD restores homodimer symmetry

Considering that the protomer arms are chemically identical, we questioned how the observed asymmetric conformation is formed. Fortunately, crystal trials with full-length zTRAP1 mutated at the MD:CTD interface and in the presence of AMPPNP resulted in a distinct crystal form with higher symmetry and a smaller unit cell (Table S1). The structure was solved by molecular replacement and refined to a resolution of 1.75 Å. The asymmetric unit contained a single protomer ending at residue Asp568, and lacking a CTD. However, unlike other NTD:MD constructs examined previously [39, 49]

NTD dimerization is preserved by the perfect two-fold symmetry axis in the crystal lattice (Figure 6A, Movie S4). Given that the full-length protein was used to produce crystals, we reasoned the protein had locked in a closed, NTD-dimerized state, was proteolyzed, and subsequently crystallized. This was confirmed by dissolving the crystals used to generate diffraction data (Figure S5).

The NTD:NTD interface in this structure is very similar to that in full-length TRAP1, and the lid remains disordered between residues 203-205 despite the lower overall B-factors and higher resolution. Importantly, by removing constraints resulting from CTD dimerization, the TRAP1 NTD:MD dimer is able to adopt a symmetric configuration and rotates outward by  $10.5^\circ$  pivoting from the NTD:MD interface. This movement results in a maximum change of  $\sim 10 \text{ \AA}$  measured at the SMD (Figure 6B, S6, Movie S5). This dimeric NTD:MD structure suggests that the simultaneous dimerization of NTDs and CTDs in the full length protein results in a highly strained state, which is at least partially relieved by forming the asymmetric conformation. Proteolysis and removal of the CTDs allows for relaxation to a more open, symmetric state.

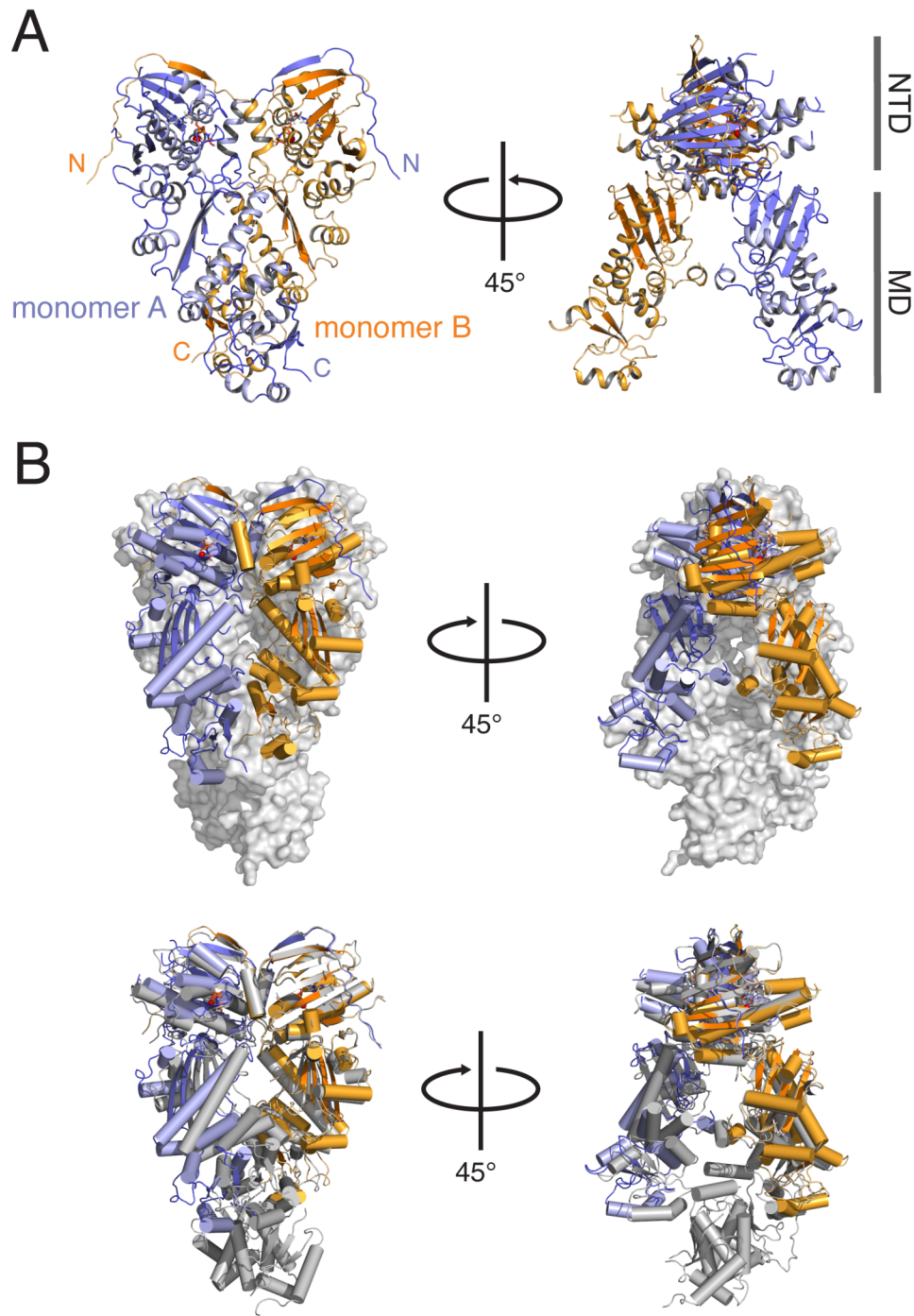


**Figure 6. NTD:MD crystal structure and implications for a strained closed state.** A) Crystal structure of a closed NTD:MD dimer of TRAP1. The CTD has been cleaved during crystallization and leads to a homo-dimeric structure dimerized at the NTD while bound to AMPPNP. Cleavage of the CTD results from destabilization of the MD:CTD interface with the Glu566Ala.Ile569Lys point mutations. B) Overlay of the NTD:MD state with the full-length TRAP1 crystal structure. In absence of strain imposed by CTD dimerization, TRAP1 protomers relax outward to reach a symmetric conformation.

## Discussion

Here we present the first structure of the mitochondrial homolog of Hsp90, TRAP1. Perturbation of TRAP1 activity is linked to a number of human diseases including several cancers and neurodegeneration [27, 28, 32, 50]. Though much work remains to identify particularly critical TRAP1 clients and signaling pathways, the data presented here provides a structural framework for further studies and design of TRAP1 specific therapeutic agents. Indeed, intervention with TRAP1 targeted inhibitors has already shown differential efficacy in diverse cancer models [50].

While it is well appreciated that Hsp90s can dynamically sample a broad range of conformations, our full-length X-ray crystal structures in complex with ATP analogs show an unexpected asymmetric conformation previously unknown in Hsp90 chaperones. This significant asymmetry is rarely observed in homo-oligomers [51, 52] but notably has been reported to be an important mechanistic feature of related GHKL family members [53]. Through the use of SAXS and DEER we confirm the existence of the observed asymmetry in solution, show that it is conserved from bHsp90 to hTRAP1, and use structure-based point mutations to support a functional role for asymmetry *in vitro*.

Our proteolyzed, dimeric NTD:MD structure suggests that simultaneous dimerization of NTD and CTD in the ATP bound closed state results in a significantly strained state, which is relieved by buckling at the MD:CTD interface to form the asymmetric conformation. Proteolysis and removal of the CTDs allows for relaxation to a more open, symmetric state. In support of strain being a conserved property of the

closed state, single-molecule FRET experiments with yHsp90 show that binding of nucleotide in the closed state can lead to transient opening of the CTD dimer interface [54]. As discussed below, we suggest that strain driven by ATP-induced closure and the consequent asymmetry gives rise to two conformational states having distinct functions in client maturation.

### *Asymmetry in the Hsp90 mechanism*

Recent biochemical and structural investigations have begun to reveal asymmetric themes in the mechanism of Hsp90 function. The co-chaperone Aha1 stimulates the ATPase activity of Hsp90 by binding asymmetrically at the NTD:MD interface [55], while binding a single Hop co-chaperone is sufficient to block ATPase activity of both protomers [56]. Asymmetry in the Hsp90:Hop client loading complex has been directly observed by single particle EM [57]. Additionally, many client proteins have been shown to bind with a 1:1 stoichiometry [58, 59] and wherever examined at higher resolution, structural and mutational data directly support asymmetric binding [60, 61]. Together these studies point to the Hsp90 chaperone functioning asymmetrically in concert with various co-chaperones and client proteins.

### *Previous models of the Hsp90 closed state*

Prior to the TRAP1 structure presented here, the only available closed state structure was of yHsp90 in the presence of AMPPNP and the co-chaperone p23 [15], required to obtain reasonable diffraction. Binding of p23 is important for steroid hormone



receptor maturation [62] and has been shown to inhibit Hsp90 ATPase activity [63, 64]. In the yHsp90 structure, NTDs are dimerized with both nucleotide pockets occupied by AMPPNP and two p23 monomers bound on either side of the NTD interface, making contact with both the NTD and MDs. Notably, if yHsp90 were to assume the TRAP1 asymmetric conformation, only one p23 could bind as there would be a steric clash with the second. We suggest that binding of the two p23 co-chaperones could be responsible for promoting the yHsp90 symmetric conformation. In support of this, NMR data has shown that binding of two p23s on hHsp90 can induce changes in the MD significantly removed from where p23 makes direct contacts [65]. Such changes would be expected if p23 binding were to induce a rotation in the MD towards a more symmetric state.

#### *Extension of asymmetry to other Hsp90 systems*

Our data demonstrates the asymmetric closed state is conserved in bHsp90 and multiple species of TRAP1. This would suggest that early on, Hsp90 evolved an ability to adopt unique conformations between protomers and that these persisted presumably due to functional pressure. Information on the broader relevance of this new closed state conformation to eukaryotic cytosolic Hsp90s is also suggested by data with yHsp90 that seems to be better explained by the asymmetric model presented here. Previous kinetic studies have shown that mutation of T22 (yHsp90, Hsp82 numbering) to Ile or Phe enhanced ATP hydrolysis while seeming to be sterically incompatible with the yeast closed state model [16, 66, 67]. By contrast, these residue changes would be

readily accommodated in our TRAP1 structure suggesting that yHsp90 may also adopt a conformation similar to our TRAP1 model during ATP hydrolysis. The p23 binding surface involves the NTD:LMD interface where T22 is located [15]; thus the position of T22 would likely be altered by the binding of two copies of p23 which would force symmetry by repositioning the yHsp90 main chain and modulating the NTD:LMD interface.

While partially buried in the yHsp90 structure (60%, calculated by PISA), phosphorylation of Ser485 of yHsp90 (Ser526, zTRAP1) leads to a decrease in function both *in vitro* and *in vivo* [68]. Phosphomimetic versions of yHsp90 at this position showed even more profound effects on *in vitro* and *in vivo* function with several client proteins, and substitution of Ser to Ala also displays *in vitro* defects. This Ser is conserved among Hsp90s and fully exposed in protomer B of our TRAP1 model where it would be available for modification. By contrast, phosphorylation of this residue in protomer A would disrupt the MD:CTD interface as it is fully buried. The degree of conservation and lack of modifying enzymes in lower species indicates this position is structurally important and perhaps was later utilized as a point of regulation by post-translational modifications. The varying degree of exposure in the TRAP1 structure is indicative of a point of structural regulation.

Preliminary investigations directly probing asymmetry in yHsp90 have been ambiguous thus far and thus remain a future direction.

### *A new model for the Hsp90 conformational cycle and utilization of ATP*

Although it is well accepted that both ATP binding and hydrolysis are essential for Hsp90 function *in vivo* [1] it remains unclear how any Hsp90 homolog utilizes the available energy from two ATPs for client maturation. Significant evidence suggests that initial client binding involves selection of a preferred conformation from an ensemble of open apo states that largely arises from variations in the rotation about the MD:CTD interface [58]. Details of potential client binding sites are emerging through combinations of NMR, genetic screens and mutagenesis [44, 60]. Particularly well characterized is the binding site highlighted in Movie S3 composed of variably exposed hydrophobic residues from both the SMD and CTD. The location of these residues explains why different clients might prefer differing MD:CTD orientations.

While simple anti-aggregation functionality for Hsp90s is independent of nucleotide *in vitro* [5], *in vivo* data clearly demonstrates the requirement for both ATP binding and hydrolysis in client maturation [1]. An attractive hypothesis is that client maturation is driven by rearrangements of these binding site residues that occur upon transition to the closed state, the rate-limiting step to hydrolysis [58, 69]. ATP hydrolysis would then lead transiently through the compact ADP state in which these residues are buried within Hsp90, leading to client release. The challenge then is to understand the role of ATP in this process as affinities for Hsp90 clients are in the 1-100 $\mu$ M range. Given the slow closure kinetics of Hsp90, the client would be predicted to fall off more than once in the time it takes Hsp90 to reach a closed state. Therefore it is hard to

understand how 7-14 kcals of energy available from hydrolysis of ATPs would benefit a release process. Moreover ATP binding is weak, such that at physiological concentrations both ATP-bound and free Hsp90 are present, thus ATP binding is unlikely to provide a significant driving force for client rearrangement.

As an alternative, we propose an updated model for the chaperone cycle of Hsp90 that integrates a broad array of available information and incorporates the novel asymmetry reported here into the ATP-driven cycle of client binding, maturation and release (Figure 7). Newly added are two closed states that exploit differential ATP hydrolysis by the two protomers. Upon ATP binding by both protomers the population shifts to a closed high-energy asymmetric state as revealed in our full-length TRAP1 structure. Unique to this model is the suggestion that hydrolysis of one ATP leads to a symmetric closed state much more like the  $\gamma$ Hsp90 crystal structure. As a consequence, rearrangement of the asymmetric client binding site residues is directly coupled to the hydrolysis of the first ATP and would then be coupled to structural changes in client bound in this region. Hydrolysis of the second ATP would cause the chaperone to transiently populate a compact ADP state, releasing clients, before releasing ADP and returning to the apo state. P23 would then be expected to preferentially interact with the single ATP more symmetric conformation, requiring both ATPs to bind, but also blocking further ATP hydrolysis.

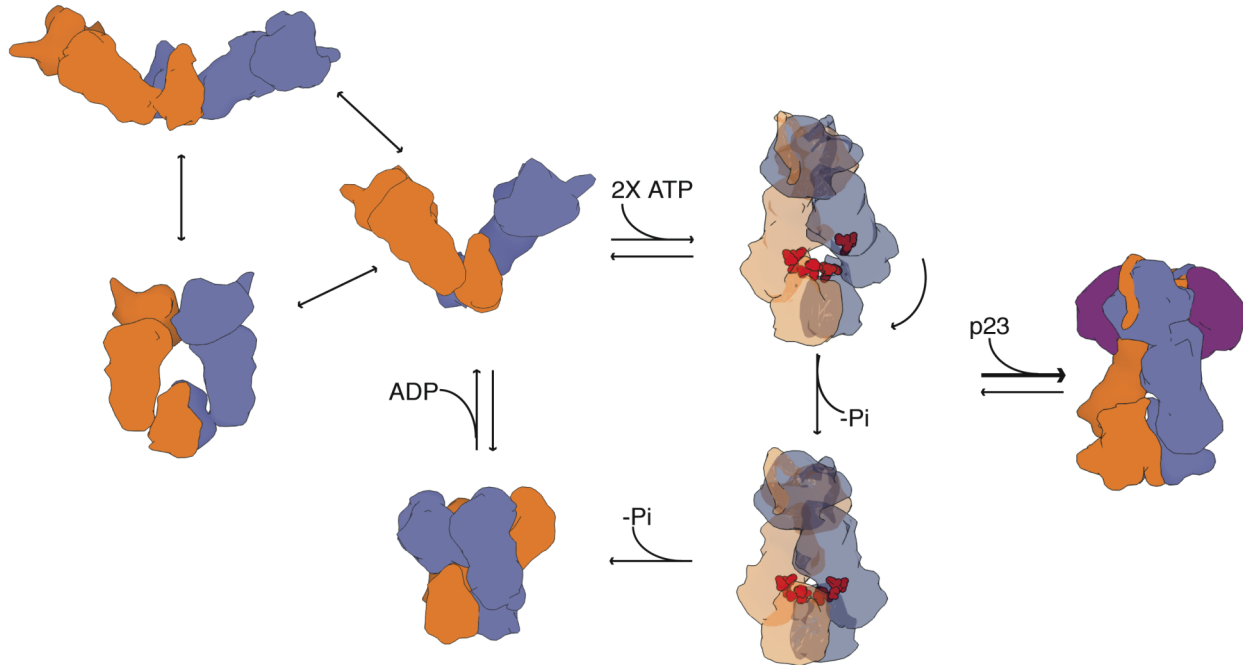


**Figure 7. New model for the conformational cycle of Hsp90.** In the absence of nucleotide, Hsp90 exists in an equilibrium of states with varying open conformations. Upon ATP binding the chaperone shifts to an asymmetric closed conformation that is significantly strained leading to buckling of the MD:CTD interface (proposed client binding residues in red [44], transparency for visualization). Upon ATP hydrolysis, strain is relieved and the MD:CTD interface is re-arranged to form a symmetric state reminiscent of the  $\gamma$ Hsp90 conformation. This conformation can be stabilized by dual binding of co-chaperone p23 (purple) at the NTD interface stalling the progression of the cycle. Upon hydrolysis of the second ATP, the ADP state is transiently formed and ADP release resets the cycle to the apo state equilibrium.

While we propose a model where the first ATP hydrolysis leads to a closed state reminiscent of the previous  $\gamma$ Hsp90 structure in the main text, it is also possible that the protomer arms could flip-flop between conformations, or that both would assume the conformation of either protomer A or protomer B. Notably, an advantage of the “flip-flop” mechanism is that both MD:CTD interfaces change upon the first hydrolysis event, which would ensure structural re-arrangements to clients bound on either of the initial protomer conformations (protomer A or B) (Figure S7). Importantly, for each of these possibilities the MD:CTD interface must re-arrange to progress through the cycle,

preserving the possibility of utilizing ATP hydrolysis for doing work on a client bound to this region.

With the introduction of inherent structural asymmetry to the Hsp90 model comes a combinatorial expansion of conformations possible for interaction with clients and co-chaperones. Modulating the asymmetry or the rate of forming the asymmetric state thus provides a convenient mode of regulation for overall Hsp90 function in various pathways. In support of this, several post-translational modifications that dramatically perturb Hsp90 function are located in or near the MD:CTD interface including the previously discussed Ser485 in  $\gamma$ Hsp90 [68, 70].

Despite sequence variation there is strong structural conservation of Hsp90 from bacteria to humans. Thus, the ability of Hsp90 to sample an asymmetric conformation in a closed state is likely an intrinsic feature of several and potentially all Hsp90 homologs. Though future experiments are required to precisely define the progression of conformational states and how the structural asymmetry shown here is utilized for diverse Hsp90 functions, our findings provide a new hypothesis for how ATP hydrolysis could be directly coupled to client maturation.

## **Accession Numbers**

Atomic coordinates have been deposited in the Protein Data Bank (PDB) under the accession codes: 4IVG, 4IPE, 4IYN, and 4JOB.

## **Acknowledgements**

We thank J. Holton, G. Meigs and ALS staff of beamline 8.3.1 for data collection and helpful discussions. We thank G. Hura, K. Dyer, J. Tanamachi and staff of beamline 12.3.1 for SAXS data collection and helpful discussions. We thank L. Peng of the M. Jacobson lab for building symmetric models of our TRAP1 structure and N. Naber of the R. Cooke lab for assistance with labeling and CW EPR. Special thanks to K. Krukenberg for bHtpG solution data and helpful discussions. Finally we thank members of the Agard lab for helpful discussions. Support for this work was provided by the National Institute of General Medical Sciences Protein Structure Initiative - Biology (PSI-Biology); Grant number: U01 GM098254 (DAA) and U54-GM094597 (MAK), the Larry L. Hillblom Center for the Biology of Aging (LAL), and HHMI.

## **Supplemental Information**

The manuscript presented in chapter 1 is currently in revision at Molecular Cell. From the reviewers comments we set out to test if the unique MD:CTD interfaces in our asymmetric closed state structure of TRAP1 had any effect on client interactions as proposed. From previous experiments we knew that the model substrate  $\Delta 131\Delta$  (a fragment of staphylococcal nuclease) could bind and accelerate the rate of

closure/ATPase of TRAP1. For the follow up, Daniel Elnatan (an author on this paper) has done the experiment in figure S9A and Timothy Street and I did the initial binding experiment shown in figure S9B. Daniel is now repeating the experiment in figure S9B and including the hTRAP1 L507K mutant to complete the experiment. Importantly, these data suggest that both MD:CTD interfaces observed in our structure are necessary for functional interaction with clients. Further, we were asked us to test if mixing the two mutants (where only one MD:CTD interface is perturbed in either mutant) would alter the mutations effects on ATPase. To this end we had done a mixing experiment (figure S8) and see no change in ATPase upon titration. Our model predicts (either figure 7 or figure S7) that the Hsp90 dimer must switch symmetries from the initial asymmetric state. If this is the case then mixing the two orthogonal mutants should still be impaired as either arm is impaired in the ability to switch to the opposite conformation (protomer A  $\leftrightarrow$  protomer B). These data are consistent with our model. Further, we have demonstrated a predictable effect of mutations in the observed MD:CTD interfaces where the severity (size/charge, %buried surface area) of mutated residue correlates with the measured effect on ATPase. As shown in the main text, mutation of Leu507Lys (hTRAP1) showed a ~70% decrease in ATPase activity where a mutation to a smaller/non-charged serine shows a less severe phenotype at ~50% decrease in ATPase. An additional mutation on the MD:CTD interface in protomer B was tested. Here we mutated Val555 (hTRAP1) towards the end of H19 (and only partially buried) to a serine and see a smaller ~30% drop in ATPase activity relative to WT. These mutations demonstrate a predictable trend that correlates with the MD:CTD



interfaces observed in our crystal structure of TRAP1. Lastly, we have shown that mutations at the MD:CTD region need not be deleterious as mutating the cysteine residues in this region to alanine actually increases the ATPase rate by  $\sim 2$ -fold (Table S3).

### Supplemental Figures and Legends

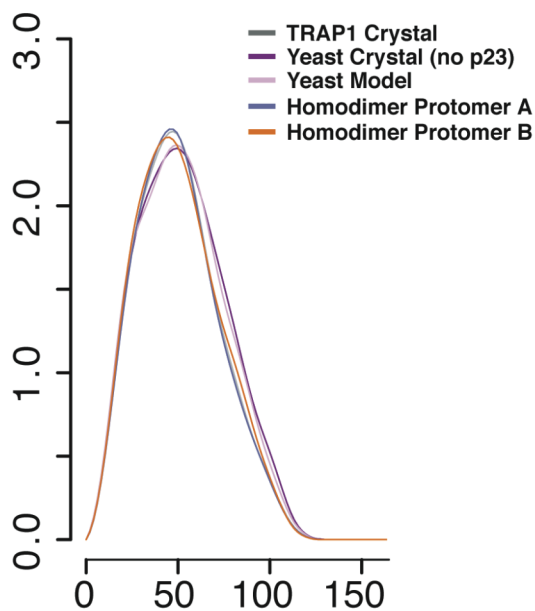


**Figure S1. Theoretical SAXS curves for closed state models.** Normalized theoretical scattering curves generated for a series of closed state models using CRY SOL [71] and GNOM [72]. Here we see differences in the distributions for each model. These curves were used for further fitting and assessment of the closed state conformation in solution.

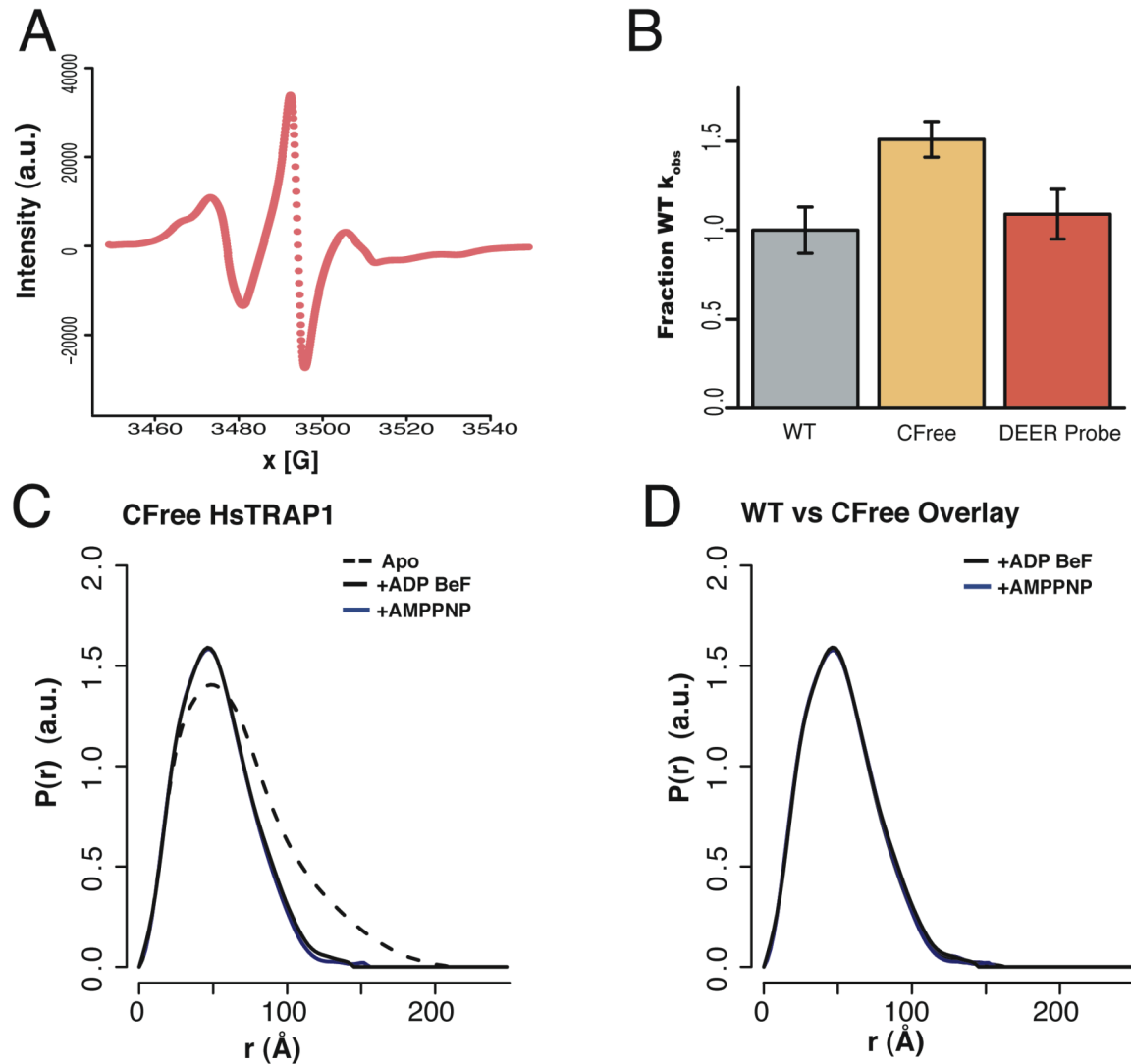


**Figure S2. DEER probe is labeled, active and forms an asymmetric closed state.** A) CW EPR confirming site-specific labeling of the MSL spin probe. Scans show no signs of free MSL. B) ATPase measurements of WT, cysteine-free (CFree), and probe used in DEER measurements in figure 4D. C) SAXS measurements for CFree human TRAP1 (hTRAP1) showing characteristic shift with addition of ATP analogs. D) Overlay of normalized SAXS curves of WT and CFree hTRAP1 illustrating conservation of overall closed state conformation.

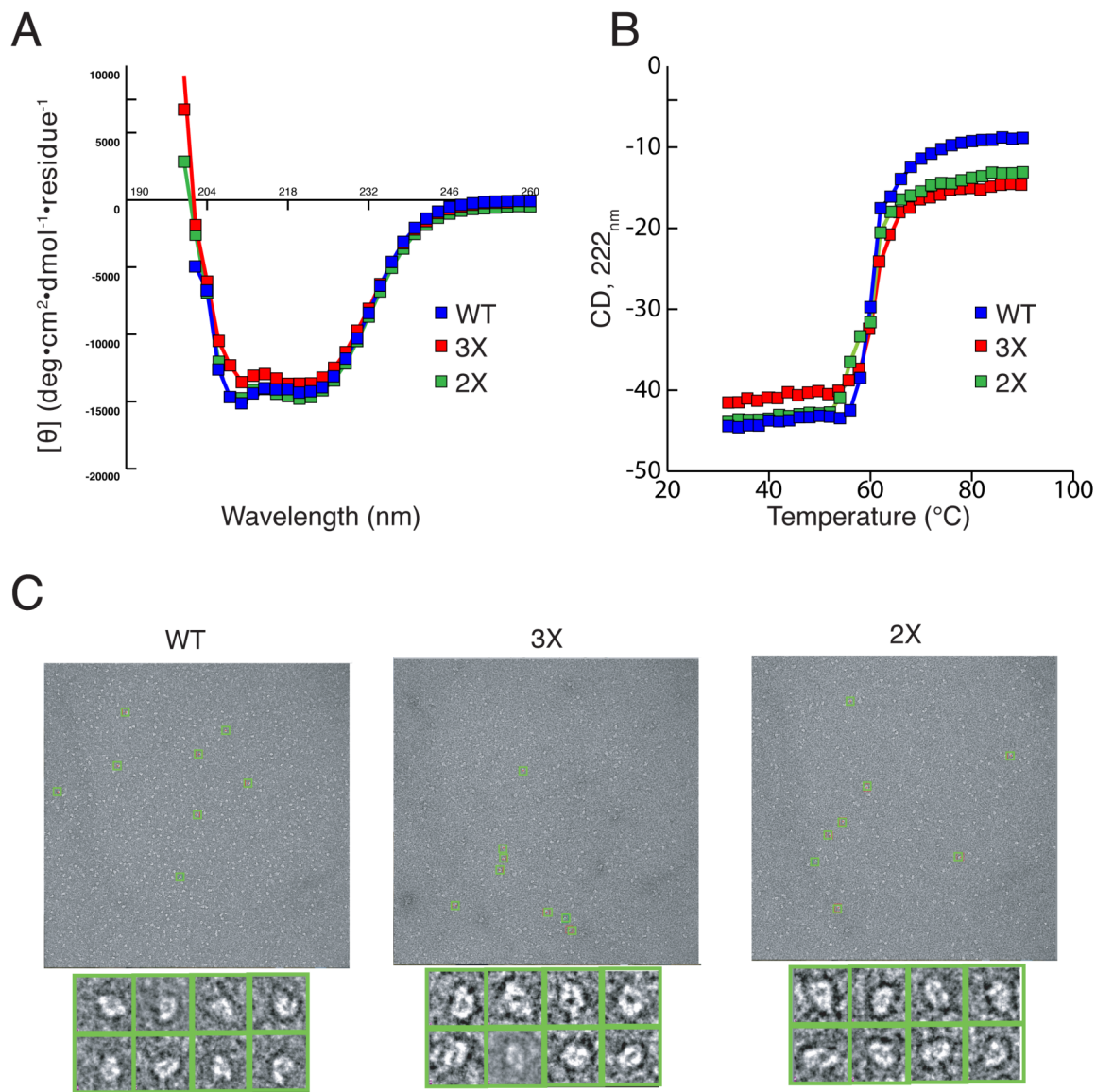


**Figure S3. MD:CTD Interface mutations do not prevent TRAP1 from reaching a closed state or effect overall fold.** A) CD spectra and B) melting curves of apo WT and mutants from A revealing that the overall secondary structure and stability of zebrafish TRAP1 (zTRAP1) is not significantly altered with the aforementioned mutations. C) Negative stain EM micrographs of pre-closed WT zTRAP1 and the two most severe mutants (Asp519Ala.His521Ala.Leu522Lys (3X), Glu566Ala.Ile569Lys (2X)) aimed at disrupting the unique MD:CTD interfaces of protomer A and protomer B, respectively. Particles representing a closed form of the chaperone are shown below their respective micrographs.

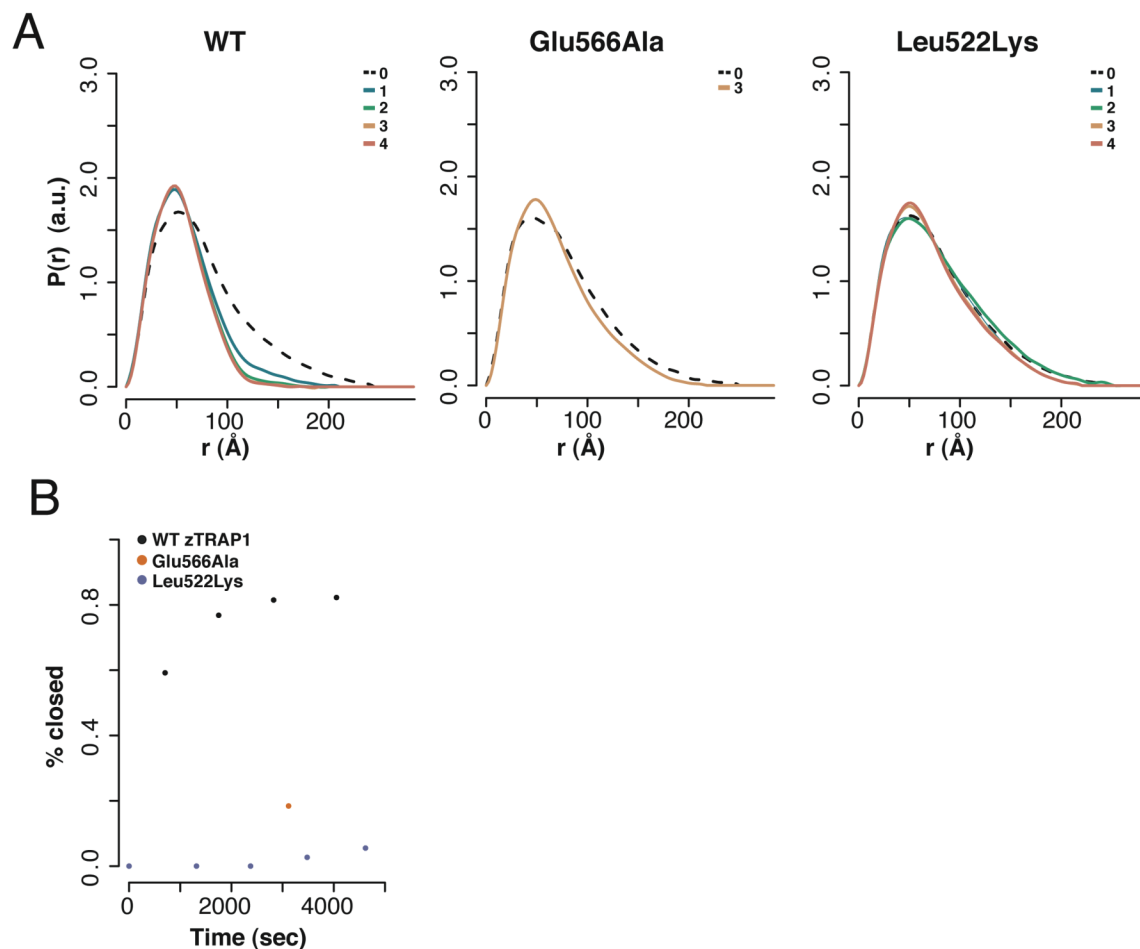


**Figure S4. MD:CTD interface mutants destabilize the closed state.** A) SAXS curves of zTRAP1 in the apo state (0) and time points following addition of ADP-BeF (1-4). For WT, the addition of ADP-BeF shows initiation of closure reaction at time point 1 and continues to accumulate over time. Although the MD:CTD interface mutants do accumulate closed state molecules, the percent of the population at the later time points is significantly less than WT. B) Plotting the percent closed state over time (least squares fitting, see methods) demonstrates that the approach to a closed state equilibrium is much slower for both mutants.

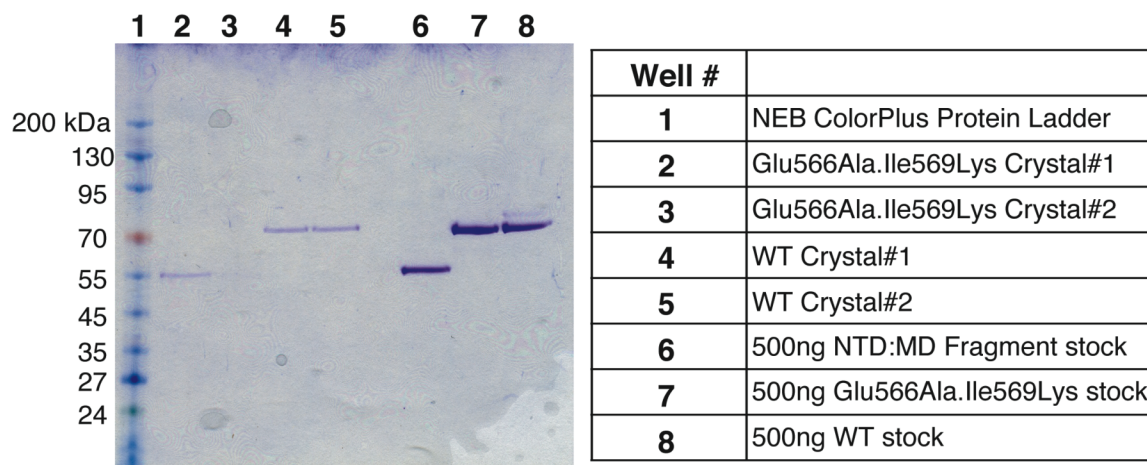


**Figure S5. NTD:MD crystal is formed after cleavage of full-length TRAP1 at a destabilized MC interface.** Coomassie stained gel of stock protein and representative WT and mutant crystals that led to the structures presented in Figures 1 and 4, respectively. Pre- and post-crystallization the WT protein remains full-length. The crystallized mutant protein has been cleaved between the Middle and C-Terminal domains leading to a NTD:MD dimer while keeping the catalytic machinery intact (Figure 4).

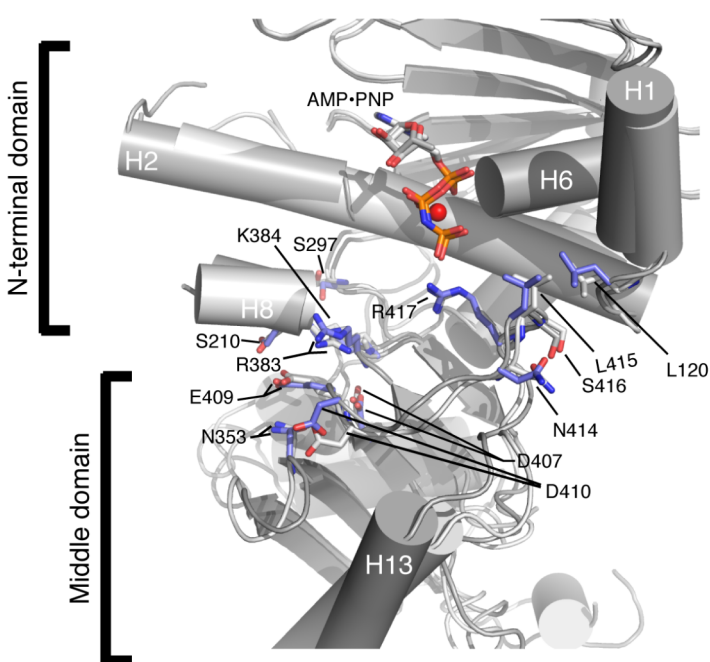


**Figure S6. NTD alignment of Full-length and NTD:MD TRAP1.** NTD alignment of the full-length and NTD:MD TRAP1 structures with a view of the NTD and LMD interface similar to Figure 3C. Sticks from protomer A of full-length and NM:MD structure are colored in slate and grey, respectively. Although the catalytic machinery remains more or less intact, structural deviations start to become apparent past Arg417.

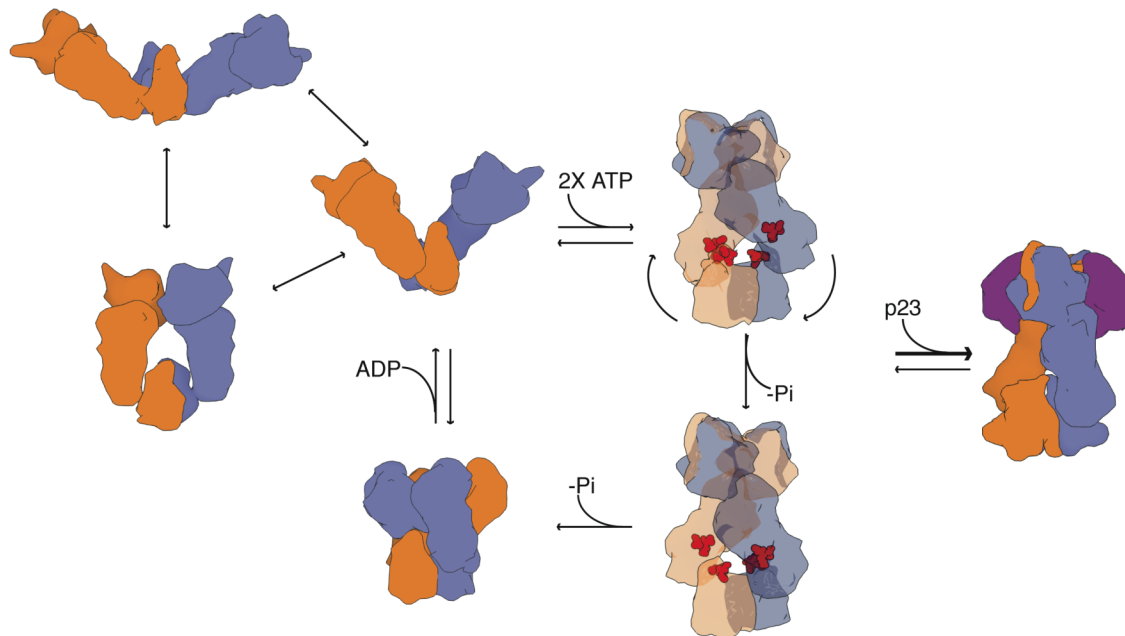


**Figure S7. Alternative Model for the chaperone cycle of Hsp90.** Model proposed in figure 7 of the main text with an alternative progression of states during sequential hydrolysis. Here instead of progression from asymmetric conformation (observed in the crystal structure of TRAP1, pdb: 4IPE) to a symmetric conformation (similar to the  $\gamma$ Hsp90:p23 closed state complex, pdb: 2CG9), the protomer arms flip-flop conformations after the first hydrolysis event before progression to the ADP and apo states to reset the cycle. One advantage of this mechanism is that both MD:CTD interfaces change upon the first hydrolysis event, which would ensure structural re-arrangements to clients bound on either of the initial protomer conformations (protomer A or B).

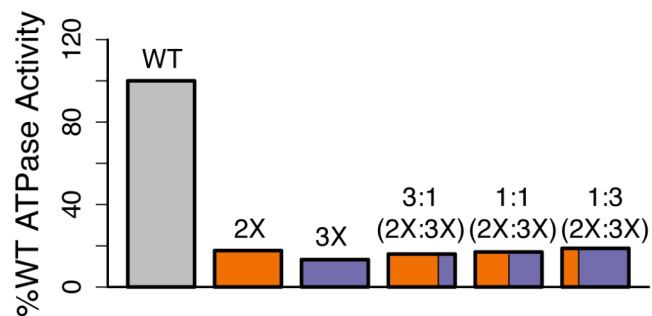


**Figure S8. Heterodimers of MD:CTD interface mutants do not rescue ATPase.** Percent of WT steady-state ATPase rates for heterodimers of the most severe MD:CTD interface mutants for zTRAP1 designed to disrupt protomer A (3X) or protomer B (2X) mixed at different ratios (for definition of “2X” and “3X” see Figure S3). Homodimers of WT and each mutant are plotted for comparison and to show that a mixing the distinct MD:CTD mutants shows no change in ATPase. Consistent with the model, which predicts that you have to be able to change symmetries from the starting state.

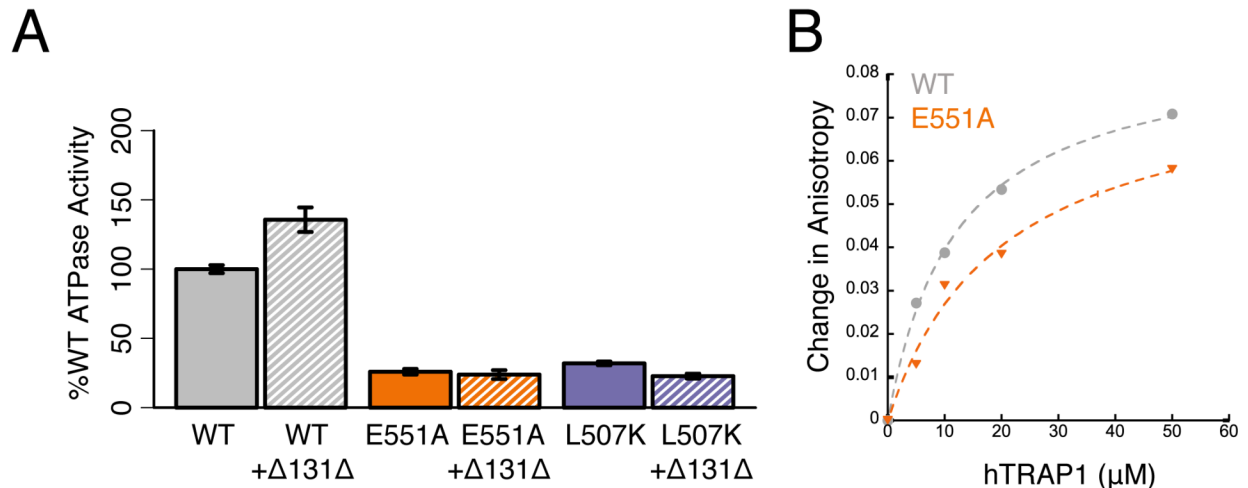


**Figure S9. MD:CTD interface mutants have altered interaction with  $\Delta 131\Delta$ .** **A)** Comparison of steady-state hydrolysis rates for WT hTRAP1 and MD:CTD mutants +/- 15 $\mu$ M  $\Delta 131\Delta$ . While  $\Delta 131\Delta$  can stimulate the ATPase of WT hTRAP1 similar to bHsp90 [58], in the presence of the MD:CTD interface mutants, the substrate acceleration is no longer observed. **B)** Anisotropy binding assay with IAEDANS-labeled  $\Delta 131\Delta$  demonstrating binding of WT hTRAP1 with a  $\sim 12\mu$ M  $K_d$  and a lower  $K_d$  of  $\sim 20\mu$ M for the MD:CTD interface mutant aimed to disrupt protomer B (E551A). Together these data suggest altered interaction of  $\Delta 131\Delta$  due to changes in the distinct MD:CTD interfaces reported here.

**Movie S1. View of full-length TRAP1 crystal structure.** 360° rotation of the full-length TRAP1 crystal structure bound to AMPPNP. (Non-printable Material, Movies can be found in final publication).

**Movie S2. Morph between the TRAP1 and yHsp90 conformations.** Morph between the TRAP1 crystal structure and the yHsp90 crystal structure clearly shows the dramatic conformational changes compatible with full-length Hsp90 structures. Morph made using [UCSF Chimera Package](#) [73]. (Non-printable Material, Final Movies can be found in final publication).

**Movie S3. Residues that bind with client protein change conformation between asymmetric states.** Residues previously shown to bind with client proteins are colored red. A morph between the two protomers of the TRAP1 crystal structure clearly demonstrate the drastic conformational change at the MD:CTD interface. (Non-printable Material, Final Movies can be found in final publication).

**Movie S4. View of NTD:MD TRAP1 crystal structure.** 360° rotation of NTD:MD TRAP1 crystal structure bound to AMPPNP. (Non-printable Material, Final Movies can be found in final publication).

**Movie S5. Conformational morph of full-length TRAP1 to NTD:MD crystal structure.** Morph (UCSF Chimera) of asymmetric conformation seen in the full-length structure of TRAP1 to the symmetric NTD:MD structure. Here we see that cleavage of the CTD in the asymmetric closed state relieves strain at the MD:CTD interface resulting in slight shifts in the in NTD and NTD:LMD interface, as well as swinging out of the MDs. These shifts ultimately result in restoration of symmetry. (Non-printable Material, Final Movies can be found in final publication).

**Table S1. Crystallographic Data Table**

Data Set	Trap1 AMPPNP native	Trap1 AIF native	Trap1 BeF native	TRAP1 ( NTD:MD) AMPPNP native	Trap1 AIF Se- methionine	Trap1 BeF Se- methionine
PDB Code	4IPE	4IYN	4JOB	4IVG		
<b>Data Collection</b>						
Wavelength	1.1159	1.1159	1.1159	1.1159	0.9796	0.9796
Space group	C2	C2	C2	I222	C2	C2
Cell dimensions:						
a, b, c (Å)	176.0, 96.1, 124.5	178.9, 96.6, 125.9	177.8, 96.6, 125.0	85.1, 94.5, 155.5	177.9, 96.7, 125.2	177.4, 96.8, 125.3
$\beta$ (°)	134.6	134.3	134.3	90.0	134.6	133.8
Resolution (Å)	50-2.3 (2.4-2.3)	50-2.3 (2.4-2.3)	45-2.35 (2.43-2.35)	50-1.75(1.81-1.75)	50-3.0 (3.1-3.0)	45-2.7 (2.8-2.7)
$R_{\text{sym}}^a$ (%)	5.1 (39.5)	9.0 (43.1)	8.7 (54.4)	8.0 (99.9)	10.0 (28.7)	12.0 (95.3)
$R_{\text{rel.m.}}^b$ (%)	5.2 (37.6)	6.8 (36.0)	5.8 (50.8)	9.1 (99.9)	9.4 (24.3)	12.6 (98.0)
$R_{\text{p.i.m.}}^c$ (%)	2.6 (18.7)	3.4 (18.3)	3.3 (29.1)	3.4 (45.8)	3.4 (8.7)	4.9 (40.1)
Completeness (%)	98.6 (97.6)	99.1 (91.1)	99.5 (98.1)	99.4 (94.6)	100 (100)	100 (99.8)
Redundancy	4.1 (4.1)	4.8 (3.8)	3.8 (3.1)	7.8 (6.2)	14.3 (8.0)	7.4 (6.7)
$I/\sigma$	24.9 (3.1)	18.6 (2.4)	18.0 (1.9)	24.9 (1.43)	25.6 (7.7)	16.8 (1.2)
Wilson B factor (Å <sup>2</sup> )	48.16	50.2	59.1	29.8	69.9	56.84
					FOM 0.44	FOM 0.40
<b>Refinement</b>						
Resolution (Å)	26-2.3	30-2.3	30-2.3	30-1.75		
Reflections	67,272	66,710	62,239	63,000		
Nonhydrogen Atoms	9,684	10,148	9,705	3,913		
Water Molecules	279	288	189	344		
$R_{\text{work}}^d$	18.0	18.5	20.5	18.86		
$R_{\text{free}}^e$	22.5	23.14	24.8	20.26		
R.m.s. deviations						
Bond lengths (Å)	0.01	0.01	0.01	0.008		



Bond angles (°)	1.16	1.18	1.17	1.17
B factors (Å <sup>2</sup> )				
Protein	73.5	67.8	82.3	47.8
Water	59.6	51.2	59.4	49.8
Coordinate error (Å)	0.25	0.27	0.33	0.20
Ramachandran plot <sup>f</sup>				
Favoured (%)	95.22	94.75	95.01	97.05
Allowed (%)	4.61	4.08	4.65	2.53
Outliers (%)	0.17	1.17	0.34	0.42

a  $R_{\text{sym}} = \sum |I_i - \langle I_i \rangle| / \sum I_i$ , where  $I_i$  is the intensity of the  $i$ th observation and  $\langle I_i \rangle$  is the mean intensity of the reflection.

b  $R_{\text{r.i.m.}} = \sum hkl [N(N-1)]^{1/2} \sum |I_i(hkl) - \langle I(hkl) \rangle| / \sum hkl \sum I_i(hkl)$ , where  $I_i(hkl)$  is the observed intensity and  $\langle I(hkl) \rangle$  is the average intensity of multiple observations of symmetry-related reflections.

c  $R_{\text{p.i.m.}} = \sum hkl [1/(N-1)]^{1/2} \sum |I_i(hkl) - \langle I(hkl) \rangle| / \sum hkl \sum I_i(hkl)$ , where  $I_i(hkl)$  is the observed intensity and  $\langle I(hkl) \rangle$  is the average intensity of multiple observations of symmetry-related reflections.

d  $R_{\text{work}} = \sum (|F_{\text{obs}}| - |F_{\text{calc}}|) / \sum |F_{\text{obs}}|$

e  $R_{\text{free}}$  = R value for a randomly selected subset (2000 reflections) of the data that were not used for minimization of the crystallographic residual.

Highest resolution shell is shown in parenthesis.

<sup>f</sup> Calculated with the program PROCHECK [74].

**Table S2. R values for closed state model fitting of SAXS data**

SAXS data	Model	R value
WT hTRAP1 ADP BeF	TRAP1 Crystal	<b>0.015</b>
WT hTRAP1 ADP BeF	Hsp82 Crystal (no p23)	0.072
WT hTRAP1 ADP BeF	Hsp82 Model	0.064
WT hTRAP1 ADP BeF	Homodimer models A+B	0.021
WT hTRAP1 AMPPNP	TRAP1 Crystal	<b>0.016</b>
WT hTRAP1 AMPPNP	Hsp82 Crystal (no p23)	0.063
WT hTRAP1 AMPPNP	Hsp82 Model	0.057
WT hTRAP1 AMPPNP	Homodimer models A + B	0.021
WT zTRAP1 ADP BeF	TRAP1 Crystal	<b>0.026</b>
WT zTRAP1 ADP BeF	Hsp82 Crystal (no p23)	0.057
WT zTRAP1 ADP BeF	Hsp82 Model	0.05
WT zTRAP1 ADP BeF	Homodimer models A + B	0.031
WT zTRAP1 AMPPNP	TRAP1 Crystal	<b>0.030</b>
WT zTRAP1 AMPPNP	Hsp82 Crystal (no p23)	0.070
WT zTRAP1 AMPPNP	Hsp82 Model	0.061
WT zTRAP1 AMPPNP	Homodimer models A + B	0.035
CFree hTRAP1 ADP BeF	TRAP1 Crystal	<b>0.015</b>
CFree hTRAP1 ADP BeF	Hsp82 Crystal (no p23)	0.063
CFree hTRAP1 ADP BeF	Hsp82 Model	0.059
CFree hTRAP1 ADP BeF	Homodimer models A + B	0.016
CFree hTRAP1 AMPPNP	TRAP1 Crystal	<b>.017</b>
CFree hTRAP1 AMPPNP	Hsp82 Crystal (no p23)	.067
CFree hTRAP1 AMPPNP	Hsp82 Model	.059
CFree hTRAP1 AMPPNP	Homodimer models A + B	0.020

Note: **Bold** represents the best fit.

**Table S3. Steady-state kinetic values**

	zTRAP1 (min <sup>-1</sup> )	K <sub>obs</sub>	hTRAP1 (min <sup>-1</sup> )	K <sub>obs</sub>
WT	1.21 +/- 0.07		0.32+/- .01	
E/A./K	0.29 +/- 0.01			
N/A.H/A.L/K	0.22 +/- 0.01			
E/A	0.46+/- .02		0.10+/- .01	
L/K	0.34 +/- .05		0.07+/- .01	
L/S			0.16 +/- .01	
V/S			.22+/- .02	
Cys Free			.67+/-0.03	
WT Km (25C)			8.3 μM	
WT Km (30C)	25.1 μM		8.5 μM	

## Supplemental crystal trial information

Upon first working with human TRAP1, I discovered a large temperature dependant kinetic barrier between the apo and closed state (described in chapter 2). With this initial finding, I saw potential for structural studies in that what seemed to be the biggest hurdle for high-resolution crystal structures were two properties of the Hsp90 system: 1) the chaperone is highly flexible [19], and 2) the conformational changes are non-deterministic leading to a mix of states under different nucleotide conditions [2]. With hTRAP1, however, the unique kinetic barrier allowed for a synchronous transition of the population to the closed state (heating +AMPPNP). Then, once closed, the chaperone was kinetically trapped in that state (chapter 2, figure 1). These data and led me to pursue crystal trials mirroring the initial EM experiments, whereby reactions containing TRAP1 and AMPPNP were heated for ~1hr to ensure ~100% closed state followed by 96-well screens at RT and grown at either RT or 4°C.

From this, I chose two of the most promising hits (many more hits than screened) and scaled up to 15-well grid screens. The best was an optimized hit originally found in the PEGs screen (well-E2) (Figure S10A, Table S4) was selected for further optimization. Joining forces with James we obtained highly geometric full-length hTRAP1 crystals, where heating was still required for crystallization (Figure S10B). Though we were able to attain good diffraction, these crystals were only found ~1/100 and displayed a diffraction pattern indicative of non-optimal lattice packing. One characteristic feature of the diffraction was decent diffraction at one angle, but then upon rotating the crystal 90° from this position, the spots would overlap producing a

checkerboard like pattern (Figure S10C). We obtained one dataset with an estimated resolution of 3.5Å that was initially judged to be 98% complete, though upon further investigation was likely only ~84% complete. Regardless, these crystals were so rare with lattice issues, that we sought the alternative strategy of species screening.

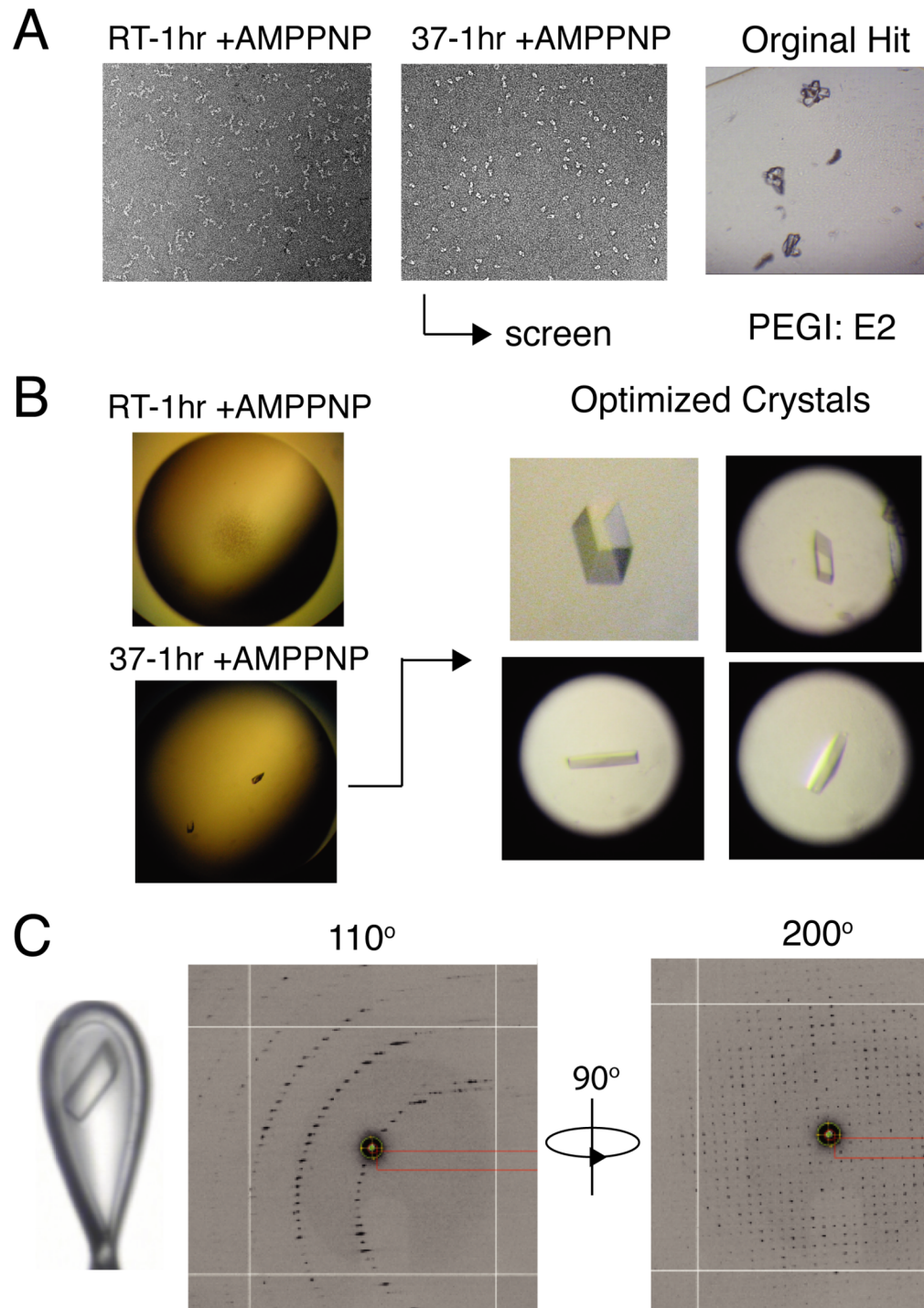


**Figure S10. Crystal trials with hTRAP1.** A) Negative stain EM images (right) for hTRAP1 showing that a temperature jump in the presence of AMPPNP could shift the chaperone to a homogeneous population of closed state molecules. These conditions were used to generate crystal hits (right). B) Images of crystal drops for the condition isolated in A demonstrating the need for the temperature jump to obtain crystals (right). Example of optimized crystals (left). C) Example of an optimized/cryoprotected hTRAP1 crystal that produced diffraction seen in the right two panels. Apparent are multiple overlapping spots and overlapping spots when the crystal is rotated 90°.

Here we chose four TRAP1 homologs with varying identity to hTRAP1, and then cloned, purified and screened to varying success. All initial screens were set up by first heating the homolog with AMPPNP for ~1hr before setting 96-well screens. From this two of the three gave promising crystals. The slime mold, *Dictyostelium discoideum* produced crystals that appeared as stacked triangular prisms. Upon grid screening it was apparent that varying the condition would merge the prisms into crystals that appeared to be single, but were likely not (Figure S11B, far right). Notably, this may be the case for the hTRAP1 crystals described, as upon optimization the crystals went from “stacked” to “single” crystals. For the TRAP1 homolog from *Danio rerio* (zebrafish, zTRAP1), and promising initial hit was found in the Index HT screen (well- H3) and reproduced by scaling up to 15-well screens.

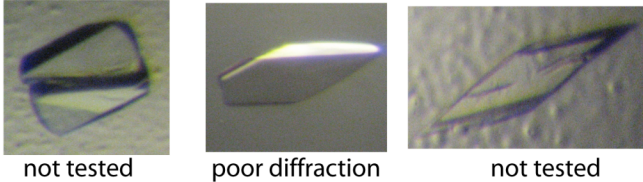
Taking the best crystal for both homologs to the ALS (8.3.1) we saw poor diffraction for *Dictyostelium discoideum*, but very promising diffraction for *D. rerio*. Further optimization was sought for the *D. rerio* crystals, where James isolated hexamine cobalt (III) chloride from an additive screen that produced high-quality diffracting crystals (Figure S11C). After the additive was isolated, heating was no longer necessary to obtain crystals, and were better without heating in fact.

A

Species	%Identity	%Similar	Notes
<i>H. sapien</i> (human)	100	100	-
<i>M. musculus</i> (mouse)	88	92	cloned, purified, screened
<i>D. rerio</i> (zebrafish)	74	84	cloned, purified, screened
<i>D. melanogaster</i> (fruit fly)	47	66	gene clone obtained
<i>D. discoideum</i> (slime mold)	40	59	cloned, purified, screened

B

*D. discoideum* (slime mold)



C

*D. rerio* (zebrafish)

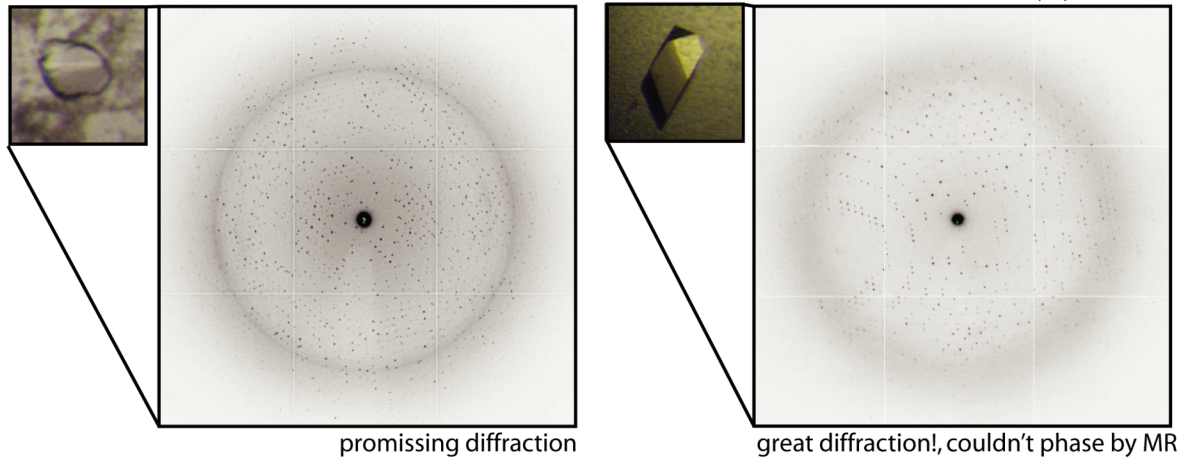


**Figure S11. Species screening produces better crystals.** A) Table of chosen TRAP1 homologs with their corresponding percent identity/similarity to hTRAP1, and their progress in the trials. B) Example crystals for *Dictyostelium discoideum* with results from the 8.3.1 (ALS) summarized below. C) Original hit and diffraction for *D. rerio* crystals showing promising diffraction (left). With the isolated additive we saw great diffraction out to 2.3Å.

Though we obtained 2.3Å diffraction we were unable to solve the dataset by molecular replacement (for reasons outlined in the main text). We then sought derivative crystals in an effort to solve the structure by experimental phasing using selenomethionine (Se-Met) and SAD. While the Se-Met protein expressed and purified quite well, the AMPPNP crystals did not diffract well and the drop had a film that was

hard to get rid of (potentially creating diffraction issues) (Figure S12A). From other biochemical experiments I was doing at the time, I had started using alternative ATP analogs (ADP-BeF and ADP-AIF) and decided to try these analogs in place of AMPPNP to see if the crystals and drop conditions would improve. Under these conditions we were able to get high-quality Se-Met crystals that diffracted to  $\sim 3\text{\AA}$ , as well as matching native crystals (Figure S12B). With the data in hand, James solved the structures of all three analog states (using the Se-Met data from the ADP-AIF crystals). From here we moved forward to try to understand the mechanistic consequences of asymmetry observed in our full-length crystal structure of zTRAP1 in the active closed state.



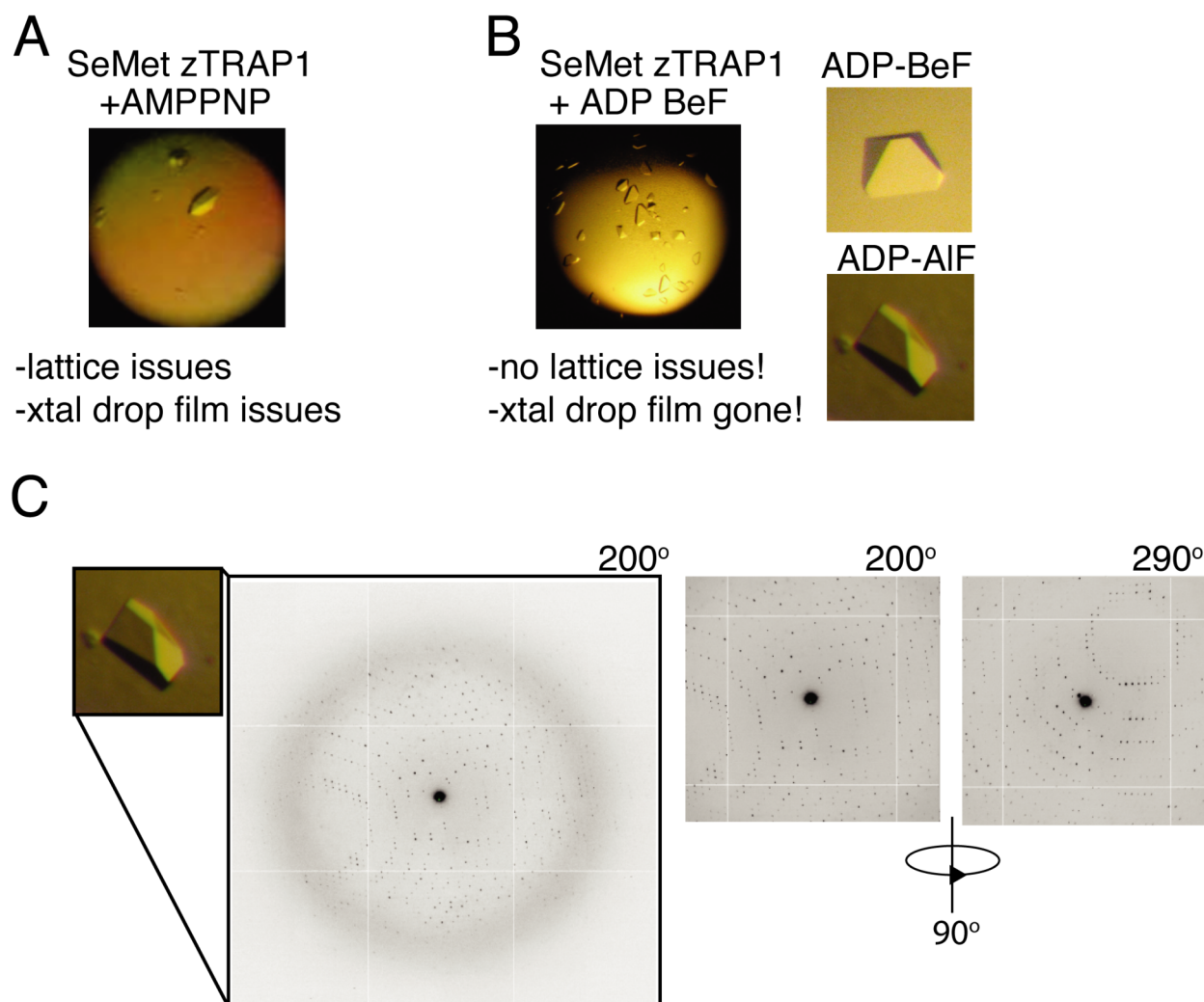


**Figure S12. Se-Met Crystals require alternative ATP analogs to produce experimental maps.** A) Example of the crystals produced by Se-Met zTRAP1 when incubated with AMPPNP. These crystals did not diffract well and had further issues with a film that formed in the drop (discussed above). B) Crystals of Se-Met zTRAP1 grown under ADP-BeF/AIF conditions. Here we see great improvement in morphology and C) diffraction quality. Zooming into look at the spots (right), no diffraction issues upon rotation of the crystal were observed in contrast to the original hTRAP1 crystals (Figure S10C).

From these trials there were several hits that we were not able to pursue. These are listed in Table S4. Additionally, we learned that while ADP-BeF, ADP-AIF and AMPPNP appear to stabilize the same closed state (as judged by the crystal structures and SAXS data in the main text), the kinetics of the transition are ~10X faster (figure S5, chapter 2) in the case of ADP-BeF (ADP-AIF is not as well behaved in solution). This

was the motivation for re-screening hTRAP1 with ADP-BeF, outlined in Table S4. These crystals as well as the ones obtained for the Dictyostelium *discoideum* homolog are potentially worth pursuing.

**Table S4. Table of promising crystal results.**

Construct	Residues	Screen Setup	Original Condition	Optimized condition	Notes	date
<b>hTRAP1 NTD:MD</b>	60-296	24mg/mL +2mM AMPPNP 42°C-1hr	Index B7	TBD	-Preliminary but promising hit. -See NB#9	06/22/2011
<b>sTRAP1</b>	63-711	5mg/mL +2mM AMPPNP 40°C-45min	PEGs H2	TBD	-Grid screened. -See NB #9	08/19/2011
<b>hTRAP1</b>	60-704	5 or 10mg/mL +2mM AMPPNP 40°C-45min	FEGs H2	TBD	-no pursued -resembles original zTRAP1 hit	08/08/15
<b>hTRAP1</b>	60-704	20mg/mL +2mM AMPPNP 37°C- 1hr	PEGls E2	.3M KF 15% PEG .1M MES pH 6.6 (42°C-1hr)	-Optimized, diffraction issues, moved on -required heating and grid screen around condition each prep to get good xtals	08/25/2010
<b>hTRAP1</b>	60-704	20mg/mL +2mM AMPPNP 37°C- 1hr	JCSG+ A3	TBD	-Good original hit -Grid screened -above looked more promising so stopped pursuing	08/25/2010
<b>hTRAP1</b>	60-704	10mg/mL +2mM AMPPNP 37°C- 1hr	Classics II H2	TBD	Good original hit	08/25/2010
<b>hTRAP1</b>	60-704	20mg/mL +2mM AMPPNP 37°C- 1hr	Classics II H4	TBD	Good original hit	08/25/2010
<b>hTRAP1</b>	60-704	10mg/mL +2mM AMPPNP 37°C- 1hr	Classics II H5	TBD	Good original hit	08/25/2010
<b>hTRAP1</b>	60-704	20mg/mL +2mM AMPPNP 37°C- 1hr Growth at 4°C	Procompl ex C1	TBD	Good original hit	08/25/2010
<b>hTRAP1</b>	60-704	7mg/mL +2mM ADP +1X BeF Mix RT-2hr	Classics II H5	-.1M Succinic Acid pH6, 15% PEG3350, +Trimethyl- amine HCl	-*ADP-BeF screen Hit -Additive screen gave Trimethyl aimine. -Didn't have time to follow up (NB #11, pg 105)	08/08/2012

**Note:** All homolgs listed here were set up after purification in a final buffer of 20mM Hepes pH 7.5, 50mM KCl, 2mM MgCl<sub>2</sub>, 1mM DTT. Multiple concentrations were screened, "mg/mL" listed is the one that produced

the hits listed. Unless otherwise noted, all xtals were grown at RT after heating step (except ADP-BeF). For explanation of "1X BeF", see methods for chapter 1. For more information, see my lab notebooks (dates are listed as **yy/dd/mm** in my lab notebook).

**\*For a list of all original hits in the ADP-BeF screen see NB#11, pg91.**

**Naming Key:** hTRAP1(human), sTRAP1 (slime mold TRAP1). NB (notebook)

## Experimental Procedures

### Protein Production and Purification

We obtained the full-length TNF receptor-associated protein 1 (TRAP1) gene of *Homo sapiens* and *Danio rerio* from the mammalian and zebrafish gene collections (Invitrogen and Thermo Scientific, respectively). The mature sequences (residues 60-704 and 73-719 *H. sapiens* and *D. rerio*, respectively) of TRAP1 were cloned into the pET151/D-TOPO bacterial expression plasmid (Invitrogen), resulting in N-terminally His-tagged TRAP1 fusion proteins. Between the 6x-His-tag and TRAP1 is a TEV protease cleavage site. The resulting plasmid was transformed into *E. coli* BL21 (DE3)-RIL for protein expression.

For expression of TRAP1 from *D. rerio* (zTRAP1, WT and mutant forms), cells were grown at 30°C in Luria-Bertani broth supplemented with 0.4% glucose to OD600 = 0.8 and induced with 0.4 mM IPTG at 16°C for 18 hours. Cells were harvested by centrifugation, resuspended in 50 mM potassium phosphate pH 8.0, 500 mM NaCl, 20 mM imidazole, and 3 mM  $\beta$ -mercaptoethanol. Cells were lysed using an EmulsiFlex-C3 (Avestin). The crude lysate was immediately supplemented with 0.2 mM phenylmethylsulfonyl fluoride (PMSF) and centrifuged at 20,000 g for 20 minutes. The soluble fraction was subsequently incubated with 2 mL Ni-NTA (GE Healthcare) per 1,000 ODs for 1 hour at 4°C. Following incubation with the Ni-NTA resin, lysate was

removed by pelleting resin at 2,500 g for 3 minutes and washed 3 times with 9 bed volumes of 50 mM potassium phosphate pH 8.0, 500 mM NaCl, 20 mM imidazole, and 3 mM  $\beta$ -mercaptoethanol (BME). Following the batch wash Ni-NTA resin was loaded onto a gravity column and His-tagged protein was eluted with 6 bed volumes of 50 mM potassium phosphate pH 8.0, 300 mM NaCl, 500 mM imidazole, and 3 mM  $\beta$ -mercaptoethanol. Eluted protein was dialyzed overnight against 10 mM Tris/HCl pH 8.0, 200 mM NaCl, and 1 mM DTT and the 6x-His-tag was cleaved using a 20:1 molar ratio of protein:TEV protease. The protein was purified by anion exchange chromatography on a HiTrapQ or MonoQ 10/100 GL column (GE Healthcare) via a linear NaCl gradient and twice by size exclusion chromatography using a Superdex S200 26/60 column (GE Healthcare) run in 10 mM Tris/HCl pH 8.0, 100 mM NaCl, 1 mM DTT. Selenomethionine derivatized WT zTRAP1 was prepared by growing BL21 (DE3)-RIL cells in M9 Medium (Sigma) supplemented with 1 mM  $\text{MgSO}_4$ , 6.6  $\mu\text{M}$   $\text{CaCl}_2$ , 1 ml  $\text{FeSO}_4$  (4.2 mg/ml), 0.4% glucose, and 100  $\mu\text{l}$  0.5% (w/v) thiamine at 37°C (modified from [75]). At  $\text{OD}_{600} = 0.5$  solid amino acid supplements were added (100 mg/ml L-lysine, L-phenylalanine, and L-threonine; 50 mg/ml L-isoleucine, L-leucine, L-valine, and L-selenomethionine). After 30 minutes, cultures were transferred to 22°C for 20 minutes and then induced with 0.2 mM IPTG for 18 hours. The selenomethionine-derivatized protein was purified as described for the native version with a final buffer of 20 mM Hepes pH 7.5, 50 mM KCl, 2 mM  $\text{MgCl}_2$ , and 5 mM DTT. Incorporation of selenomethionine was confirmed by mass spectrometry (data not shown). Both the native and selenomethionine derivative proteins were concentrated to ~25 mg/mL for crystallization and flash frozen for storage.

TRAP1 from *H. sapiens* (hTRAP1, WT and mutant forms) was purified in a similar fashion to zTRAP1 proteins with a final buffer of 20 mM Hepes pH 7.5, 50 mM KCl, 2 mM MgCl<sub>2</sub>, and 1 mM DTT.

Mutant forms for all homologs were made from the vector constructs described above using standard PCR methods.

### **Crystallography**

WT zTRAP1 was screened for crystallization conditions at a concentration of 10 mg/mL and incubated in a crystallization buffer (20 mM Hepes 7.5, 50 mM KCl, and 2 mM MgCl<sub>2</sub>, 2 mM AMPPNP or 2 mM ADP + 1X BeF<sub>2</sub> / AlF<sub>3</sub>) for 30 minutes prior to crystallization. BeF<sub>2</sub> and AlF<sub>3</sub> were made by mixing 200 mM BeCl<sub>2</sub> / AlCl<sub>3</sub> and 1 M KF to make a 5X BeF<sub>2</sub> / AlF<sub>3</sub> solution of 10 mM BeCl<sub>2</sub> / AlCl<sub>3</sub> and 50 mM KF.

For screening we used a mosquito liquid handling robot (TTP Lab Tech) and three commercially available deep well screening blocks: JCSG+ and Protein Complex Suite (Qiagen) as well as the Index HT screen (Hampton Research). The initial crystallization hit was refined to 18% (v/v) PEG3350 and 0.2 M sodium malonate pH 6.6 by the hanging drop vapor diffusion method at 23°C. The additive screen HT (Hampton Research) was used to isolate hexamine cobalt (III) chloride as an additive that greatly improved crystal size and overall morphology. The final crystallization condition used was 18% (v/v) PEG3350, 0.2 M sodium malonate pH 6.6 - 7, 20 – 42 mM hexamine cobalt mixed 1:1 with TRAP1 protein at 7-10 mg/mL. Our optimized crystals grew in 7-10 days at 23 °C using the hanging drop vapor diffusion method forming 100 μm x 100

$\mu\text{m}$  x  $200 \mu\text{m}$  crystals. The selenomethionine derivative protein crystallized in a similar condition. Both native and derivative crystals were cryoprotected by adding glycerol (10-12% (v/v) final concentration) to the reservoir solution before flash-freezing in liquid nitrogen. Crystal screening and data collection were carried out at beamlines 8.3.1, 8.2.1, and 8.2.2 at the Advanced Light Source (ALS) and the final X-ray data was collected at beamline 8.3.1. The native and selenomethionine derivatized protein of TRAP1 were crystallized in the  $C2_1$  spacegroup with one TRAP1 dimer per asymmetric unit (PDB codes: 4JOB, 4IYN, and 4IPE).

For the N-terminal:Middle domain (NTD:MD) crystal structure, full-length protein was purified and screened in a similar fashion (buffer condition at the time of screening was 20mM Hepes pH7.5, 50mM KCl, 2mM  $\text{MgCl}_2$ , 1mM DTT), using full-length zTRAP1 with a double point mutation at Glu556Ala.Ile569Lys. These mutations effectively destabilize the Middle-CTD (MD:CTD) interface present in monomer B of the full length crystal structure. The initial crystallization hit was refined to a final condition of 5mg/mL protein in a 1:1 ratio with 0.1M Sodium Phosphate monobasic pH 6.5, and 12% PEG 8000. Our optimized crystals grew in 10-14 days at 23 °C using the hanging drop vapor diffusion method forming  $100 \mu\text{m}$  x  $100 \mu\text{m}$  x  $200 \mu\text{m}$  crystals. Crystals were harvested and cryoprotected with 12% (v/v) glycerol prior to flash-freezing in liquid nitrogen. Data collection was carried out at the ALS at beamline 8.3.1. This data set could easily be scaled and merged in the I222 spacegroup containing a single TRAP1 protomer, already indicative of a high degree of symmetry between protomers. We chose to build and refine the structure in the  $C2_1$  spacegroup, and similar to the full-length structure the

spacegroup  $C2_1$  contains two protomers to complete one dimerized biological unit. This symmetry persisted in  $C2_1$  and we chose to build our final model in the I222 spacegroup, as we saw no significant differences between protomers in the ASU (PDB code: 4IVG).

## Structure Determination

Data reduction was carried out using HKL2000 [76]. Structures of zTRAP1 bound to ADP-AIF<sub>4</sub> and ADP-BeF<sub>3</sub> were solved using the single-wavelength anomalous dispersion (SAD) method with selenomethionine derivatives. The positions of 36 selenium sites (out of 38 possible per zTRAP1-dimer) were found using AutoSol from the PHENIX program suite and used for subsequent phasing [77]. The selenium positions and experimental map allowed us to clearly define domains of zTRAP1 that allowed us to build a full-length model. The final models for zTRAP1 bound to ADP-AIF<sub>4</sub> or ADP-BeF<sub>3</sub> were built with native data and refined to an extended resolution of 2.3 Å. The structure of zTRAP1 bound to AMPPNP was solved using molecular replacement and the zTRAP1 model bound to ADP-AIF<sub>4</sub>. The final NTD:MD zTRAP1 structure bound to AMPPNP was solved with molecular replacement and a monomer of the full-length zTRAP1 model truncated at the MC interface. All models of TRAP1 were built using COOT [78] and further refinement was carried out using the latest builds of PHENIX suite [77].

A majority of the secondary structural elements have been built with the exception of helix 5 (residues 132-136) of protomers B and helix 21 (residues 568-579)



in the C-terminal domain of both protomers in the full-length structure. Some loops have been omitted due to poor electron density and very high B-factors. Figures were made using PyMOL [79] and [UCSF Chimera Package](#) [73]. Chimera is developed by the Resource for Biocomputing, Visualization, and Informatics at the University of California, San Francisco (supported by NIGMS 9P41GM103311).

### **Structural Comparisons**

In Figure 3 the four major domains of TRAP1-AMPPNP were individually aligned using monomer A and monomer B and the “*match*” command in Chimera to obtain RMSD values for every residue. These RMSD values were then imported into the B-factor column of monomer B from the TRAP1-AMPPNP structure. The “cartoon putty” feature of PyMOL was used to represent increasing RMSD values as thicker tubes with a transition in color from blue to yellow.

### **Steady-state Hydrolysis Measurements**

Protein concentration was calculated using the Edelhauc method [80]. Steady-state hydrolysis rates were measured using the previously described ATP regenerating assay [48] on an Agilent 8453 diode array. Assay components were mixed to a final concentration of 200  $\mu$ M NADH, 400  $\mu$ M PEP, 50 U/mL PK, 50 U/mL LDH, and ATP at least 10-fold over the measured  $K_m$  (Table S3). Background change in NADH absorbance (340 nm) was monitored to ensure a flat baseline before addition of 5  $\mu$ M chaperone (monomer concentration). The change in NADH absorbance after protein

addition was monitored and slope obtained by subtracting baseline at 750 nm followed by least squares fitting to a simple linear regression model.  $K_{obs}$  values were calculated using the equation below:

$$k_{obs} = \text{slope} / (E_{nadh} * c)$$

where  $k_{obs}$  is the observed rate of hydrolysis ( $s^{-1}$ ),  $E_{nadh}$  is the extinction coefficient of NADH ( $6220 M^{-1}s^{-1}$ ), and  $c$  is the monomer protein concentration (M). For bar plots the rates were normalized by the WT rate and standard deviations were error propagated according to the equation below:

$$\text{Stdev}_{propagated} = \%WT * \sqrt{((WT_{stdev}/WT_{mean})^2 + (Mutant_{stdev}/Mutant_{mean})^2)}$$

For MD:CTD interface mutant mixing experiment (Figure S8), we used a previously reported radioactive assay [67], with 2uM protein (monomer), 650uM ATP at 37°C in a buffer containing of 20 mM Hepes pH 7.5, 50 mM KCl, 2 mM MgCl<sub>2</sub>, and 1 mM DTT. Prior to initiating the reaction with ATP, heterodimers were formed under apo conditions at 30°C for 30 minutes.

All homologs were inhibited with the Hsp90 specific inhibitors (Radicicol, data not shown) and results were plotted using the program R [81].

## Negative Stain Electron Microscopy

WT zTRAP1, zTRAP1 Glu566Ala.Ile569Lys and zTRAP1 Asn519Ala.His521Ala.Leu522Lys were initially diluted to .1 mg/mL in a buffer containing 20 mM Hepes 7.5, 50 mM KCl, and 2 mM MgCl<sub>2</sub>, + 2 mM ADP-BeF<sub>3</sub> (BeF prepared as above). Reactions were incubated at RT for 30 minutes, followed by dilution to 0.01 mg/mL in the buffer above including ADP-BeF<sub>3</sub>. 5  $\mu$ L of the resulting reactions were then incubated for ~1 minute on 400 mesh Cu grids (Pelco). Grids were previously coated with Collodion (EMS) and then coated with a thin carbon layer (~100 Å). Following sample incubation was a 3X wash with miliQ water, and lastly stained 3X with uranyl formate, pH 6. The last stain was removed by vacuum until the surface of the grid was dry. Prepared grids were imaged with a TECNAI 20 (FEI) operated at 120 kV. Images were recorded using a 4k x 4k CCD camera (Gatan) at 62,000 magnification, at -1.5  $\mu$ m defocus. Representative closed state particles (Figure S3C) were selected in EMAN [82].

## Circular Dichroism Spectroscopy

zTRAP1 Glu566Ala.Ile569Lys and zTRAP1 Asn519Ala.His521Ala.Leu522Lys were buffer exchanged with size exclusion chromatography into a 5 mM Hepes/NaOH pH 7.4 and 150 mM NaCl buffer immediately prior to the experiment. An Aviv Model 202 CD spectrometer was used for all experiments. CD signal at 220 nm of 0.5 mg/mL protein in a 1 mm path length cell was recorded at every degree during a 25-80°C temperature ramp with two minutes of equilibration time at each step. Raw CD data was

converted to units of mean residue ellipticity  $[\theta]$  (degrees  $\text{cm}^2 \text{dmol}^{-1} \text{residue}^{-1}$ ).

### **SAXS Reaction, Data Collection and Analysis**

WT TRAP1 homologs and mutant proteins were buffer exchanged into 20 mM Hepes pH 7.5, 50 mM KCl, 2 mM  $\text{MgCl}_2$ , 1mM DTT immediately prior to the experiment. 75  $\mu\text{M}$  protein (monomer) was used as the final concentration for all reactions. In the reactions where ADP- $\text{BeF}_3$  was used as the nucleotide analog, 1X  $\text{BeF}$  was made as described in the crystallography methods section above and added to both reactions to allow for direct comparison. 2 mM nucleotides were used to initiate closure and the reactions were incubated at 30°C for 10 hours. Reactions were spun down at max speed in a tabletop centrifuge for 10 minutes immediately prior to data collection to remove any trace aggregation.

For time course experiments, zTRAP1 proteins were mixed as above without addition of nucleotide until the day of SAXS data collection. Once ADP- $\text{BeF}_3$  was added to the reaction 20  $\mu\text{L}$  time points were taken spun down at max speed in a tabletop centrifuge for ten minutes, and then data was collected. Time points were recorded at the time of exposure.

Data was collected at the ALS at beamline 12.3.1 [83] with exposure times of 0.5, 1, and 5 seconds. An additional 2 second exposure was used for the aforementioned time course. Each sample collected was subsequently buffer subtracted and time points were averaged using scripts at beamline 12.3.1 (ogreNew) and in-house software. The scattering data was transformed to  $P(r)$  vs.  $r$  using the program GNOM [72] and  $D_{\text{max}}$

was optimized. To assess the nature of the closed state the resulting distributions were fit using in house least squares fitting program in the region where non-zero data was present for the target data and each model tested. For the fitting we chose to test a combination of a theoretical scattering curve for each closed state in question and the respective apo data for each reaction. Theoretical scattering curves were generated for each model PDB in the program CRYSQL [71]. The resulting normalized target data and model fit are output from our fitting program with an R-factor that is similar to a crystallography R-factor in nature. R is defined as the equation below:

$$R_{\text{merge}} = \frac{\sum |I_{\text{Pobs}}(r) - I_{\text{Pcalc}}(r)|}{\sum I_{\text{Pobs}}(r)}$$

where  $P_{\text{obs}}(r)$  is the observed probability distribution and  $P_{\text{calc}}(r)$  is the calculated modeled fit. Residuals were calculated using the equation below:

$$\text{Residuals} = P_{\text{calc}}(r) - P_{\text{obs}}(r)$$

### **DEER Spectroscopy**

Native cysteine residues were replaced in the mature form of human TRAP1 (vector description above) based on conservation with TRAP1 homologs (Cys261Ser, Cys527Ala, Cys573Arg). Two residue positions (within one protomer) were chosen computationally based on solvent accessibility, as well as for optimal resolution between the theoretical distances of asymmetric protomer conformations. Chosen positions

(Lys439 and Asp684) were replaced with cysteine residues using standard PCR methods to allow for site specific labeling with maleimide functionalized MSL (Sigma). Distance simulations were performed on our closed state model at cryogenic temperatures using rotameric modeling of MTSL labels (MSL not available) at the chosen residue positions using the latest version of multiscale modeling of macromolecular systems, MMM2013 [84].

Cysteine-free hTRAP1 and cysteine variant for double electron-electron resonance measurements (DEER) were purified as described above with a size exclusion buffer of 20mM Sodium Phosphate pH 7, 50 mM KCl, 2 mM MgCl<sub>2</sub> degassed by purging with N<sub>2</sub> gas to protect cysteine residues of the DEER probe construct. Following size exclusion chromatography, DEER probe protein was labeled ON at 4°C with a 2:1 excess of MSL:cysteine residue. Excess label was removed by extensive dialysis in size exclusion buffer and labeling was confirmed by CW EPR as in Naber et al (Figure S7 A) [85]. Removal of native cysteine residues or spin-labeling did not negatively impact ATPase activity (Figure S72B). Importantly, the closed state distribution shows conservation of state as compared to WT (Figure 2C, 2D).

Cysteine-free and DEER probe protein were then exchanged into a D<sub>2</sub>O version of the size exclusion buffer by concentration/dilution in Centricon concentrators (10,000 mwco, Millipore) until the concentration of H<sub>2</sub>O was <1%. Unlabeled and labeled proteins were mixed in a 10:1 ratio (final concentration of 30 μM labeled protein) and exchanged at 30°C for 30 minutes. Reactions were incubated with addition of 2 mM ADP-BeF at 30°C for 10 hours (as in SAXS) followed by addition of 30% deuterated

glycerol (Sigma). Four-pulse DEER data were collected using a Bruker ELEXSYS E580 spectrometer at 34 GHz equipped with a SuperQ-FT pulse Q-band system with a 10 W amplifier and a 5 mm EN5107D2 resonator located at the Ohio Advanced EPR laboratory. Samples of  $\sim 10 \mu\text{l}$  were loaded into a 1.1 mm inner diameter quartz capillary tubes and frozen in liquid nitrogen prior to insertion into the pre-cooled resonator set at 80 K. Data were collected with probe  $\pi/2$  and  $\pi$  pulse widths of 10 and 20 ns and a pump  $\pi$  pulse width of 24 ns with a repetition time of 700-800  $\mu\text{s}$  and 100 shots/point. The frequency of the pump pulse was adjusted to the maximum in the nitroxide field sweep spectrum and the observed pulse was applied 80 MHz upfield from the pump frequency. The DEER evolution time periods were from 3.6 – 4.3  $\mu\text{s}$ .  $T_1$  and  $T_2$  values were  $\sim 400 \mu\text{s}$  and  $\sim 4.7 \mu\text{s}$ , respectively. Data were processed and analyzed using DEERAnalysis2013 [46] and distance distributions  $P(r)$  were obtained from Tikhonov regularization [86], incorporating the constraint  $P(r) > 0$ . The regularization parameter was optimized to fit the time-domain data without overfitting. The distance distribution data was normalized with an integral of 0.01.

### **Anisotropy binding measurements**

75  $\mu\text{M}$  WT hTRAP1 or hTRAP1 E551A were pre-closed with 2mM AMPPNP at 40°C for 3.5 hours to ensure  $\sim 100\%$  closed state. Buffer conditions were 20mM Hepes pH 7.5, 50mM KCl, 2mM  $\text{MgCl}_2$ , and 1mM DTT. Following this steady-state anisotropy measurements with IAEDANS-labeled  $\Delta 131\Delta$  with WT or E551A were titrated (maintaining AMPPNP concentration) to obtain the affinity for the model substrate. Anisotropy measurements were done as in Street et. al., 2011 [58].

## Postscript

This work has provided the first model for direct coupling of ATP hydrolysis to client remodeling. As discussed above we propose that sequential hydrolysis from the asymmetric closed state leads to a novel conformational change in Hsp90 that re-arranges a known client interface, and that the potential to do work on a client is not equal for both hydrolysis events. Here we propose that it is the first event from the highly strained state that is functioning to actively re-model.

From this there are several questions that remain. First, what is the order of events (ie model in figure 7 or S7)? Utilizing the new DEER assay and a creative strategy for forming permanent heterodimers, Daniel Elnatan has new data that suggests that the “flip-flop” mechanism is actually correct. As discussed above, this model has the advantage of ensuring structural re-arrangements to clients bound on either of the initial protomer conformations (protomer A or B). Secondly, our model predicts that only one of the conformations in the protomers of our crystal structure is in the hydrolysis competent state. Given the difference in B-factors of the loop that contains the  $\gamma$ -phosphate contact (Arg417) from the MD, I first hypothesize that protomer A displays the hydrolysis competent state as Arg417 is more stably contacting the  $\gamma$ -phosphate. Experiments to directly test this hypothesis require single-turnover conditions and a strategy for biasing the MD:CTD conformation of the protomer arms. For the latter, the MD:CTD mutations outlined above should be very useful, and as a first step will DEER measurements with either homodimers or heterodimers of these mutants will provide direct detection of the bias.



Finally, the idea of coupling hydrolysis dependant changes in the MD:CTD conformation to client structure is well founded and exciting but experiments to test this are of highest priority. To do this one must be able to correlate the changes to the MD:CTD interface to changes in client fold/activity. Daniels permanent heterodimer strategy and the knowledge of key residues for client binding (W467, bHsp90/HtpG) should allow one to simulations bias/dictate which arm is bound to a client while manipulating the MD:CTD conformation (MD:CTD mutants) and/or hydrolysis capability. If an activity can be measured for the client (ala GR ligand binding- see work by Elaine Kirschke) or a measure of fold is possible ( $^{13}\text{C}$ -Alanine NMR- see chapter 3) then it should be possible to do so. Then the challenge is to choose an appropriate client for these studies.

When considering clients for the TRAP1 there are several avenues of pursuit. In the case of the most well studied of the clients (CypD), the protein is very stable and thus calls into question weather the chaperone is simply “holding” CypD to regulated the necrotic response, or if there is a structural change to this client. This could be tested by a few key “make or break” experiments. First, hydrogen exchange on the client monitored either by NMR or mass spectrometry would show if there was any change to the fold of CypD. If so it may be possible to work to stabilize the near-native state for CypD through varying conditions or targeted mutations. For the latter a high-resolution picture of the intermediate is necessary.

Though CypD and a few other clients for TRAP1 have been identified, these systems lack some of the advantages that a model substrate ( $\Delta 131\Delta$ ) provides (see

chapter 4). I have shown that the  $\Delta 131\Delta$  model substrate system extends to TRAP1 (above and chapter 2) and future investigation of  $\Delta 131\Delta$  with TRAP1 promises to further elucidate chaperone mechanism in this system. Because the measured affinity for  $\Delta 131\Delta$  is weaker (figure S9 and chapter 4) in the case of TRAP1, I think it could be quite useful to make key mutations to the known binding residues to increase this affinity. Most key would be a mutation of the leucine in TRAP1 that is analogous to W467 in bHsp90 (HtpG).

Finally, a strategy for finding new clients for TRAP1 (outlined in chapter 3) provides an avenue to discover novel mitochondrial pathways that specifically depend on the chaperone for faithful signaling, as well as new tools for the study of TRAP1 mechanism *in vitro*.

## References:

1. Panaretou, B., et al., *ATP binding and hydrolysis are essential to the function of the Hsp90 molecular chaperone in vivo*. The EMBO journal, 1998. **17**(16): p. 4829-36.
2. Southworth, D.R. and D.A. Agard, *Species-dependent ensembles of conserved conformational states define the Hsp90 chaperone ATPase cycle*. Mol Cell, 2008. **32**(5): p. 631-40.
3. Hartl, F.U., A. Bracher, and M. Hayer-Hartl, *Molecular chaperones in protein folding and proteostasis*. Nature, 2011. **475**(7356): p. 324-32.
4. Zhao, R., et al., *Navigating the chaperone network: an integrative map of physical and genetic interactions mediated by the hsp90 chaperone*. Cell, 2005. **120**(5): p. 715-27.
5. Jakob, U., et al., *Transient interaction of Hsp90 with early unfolding intermediates of citrate synthase. Implications for heat shock in vivo*. J Biol Chem, 1995. **270**(13): p. 7288-94.
6. Taipale, M., et al., *Quantitative analysis of HSP90-client interactions reveals principles of substrate recognition*. Cell, 2012. **150**(5): p. 987-1001.
7. Echeverria, P.C., et al., *An interaction network predicted from public data as a discovery tool: application to the Hsp90 molecular chaperone machine*. PLoS One, 2011. **6**(10): p. e26044.
8. Rutherford, S.L. and S. Lindquist, *Hsp90 as a capacitor for morphological evolution*. Nature, 1998. **396**(6709): p. 336-42.
9. Lindquist, S., *Protein folding sculpting evolutionary change*. Cold Spring Harbor symposia on quantitative biology, 2009. **74**: p. 103-8.
10. Whitesell, L. and S.L. Lindquist, *HSP90 and the chaperoning of cancer*. Nat Rev Cancer, 2005. **5**(10): p. 761-72.

11. Shah, V., et al., *Hsp90 regulation of endothelial nitric oxide synthase contributes to vascular control in portal hypertension*. Am J Physiol, 1999. **277**(2 Pt 1): p. G463-8.
12. Luo, W., et al., *Heat shock protein 90 in neurodegenerative diseases*. Mol Neurodegener, 2010. **5**: p. 24.
13. Krukenberg, K.A., et al., *pH-dependent conformational changes in bacterial Hsp90 reveal a Grp94-like conformation at pH 6 that is highly active in suppression of citrate synthase aggregation*. J Mol Biol, 2009. **390**(2): p. 278-91.
14. Krukenberg, K.A., et al., *Multiple conformations of E. coli Hsp90 in solution: insights into the conformational dynamics of Hsp90*. Structure, 2008. **16**(5): p. 755-65.
15. Ali, M.M., et al., *Crystal structure of an Hsp90-nucleotide-p23/Sba1 closed chaperone complex*. Nature, 2006. **440**(7087): p. 1013-7.
16. Prodromou, C., et al., *The ATPase cycle of Hsp90 drives a molecular 'clamp' via transient dimerization of the N-terminal domains*. EMBO J, 2000. **19**(16): p. 4383-92.
17. Richter, K., et al., *Coordinated ATP hydrolysis by the Hsp90 dimer*. J Biol Chem, 2001. **276**(36): p. 33689-96.
18. Shiau, A.K., et al., *Structural Analysis of E. coli hsp90 reveals dramatic nucleotide-dependent conformational rearrangements*. Cell, 2006. **127**(2): p. 329-40.
19. Krukenberg, K.A., et al., *Conformational dynamics of the molecular chaperone Hsp90*. Quarterly reviews of biophysics, 2011. **44**(2): p. 229-55.
20. Johnson, J.L., *Evolution and function of diverse Hsp90 homologs and cochaperone proteins*. Biochim Biophys Acta, 2012. **1823**(3): p. 607-13.
21. Liu, B., et al., *Folding of Toll-like receptors by the HSP90 paralogue gp96 requires a substrate-specific cochaperone*. Nat Commun, 2010. **1**: p. 79.

22. Song, H.Y., et al., *Identification of a protein with homology to hsp90 that binds the type 1 tumor necrosis factor receptor*. J Biol Chem, 1995. **270**(8): p. 3574-81.
23. Felts, S.J., et al., *The hsp90-related protein TRAP1 is a mitochondrial protein with distinct functional properties*. J Biol Chem, 2000. **275**(5): p. 3305-12.
24. Cechetto, J.D. and R.S. Gupta, *Immunoelectron microscopy provides evidence that tumor necrosis factor receptor-associated protein 1 (TRAP-1) is a mitochondrial protein which also localizes at specific extramitochondrial sites*. Exp Cell Res, 2000. **260**(1): p. 30-9.
25. Altieri, D.C., et al., *TRAP-1, the mitochondrial Hsp90*. Biochim Biophys Acta, 2012. **1823**(3): p. 767-73.
26. Takamura, H., et al., *TRAP1 controls mitochondrial fusion/fission balance through Drp1 and Mff expression*. PLoS One, 2012. **7**(12): p. e51912.
27. Zhang, L., et al., *TRAP1 rescues PINK1 loss-of-function phenotypes*. Hum Mol Genet, 2013.
28. Costa, A.C., S.H. Loh, and L.M. Martins, *Drosophila Trap1 protects against mitochondrial dysfunction in a PINK1/parkin model of Parkinson's disease*. Cell Death Dis, 2013. **4**: p. e467.
29. Kang, B.H., et al., *Regulation of tumor cell mitochondrial homeostasis by an organelle-specific Hsp90 chaperone network*. Cell, 2007. **131**(2): p. 257-70.
30. Yoshida, S., et al., *Molecular chaperone TRAP1 regulates a metabolic switch between mitochondrial respiration and aerobic glycolysis*. Proceedings of the National Academy of Sciences of the United States of America, 2013. **110**(17): p. E1604-12.
31. Sciacovelli, M., et al., *The Mitochondrial Chaperone TRAP1 Promotes Neoplastic Growth by Inhibiting Succinate Dehydrogenase*. Cell metabolism, 2013. **17**(6): p. 988-99.
32. Butler, E.K., et al., *The Mitochondrial Chaperone Protein TRAP1 Mitigates alpha-Synuclein Toxicity*. PLoS genetics, 2012. **8**(2): p. e1002488.

33. Chen, B., D. Zhong, and A. Monteiro, *Comparative genomics and evolution of the HSP90 family of genes across all kingdoms of organisms*. BMC Genomics, 2006. **7**: p. 156.
34. Richter, K., J. Reinstein, and J. Buchner, *N-terminal residues regulate the catalytic efficiency of the Hsp90 ATPase cycle*. J Biol Chem, 2002. **277**(47): p. 44905-10.
35. Richter, K., et al., *Intrinsic inhibition of the Hsp90 ATPase activity*. J Biol Chem, 2006. **281**(16): p. 11301-11.
36. Prodromou, C., et al., *Identification and structural characterization of the ATP/ADP-binding site in the Hsp90 molecular chaperone*. Cell, 1997. **90**(1): p. 65-75.
37. Li, J., et al., *Structure insights into mechanisms of ATP hydrolysis and the activation of human heat-shock protein 90*. Acta biochimica et biophysica Sinica, 2012. **44**(4): p. 300-6.
38. Dollins, D.E., R.M. Immormino, and D.T. Gewirth, *Structure of unliganded GRP94, the endoplasmic reticulum Hsp90. Basis for nucleotide-induced conformational change*. The Journal of biological chemistry, 2005. **280**(34): p. 30438-47.
39. Dollins, D.E., et al., *Structures of GRP94-nucleotide complexes reveal mechanistic differences between the hsp90 chaperones*. Mol Cell, 2007. **28**(1): p. 41-56.
40. Morra, G., et al., *Corresponding functional dynamics across the Hsp90 Chaperone family: insights from a multiscale analysis of MD simulations*. PLoS Comput Biol, 2012. **8**(3): p. e1002433.
41. Morra, G., G. Verkhivker, and G. Colombo, *Modeling signal propagation mechanisms and ligand-based conformational dynamics of the Hsp90 molecular chaperone full-length dimer*. PLoS Comput Biol, 2009. **5**(3): p. e1000323.

42. Meyer, P., et al., *Structural and functional analysis of the middle segment of hsp90: implications for ATP hydrolysis and client protein and cochaperone interactions*. Mol Cell, 2003. **11**(3): p. 647-58.
43. Cunningham, C.N., et al., *The conserved arginine 380 of Hsp90 is not a catalytic residue, but stabilizes the closed conformation required for ATP hydrolysis*. Protein Sci, 2012. **21**(8): p. 1162-71.
44. Genest, O., et al., *Uncovering a region of heat shock protein 90 important for client binding in E. coli and chaperone function in yeast*. Mol Cell, 2013. **49**(3): p. 464-73.
45. Krukenberg, K.A., et al., *Grp94, the endoplasmic reticulum Hsp90, has a similar solution conformation to cytosolic Hsp90 in the absence of nucleotide*. Protein Sci, 2009. **18**(9): p. 1815-27.
46. Jeschke, G., *DEER distance measurements on proteins*. Annual review of physical chemistry, 2012. **63**: p. 419-46.
47. Krissinel, E. and K. Henrick, *Inference of macromolecular assemblies from crystalline state*. J Mol Biol, 2007. **372**(3): p. 774-97.
48. Leskovar, A., et al., *The ATPase cycle of the mitochondrial Hsp90 analog Trap1*. J Biol Chem, 2008. **283**(17): p. 11677-88.
49. Huai, Q., et al., *Structures of the N-terminal and middle domains of E. coli Hsp90 and conformation changes upon ADP binding*. Structure, 2005. **13**(4): p. 579-90.
50. Kang, B.H., *TRAP1 regulation of mitochondrial life or death decision in cancer cells and mitochondria-targeted TRAP1 inhibitors*. BMB Rep, 2012. **45**(1): p. 1-6.
51. Goodsell, D.S. and A.J. Olson, *Structural symmetry and protein function*. Annu Rev Biophys Biomol Struct, 2000. **29**: p. 105-53.
52. Swapna, L.S., K. Srikeerthana, and N. Srinivasan, *Extent of structural asymmetry in homodimeric proteins: prevalence and relevance*. PLoS One, 2012. **7**(5): p. e36688.

53. Schoeffler, A.J. and J.M. Berger, *Recent advances in understanding structure-function relationships in the type II topoisomerase mechanism*. Biochemical Society transactions, 2005. **33**(Pt 6): p. 1465-70.
54. Ratzke, C., et al., *Dynamics of heat shock protein 90 C-terminal dimerization is an important part of its conformational cycle*. Proceedings of the National Academy of Sciences of the United States of America, 2010. **107**(37): p. 16101-6.
55. Retzlaff, M., et al., *Asymmetric activation of the hsp90 dimer by its cochaperone aha1*. Mol Cell, 2010. **37**(3): p. 344-54.
56. Li, J., K. Richter, and J. Buchner, *Mixed Hsp90-cochaperone complexes are important for the progression of the reaction cycle*. Nature structural & molecular biology, 2011. **18**(1): p. 61-6.
57. Southworth, D.R. and D.A. Agard, *Client-loading conformation of the Hsp90 molecular chaperone revealed in the cryo-EM structure of the human Hsp90:Hop complex*. Mol Cell, 2011. **42**(6): p. 771-81.
58. Street, T.O., L.A. Lavery, and D.A. Agard, *Substrate binding drives large-scale conformational changes in the Hsp90 molecular chaperone*. Molecular cell, 2011. **42**(1): p. 96-105.
59. Motojima-Miyazaki, Y., M. Yoshida, and F. Motojima, *Ribosomal protein L2 associates with E. coli HtpG and activates its ATPase activity*. Biochem Biophys Res Commun, 2010. **400**(2): p. 241-5.
60. Street, T.O., et al., *Cross-monomer substrate contacts reposition the Hsp90 N-terminal domain and prime the chaperone activity*. Journal of molecular biology, 2012. **415**(1): p. 3-15.
61. Vaughan, C.K., et al., *Structure of an Hsp90-Cdc37-Cdk4 complex*. Mol Cell, 2006. **23**(5): p. 697-707.
62. Hutchison, K.A., et al., *The 23-kDa acidic protein in reticulocyte lysate is the weakly bound component of the hsp foldosome that is required for assembly of*



- the glucocorticoid receptor into a functional heterocomplex with hsp90*. The Journal of biological chemistry, 1995. **270**(32): p. 18841-7.
63. McLaughlin, S.H., et al., *The co-chaperone p23 arrests the Hsp90 ATPase cycle to trap client proteins*. J Mol Biol, 2006. **356**(3): p. 746-58.
  64. Richter, K., S. Walter, and J. Buchner, *The Co-chaperone Sba1 connects the ATPase reaction of Hsp90 to the progression of the chaperone cycle*. J Mol Biol, 2004. **342**(5): p. 1403-13.
  65. Karagoz, G.E., et al., *N-terminal domain of human Hsp90 triggers binding to the cochaperone p23*. Proceedings of the National Academy of Sciences of the United States of America, 2011. **108**(2): p. 580-5.
  66. Nathan, D.F. and S. Lindquist, *Mutational analysis of Hsp90 function: interactions with a steroid receptor and a protein kinase*. Mol Cell Biol, 1995. **15**(7): p. 3917-25.
  67. Cunningham, C.N., K.A. Krukenberg, and D.A. Agard, *Intra- and intermonomer interactions are required to synergistically facilitate ATP hydrolysis in Hsp90*. J Biol Chem, 2008. **283**(30): p. 21170-8.
  68. Soroka, J., et al., *Conformational switching of the molecular chaperone Hsp90 via regulated phosphorylation*. Mol Cell, 2012. **45**(4): p. 517-28.
  69. Hessling, M., K. Richter, and J. Buchner, *Dissection of the ATP-induced conformational cycle of the molecular chaperone Hsp90*. Nat Struct Mol Biol, 2009. **16**(3): p. 287-93.
  70. Martinez-Ruiz, A., et al., *S-nitrosylation of Hsp90 promotes the inhibition of its ATPase and endothelial nitric oxide synthase regulatory activities*. Proc Natl Acad Sci U S A, 2005. **102**(24): p. 8525-30.
  71. Svergun D.I., B.C.a.K.M.H.J., *CRY SOL - a Program to Evaluate X-ray Solution Scattering of Biological Macromolecules from Atomic Coordinates*. J. Appl. Crystallogr, 1995(28): p. 768-773.

72. Svergun, D., *Determination of the regularization parameter in indirect-transform methods using perceptual criteria*. J. Appl. Crystallogr, 1992(25): p. 495-503.
73. Pettersen, E.F., et al., *UCSF Chimera--a visualization system for exploratory research and analysis*. J Comput Chem, 2004. **25**(13): p. 1605-12.
74. Laskowski, R.A., et al., *PROCHECK: a program to check the stereochemical quality of protein*. Journal of Applied Crystallography, 1993.
75. Doublet, S., *Preparation of selenomethionyl proteins for phase determination*. Methods Enzymol, 1997. **276**: p. 523-30.
76. Otwinowski, Z. and W. Minor, *Processing of X-ray diffraction data collected in oscillation mode*. Macromolecular Crystallography, Pt A, 1997. **276**: p. 307-326.
77. Adams, P.D., et al., *PHENIX: a comprehensive Python-based system for macromolecular structure solution*. Acta Crystallogr D Biol Crystallogr. **66**(Pt 2): p. 213-21.
78. Emsley, P. and K. Cowtan, *Coot: model-building tools for molecular graphics*. Acta Crystallogr D Biol Crystallogr, 2004. **60**(Pt 12 Pt 1): p. 2126-32.
79. Schrödinger, L., *The PyMOL Molecular Graphics System*. 2010.
80. Gill, S.C. and P.H. von Hippel, *Calculation of protein extinction coefficients from amino acid sequence data*. Analytical biochemistry, 1989. **182**(2): p. 319-26.
81. R Development Core Team. *R: A language and environment for statistical computing*. 2010 [cited 2013; Available from: <http://www.r-project.org>].
82. Ludtke, S.J., P.R. Baldwin, and W. Chiu, *EMAN: semiautomated software for high-resolution single-particle reconstructions*. J Struct Biol, 1999. **128**(1): p. 82-97.
83. Hura, G.L., et al., *Robust, high-throughput solution structural analyses by small angle X-ray scattering (SAXS)*. Nature methods, 2009. **6**(8): p. 606-12.

84. Polyhach, Y., E. Bordignon, and G. Jeschke, *Rotamer libraries of spin labelled cysteines for protein studies*. Physical chemistry chemical physics : PCCP, 2011. **13**(6): p. 2356-66.
85. Naber, N., et al., *Dynamics of the nucleotide pocket of myosin measured by spin-labeled nucleotides*. Biophysical journal, 2007. **92**(1): p. 172-84.
86. Chiang, Y.W., P.P. Borbat, and J.H. Freed, *Maximum entropy: a complement to Tikhonov regularization for determination of pair distance distributions by pulsed ESR*. Journal of magnetic resonance, 2005. **177**(2): p. 184-96.

## Chapter 2

A novel N-terminal extension in mitochondrial Hsp90  
(TRAP1) serves as a kinetic regulator of chaperone  
activity

**Contributing Authors:** James R. Partridge, Nariman Naber, Roger Cooke,  
and David A. Agard.

## **Preface**

Hsp90 is an essential molecular chaperone that undergoes ATP dependant conformational changes, which are intimately linked to the chaperones function of client re-modeling (see introduction and chapter 1). Evolution has produces several forms of Hsp90 found in divergent species and cellular compartments [1]. These homologs display differences in primary amino acid sequence and sequence length [2], with the latter being observed mainly at the N and C-termini or the boundaries between the major domains (NTD, MD and CTD). Though the overall structure, conformational states and dependence on ATP binding and hydrolysis for function are conserved, the kinetic rates of conformational changes and thermodynamics are unique to the different homologs [3, 4]. These data suggest that the function of each homolog requires optimal energetic landscape that has been tuned through evolution of the root Hsp90 gene.

This chapter of my thesis describes the regulatory function of a novel N-terminal extension in the mitochondria Hsp90 (TRAP1), first observed in our full-length crystal structure of zTRAP1 (chapter 1). We find that this extension, termed the “strap”, is responsible for a unique thermal sensitive kinetic barrier between the apo and closed states of TRAP1 and demonstrate that the concept of kinetic regulation by N-terminal residues for Hsp90 is conserved. These data suggest a unique evolutionary strategy for evolving novel properties in Hsp90 homologs to optimize function in diverse environments.

A manuscript describing this study is currently in preparation. James Partridge (post-doc) and I worked together to accomplish this work and are listed as co-first

authors where James appears first in the author list. In the version of the manuscript that follows James is responsible for identifying the “strap”, initial design and ATPase for zTRAP1 strap mutants (chapter 1), human Hsp90 (hHsp90) ATPases, zTRAP1 SAXS, and EPR assay development. I am responsible for the identification of the thermal sensitive kinetic barrier in hTRAP1, EM, hTRAP1 SAXS, zTRAP1 SAXS data analysis, hTRAP1 ATPases, and FRET assay development for TRAP1. In-house SAXS analysis software was written and optimized for this study by David Agard. Our collaborators Nariman Naber and Roger Cooke have provided expert assistance for the EPR experiments presented.

Finally, the following chapter is a draft of the manuscript that I prepared, where not all the data that will go into the final manuscript is represented. To this end, the supplemental section provides a layout for the experiments that will be done in the near future and subsequently incorporated into the manuscript.

## Summary

Hsp90 is a highly conserved molecular chaperone that regulates protein homeostasis inside the cell. Most eukaryotes have four different isoforms: two cytosolic versions, Hsp90 $\alpha/\beta$ , a homolog in the ER called Grp94 and in the mitochondria called TRAP1. Our recent X-ray crystallographic efforts with TRAP1 highlight an extension of the N-terminal “ $\beta$ -strand swap” that we previously described to affect catalytic turnover. Here we have addressed the regulatory function of this N-terminal extension, or “strap”, with a combination of biophysical techniques and demonstrate this structural element is responsible for a unique thermal barrier between apo and the active closed conformation. Further, we demonstrate that the strap functions to limit dimer closure and is coupled to local conformational changes of N-terminal domain (NTD) rotation and lid closure. The extension is conserved in higher eukaryotes and absent in yeast and the prokaryotic family members suggesting this structural element can serve as a novel kinetic regulator for specific homologs. Altogether we highlight the structural and functional relevance of an N-terminal strap that serves as a global regulator of Hsp90 activity and suggest that the evolution of this element can serve to impart novel kinetic properties to diverse homologs.

## Introduction

Hsp90 is a highly conserved molecular chaperone and essential for protein and cellular homeostasis. Although all molecular chaperones promote protein folding and prevent aggregation, Hsp90 is unique in that it interacts with substrate (“client”) proteins

that are already in a semi-folded state to facilitate downstream protein-protein interactions and promote client function in diverse biological pathways [5, 6]. Hsp90 is thought to interact with nearly 10% of the eukaryotic proteome [7] with client proteins that vary in sequence and structure and are known to have transient interactions with the chaperone [8]. For this reason little is known about the biochemical characteristics that regulate client interaction and specificity. Deregulation of Hsp90 protein levels and function has been linked to multiple human diseases and for this reason Hsp90 is a target for biochemical characterization, structural studies, and drug targeting [6, 9].

Hsp90 exists as a homodimer, with each individual protomer consisting of three major domains. The N-terminal domain (NTD) binds to nucleotide, the C-terminal domain (CTD) provides a dimerization interface between protomers, and the middle domain (MD) about which the NTD and CTD sample larger rigid body rearrangements to orchestrate a remarkable concert of conformations that dictate the functional Hsp90 cycle [4, 10-13]. Notably, the MD can be separated into two domains, the large and small MDs (LMD/SMD, N to C-terminus), based on known conformational motions at a hinge point between helix 14 and 15 (H14 and H15) [13-15]. This conserved conformational cycle is regulated by steps of ATP binding and subsequent hydrolysis [4] that are linked to client maturation *in vivo* [3]. Previous studies have shown that the limiting factor of Hsp90 ATPase activity is the rate of dimer closure to form an NTD-dimerized state [16]. Binding of ATP to the NTD nucleotide-binding pocket triggers a series of conformational changes towards an NTD-dimerized state including ATP binding, closure of the lid, a 90° rotation of the NTD relative to the MD [17].



Evolution has given rise to several Hsp90 homologs and isoforms within different species and compartments of the cell, each with unique biological functions [1, 2]. Plants have among the largest number of the chaperone with seven genes identified in *Arabidopsis thaliana* [18]. In most eukaryotes, there are four different homologs of Hsp90: Hsp90 $\alpha$  and Hsp90 $\beta$  in the cytoplasm, GRP94 in the endoplasmic reticulum, and TRAP1 is localized to the mitochondria. Previous studies have demonstrated that though each Hsp90 homolog has a unique conformational equilibrium and catalytic rate, the underlying conformational cycle and mechanism appears conserved [3, 4, 19].

Recently, we solved the crystal structure of TRAP1 in an asymmetric closed state bound to AMPPNP [13]. The crystal structure of full-length TRAP1, solved at 2.3 Å resolution, provides significant insight into previously unknown features of Hsp90. One feature is the dramatic presence of asymmetry between protomers, primarily at the interface between the MD and CTD. We demonstrated that the asymmetry is sampled in solution, functional for catalytic turnover, and provided a model for coupling the energy of ATP hydrolysis to client re-modeling. A second feature highlighted in the TRAP1 crystal structure is the observation of a long extension of the N-terminal  $\beta$ -stand swap. This extension, or “strap,” is found in all forms of Hsp90 from metazoans, including the cytosolic varieties as well as TRAP1 and GRP94. Interestingly, the strap is absent from both yeast and bacterial Hsp90s [2]. Structure based point mutations and complete removal of the strap ( $\Delta$ strap) resulted in 4-fold increase in ATPase activity, evidence that the strap plays some role in regulating TRAP1, though the mechanism remained unclear. In this study we explore the conformational cycle of TRAP1 and demonstrate

that the strap is responsible for a large thermal barrier between the apo and ATP-closed state. Using Negative-stain electron microscopy (EM) and Small-Angle X-ray Scattering (SAXS) we show that removal of the strap results in a complete loss of temperature response in multiple TRAP1 homologs, demonstrating that the strap is responsible for the gain of unique properties observed in this homolog. Additionally, we explore the role of the strap in conformational transitions preceding closure of NTD rotation and lid closure. Here we show that the strap regulates the rates of these conformational changes, which are necessary to form the active closed state dimer. Altogether we show that the unique energy landscape of TRAP1 is intimately linked to the NTD-strap that regulates the rate of dimer closure. These results suggest a unique evolutionary strategy for editing the landscape of diverse Hsp90s for new properties and optimal function *in vivo*.

## **Results**

### **A thermal sensitive kinetic barrier limits the conformational transition from apo to the closed state in TRAP1**

Our initial experiments with human TRAP1 (hTRAP1) demonstrated that the mitochondrial homolog has different closure properties than other hsp90 family members, where hTRAP1 remained in the open conformation despite saturating non-hydrolyzable ATP (AMPPNP) (data not shown). Previous kinetic studies had demonstrated the correlation between temperature and ATPase activity in hTRAP1, with

ATPase rates increasing by nearly 200-fold with a temperature ramp between 25°C and 55 °C [20]. In addition, ATPase activity and closure rates are tightly correlated in the Hsp90 system where the human cytosolic Hsp90 (hHsp90) has the lowest measured ATPase activity and samples the closed conformation quite rarely *in vitro* [4, 16, 19]. Therefore we monitored the ability of hTRAP1 to close as a function of temperature. Reactions containing hTRAP1 and saturating AMPPNP were incubated at increasing temperatures and closure was monitored by negative-stain EM. After an hour of incubation at a given temperature it was clear that while at room temperature (RT, ~23°C) hTRAP1 remained in the apo state, at higher temperatures the closed state was populated at increasing amounts with 30°C populating an intermediate equilibrium and 37°C being almost all in the closed state (Figure 1A). These results correlate with the temperature sensitive steady-state hydrolysis rates of hTRAP1 [20] and are consistent with closure being rate-limiting for hydrolysis in TRAP1. Surprisingly, after removing the reactions from the initial heat perturbation the equilibrium appears to remain fixed (Figure 1B) overnight suggesting a highly stable closed state.

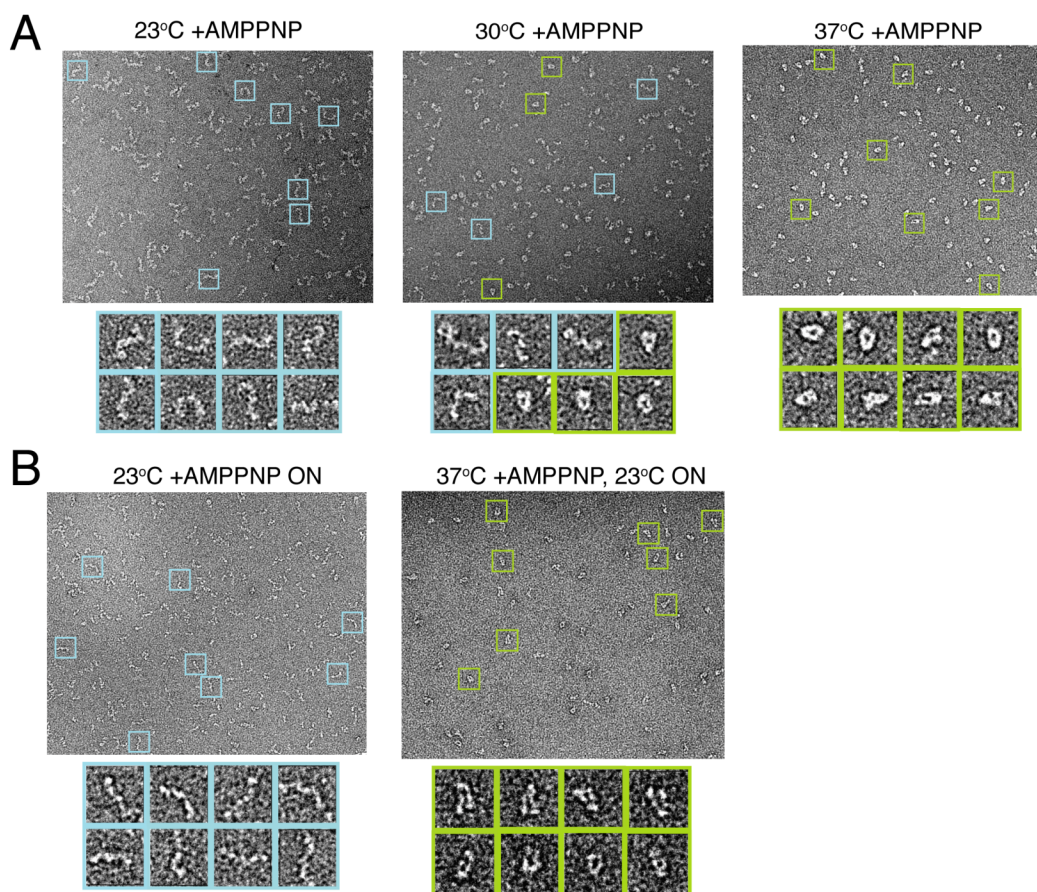


**Figure 1: A temperature dependent kinetic barrier separates the apo to closed state transition of TRAP1.** A) Negative stain electron microscopy (EM) images of hTRAP1 in the presence of AMPPNP at increasing temperatures for 1hr. While the population appears to remain in an apo conformation at RT, conversion to the closed state appears to be intermediate at 30 °C and nearly complete at 37°C. B) Negative stain EM images of reactions set at 23°C and 37°C from A after returning the sample to RT. Both populations remain apo and closed (respectively) demonstrating the large kinetic barrier that limits the conformational transition from apo to the closed state.

To better quantify the equilibrium at each temperature we chose to mirror the experiments above utilizing SAXS. Incubations of TRAP1 homologs with AMPPNP at increasing temperatures were set for one hour prior to exposure and data collection (methods). As expected, the resulting distributions clearly showed a temperature

dependence in transitioning to the closed state as seen by the change in shift towards a more compact distribution (indicative of closure) as a function of temperature (Figure 2A). Fitting the distributions as previously [13] indicated that after an hour at 20°C only .4% of the molecules populate the closed conformation in hTRAP1, while ~74% are closed at 36°C (Figure 2C and Table S1). Though further elucidation of the conformations populated in the apo distribution are necessary to obtain exact values for the percentage of closed state, our values are likely a close estimate given the correlation with the observed EM conformational equilibria above (Figure 1A). Interestingly, the TRAP1 from zebrafish (zTRAP1) displays a shifted temperature dependent closure (Figure 2A and 2C) that correlates a higher ATPase rate and the lower physiological temperature for the organism. The observed species variation is potentially indicative of evolved changes to accommodate chaperone activity at the steady-state temperature of each organism. As above, when returned to the lowest temperature post heating the equilibrium does not revert to apo (Figure S1). Together these data indicate a unique energy landscape for TRAP1 with a large kinetic barrier that limits closure as well as contributes to the stability of the closed conformation once this state is achieved.

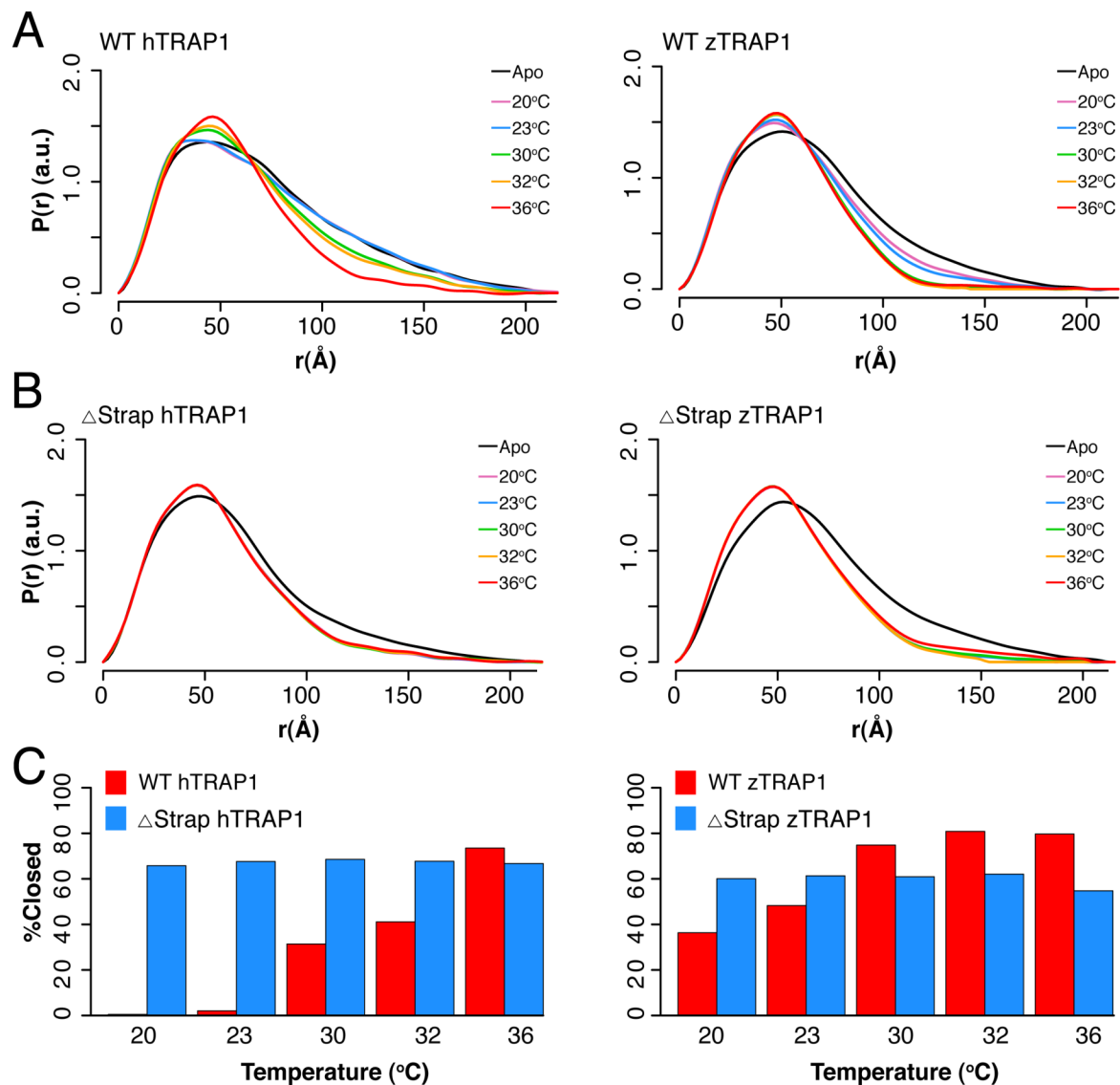


**Figure 2: Kinetic barrier to closed state is modulated by the NTD-strap.** A) SAXS distributions for hTRAP1 (left) and zTRAP1 (right) (84% identical to hTRAP1) in apo and with AMPPNP at increasing temperatures from 20°C to 36°C. Conversion of the population to the closed state is seen at 36°C for hTRAP1 and at 32°C of zTRAP1 consistent with the trend in physiological temperatures of the different species. B) SAXS distributions of  $\Delta$ strap in matching conditions from A. Here we see removal of the strap mitigates the temperature dependent barrier between the apo and closed states. C) Quantification of percent closed for both species of TRAP1 in the presence or absence of the strap. Apparent is the different temperature dependence of hTRAP1 and zTRAP1 and the loss of temperature response of the chaperone in the case of  $\Delta$ strap.

## **The N-terminal strap regulates the large kinetic barrier of TRAP1**

Our prior crystallographic studies highlighted a novel extension of the N-terminal  $\beta$ -strand swap, shown to strongly regulate the ATPase rate of zTRAP1 [13]. Point mutations within the “strap” aimed to disrupt electrostatic interactions between the strap and the neighboring protomer accelerate ATP-hydrolysis activity by 4-fold. Further, zTRAP1 protein lacking the strap (73-100 in zTRAP1) showed up to a 6-fold acceleration of activity.

Given the unique energy landscape of TRAP1 described above, we wondered if the gain of an N-terminal strap could be responsible for unique properties observed in TRAP1. To test this hypothesis, hTRAP1 and zTRAP1 lacking the strap (residues 60-85 in hTRAP1) were tested for their ability to close as a function of temperature by SAXS. Reactions were mixed as with the WT above. Strikingly, at every temperature measured hTRAP1 and zTRAP1 immediately transition to a closed conformation after addition of AMPPNP (Figure 2B), clearly demonstrating the significance of the strap in regulating the transition from apo to the closed conformation. This indicates that the strap has a role in inhibiting the transition to the closed state likely via cis-protomer interactions with the NTD. Further, removal of the strap results in a complete loss of temperature sensitivity in closure as illustrated by the calculated percent closed state at each temperature compared to WT (Figure 2C). This demonstrates that the strap region of the N-terminal  $\beta$ -strand swap is responsible for the gain of a unique landscape observed in TRAP1.

To test if the changes in ATPase extended to hTRAP1 we measured the ATPase activity as previously described [13]. As with zTRAP1, removal of the strap lead to an increase in activity but to a much larger degree at 30-fold for hTRAP1 (Figure 3A, Table S2). This larger fold increase in ATPase correlates with the difference in temperature dependant closure between zTRAP1 and hTRAP1, with hTRAP1 having the more significant dependence and thus a higher kinetic barrier at the experimental temperature (30°C). Notably, truncations ( $\Delta 9$ , residues 69-704) prior to where the contacts in the strap region begin (His71:Glu142 hTRAP1, conserved salt-bridge) did not have an effect on ATPase suggesting that the strap contacts are likely the same in cis (apo) and trans (closed state) (Figure 3A, Table S2).

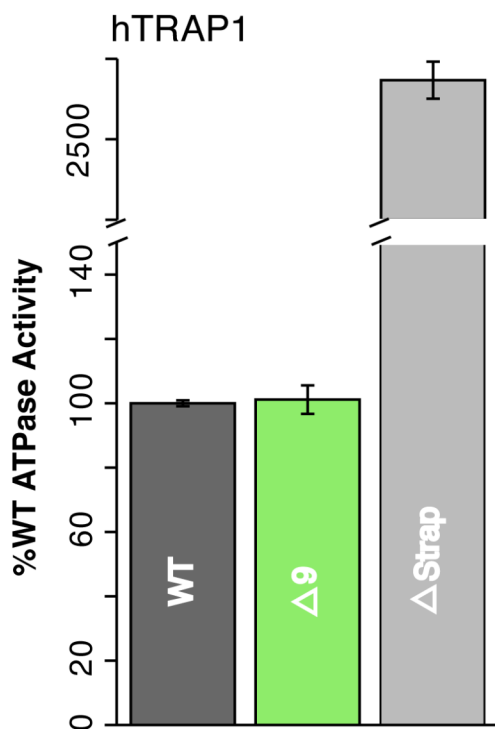


**Figure 3: NTD-strap regulates the ATPase of Hsp90 homologs.**

A) WT and strap mutants for hTRAP1. Removal of the strap ( $\Delta$ Strap) results in a ~30-fold increase in ATPase rate, while truncations before the previously reported salt bridge contact [13] shows no change in activity.



From sequence alignments, the strap region is conserved in Grp94 and cytosolic Hsp90s in higher eukaryotes. Therefore, we questioned if the strap played similar roles in other Hsp90 homologs. From previous studies, deletion of the strap in Grp94 (residues 22-72, referred to as the 'pre-N domain') results in a 5-fold increase in ATPase [11] indicating a role in kinetic regulation as seen in TRAP1. We then tested the effect of the smaller strap region present in the sequence of human Hsp90 (hHsp90, residues 1-14, alpha isoform). Making similar point mutants we see a slight increase in activity with the salt-bridge point mutants that is the same magnitude as the strap deletion, similar to our zTRAP1 results (Figure S2). Upon mutation of F22S in the  $\beta$ -strand (further into the N-terminal sequence of hHsp90) we observe a more significant increase in ATPase of ~6-fold. This mutation is similar to the ' $\Delta 8$ ' mutation in yHsp90 [21] and demonstrates the conservation of N-terminal regulation of Hsp90 homologs. All together these data demonstrate unique properties that the strap imparts to TRAP1 and suggest a role for the strap in regulating catalytic activity across higher eukaryotic Hsp90s.

### **The N-terminal strap regulates the closure rate of TRAP1**

The above results predict that the rate of closure should positively correlate with increasing temperatures. To test this we chose Fluorescence Resonance Energy Transfer (FRET) as a method that could directly measure the rate of this conformational transition [16, 22]. Utilizing our cysteine free version of hTRAP1 [13], two site-specific cysteine residues were added modeled after our previously reported FRET pair for

bacterial Hsp90 (bHsp90) [23], which tracks NTD rotation on path to the active closed state. After forming heterodimers (methods), closure reactions were initiated with AMPPNP and the change in FRET was monitored over time at a temperature range from 20°C to 42°C. Pre and post reaction scans were taken to show the predicted FRET change (high to low FRET) indicating closure has occurred (Figure 4A). As expected the rate of closure increased with higher temperature as quantified by the change in donor fluorescence (Figure 4B, Table 3).

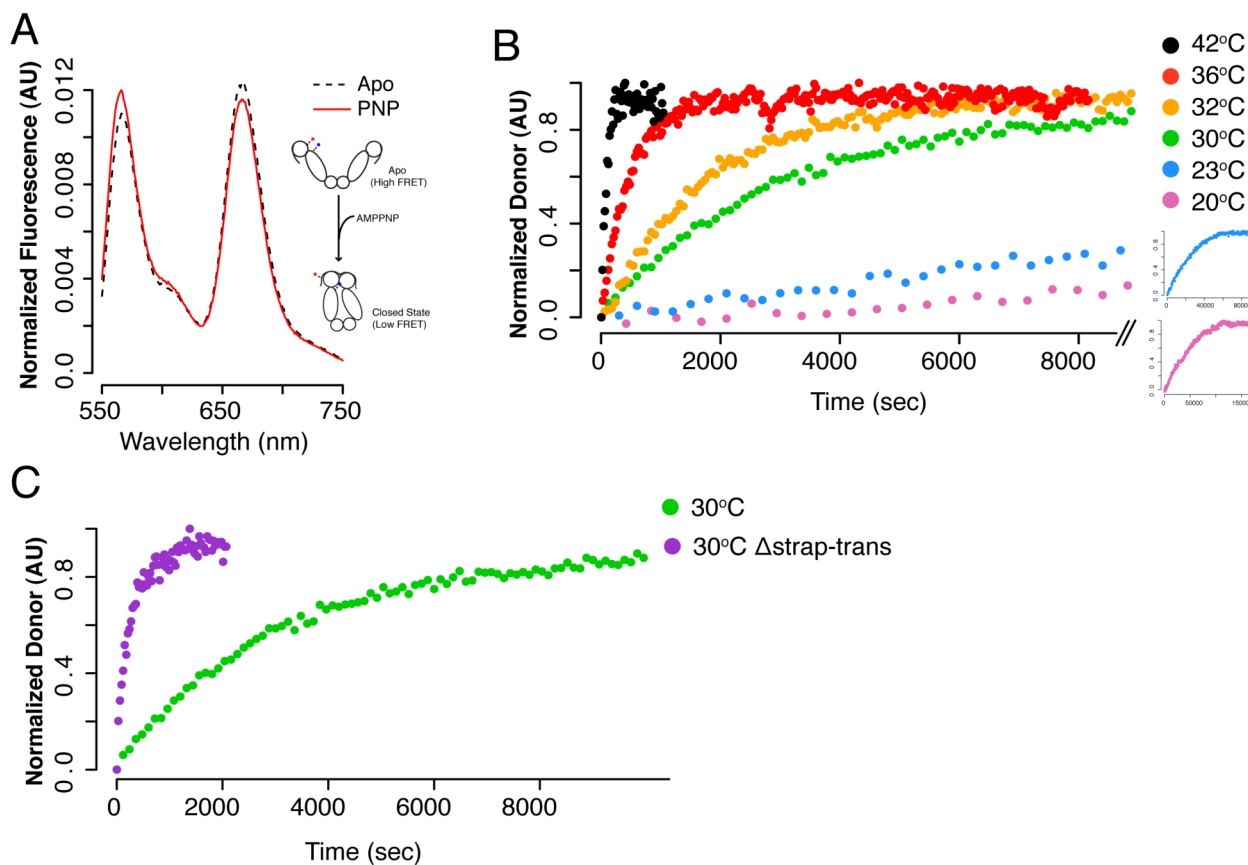


**Figure 4: The NTD-strap regulates closure rate of TRAP1.** A) Steady-state FRET scans for apo and AMPPNP reactions illustrating the anti-correlated change in FRET upon closure (high to low FRET) as measured by the rotation of the NTD from apo to the closed state. B) Temperature dependant closer rates for WT hTRAP1. Here a predicted increase in rate at higher temperatures is apparent. C) Closure at 30°C of WT versus a heterodimer lacking one NTD-strap. Consistent with the steady-state SAXS and ATPase, these data suggest removal of the strap region lowers the energy barrier between apo and the closed state.

Removal of the strap region from the trans protomer resulted in an intermediate ~12-fold acceleration (Figure 4C). Though further truncations are necessary to confirm, these results suggest that the cis and trans straps are independent with a prediction that removal of the second strap will result in the full 30-fold acceleration observed in the ATPase measurements. These data suggest that the N-terminal strap limits the rotation of the NTD and thus transition to the closed state.

### **Lid dynamics and closure are coupled to the N-terminal strap**

Previous studies indicate a correlation between the  $\beta$ -strand swap in yHsp90 and dynamics of the NTD lid [24]. The “lid” of Hsp90 (residues 191-217 zTRAP1) is a structural feature, typical of many ATPases, that rearranges upon ATP binding to “close” over the bound nucleotide. Given the exaggerated extension of the  $\beta$ -strand swap in TRAP1 we questioned if the strap has a novel role in lid stabilization. In the closed state structure of TRAP1, the lid is folded down and interacting with nucleotide via side chains of Ser193 and Ser195 [13]. Looking at the alignment of lid amino acid sequence amongst diverse Hsp90 homologs, Ser193 and Ser/Thr195 are highly conserved with a Gly residue separating the two residues. Considering the length of the lid, 96 residues in zTRAP1, it’s curious to see limited contact with nucleotide in the closed conformation. In fact, deletion of the lid does not affect the affinity of Hsp90 for nucleotide [21]. Although lidless Hsp90 mutants are ATPase inactive, deletion of the lid does have the profound affect of increasing the rate of Hsp90 activity when paired with a WT protomer. Removal

of the lid also results in an increased dimerization affinity, indicating that the lid functions as an inhibitor of NTD-dimerization [24]. Considering these previous studies and our own results, we questioned if the lid had any connection with the observed strap extension of the  $\beta$ -strand swap.

To test this, we developed an electron paramagnetic resonance (EPR) spectroscopy assay to track lid mobility in the apo or closed state (methods). In addition, we aimed to monitor stability of the lid in relation to the presence or absence of the strap. A cys-free version of zTRAP1 was used with a Ala201Cys allowing for malimide based labeling with N-(1-oxy-2,2,6,6-tetramethyl-4-piperidinyl)maleimide (MSL). TRAP1 labeled with MSL additionally has comparable activity to WT TRAP1.

EPR spectra of full-length TRAP1 was recorded at 23 °C and shown to be predominantly immobile in the apo state and increasingly mobile in the nucleotide bound state (Figure 5A). The measured mobility of the lid is consistent with apo structures showing low B-factors for this region due to contacts with H1 of the cis protomer [10, 24]. Conversely, crystal structures of TRAP1 and other Hsp90 homologs bound to triphosphate nucleotide in the closed and dimerized conformation have a lid folding over the nucleotide lacking many stable contacts with the N-terminal domain [12, 13]. In these structures the lid has comparatively heightened B-factors, typically indicative of structural regions that are only loosely ordered and consistent with the mobile signature for the closed conformation in our assay.

Comparing our measurements for WT and  $\Delta$ strap shows that the presence or absence of the N-terminal strap gives comparable results (Figure 5A). We next asked if

there was a change in closure rate. To measure this we tracked the change in lid state from apo (immobile) to the closed (mobile) by monitoring the change in EPR scans over time at 23°C. By plotting the change in the ratio of peak heights (mobile maximum/immobile maximum) over time (Figure 5B), it is apparent that the rate of change is much faster for the  $\Delta$ strap sample compared to WT. These results suggest coupling of conformational changes in the lid to the release of the strap on-path to the closed state and provide significant understanding of the role of the N-terminal strap in conformational changes that regulate NTD-dimerization and ATPase activity of Hsp90.

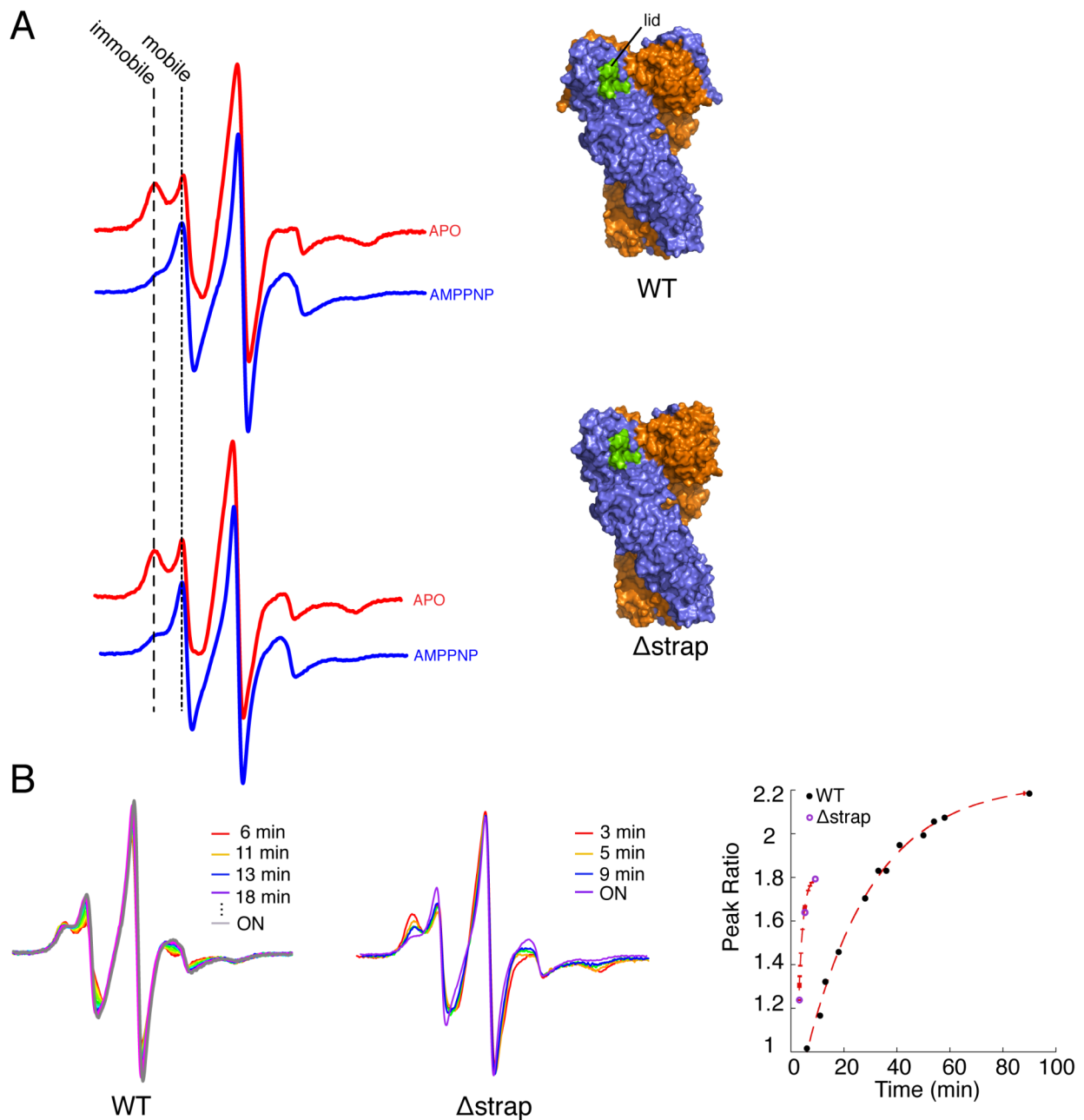


**Figure 5: Lid Closure rate is regulated by the NTD-strap.** A) Continuous Wave (CW) EPR scans of cysteine Free WT (top) and  $\Delta$ strap zTRAP1 (bottom) labeled with a spin-probe on the NTD-lid (green) in order to observe changes to the lid in the apo and closed states (see Methods). In the apo state the lid is in equilibrium with the closed state and more immobile. After addition of AMPPNP the population shifts to the closed conformation as measured by the mobile peak. In the presence or absence of the strap the scans look similar. B) CW-EPR scans at  $\sim 23^\circ\text{C}$  taken for the cysteine Free WT (right) and  $\Delta$ strap zTRAP1 (left) over time after addition of AMPPNP. Tracking the ratio of closed/apo state peak height (mobile/immobile) over time shows an increase rate of the lid conformational change to the closed state, suggesting coupling between the strap and the NTD-lid.

## Discussion

The conservation of Hsp90 has been established from bacteria to humans, giving rise to several homologs in different species and multiple versions of the chaperone in different cellular compartments [1]. Though biochemical and structural studies have identified key differences in the thermodynamic and kinetic properties of the homologs, the underlying a set of conformations [4] and ATP dependant mechanism appears conserved and is essential for client maturation *in vivo* [3]. This suggests the evolution of the Hsp90 gene was accompanied by optimization of the chaperones energetic landscape in order to productively interact with client proteins within diverse environments.

Here we have identified unique kinetic and thermodynamic properties of the mitochondrial Hsp90 (TRAP1) and use a combination of structural and biochemical techniques to show that an addition in N-terminal sequence gives rise to a large thermal barrier that serves to kinetically regulate the formation of the active closed state conformation. Further, we establish coupling of the “strap” to steps preceding closure of NTD rotation and lid closure, transitions necessary for the formation of the NTD-dimerization interface and ATP hydrolysis [17]. As discussed below, these results are consistent with that conformational closer is rate-limiting and suggest that elaborations in sequence at the N-terminus of Hsp90 can be used to evolved different kinetic properties to influence chaperone function.

**NTD:MD rearrangements are required to form the active closed state.**

When considering the transition from apo to the closed state, several local rearrangements in the NTD and between the NTD and MD are necessary. Before nucleotide binding, the element in the NTD known as the “lid” makes contacts with H1 [10, 24], while in the closed state flips over H2 and nucleotide [11-13]. This closed state lid conformation is incompatible with the NTD:MD conformation in the apo state as it would sterically clash with the MD [10, 11]. Further biochemical studies have shown that the lid inhibits the ATPase of Hsp90 by blocking nucleotide binding and favoring the apo state through stabilizing contacts with H1 [10, 24]. In line with this, removal of the lid results in an increase in ATPase and closure rates experimentally demonstrating the lids inhibitory function [24, 25].

After nucleotide binding, a large NTD rotation of  $90^\circ$  relative to the MD must occur to align cis and trans contacts thus completing the dimers catalytic machinery [11-13, 26]. Unlike the MD:CTD, changes in the NTD:MD orientation are rarely sampled in the apo equilibrium without stimulation by co-chaperones or clients, suggesting the transition is unfavorable [23, 27, 28]. These results suggest that these local conformational changes are part of the rate-limiting barrier to the closed state, and as discussed below are regulated in Hsp90 by N-terminal residues of varying lengths.

### **N-terminal Residues and kinetic regulation of Hsp90**

In this study we show that the N-terminal residues that make up the strap limit the closure kinetics and ATPase activity of TRAP1. Removal of the strap leads to a 30-



fold increase in ATPase rate, faster closure kinetics, and loss of thermal regulation of dimer closure.

Beyond TRAP1, regulation of the chaperone's ATPase appears to be a conserved feature of the Hsp90 family. In yHsp90, the 'β-strand swap' (residues 1-8) [21, 24] makes contacts with the cis-NTD in the apo state and forms analogous contacts on the trans-protomer in the closed state [12, 13]. Deletion of the first β-strand ('Δ8') was shown to accelerate the ATPase rate by ~1.5 fold by releasing cis-contacts allowing H1 and the lid to undergo conformational changes necessary to form the NTD-dimer interface [21]. These N-terminal residues are further into the amino acid sequence of TRAP1 and separable from the observed N-terminal strap by the change in secondary structure from a loop to a β-sheet (moving from N to C-terminus), with the strap adding an additional 771Å of buried surface area and several new trans-protomer contacts [13]. Given the similar accelerating effects on ATPase, it is likely that the β-strand and the strap are acting on the same barrier.

In GRP94 and Hsp90 found in chloroplasts, the strap region is similar in length to that seen in the TRAP1 gene [2]. Though ATPase effects are unknown for the chloroplast homolog, the analogous strap region in GRP94 serves to inhibit ATP hydrolysis by 5-fold [11] suggesting similar regulatory function demonstrated in our study of TRAP1. In our own measurements of the ATPase of hHsp90, we find that contacts unique to the strap accelerate ATPase rates by ~1.3 fold and ~6-fold if mutations mimicking the Δ8 mutant in yHsp90 are tested. Together these data point to conservation of kinetic regulation by N-terminal residues in Hsp90 family and bring forth

the concept that extensions of this region can serve to impart new properties to the chaperone as demonstrated here with TRAP1.

Altogether we propose a model for the conformational cycle of Hsp90 (Figure 6A) where we outlined a series of steps that slow closure and consequently ATP hydrolysis. Specifically, after ATP is bound, release of cis contacts of the  $\beta$ -strand/strap allows for lid closure and NTD rotation resulting in an asymmetric conformation [13]. Sequential hydrolysis leads to rearrangement of client binding residues (red) between the MD:CTD thus coupling ATP hydrolysis to client remodeling when clients are bound to this region.

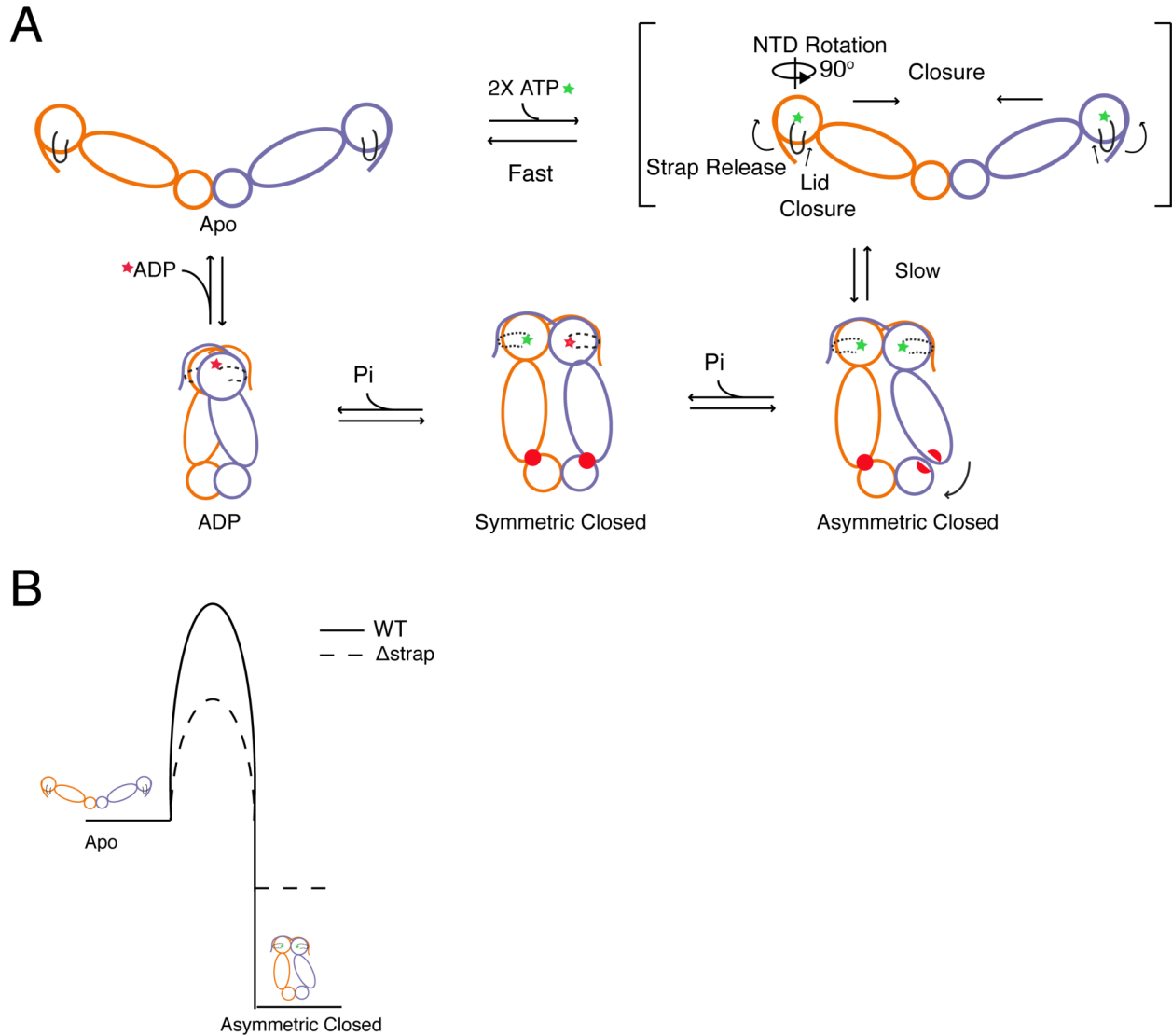


**Figure 6. Model for the conformational cycle and unique energy landscape of TRAP1.** A) In the absence of nucleotide the chaperone is in an equilibrium of open conformations (most open shown for simplicity) with the strap folded back onto the cis protomer. Upon binding of ATP conformational changes necessary for the closed state transition are initiated. Here we propose that the cis contacts of the strap are broken allowing the lid and NTD to undergo conformational changes towards the closed state. After the slow closure step the chaperone assumes the previously reported asymmetric conformation [13]. Sequential hydrolysis leads to changes in symmetry rearranging the unique MD:CTD interfaces and client binding residues (red) before sampling the ADP conformation and resetting the cycle to the apo state equilibrium. B) Model for the unique energy landscape of TRAP1. Dashed lines illustrate the energy landscape of WT TRAP1, and the solid lines depict the change in landscape upon the loss of the extended N-terminal sequence in TRAP known as the ‘strap’ illustrating the unique properties to the landscape that the strap imparts.

From our previous study defining structural asymmetry in the closed state of TRAP1 [13], the progression of conformations post the first hydrolysis remains a hypothesis. Therefore, an alternative model with an alternative conformational progression is described in figure S3. After the second ATP is hydrolyzed the chaperone assumes a compact ADP conformation before resetting the cycle to the apo state.

Specific changes to the TRAP1 energetic landscape imparted by the strap are depicted in figure 6B. Here the barrier between the apo and closed conformation is accentuated by the addition of this structural element at the N-terminus. Further, the closed state is more stable as observed in Figure 1 and Figure S1, presumably due to cross-protomer strap contacts observed in the crystal structure of TRAP1 [13].

### **Functional implications for the evolution of an N-terminal strap**

The observation that the catalytic efficiency of different Hsp90s vary by ~15-fold [19] suggest that regulation of the rate-limiting step has been highly tuned through evolution for functional importance. In support of this, mutations demonstrated to accelerate or decelerate ATPase rates result in significant growth defects and loss of client protein folding *in vivo* [25, 29]. The evolution of additional residues at the N-terminus of the Hsp90 gene provides a convenient way to edit the chaperone's conformational cycle to function with diverse clients encountered by the different homologs. Additionally, while the cytosolic Hsp90s are highly regulated by several co-chaperones [30], only one co-chaperone has been identified for the organelle

homologs [31]. This brings forth the possibility that the more extended strap in these homologs function to perform regulation that co-chaperones proved to Hsp90 in the cytosol. Additionally, as Hsp90 is a heavy target for post-translational modifications (PTMs) [32] added contacts that the strap provides a target for PTMs that could modulate the regulatory function of this element. Unique to TRAP1 is the possibility that the thermal response of the kinetic barrier is biologically relevant in the mitochondria where heat is generated through uncoupling of the electron transport chain [33]. Perhaps the catalytic response of TRAP1 to temperature is an adaptation to thermal fluctuations in this environment or perhaps more intimately tied to sensing temperature as part of a feedback mechanism for the organelle or under stress conditions. Though the *in vivo* purpose of the conserved strap remains to be uncovered, we demonstrate that this region is responsible for the unique thermal properties of TRAP1 and coupled to a series of smaller conformational changes in the NTD:MD on pathway to the closed state. Altogether our findings suggest a way that the Hsp90 family can evolve new kinetic properties for the purpose of optimal function.

### **Supplemental Information**

The work presented in this chapter is an initial draft for a manuscript that is in the beginning stages of writing with a few questions and thus experiments left to finish in the near future. The major question I feel is lacking is- is the strap's role largely limited to the on-rate component of the closure reaction ('closure'), or is the off-rate ('re-opening') contributing in a significant way? Initial experiments suggest that the latter could be

true, though these experiments need to be repeated and re-thought. If the latter turns out to be true this result is also quite interesting in that it has been known for quite awhile that the hydrolysis rate, which correlates to the amount of time spent in the closed state, is intimately linked to client maturation [25]. The strap could be acting as a kinetic ‘tuner’ for TRAP1 that allows for proper function in the unique environment of the mitochondria. In line with the above, an explanation and outline for experiments are below.

For the FRET experiments and initial re-opening experiment was tried by chasing the reaction with 10-fold excess ADP or ATP. This experiment was modeled after experiments I had done with the bHsp90 (HtpG specifically) (chapter 5) [22]. In this case after TRAP1 had equilibrated to the closed-state (as judged by the plateau) I challenged the population with 10-fold excess ADP or ATP. However, unlike in the case of bHsp90 the population remained in the closed state for more than 6 hours indicating a very stable closed conformation (Figure S4). It is possible that without the strap the re-opening will look like bHsp90 and closely match the closure rate, or perhaps hydrolysis is necessary to re-open. In the latter case it should be possible to re-do the experiment with ATP $\gamma$ S, where I would predict that the re-opening rate (increase in FRET for the NM rotation FRET pair) should match the hydrolysis rate of this analog (~7-fold slower relative to the ATPase rate). Alternatively, one could try a different experiment by using the FRET pair that measure closure across the dimer [16, 22] and add either ADP, ATP $\gamma$ S, or measure monomer exchange as a proxy for re-opening by adding excess

unlabeled WT. A repeat of the initial experiments as well as these alternatives will be done to ascertain the role of the strap in the re-opening reaction for TRAP1.

Curiously, comparing scans from the apo reactions for WT and  $\Delta$ strap we observe a small FRET change consistent with a rotation towards the closed state (low to high FRET) (data not shown). Here the strap deletion is in the trans protomer, so any effect must happen in trans. This signal suggests that the trans protomer can influence closure of the dimer. This is consistent with the apo SAXS data for  $\Delta$ strap (also in hTRAP1), which show a shift in the apo distribution towards the closed state (data not shown). In this case, both straps truncated so there isn't a separable cis/trans effect. These data indicate that removal of the strap shifts the apo distribution towards the closed state.

Previous to the FRET experiments in the main text figures, I had done some initial experiments showing the temperature dependence of the closure rate using the same NTD:MD intra-FRET pair. In this case a few of the conditions (buffer: 50mM Hepes pH7.5, 50mM KCl, 5mM MgCl<sub>2</sub>, nucleotide concentration: 2-5mM) were a bit different, but the experiments were conducted in a similar fashion. In this initial round the donor and acceptor fluorescence seemed well behaved and calculating the rates with either donor, acceptor or the D/A ratio resulted in approximately the same  $K_{obs}$  (Figure S5A, Table S2). In some experiments the rates are not as well behaved for this pair. In principle the rate of closure should be the same whether the Donor, Acceptor, or D/A ratio is fit. In the case of NTD:MD intra-FRET pair the signals/rates seem to be more stable across experiments with the Donor, though the alternative pair that

measures across the dimer in general seems to give more consistent results (E140C, E407C in hTRAP1). Additionally, I tested the closure rate in the presence of different ATP analogs ADP/ATP BeF, here the rates were much faster and closer to measured hydrolysis rates (Figure S5B, Table S4). These data suggest that either a different pathway to closer is being used with ADP/ATP BeF, or that the chemical nature of AMPPNP doesn't induce closure as effectively as the other analogs. In this study I believe our conclusions are valid either way. AMPPNP affords us a better dynamic range to view the temperature dependence and to clearly see the NTD-Straps role in the unique landscape of TRAP1.

Also tested was the ability of  $\Delta 131\Delta$  to accelerate hTRAP1 at the various temperatures. Initial experiments indicate an acceleration at every temperature (further measurements are necessary to get better statistics for quantitative comparison) (Figure S5C) suggesting that temperature and client are potentially working independently on the same energy barrier. Further experiments are planned to repeat this observation and to test if removal of the strap mitigates the client effect.

Lastly, there are plans to repeat the EPR time course. With repeats it should be possible to get a better idea for the change in rate observed in when comparing the WT to the  $\Delta$ strap (simply illustrated in the main text and figures). As an initial estimate of the rates I fit the change in closed state peak height over time from the raw data (not including the ON time point as there was not an exact time known). From this I get a ~8-fold increase in lid closure for the  $\Delta$ strap (Figure 5B). In order to get accurate rates and correlate the EPR data with the fold change in hydrolysis rate we need better



sampling, to ensure the reaction is finished. Further we will need to measure the ATPase rates for WT and  $\Delta$ strap zTRAP1 at RT as current measurements are at 30°C. At 30°C the fold difference is likely to be smaller given the temperature dependant range for zTRAP1. Initial rate measurements for WT zTRAP1 at RT are  $.454 \text{ min}^{-1}$  (calculated per monomer), however the  $\Delta$ strap still needs to be measured. Ultimately, the qualitative observation of the acceleration of lid closure suggests that the conformational change of the lid necessary to closure is coupled to release of the cis strap on pathway to the closed conformation as discussed in the main text. The necessary repeats and data analysis will require some work in collaboration with Nariman Naber and Roger Cooke.

### Supplemental Figures and Legends

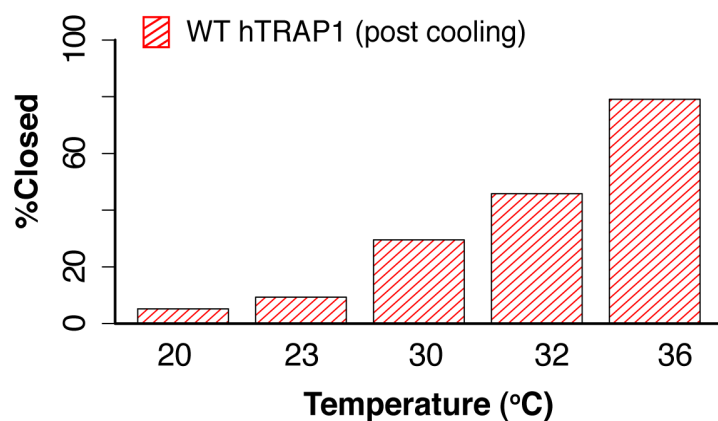


**Figure S1. The closed conformation of TRAP1 is stable post temperature induced closure.** A plot of percent closed state versus temperature of WT hTRAP1 after closure has completed at each given temperature and then cooled to the 20°C for 2 hours. This data was taken for the same samples of in figure 2C and suggests a highly stable closed state.

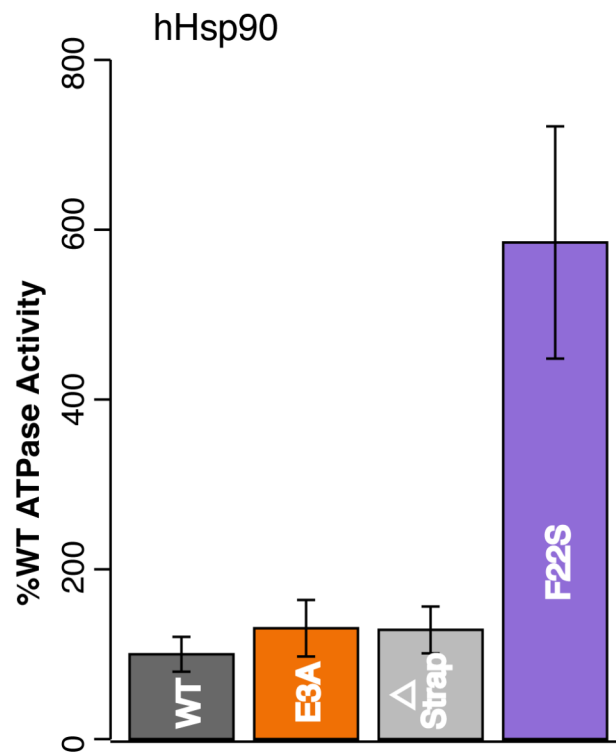


**Figure S2. WT and strap mutants for hHsp90.** Removal of the strap region of hHsp90 (alpha isoform) results in an increase in a modest ~1.3-fold ATPase rate that is the same fold as mutation of the analogous salt bridge residue from TRAP1 [13]. Making a mutation of F22S in hHsp90 $\alpha$  shows a ~6-fold increase and is similar to the 'Δ8' from yeast Hsp90 [21].

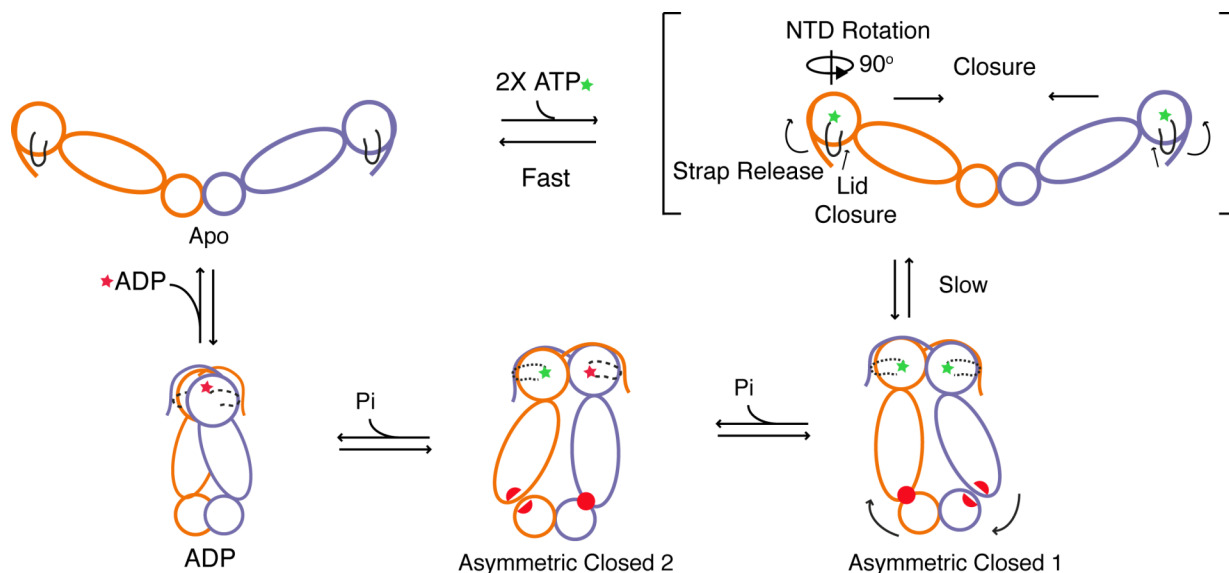


**Figure S3. Alternative Model for the chaperone cycle.** Model proposed in figure 6 of the main text with an alternative progression of states during sequential hydrolysis. Here the protomer arms flip-flop conformations after the first hydrolysis event before progression to the ADP and apo states to re-set the cycle. This alternative figure is similar to the one that can be found in chapter 1 (Figure S7), and is proposed here due to the fact that we cannot distinguish the two models with the data presented in chapter 1.

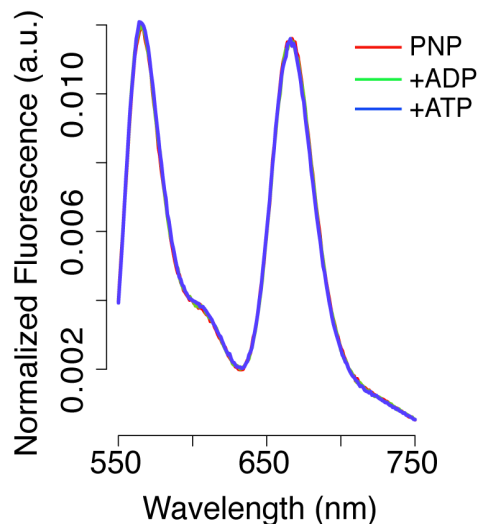


**Figure S4. The closed state of TRAP1 is a stabilized state.** Steady-state FRET scans for the NTD:MD Intra-FRET pair (both straps are still present) after closure with AMPPNP has completed at  $30^\circ\text{C}$ . Upon addition of 10-fold excess ADP or ATP the distribution remains stable. These results are in contrast to previous experiments with bHsp90 [22] and suggest a more stable state for TRAP1.

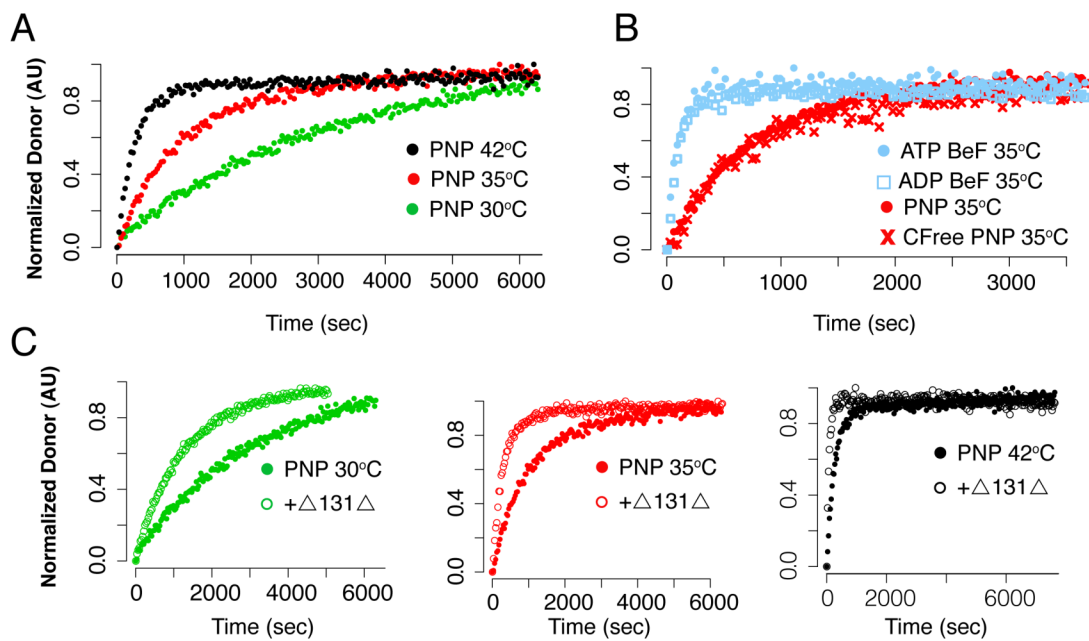


**Figure S5. Previous FRET measurements for the NTD:MD Intra-FRET pair.** A) Temperature dependant closure experiments. B) FRET kinetics of different ATP analogs (AMPPNP, ATP-BeF, or ADP-BeF) and in the presence of either WT or a Cys Free trans protomer. WT and cysteine free give the same rate, while the other analogs are estimated to be ~7-fold faster than AMPPNP. C) Temperature dependant substrate stimulation of  $\Delta 131\Delta$ . Heterodimers were formed as usual and then mixed with 75uM  $\Delta 131\Delta$  before closure was initiated with AMPPNP. Acceleration of closure is observed at all temperatures.

**Table S1. Percent closed state for TRAP1 homologs at varying temperatures.**

Temperature (Celsius)	Protein	%closed state	R
20	WT hTRAP1	.5	0.042
23	WT hTRAP1	2	0.042
30	WT hTRAP1	31	0.024
32	WT hTRAP1	41	0.019
36	WT hTRAP1	74	0.011
20	WT zTRAP1	36	0.015
23	WT zTRAP1	48	0.011
30	WT zTRAP1	75	0.027
32	WT zTRAP1	81	0.033
36	WT zTRAP1	80	0.030
20	hTRAP1 $\Delta$ strap	66	0.015
23	hTRAP1 $\Delta$ strap	68	0.014
30	hTRAP1 $\Delta$ strap	69	0.014
32	hTRAP1 $\Delta$ strap	68	0.015
36	hTRAP1 $\Delta$ strap	67	0.018
20	zTRAP1 $\Delta$ strap	60	0.016
23	zTRAP1 $\Delta$ strap	64	0.014
30	zTRAP1 $\Delta$ strap	61	0.015
32	zTRAP1 $\Delta$ strap	62	0.014
36	zTRAP1 $\Delta$ strap	55	0.016

**Table S2. ATPase rates for WT and strap mutants**

Protein	hTRAP1 $K_{obs}$ ( $\text{min}^{-1}$ )	hHsp90 alpha $K_{obs}$ ( $\text{min}^{-1}$ )
WT	0.463 $\pm$ 0.003	0.073 $\pm$ 0.015
$\Delta$ salt bridge (E/A)		0.096 $\pm$ 0.015
$\Delta$ strap	13.284 $\pm$ 0.526	0.094 $\pm$ 0.006
$\Delta$ 9	0.468 $\pm$ 0.020	
F22S		0.43 $\pm$ 0.05

**Table S3. FRET closure rates for main text experiments**

Temperature (Celsius)	Donor Rate $K_{obs}$ ( $\text{min}^{-1}$ )
20	0.0012 $\pm$ 0.00002
23	0.0022 $\pm$ 0.0001
30	0.016 $\pm$ 0.0002
32	0.035 $\pm$ 0.0015
36	0.125 $\pm$ 0.003
42	0.81 $\pm$ 0.032

**Table S4. FRET closure rates for supplemental experiments**

Temperature	Nucleotide	+75uM $\Delta 131\Delta$ Y/N	Donor Rate $K_{obs}$ ( $\text{min}^{-1}$ )	Acceptor Rate $K_{obs}$ ( $\text{min}^{-1}$ )	D/A Ratio Rate $K_{obs}$ ( $\text{min}^{-1}$ )
30	AMPPNP	N	0.017	0.021	0.019
30	AMPPNP	Y	0.044	0.042	0.043
35	AMPPNP	N	0.055 (.064 +/- .007)	0.055	0.050
35	AMPPNP	Y	0.180	0.180	0.180
35	ATP BeF	N	0.6 (0.50 +/- .09)	0.33	0.5
35	ADP BeF	N	0.58	0.33	0.43
35*	AMPPNP	N	0.078	.046	.053
40	AMPPNP	N	0.192	0.23	0.19
40	AMPPNP	Y	0.780	0.53	0.55

\*Denotes Cysteine Free protein used as trans protomer.

Rates represent a single run of FRET kinetics. () are average rates calculated from the donor across experiments, but this was only possible for two of the conditions.

## Experimental Procedures

### Protein Production and Purification

Full-length and mutant versions of TNF receptor-associated protein 1 (TRAP1) from *Homo sapiens* and *Danio rerio* (hTRAP1, zTRAP1), as well as human Hsp90 $\alpha$  (hHsp90) were purified as using a previously described protocol [13]. Mutant versions of Hsp90 homologs were generated by standard PCR based methods.

### Negative-Stain Electron microscopy

WT hTRAP1 was initially diluted to .1 mg/mL in a buffer containing 20 mM  $\text{NaH}_2\text{PO}_4$ , 7, 500 mM KCl, and 2 mM  $\text{MgCl}_2$ , .02% n-octyl- $\beta$ -D-glucoside + 2 mM AMPPNP. Reactions were incubated at various temperatures one hour, followed by dilution to 0.01 mg/mL in the buffer above including 2mM AMPPNP to maintain nucleotide concentration. 5  $\mu\text{L}$  of the resulting reactions were then incubated for ~1

minute on 400 mesh Cu grids (Pelco) coated with a thin carbon layer (~50-100 Å). Following sample incubation was a 3X wash with milliQ water, and lastly stained 3X with uranyl formate pH 6. The last stain was removed by vacuum until the surface of the grid was dry. Prepared grids were imaged with a TECNAI 20 (FEI) operated at 120 kV. Images were recorded using a 4k x 4k CCD camera (Gatan) at 62,000 magnification, at -1.5 μm defocus. Representative closed state particles were selected in EMAN [34].

### **SAXS data collection and analysis**

TRAP1 homologs and mutant proteins were buffer exchanged into 20 mM Hepes pH 7.5, 50 mM KCl, 2 mM MgCl<sub>2</sub>, 1mM DTT immediately prior to the experiment. 75 μM protein (monomer) was used as the final concentration for all reactions. 2 mM nucleotides were used to initiate closure and the reactions were incubated at various temperatures for one hour prior to data collection. Reactions were spun down at max speed in a tabletop centrifuge for ten minutes immediately prior to data collection to remove any trace aggregation.

Data was collected at the ALS at beamline 12.3.1 with sequential exposure times of 0.5, 1, and 0.5 seconds. Each sample collected was subsequently buffer subtracted and time points were averaged using scripts at beamline 12.3.1 and our own in-house software. The scattering data was transformed to  $P(r)$  vs.  $r$  using the program gnom [35] and Dmax was optimized for a smooth approach to zero. The resulting distributions were fit using in-house least squares fitting program in the region where non-zero data was present for the target data and closed state model. For the fitting we chose to

theoretical scattering data for our TRAP1 closed state model [13] and the WT apo data for each TRAP1 homolog. The WT apo data was chosen as the best representation of apo for two reasons. 1) The apo state of Hsp90 proteins consist of a mix of conformations [4] of which the various conformations and percent of each remains to be elucidated for TRAP1, and 2) removal of the strap (particularly in hTRAP1) induces a shift of the apo distribution towards the closed state (data not shown), which would result in a value of percent closed for the  $\Delta$ strap protein that would under represent the true value relative to WT. Theoretical scattering curve for the TRAP1 crystal structure was generated in the program CRY SOL [36]. The percent of components utilized in the fit, and an R factor (R\_merge) that is similar to a crystallography R factor in nature is output from our least-squares fitting program and values reported in Table 1. R\_merge is defined as the equation below

$$R\_merge = \frac{\sum |P_{obs}(r) - P_{calc}(r)|}{\sum P_{obs}(r)}$$

where  $P_{obs}(r)$  is the observed probability distribution and  $P_{calc}(r)$  is the calculated modeled fit. Residuals were calculated using the equation below

$$Residuals = P_{calc}(r) - P_{obs}(r)$$



## **Point mutations based on previously solved structure of TRAP1**

Our recently published structures of TRAP1 indicate several key interactions between protomers of the TRAP1 dimer that potentially play a key role in regulating TRAP1 function [13]. A series of point mutations were designed to disrupt and eliminate interactions between N-terminal domains and the N-terminal extension “strap” of the neighboring protomer. These include disrupting the interaction between His87 and Glu157 from zTRAP1 and removing the first 100 residues of zTRAP1 ( $\Delta$ strap zTRAP1) in order to eliminate a majority of the “strap” interface. Similar mutations were carried out using hTRAP1, to demonstrate the mechanism of regulation via strap is conserved between multiple species. To further judge the pervasiveness of NTD-strap regions in Hsp90 homologs, similar mutations were introduced into the alpha isoform of human Hsp90 (hHsp90). Standard PCR methods were used to introduce all mutations to parental plasmids. All genes were cloned into the pET151/D-TOPO bacterial expression plasmid (Invitrogen) and purified as referenced above.

## **Steady-State ATPase measurements**

Steady-state kinetic measurements for various Hsp90 homolog and mutants were carried out as previously described [13]. Results were plotted using the program R [37].

## **Fluorescence Resonance Energy Transfer (FRET) measurements**

Cysteine Free hTRAP1 with encoded cysteine positions (Ser133Cys, Glu407Cys) on a single protomer allowed for site-specific labeling and was purified as previously described [13], with a final S200 (storage) buffer of 50mM Hepes pH 7.5, 100mM KCl, 500uM TCEP. Purified protein was then dual labeled with AlexaFluor 555 (Donor) and 647 (Acceptor) (Invitrogen) at 5-fold excess over protein (pre-mixed at 2.5-fold concentration each) overnight at 4°C. Labeling reactions were then quenched with 2-fold  $\beta$ -mercaptoethanol over dye concentration and free dye was removed with desalting columns containing Sephadex G-50 resin (illustra Nick Columns, GE Healthcare).

For FRET measurements, WT hTRAP1 was mixed in 20-fold excess over labeled protein in a 10X reaction (2.5uM labeled protein:50uM WT) in a 1X buffer (40mM Hepes pH7.5, 150mM KCl, 5mM MgCl<sub>2</sub>) and heterodimers were formed at 30°C for 30 minutes. Final reactions were mixed to 1X in the buffer above and closure was initiated by addition of 2mM AMPPNP at various temperatures. Experiments were carried out using a Jobin Yvon fluorometer with excitation and emission monochromator slits set to 2 nm/3nm (respectively), an integration time of .3 seconds, and excitation/emission wavelengths of 532/567nm (donor) and 532/667nm (acceptor). Kinetic measurements were taken at a time interval to minimize photobleaching. The change in donor fluorescence was well fit with a single exponential to obtain the rate of closure/NTD rotation. For steady-state FRET scans (taken before and after kinetic measurements), reactions were excited at 532nm and emission was collected from 550nm-750nm. FRET scans were normalized such that the area under the curve is 1.

For FRET experiments in the supplemental section, kinetic measurements were carried out as above with slight differences in buffer and nucleotide concentrations. For the ATP/ADP-BeF experiments the buffer was supplemented using a 5X master mix of BeCl<sub>2</sub>/KF (10mM BeCl<sub>2</sub> and 50mM KF, to form BeF) to a final concentration of 2mM BeF (dilution of master mix to 1X), and 2mM ATP or ADP was added to initiate dimer closure. Experiments with the model substrate, Δ131Δ, heterodimers were performed as above followed by incubation with 75uM substrate at 30°C for 30minutes. Closure was initiated with AMPPNP and measurements were carried out on a Jobin Yvon fluorometer as above.

### **Continuous-Wave Electron Paramagnetic Resonance (EPR)**

Cysteine free zTRAP1 with a Ala201Cys mutation on the lid was exchanged into non-reducing EPR buffer (25 mM Hepes pH 7.4, 150 mM NaCl) at 100 μM (monomer concentration) and labeled by the addition of N-(1-oxyl- 2,2,6,6-tetramethyl-4-piperidiny)maleimide (MSL, Sigma) to 2.5x concentration of protein overnight at 4°C. The labeled protein was then run through a Micro Bio-Spin column P-30 (Bio-Rad) to eliminate free probe. EPR spectra were obtained at ~100uM labeled protein +/- 2mM AMPPNP in the buffer above with addition of 2mM MgCl<sub>2</sub> and after heating at 30°C for 30 minutes to ensure closure has completed (Figure 5A). For the time course (Figure 5B), protein was spiked with AMPPNP and EPR scans recorded overtime at room temperature (~23°C).

EPR measurements were performed with a Bruker EMX EPR spectrometer (Bruker, Billerica, MA) in a 50-  $\mu$ l glass capillary. First derivative X-band spectra were recorded in a high- sensitivity microwave cavity using 50-s, 10-mT-wide magnetic field sweeps. The instrument settings were as follows: microwave power, 25 mW; time constant, 164 ms; frequency, 9.83 GHz; modulation, 0.1 mT at a frequency of 100 kHz. Each spectrum used in data analysis was an average of 10-20 sweeps from an individual experimental preparation. Data was collected at room temperature and monitored using a thermistor placed close to the experimental sample.

Rates of lid closure for WT and  $\Delta$ strap were estimated by fitting the ratio of peak heights (mobile/immobile) representing the apo (immobile) and closed (mobile) states over time. Both rates were well fit using single exponentials.

## **Postscript**

From the work above we learn how evolved extensions in sequence the N-terminus can influence chaperone activity. The question then is why is the rate of hydrolysis so finely tuned in the case of different Hsp90 homologs and what is the “strap” doing *in vivo*? The functional relevance for this is suggested by the observation that if the ATPase rate of Hsp90 is decreased or increased there are detrimental effects on cellular growth and client maturation (see discussion). Coupled to our findings, one important question is is the strap functional for client binding and/or re-modeling? An outline to test this *in vitro* can be found above with the  $\Delta$ 131 $\Delta$  system. To elucidate the functional consequences of the strap *in vivo* it should be possible to replace endogenous TRAP1 (as TRAP1 can be knocked out without a lethal phenotype- as

apposed to cytosolic Hsp90 or Grp94 in eukaryotes) with either a TRAP1 homolog with a shifted temperature dependence or with the strap mutations presented above. Here the advantage is that the TRAP1 KO or KD phenotypes have been characterized, so one can look for changes in mitochondrial morphology, bioenergetics, apoptosis/necrosis, or PD related phenotypes (see chapter 3). We have TRAP1 KO cells in house (chapter 3 and Appendix), as well as an established collaboration with Dr. L. Miguel Martins (University of Leicester) to do experiments in TRAP1 KO flies. Further from pursuits in chapter 1, we have a variety of TRAP1 homologs in house. All of the homologs express and purify quite well. It could be interesting to utilize these to investigate the evolution and mechanism of the strap in the different species.

## References:

1. Johnson, J.L., *Evolution and function of diverse Hsp90 homologs and cochaperone proteins*. Biochim Biophys Acta, 2012. **1823**(3): p. 607-13.
2. Chen, B., D. Zhong, and A. Monteiro, *Comparative genomics and evolution of the HSP90 family of genes across all kingdoms of organisms*. BMC Genomics, 2006. **7**: p. 156.
3. Panaretou, B., et al., *ATP binding and hydrolysis are essential to the function of the Hsp90 molecular chaperone in vivo*. The EMBO journal, 1998. **17**(16): p. 4829-36.
4. Southworth, D.R. and D.A. Agard, *Species-dependent ensembles of conserved conformational states define the Hsp90 chaperone ATPase cycle*. Mol Cell, 2008. **32**(5): p. 631-40.
5. Taipale, M., et al., *Quantitative analysis of HSP90-client interactions reveals principles of substrate recognition*. Cell, 2012. **150**(5): p. 987-1001.
6. Taipale, M., D.F. Jarosz, and S. Lindquist, *HSP90 at the hub of protein homeostasis: emerging mechanistic insights*. Nat Rev Mol Cell Biol, 2010. **11**(7): p. 515-28.
7. Zhao, R., et al., *Navigating the chaperone network: an integrative map of physical and genetic interactions mediated by the hsp90 chaperone*. Cell, 2005. **120**(5): p. 715-27.
8. Echeverria, P.C., et al., *An interaction network predicted from public data as a discovery tool: application to the Hsp90 molecular chaperone machine*. PLoS One, 2011. **6**(10): p. e26044.
9. Luo, W., et al., *Heat shock protein 90 in neurodegenerative diseases*. Mol Neurodegener, 2010. **5**: p. 24.
10. Shiau, A.K., et al., *Structural Analysis of E. coli hsp90 reveals dramatic nucleotide-dependent conformational rearrangements*. Cell, 2006. **127**(2): p. 329-40.

11. Dollins, D.E., et al., *Structures of GRP94-nucleotide complexes reveal mechanistic differences between the hsp90 chaperones*. Mol Cell, 2007. **28**(1): p. 41-56.
12. Ali, M.M., et al., *Crystal structure of an Hsp90-nucleotide-p23/Sba1 closed chaperone complex*. Nature, 2006. **440**(7087): p. 1013-7.
13. Lavery, L.A., et al., *Structural asymmetry in the closed state of mitochondrial Hsp90 (TRAP1) supports a two-step ATP hydrolysis mechanism* 2013.
14. Morra, G., et al., *Corresponding functional dynamics across the Hsp90 Chaperone family: insights from a multiscale analysis of MD simulations*. PLoS Comput Biol, 2012. **8**(3): p. e1002433.
15. Meyer, P., et al., *Structural and functional analysis of the middle segment of hsp90: implications for ATP hydrolysis and client protein and cochaperone interactions*. Mol Cell, 2003. **11**(3): p. 647-58.
16. Hessling, M., K. Richter, and J. Buchner, *Dissection of the ATP-induced conformational cycle of the molecular chaperone Hsp90*. Nat Struct Mol Biol, 2009. **16**(3): p. 287-93.
17. Krukenberg, K.A., et al., *Conformational dynamics of the molecular chaperone Hsp90*. Quarterly reviews of biophysics, 2011. **44**(2): p. 229-55.
18. Krishna, P. and G. Gloor, *The Hsp90 family of proteins in Arabidopsis thaliana*. Cell Stress Chaperones, 2001. **6**(3): p. 238-46.
19. Richter, K., et al., *Conserved conformational changes in the ATPase cycle of human Hsp90*. J Biol Chem, 2008. **283**(26): p. 17757-65.
20. Leskovar, A., et al., *The ATPase cycle of the mitochondrial Hsp90 analog Trap1*. J Biol Chem, 2008. **283**(17): p. 11677-88.
21. Richter, K., J. Reinstein, and J. Buchner, *N-terminal residues regulate the catalytic efficiency of the Hsp90 ATPase cycle*. J Biol Chem, 2002. **277**(47): p. 44905-10.

22. Street, T.O., L.A. Lavery, and D.A. Agard, *Substrate binding drives large-scale conformational changes in the Hsp90 molecular chaperone*. *Molecular cell*, 2011. **42**(1): p. 96-105.
23. Street, T.O., et al., *Cross-monomer substrate contacts reposition the Hsp90 N-terminal domain and prime the chaperone activity*. *Journal of molecular biology*, 2012. **415**(1): p. 3-15.
24. Richter, K., et al., *Intrinsic inhibition of the Hsp90 ATPase activity*. *J Biol Chem*, 2006. **281**(16): p. 11301-11.
25. Prodromou, C., et al., *The ATPase cycle of Hsp90 drives a molecular 'clamp' via transient dimerization of the N-terminal domains*. *EMBO J*, 2000. **19**(16): p. 4383-92.
26. Cunningham, C.N., K.A. Krukenberg, and D.A. Agard, *Intra- and intermonomer interactions are required to synergistically facilitate ATP hydrolysis in Hsp90*. *J Biol Chem*, 2008. **283**(30): p. 21170-8.
27. Krukenberg, K.A., et al., *Multiple conformations of E. coli Hsp90 in solution: insights into the conformational dynamics of Hsp90*. *Structure*, 2008. **16**(5): p. 755-65.
28. Southworth, D.R. and D.A. Agard, *Client-loading conformation of the Hsp90 molecular chaperone revealed in the cryo-EM structure of the human Hsp90:Hop complex*. *Mol Cell*, 2011. **42**(6): p. 771-81.
29. Nathan, D.F. and S. Lindquist, *Mutational analysis of Hsp90 function: interactions with a steroid receptor and a protein kinase*. *Mol Cell Biol*, 1995. **15**(7): p. 3917-25.
30. Zuehlke, A. and J.L. Johnson, *Hsp90 and co-chaperones twist the functions of diverse client proteins*. *Biopolymers*, 2010. **93**(3): p. 211-7.
31. Liu, B., et al., *Folding of Toll-like receptors by the HSP90 paralogue gp96 requires a substrate-specific cochaperone*. *Nat Commun*, 2010. **1**: p. 79.



32. Mollapour, M. and L. Neckers, *Post-translational modifications of Hsp90 and their contributions to chaperone regulation*. *Biochim Biophys Acta*, 2012. **1823**(3): p. 648-55.
33. Rousset, S., et al., *The biology of mitochondrial uncoupling proteins*. *Diabetes*, 2004. **53 Suppl 1**: p. S130-5.
34. Ludtke, S.J., P.R. Baldwin, and W. Chiu, *EMAN: semiautomated software for high-resolution single-particle reconstructions*. *J Struct Biol*, 1999. **128**(1): p. 82-97.
35. Svergun, D., *Determination of the regularization parameter in indirect-transform methods using perceptual criteria*. *J. Appl. Crystallogr*, 1992(25): p. 495-503.
36. Svergun D.I., B.C.a.K.M.H.J., *CRY SOL - a Program to Evaluate X-ray Solution Scattering of Biological Macromolecules from Atomic Coordinates*. *J. Appl. Crystallogr*, 1995(28): p. 768-773.
37. R Development Core Team. *R: A language and environment for statistical computing*. 2010 [cited 2013; Available from: <http://www.r-project.org>].

## Chapter 3

### The role of the mitochondrial Hsp90 molecular chaperone (TRAP1) in Parkinson's disease

**Contributing Authors:** Nicholas T. Hertz, Ken Nakamura, Kevan M. Shokat  
and David A. Agard.

## Preface

During the course of my graduate work, David and I had an opportunity to work with a diverse collection of PI's (Robert Edwards, Kevan Shokat, Ken Nakamura, Eric Huang, and graduate student Nicholas Hertz) to apply to the Udall Foundation to create an Udall Center for Parkinson's Disease (PD) at UCSF. In our section of the center grant, we proposed to elucidate the role of the mitochondrial Hsp90 (TRAP1) in PD through its links to the PD related kinase, PINK1.

PINK1 is a mitochondrial kinase that has been linked to genetic forms of PD, where patient derived mutations render the kinase inactive through a variety of mechanisms [1-5]. TRAP1 has been identified as a substrate for PINK1 and phosphorylation of the chaperone has been shown to be cytoprotective, however the mechanism remains unknown. Specifically, we had proposed that TRAP1 has a role downstream of PINK1, and that PINK1 specific phosphorylation could modulate the chaperone's activity and thus client interactions to affect PD phenotypes. Though well founded, a direct link between TRAP1 and the etiology of PD remained a hypothesis. Very recently, two studies have demonstrated that TRAP1 can rescue PD phenotypes *in vivo* in PINK1 models for the disease in *Drosophila melanogaster*, and that the chaperone acts in parallel and synergistically with the PD related E3 ubiquitin ligase, Parkin [6, 7]. Importantly, the ATPase activity of TRAP1 was demonstrated to be necessary for phenotypic rescue. These results clearly demonstrate that TRAP1 is linked to a disease relevant signaling pathway downstream of PINK1, as well as firmly establishes TRAP1 as a novel biological target for PD.

From our efforts, we made great progress on the proof of principal results, established collaborations, as well as pushed our ideas and project direction. To this end, the background, a summary for this project, preliminary results, on-going experiments, and future directions make up this chapter of my thesis.

The work presented here in is a collaboration, where Nicholas Hertz mapped the PINK1-specific phosphorylation sites, the Parkin recruitment and mitochondrial bioenergetic measurements on the TRAP1 KO cells were done in the Nakamura lab (Gladstone, UCSF), and the  $^{13}\text{C}$ -Alanine NMR measurements were done by Kari Pederson in the lab of James Prestegard (University of Georgia, Athens). The TRAP1 KO mouse fibroblasts were provided by Didier Picard (University of Geneva). I am responsible for the remaining data in this chapter. Select protocols can be found in the Appendix of my thesis.

## Summary

Parkinson's Disease (PD) is an age-related neurodegenerative disorder characterized by selective cell death in the substantia nigra. Mitochondrial dysfunction has been implicated in PD through several patient derived mutations in proteins that are mitochondrially localized or linked to mitochondrial signaling pathways [8-10]. Of particular relevance here are mutations in the PINK1 kinase that have been linked to PD [1]. Importantly, PINK1 protects cells from oxidative-stress-induced cell death through specific phosphorylation of the mitochondria-specific chaperone [2], TRAP1, a homolog of the Hsp90 class of chaperones. This cytoprotective effect of PINK1 requires both an active kinase and the presence of TRAP1 as a substrate for PINK1 post-translational modifications (PTMs). These data suggest that the phosphorylation of TRAP1 affects the chaperone's function likely due to changes in structure, kinetics and/or regulation of its ability to bind and produce mature clients. Here we explore the mechanism of TRAP1 in mitochondrial quality control and identify the PINK1 specific phosphorylation sites. While previous studies have demonstrated phosphomimetics inhibit Hsp90 homologs, PINK1 specific phosphomimetic human TRAP1 (hTRAP1) displays a 2-fold enhancement of catalytic activity. Though further investigation is necessary, together with previous studies linking the chaperone to idiopathic forms of the disease, these results suggest that specific targeting of TRAP1 and/or TRAP1:client complexes could have therapeutic benefit in PD.

## **Background**

### **Mitochondrial dysfunction, Protein Quality Control, and Parkinson's Disease**

In recent years, evidence has mounted implicating mitochondrial dysfunction [8, 9] in PD and data is accumulating supporting a direct linkage to mitochondrial protein quality control pathways [10]. As discussed below, the mitochondria-specific Hsp90 molecular chaperone, TRAP1, is emerging as an important, PD relevant, component of mitochondrial protein homeostasis, showing linkage to both  $\alpha$ -synuclein and Parkin pathways. Here we explore this connection in molecular detail with the goal to further validate the relevance of TRAP1 signaling for PD, understand the molecular basis for the connection, and to develop leads for potential therapeutics.

The contribution of mitochondria to PD pathogenesis was first suggested by the discovery that the neurotoxin MPTP (1-methyl-4-phenyl-1,2,3,4-tetrahydropyridine) produces an irreversible parkinsonian syndrome in humans [11]. This toxin interferes with complex I of the mitochondrial electron transport chain and can result in the accumulation of toxic reactive oxygen species (ROS) [8]. Since then, several rare recessive genetic mutations have been discovered in patients with early-onset PD, which map to proteins that localize to or function in mitochondria (PINK1, DJ1), or are involved in signaling pathways linked to mitochondria (Parkin) [8]. Importantly, more recent studies have firmly linked Parkin to sporadic PD. Indeed, Parkin appears to be inactivated in sporadic PD [12-14], and has also been linked to PGC-1 $\alpha$  [13], a

transcription factor strongly associated with late-onset PD [15]. The link between mitochondria and sporadic PD has been further strengthened with the discovery that  $\alpha$ -synuclein associates with mitochondrial membranes [16, 17] where it induces changes in mitochondrial morphology that precede neuronal death by several days [17]. These findings thus support a critical role for the interaction of Parkin and synuclein with mitochondria in the pathogenesis of sporadic PD.

Of particular motivation here are three observations linking patient derived mutations in previously distinct pathways to the same mitochondrial molecular chaperone, TRAP1. First, and of importance for detailed discussions below, are patient derived mutations in the mitochondrial PTEN-induced putative kinase 1 (PINK1) that perturb its kinase activity, and inhibit the recruitment of Parkin to damaged mitochondria. A recent study identified TRAP1 as an important, and PD-relevant, substrate for PINK1 [2]. Second, two very recent studies have demonstrated that TRAP1 can rescue PD phenotypes in a PINK1 model for the disease in *Drosophila melanogaster*, as well as show that the chaperone acts in parallel and synergistically with the PD related E3 ubiquitin ligase, Parkin [6, 7]. Importantly, the ATPase activity of TRAP1 was demonstrated to be necessary for phenotypic rescue utilizing the non-binding mutant for Hsp90 homologs [18]. These results clearly demonstrate that TRAP1 is linked to a disease relevant signaling pathway downstream of PINK1. Third, it was demonstrated [19] that TRAP1 overexpression blocks both mitochondrial fragmentation and the toxicity of A53T mutant  $\alpha$ -synuclein in *Drosophila*, rat primary neurons, and human neuronal and non-neuronal cell lines. Although a definitive role for mitochondrial

fragmentation in synuclein toxicity has not been proven, mitochondrial fragmentation precedes and predicts cell death produced by  $\alpha$ -synuclein in neurons [17]. This newly discovered link between TRAP1 and  $\alpha$ -synuclein implicates TRAP1 in the sporadic disease, suggests the existence of a common pathway, and strengthens the link between sporadic PD and mitochondria. As a molecular chaperone, we expect TRAP1 function to be mediated through functional interaction with its client proteins.

### **Hsp90, TRAP1 and Protein Quality Control**

Although not extensively studied, TRAP1 is a member of the highly abundant Hsp90 molecular chaperone family known to play a critical role in protein homeostasis within the cytoplasm [20]. In higher eukaryotes, four homologs of Hsp90 exist in each cell: two that reside in the cytosol (Hsp90 $\alpha/\beta$ ), one in the ER (Grp94) and one in mitochondria (TRAP1) [21]. Interestingly, although the conformational states are conserved, the equilibria and kinetics are specific to each Hsp90 homolog [22], suggesting an optimization for a particular set of client proteins located in each cell type or compartment. Given this and the high level of Hsp90 conservation from bacteria to mammals [23], it is likely that information gleaned from previous studies on the cytosolic Hsp90s will be quite relevant in the understanding of TRAP1 function and visa versa (in support of this, see chapters 1 and 2).

Cytosolic Hsp90s have been shown to affect the folding and activation of a broad array of substrate “client” proteins, including many involved in signaling and regulatory processes [20]. In addition to its facilitation of individual proteins, Hsp90 plays a broader



regulatory role in establishing protein homeostasis in the cytosol by suppressing the activation of the stress-response transcription factor HSF1 [24] and pro-apoptotic factors such as IP6K2 [25] and FKBP38 [26, 27]. In healthy cells the abundance of free Hsp90 allows the chaperone to simultaneously promote maturation of its specific clients, maintain inhibition of pro-apoptotic factors, as well as buffer protein damage and aggregation. Accumulation of misfolded clients leads to the release and subsequent activation of HSF1, inducing the protein stress response [24]. However, when the stress and cellular damage are prolonged, the ability of Hsp90 to balance between these functions appears to be compromised as pro-apoptotic factors are then able to initiate programmed cell death pathways.

Significantly, we expect this dual theme of protein folding and homeostatic surveillance to extend to TRAP1. Within the mitochondria, molecular chaperones and proteases work together to maintain healthy organelles. When the level of protein damage increases, the mitochondrial Unfolded Protein Response (UPR) signals to the nucleus; stimulating the levels of the protein quality control factors [28]. If homeostasis cannot be restored, then mitophagy (terminally damaged mitochondria removed by lysosomal degradation) pathways may be triggered [29]. Importantly, mitochondrial dysfunction and loss of integrity can also trigger programmed cell death pathways (reviewed in [30], which may trigger neuronal death found in vulnerable neurons such as dopaminergic neurons of the substantia nigra in PD. Studies from the cancer literature have already identified TRAP1 as a negative regulator of cell death. TRAP1 binds to and inhibits cyclophilin D (CypD), which induces cell death through opening of the

mitochondrial permeability transition pore (mtPTP) [31]. Together, these studies support a central role for TRAP1 in maintaining mitochondrial homeostasis and highlight CypD as a candidate for downstream effects upon modification by PINK1 (a potential PD-relevant PINK1:TRAP1:CypD signaling pathway).

### **Hsp90 mechanism of action**

Owing to its importance in cell function and human diseases such as cancer [32, 33] and neurodegenerative disorders [34], significant effort has focused on discovering Hsp90's molecular mechanism of function. Unique to the Hsp90 class of chaperones is the preferential interaction with near native states [35] of its client proteins and the ability to induce subtle rearrangements to activate them for downstream protein-protein and protein-ligand interactions [36].

Structurally, all Hsp90s are homodimers consisting of three domains: the N-terminal domain (NTD), which is the site for ATP binding and hydrolysis; the middle domain (MD), which aids in hydrolysis; and the C-terminal domain (CTD), which provides the dimeric interface for the molecule [37]. Full-length x-ray crystal structures [38-40] have shown that each domain exposes regions of hydrophobic surface postulated to be involved in client protein recognition. Binding and hydrolysis of ATP leads to significant conformational changes and is essential for client maturation in vivo [18] providing a model for the functional chaperone cycle (Figure 1, abstract pg vii) [37]. More recently, Small Angle X-ray Scattering (SAXS) [41, 42] and Electron Microscopy (EM) [22, 40] revealed that Hsp90 is highly dynamic and can adopt a wide variety of

structurally distinct open states. The inherent flexibility and combinatorial use of conformational states is believed to underlie Hsp90's ability to interact with such a diverse array of clients. Recently we updated this model through the elucidation of a previously unknown asymmetric closed state conformation of the Hsp90 homodimer visualized in the first crystal structure of full-length TRAP1 bound to ATP analogs [43]. Using a diverse set of biophysical and biochemical assays (SAXS, DEER, steady-state kinetics, EM, CD, crystallography) we show that this conformation is populated in solution, functional for ATP hydrolysis, and is conserved from bacterial Hsp90 (bHsp90) to human TRAP1 (hTRAP1). Importantly, the different conformation of the two chemically identical promoters results in the differential presentation of client binding residues suggesting a model for how the essential hydrolysis step is coupled to client folding (for further details, see chapter 1).

In the eukaryotic cytosol, activation of client proteins is accomplished with the aid of co-chaperones [44], in contrast the prokaryotic and organellar Hsp90s largely lack Hsp90-specific co-chaperones where only one has been identified for Grp94 [45]. In addition to co-chaperones, post-translational modifications such as acetylation, S-nitrosylation, and phosphorylation have been shown to regulate the chaperone cycle as well as affect substrate binding [46]. To date, relatively little is known about how client proteins are recognized by the chaperone, where the interaction surfaces are, or how Hsp90's highly dynamic yet conserved conformational motions are coupled to client protein maturation/regulation. As mentioned above, our recent efforts with TRAP1 have afforded traction on the latter.

## **TRAP1 regulates the Mitochondrial Permeability Transition Pore through Cyclophilin D**

TRAP1 is a nuclear encoded, 75kDa (monomer size) chaperone originally identified as a binding partner of tumor necrosis factor receptor 1 [47]. Since its identification, TRAP1 has been shown to be a mitochondrial-localized [48] Hsp90 homolog closest in origin to the bHsp90 [23]. Accordingly, TRAP1 lacks features characteristic of all eukaryotic cytosolic Hsp90s: the long charged linker near the NTD-MD interface and the C-terminal MEEVD sequence known to bind TPR containing co-chaperones [23]. Mirroring this, TRAP1 was unable to promote *in vitro* hormone binding to progesterone receptor, a classical substrate of cytosolic Hsp90 [48]. Unique features of TRAP1 also exist, including the N-terminal mitochondrial targeting signal, localization to both the matrix [31, 49] and the inner membrane space [2] and a characteristic LXCXE motif in the MD [23]. Previous studies have reported a comparable ATPase activity to other Hsp90s and inhibition by Hsp90 specific drugs [43, 50] including specific inhibitors targeted to the mitochondria [51-53].

In recent years, important biological functions of TRAP1 are beginning to emerge highlighting a critical role in regulating protein homeostasis inside the mitochondria [54]. Specifically, TRAP1 has been implicated in signaling pathways of mitochondrial fission/fusion [55], mitophagy [2, 6, 7], as well as bioenergetic maintenance [56] and the necrotic form of cell death through regulating cyclophilin D (CypD) [31]. Interestingly, recent reports have identified a role for TRAP1 in extra mitochondrial

signaling through crosstalk with the ER [57, 58]. This is compatible with the physical association of the two organelles [59]. A small number of TRAP1 specific clients have been identified [31, 57, 60-62] with the potentially most relevant here being CypD [31].

CypD (a soluble, small immunophilin protein) is a central component of the mitochondrial permeability transition pore (mtPTP) and the master regulator of its open/closed transition [30]. In healthy mitochondria, the mtPTP exists in a low conductance state [30]. The high conductance state of the pore is induced by  $\text{Ca}^{2+}$  overload, increased oxidative stress and decreased levels of adenosine nucleotides [30], although how these stressors couple to pore opening is unknown. Prolonged opening of the channel leads to loss of membrane potential ( $\Delta\Psi_m$ ), which appears to be required for Parkin recruitment. Eventually, this leads to rupturing the outer mitochondrial membrane, release of cytochrome C and cell death. This intrinsic cell death pathway results in necrosis [63] and is distinct from apoptotic pathways initiated by cell death receptors and the Bcl-2 family of proteins. In mouse models, knockout of CypD (*ppif<sup>-/-</sup>*) decreased sensitivity to oxidative stress, MPTP-induced membrane depolarization, and increased the  $\text{Ca}^{2+}$  storage capacity of the mitochondria [63-65]. Adenovirus gene transfer of WT but not a catalytically dead CypD can reverse this phenotype [64]. These data suggests that the loss of functional CypD is protective from necrotic cell death.

Not only can TRAP1 bind CypD, but its binding antagonizes the ability of CypD to open the mtPTP [31]. In keeping with this, numerous studies report that TRAP1 overexpression renders cells resistant to cell death [66, 67]. Conversely, siRNA

knockdown of TRAP1 or inhibition by mitochondria-targeted Hsp90 inhibitors increases the sensitivity to mitochondrial perturbation [2, 31, 52, 66, 67]. CypD binding by TRAP1 is observed both in vivo and in vitro, and can be inhibited by addition of TRAP1- or CypD-specific inhibitors [31]. Though it is clear that this pathway is important for regulating the cell fate decision, further investigation is necessary to understand how TRAP1 blocks CypD mediated opening of the mtPTP, as well as how the interaction between TRAP1 and CypD is modulated within mitochondria to only trigger CypD release under appropriate conditions. Reaching a molecular understanding of this process will prove invaluable in understanding a fundamental cell-death pathway and in the discovery of drugs that can appropriately modulate the TRAP1:CypD complex even in the context of patient-derived mutations in PINK1 to affect cell-fate decisions.

While CypD appears to be a very PD-relevant TRAP1 client, other identified or yet to be unidentified client proteins may be equally important in either maintaining mitochondrial homeostasis or communicating mitochondrial dysfunction. Hence, a proposal to discover, validate and structurally characterize new PD-relevant client proteins in parallel with studies aimed at CypD is outlined in the later section of this chapter.

### **Phosphorylation of TRAP1 by PINK1 affects cell fate**

Since the discovery of genetic contributions to early onset PD, disease-linked mutations have been identified in PINK1 [1]. Interestingly, PINK1 heterozygous mutations have been identified in late onset PD patients [2]. PINK1 is a 581 amino acid

mitochondrial kinase, consisting of an N-terminal localization tag, a putative transmembrane domain (residues 101-107), a serine-threonine kinase domain (residues 156-509), and a C-terminal regulatory domain [3]. Through a variety of mechanisms, disease-relevant mutations generally compromise kinase function [1-5].

PINK1 plays a role in processes necessary for normal mitochondrial biology and protein quality control [1, 68]. Several of these are in a common pathway with the E3 ubiquitin-protein ligase, Parkin. These include regulation of mitochondrial fission/fusion [69], regulation of mitochondrial motility [70], and recruitment of Parkin to damaged mitochondria for initiation of mitophagy [71]. Importantly, the latter is also promoted by low  $\Delta\Psi_m$  [72, 73], by binding of PINK1 to Beclin 1 (a protein known to regulate autophagosome formation) [74], and preceded by severing the organelle from the microtubule network [15]. Though the signaling pathway between PINK1 and Parkin leading to these later steps of mitophagy remains unclear, loss of membrane potential is thought to be required for faithful Parkin recruitment [75]. Importantly, in cultured human cells and animal models, PINK1 was shown to suppress cell death pathways initiated by several factors including high calcium levels [76, 77], reactive oxygen species [2, 4, 78] and exogenous pro-apoptotic compounds [79-81]. Though several groups had reported this phenomenon, mechanistic understanding was lacking until the discovery of the first substrate protein of the kinase, TRAP1 [2].

In a landmark study by Pridgeon et al, the authors demonstrate that PINK1 and TRAP1 co-localize in the mitochondria and show that WT, but not PD-linked mutant forms of the kinase phosphorylate TRAP1 both in vivo and in vitro. Further, siRNA

knockdown of TRAP1, WT PINK1, or the presence of PD-relevant mutants of the kinase resulted in increased cytochrome C release and cell death when challenged with oxidative stressors. PINK1 localization was not affected by pathogenic mutations tested. Importantly, overexpression of WT PINK1 was cytoprotective, whereas overexpression of WT PINK1 in TRAP1 depleted cells was not - clearly demonstrating that TRAP1 is a downstream cytoprotective effector of PINK1. These data demonstrate a novel pathway, whereby PINK1 protects cells from oxidative-stress-induced cell death through specific phosphorylation of TRAP1. Very recently, with our colleague Nicolas Hertz (Shokat Lab), it was demonstrated that an ATP analog (kinetin triphosphate, KTP) can rescue mutant PINK1 catalytic activity and phosphorylation of TRAP1 *in vitro* (recombinant purified, Appendix A) where a loop insertion in the active site of the kinase allows for analog specificity [82]. They went on to show that this drug could rescue PINK1 phenotypes *in vivo*, suggesting that downstream phosphorylation of PINK1 substrates is key to PD progression.

We hypothesize that phosphorylation of TRAP1 would mediate down-stream effects through altered interactions with key TRAP1 client proteins. By analogy with the role of cytosolic Hsp90s in monitoring protein homeostasis in the cytoplasm, we propose that TRAP1 is uniquely poised to integrate information on protein homeostasis and perhaps other aspects of physiology (pH, Ca<sup>++</sup>, etc.) within the mitochondria into a decision to either facilitate mitophagy or cell death. This could be via the CypD:mtPTP membrane depolarization pathway or presently unidentified pathways. Phosphorylation of TRAP1 could then alter the “set point” or sensitivity in signaling homeostatic failure.



While this can provide a general model of how at least some of the PINK1 mutations seen in familial PD patients may be functioning, lagging is a mechanistic understanding of how TRAP1 functions (though studies of TRAP1 have provided new mechanistic inroads chapters 1 and 2), how its behavior is modulated by PINK1 and how this might affect interactions with CypD or other key mitochondrial clients.

Through a combination of biochemical and biophysical approaches we focus on the role and mechanism of TRAP1, seeking to identify how phosphorylation by PINK1 modulates TRAP1 function and to determine if there is a direct link between phosphorylation and TRAP1's ability to bind and interact with CypD or other mitochondrial client proteins. Results from this study will information will facilitate the discovery of novel small molecules focused on modulating TRAP1 function for potential intervention in PD.

## **Results**

### **TRAP1 KO cells show defects in Parkin-mediated Mitophagy**

Depolarization of mitochondria leads to the stabilization and accumulation of PINK1 on the outer mitochondrial membrane [73, 83, 84], which leads to recruitment of Parkin and ultimately mitochondrial degradation. However, the mechanism by which PINK1 produces Parkin recruitment is not known. Considering TRAP1's known role as a PINK1 substrate, we hypothesized that TRAP1 may also play an important role in regulating Parkin recruitment. Consistent with this, (in collaboration with Ken Nakamura)

we found that cells lacking TRAP1 (TRAP1 KO, from Didier Picards's lab) are resistant to Parkin-based mitophagy following depolarization (Figure 1) with the mitochondrial uncoupler FCCP (carbonyl cyanide 4-(trifluoromethoxy) phenylhydrazone). While preliminary, these data suggests that PINK1 may promote Parkin recruitment through effects on TRAP1. One possibility is that the change in Parkin recruitment is due to changes in membrane potential through downstream effects of TRAP1 PTM, which is known to affect Parkin recruitment [75].

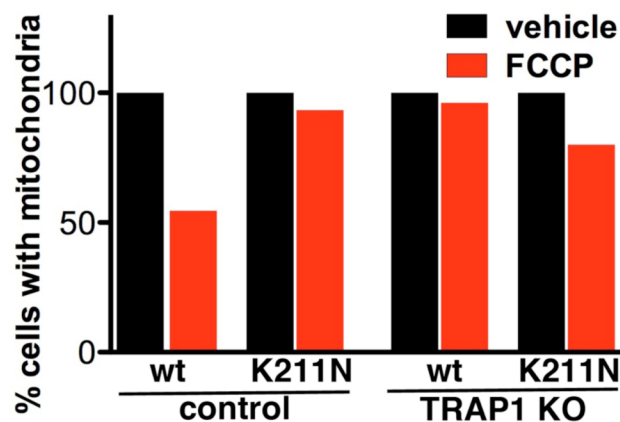


**Figure 1. TRAP1 is required for Parkin-dependent mitophagy.** TRAP1 KO or control fibroblast cells were transiently transfected with wild type (wt) or K211N mutant Parkin, treated with 10  $\mu$ M FCCP for 48 hours, fixed, immunostained for Tom20 and assessed for the presence or absence of mitochondria. Wild type Parkin produces robust mitophagy that is not evident in TRAP1 KO cells.

### **TRAP1 KO cells have impaired mitochondrial bioenergetics similar to PINK1 KO**

Although the mechanism by which PINK1 triggers Parkin recruitment is unknown, it may involve TRAP1-mediated effects on mitochondrial bioenergetics and/or the mtPTP. Indeed, PINK1 is required to maintain normal mitochondrial bioenergetics, and loss of PINK1 results in decreased basal respiration and a dramatically altered

response of membrane potential to oligomycin [76, 85]. This abnormal response to oligomycin may reflect underlying respiratory failure in PINK1 KO cells with the mitochondrial membrane maintained by reverse pumping of protons through the mitochondrial H<sup>+</sup>-ATP synthase [76]. Alternatively, the response to oligomycin could indicate aberrant regulation of the mtPTP in PINK1 KO cells. Indeed, oligomycin can also interact directly and/or indirectly with the mtPTP [86, 87], and oligomycin can produce a shift in the threshold of mtPTP opening that predisposes to a rapid loss of mitochondrial membrane potential [86]. Consistent with this, (in collaboration with Ken Nakamura) our preliminary studies show that TRAP1 KO cells also show a very anomalous response to oligomycin, exhibiting a markedly subdued glycolytic response (Figure 2) that suggests a decreased ability to compensate for respiratory dysfunction. These results are consistent with recent reports of TRAP1 mediated control of bioenergetic function [56, 88, 89]. We hypothesize that loss of PINK1 may result in a TRAP1-dependent shift in the threshold for opening of the mtPTP, and this could underlie the aberrant effects of PINK1 on bioenergetic function and may also regulate Parkin recruitment.

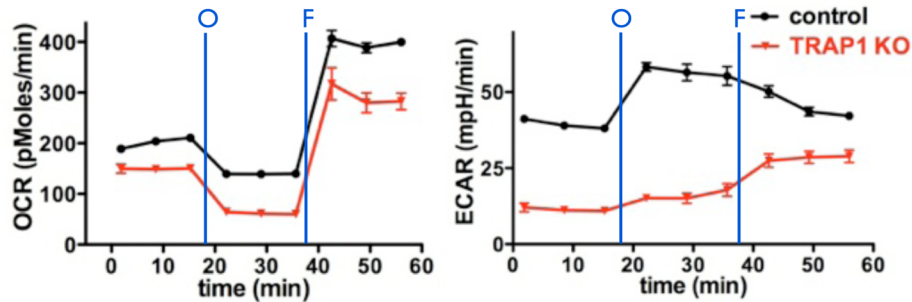


**Figure 2. Metabolic defects in TRAP1 KO cells.** Control and TRAP1 KO fibroblasts were sequentially exposed to control medium, oligomycin (O addition; inhibits ATP synthase, blocking oxygen consumption), and FCCP (F addition; uncoupler to assess maximal respiratory rate). Using a Seahorse Analyzer, respiration (left, O<sub>2</sub> consumption rate [OCR]), and glycolysis (right, extracellular acidification [ECAR]) were measured. TRAP1 KO cells showed decreased basal and maximal respiration, similar to PINK1 KO cells. In addition, there is a markedly blunted glycolytic response to oligomycin indicating a blunted glycolytic response.

### **PINK1 phosphorylates TRAP1 in known functional regions of the chaperone**

In collaboration with Nicolas Hertz in the Shokat lab, we have identified PINK1 specific phosphorylation sites in TRAP1. For this we utilized the fact that PINK1 accepts N<sup>6</sup> modified ATP analogs as a substrate where most kinases cannot and applied a phospho-peptide capture and release strategy developed in the Shokat lab [82, 90, 91]. Specifically, we incubated recombinantly expressed WT or KDDD PINK1 from a baculovirus co-expression system [82] and added the protein to isolated mouse whole brain lysate [92] along with N<sup>6</sup> furfuryl ATP $\gamma$ S (KTP $\gamma$ S) and recombinantly expressed hTRAP1, where 5% of the total protein was the chaperone (for expanded WT hTRAP1 purification see Appendix). The thiophosphate label provides a bio-orthogonal tag that can be used to affinity purify and identify sites on labeled proteins by LCMSMS. From this a handful of statistically significant peptide fragments were identified (S121, S367,

S401, S408, S454), with three containing phosphosites specific to WT PINK1 only (S121, S367, T454, Figure 3), and one found in both WT and kinase-dead (S401).

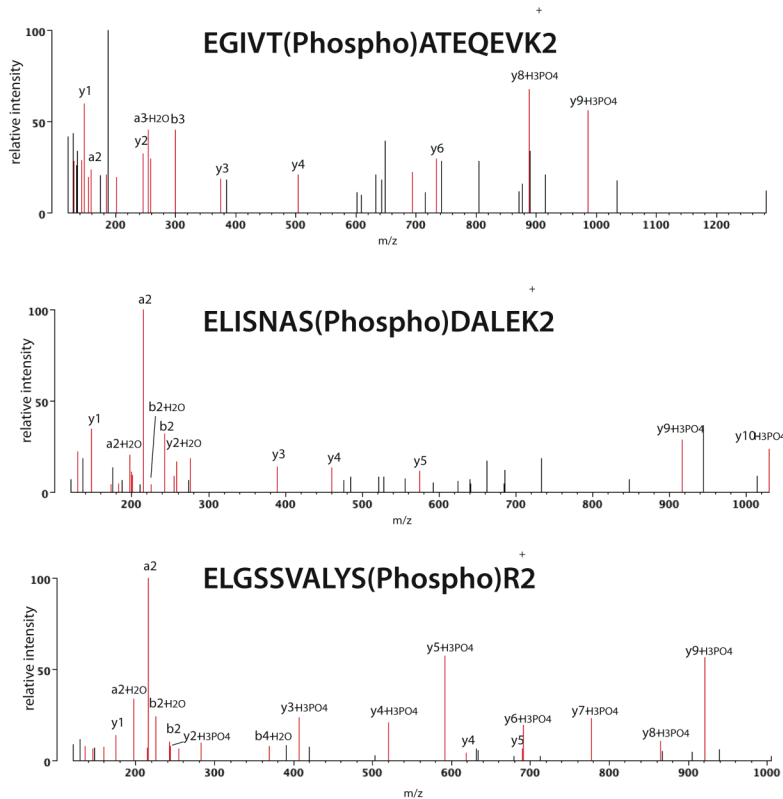


**Figure 3.** MS/MS spectra identifying the three primary PINK1-derived phosphopeptides within hTRAP1.

Interestingly the residues identified as phosphorylation sites specific to WT (S121, S367, T454) map to potentially sensitive regions of the chaperone (Figure 4, green residues). More specifically, at the N-M interface near the catalytic glutamate (Figure 4, blue residue) [18, 39, 43], as well as near in the middle domain of the chaperone in the region near the binding site for our model substrate,  $\Delta 131\Delta$  (Figure 4, red residues) [93-95]. Thus PINK1-mediated phosphorylation would be expected to alter

the conformational dynamics, ATPase rates and/or client protein binding as proposed above.

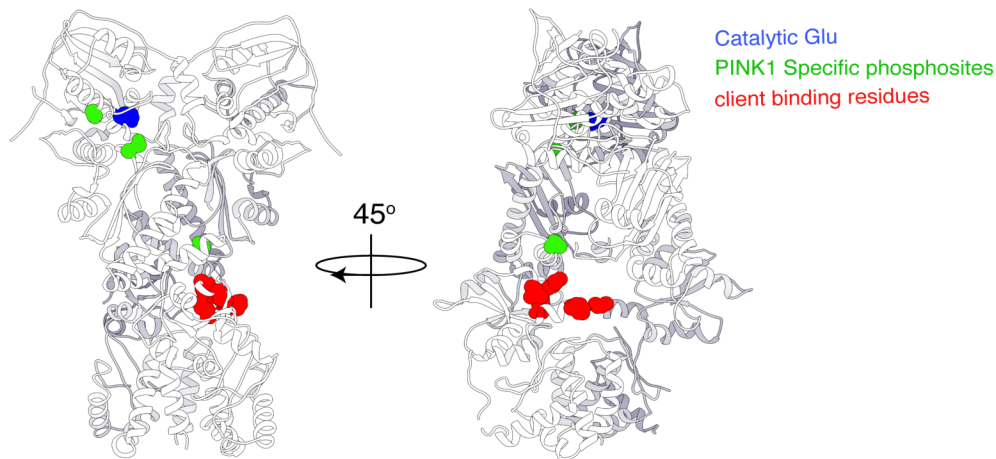


**Figure 4. PINK1 specific phosphorylation sites identified for hTRAP1.** Identified phosphosites and catalytic residues are mapped onto the crystal structure of TRAP1 from zebrafish [43] (pdb code: 4IPE) labeled in green and blue, respectively. The client binding residues are colored in red. Apparent is the proximity to the PINK1 PTM to known functional regions of Hsp90.

### **Phosphomimetic mutations at identified sites stimulate the catalytic activity of TRAP1**

While we do not yet have sufficient phosphorylated TRAP1 to directly assess effects of phosphorylation, as an initial experiment we sought to see if mimicking phosphorylation at the WT PINK1 specific sites (S121, S367, T454) would affect the ATPase activity of TRAP1 as hypothesized above. As a first step, we mutated all three sites to glutamate and tested the ATPase activity of the phosphomimetic TRAP1 relative to wild-type (WT) with a previously reported activity (assay conditions as in Lavery et al./chapter 1, temperature was 37°C) [43, 50]. In line with our hypothesis, the phosphomimetic showed a 2-fold enhancement of activity over WT (Figure 5). The next

steps will be to dissect the functional consequences of these three sites using four different assays: ATPase, closure kinetics, temperature dependence, client interactions using CypD or our model client  $\Delta 131\Delta$ , as well as *in vivo* (outlined below). We plan to try individual mutations as well as combinations, explore use of Asp as an alternative to Glu, Ala as a control, as well as making other substitutions. These results and future experiments will afford an understanding of the biochemical and biophysical consequences of PINK1 specific phosphorylation.

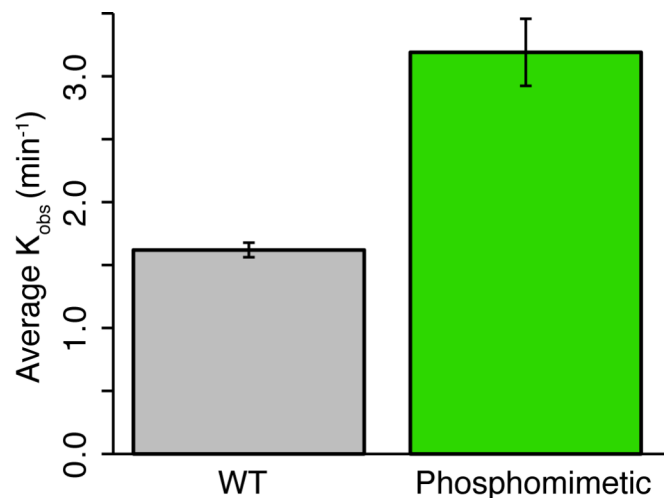


**Figure 5. Phosphomimetic hTRAP1 shows a 2-fold enhancement of ATPase.** Average ATP hydrolysis rates of WT human TRAP1 and human TRAP1 containing phosphomimetic mutations at all three sites (S/T to E). A 2-fold enhancement of TRAP1 activity is observed with phosphomimetic mutations at PINK1 specific phosphorylation sites.

To extend *in vivo*, we have established a collaboration with Dr. L. Miguel Martins (University of Leicester), whose lab published one of the recent studies demonstrating TRAP1 specific rescue of PD phenotypes in PINK1 mutant flies [7]. We have now mutated the analogous phosphosites in TRAP1 from flies (*Drosophila melanogaster*, fTRAP1) to either the phosphomimetic (all Glu mutations) or phosphomutant (all Ala

mutations) forms. The mutant fly lines are currently being generated and will be tested for their ability or deficiency (respectively) to rescue phenotypes observed in TRAP1 KO and PINK1 mutant flies. Here our hypothesis is that the phosphomimetic flies should show significant rescue and benefit to both mutant fly lines, while the phosphomutants should no longer be capable of rescue. These results would functionally validate our identified sites *in vivo*, and provide a platform to study downstream effects on client signaling, interactions and re-modeling mediated by TRAP1. For the latter, though CypD is a well-founded candidate for study, a need for the elucidation of TRAP1 clients specific to the PINK1 signaling pathway is apparent. Towards this, a proposal for identifying clients sensitive to PINK1 specific phosphorylation of TRAP1 is outlined in the sections that follow.

### **TRAP1 interaction with CypD and $\Delta 131\Delta$**

Although the ability of Hsp90s to assist both general protein folding and to activate specific classes of client proteins for downstream signaling events [20] has been appreciated for some time, working out the molecular mechanism of Hsp90 action has proven quite challenging for three main reasons: the Hsp90 structure is highly dynamic [37] making crystallization difficult; Hsp90 preferentially interacts with non-native but largely-folded states of its client proteins [35, 96] which are poorly populated and have a strong tendency to aggregate; and the eukaryotic cytosolic Hsp90s work with a large ensemble of co-chaperones [44] greatly increasing the challenge of *in vitro* reconstitution. While we continue to pursue bone fide client proteins that are strongly



dependent on Hsp90 for *in vivo* folding and function, a model non-native state protein has provided critical insights into Hsp90-client interactions and promises to do the same for TRAP1.

Extensive studies have shown that a 131-residue fragment of Staphylococcal nuclease ( $\Delta 131\Delta$ ; full length is 149 residues) is globally unfolded but remains compact with residual structured regions [97-99]. Importantly,  $\Delta 131\Delta$  is monomeric at high concentrations, stable under a wide variety of conditions, amenable to NMR, and can be refolded by the addition of a tight binding inhibitor [100]. Labeling  $\Delta 131\Delta$  with IAEDANS allows its binding to Hsp90 to be examined by fluorescence polarization anisotropy [94] ( $K_d$  of  $\sim 10\mu\text{M}$ , although the value varies slightly depending on species and conditions), and refolding  $\Delta 131\Delta$  blocks Hsp90 binding [94]. SAXS reveals that  $\Delta 131\Delta$  binding drives Hsp90 into a more V-shaped conformation with one  $\Delta 131\Delta$  bound per Hsp90 dimer [94]. Hsp90 is a slow ATPase (0.1 – 1 ATP/min). By attaching donor and acceptor fluorophores [94, 101], the large conformational changes associated with the addition of the non-hydrolysable ATP analog, AMPPNP (apo state  $\rightarrow$  ATP state) can be measured revealing that the closure transition is rate limiting for ATP hydrolysis. In a quite surprising result, addition of the model client  $\Delta 131\Delta$  greatly accelerates closure and hydrolysis revealing that while Hsp90 catalyzes conformational rearrangements in its client proteins, they too catalyze conformational changes within Hsp90 that in turn accelerate ATP hydrolysis [94, 95, 102]. This has the benefit of only utilizing significant ATP when Hsp90 is “engaged” with its clients.

A significant advantage of using  $\Delta 131\Delta$  as a model system is that it is amenable to NMR. To gain a higher resolution picture of the interaction site on  $\Delta 131\Delta$ , we measured the  $\Delta 131\Delta$   $^{15}\text{N}$  HSQC spectrum with and without bacterial Hsp90. We observe that a subset of peaks disappear while others have reduced intensity [94]. The fractional loss of peak height mapped to a  $\sim 30$  residue region of  $\Delta 131\Delta$ , corresponding to the most highly structured region [98] within the largely unfolded ensemble. These findings are consistent with previous reports that Hsp90 interacts with near-native state proteins. NMR strategies based on specific amino acid labeling [103] have also been used to determine an approximate binding site for  $\Delta 131\Delta$  or the Hsp90 middle domain and this has been confirmed by mutation [95]. Recent genetic and biochemical data in collaboration with the Wickner lab extend these results, identifying a conserved MD:CTD pocket responsible for  $\Delta 131\Delta$  binding to the bacterial chaperone and also proper function of yeast Hsp90 [93]. This demonstrates both the conserved nature of Hsp90:client interactions and the broad utility of  $\Delta 131\Delta$  for exploring these interactions in molecular detail. Importantly, the identified binding site is positioned at the region of most pronounced asymmetry in our closed state TRAP1 structure and we have proposed new mechanism for Hsp90 whereby the energy of ATP hydrolysis is directly connected to re-model clients bound to this region [43]. Our new full-length Hsp90 structure is a significant accomplishment and will be critical for mapping PINK1, CypD and novel client binding sites, as well as designing mutants and refining small molecule allosteric modulators toward our future goals. To test the function of TRAP1 with  $\Delta 131\Delta$ , we used our FRET-based closure assay for hTRAP1 (see chapter 2 methods) and

found that client acceleration by  $\Delta 131\Delta$  is conserved (chapter 2, figure S5). Towards our goals, the FRET assays have now been adapted to 384-well plates, and a post-doc in the lab (Joe Tao) has now undertaken a high-throughput screen to identify small molecules that modulate TRAP1 closure kinetics and client interactions under defined conditions.

As with our model client  $\Delta 131\Delta$ , the NMR spectra for CypD has been fully assigned (backbone and side chains) [104]. Paralleling our work with  $\Delta 131\Delta$  [95], we  $^{15}\text{N}$ -labeled human CypD, incubated it with TRAP1 and recorded HSQC spectra (Figure 6) (see lab notebook #5, pg 23-38 for expression and purification details). As is immediately apparent, while the free CypD gives an excellent, well-dispersed spectrum, the vast majority of the peaks disappear upon addition of equimolar TRAP1 (~1:1, CypD:TRAP1 dimer). The few peaks that remain correspond to the disordered N-terminal tail, some disordered loops and are generally removed from the active site. Since peaks from all over the molecule disappear, it is most likely that TRAP1 binds CypD sufficiently tightly for its tumbling to correspond to the aggregate molecular weight for the complex, thereby relaxing and broadening the peaks to the point they become unobservable.

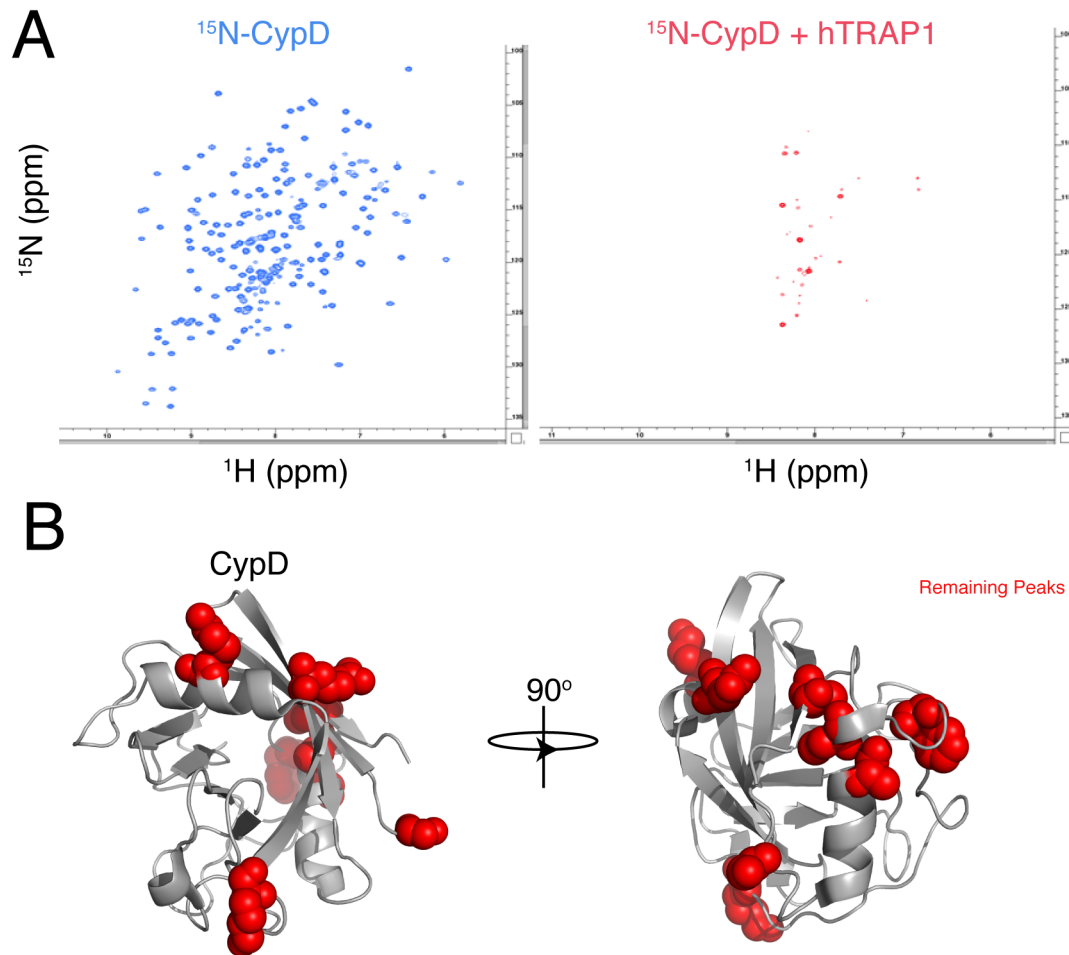


**Figure 6. hTRAP1 interacts with human CypD in vitro.** A) HSQC spectrum of CypD (left) most peaks disappear on adding equal molar hTRAP1 (right) indicating binding. B) Preliminary mapping of residues from previous assignment. Remaining peaks are generally located away from the active site (preliminary remaining peaks: M1, G2, R19, A38, C40, F46, K91, K141, C161).

While preliminary, this is an excellent beginning indicating that stable complexes of this bone fide TRAP1:client interaction form *in vitro*. It is worth noting that CypD has some advantages for investigating chaperone:client interactions *in vitro* as it is a small and soluble protein ideal for biochemical and structural studies. If necessary, it may be possible to alter the folding landscape (ala  $\Delta 131\Delta$ ) with mutations or conditions to stabilize the interaction with TRAP1 if the affinity is not high enough in the case of WT

CypD. Further, because TRAP1:CypD phenotypes are known, the functional consequences of changes to this interaction can be assayed *in vivo*.

### **Development of $^{13}\text{C}$ -labeled NMR assay for full-length hTRAP1**

Although quite challenging because of the size, NMR provides a tremendous potential to map transient binding sites onto Hsp90 and to explore the consequent conformational changes induced in clients. We have recently established a collaboration with Dr. James Prestegard (University of Georgia, Athens) to use build a NMR based assay for studies with Hsp90 (~150KDa) and have begun the first experiments using a perdeuterated  $^{13}\text{C}$ -Ala-labeled sample (Final buffer: 20mM  $\text{Na}_2\text{HPO}_4$  pH 6.5, 50mM KCl, 2mM  $\text{MgCl}_2$ , 1mM deuterated DTT in  $\text{D}_2\text{O}$ ) [105] (for  $^{13}\text{C}$ -hTRAP1 purification see Appendix). Using very little material (~70uL of 50uM dimer) we have already obtained spectra of hTRAP1 where most of the expected Ala residues (51) are visible and well dispersed (Figure 7). Further, upon addition of an ATP analog we observe shifts in a subset of peaks consistent with a conformational change as would be expected (Figure 7).

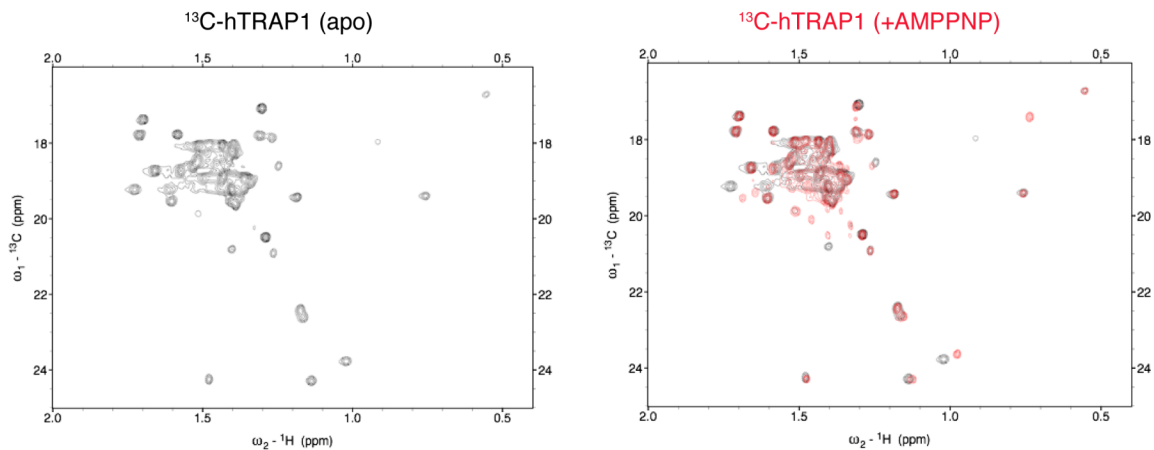


**Figure 7.  $^{13}\text{C}$ -NMR of full-length hTRAP1.** NMR spectra of full-length hTRAP1 in the apo (left) and with addition of saturating AMPPNP (right) overlaid with the apo spectra. From the spectra most of the 51 expected peaks (number of Ala residues in recombinantly purified hTRAP1) are visible. Changes to peaks observed in apo upon addition of AMPPNP are apparent from the overlaid spectra.

This is an excellent start, with more optimization to be done as well as assignment of the Ala via the individual domains and alternative strategies (on-going).  $^{13}\text{C}$ -RDCs should be particularly useful for analyzing conformational changes in the domains and are being explored. This system will provide an excellent assay for the assignment of client binding sites as well as the potential to detect structural rearrangements in client proteins if the client instead of the chaperone is  $^{13}\text{C}$ -Ala labeled. Future experiments are outlined below.

## **Proposed Future Experiments**

Though writing the Udall grant we outlined extensive future experiments toward elucidating the role that TRAP1 plays in PD. Below is a version of this plan, which I have edited with new knowledge of the TRAP1 system (contributed by us and others) and keeping in mind newly established collaborations. Additionally, an extensive plan for *in vivo* experiments aimed to assay TRAP1 effects on PINK1 and  $\alpha$ -synuclein phenotypes were outlined in the second submission of the grant. For the purposes of clarity, to focus on what I think are the most immediate/exciting next steps for the lab, and with the recent findings that TRAP1 can rescue of PINK1 phenotypes, I have omitted these sections in this chapter of my thesis. For further details please ask for a copy of the second round of our Udall Center grant proposal.

## **Experimental Approach**

As discussed above, very little is known about how the Hsp90 class of chaperones facilitates folding and activation of its diverse set of client proteins. In the case of TRAP1 even less is known about its cellular context including how this homolog functions to monitor and direct protein homeostasis within the mitochondria and, when necessary, initiate cell death pathways. Both of these activities are linked to mitochondrial dysfunction and thus likely relevant to diseases such as PD [10, 30]. It has been well demonstrated that TRAP1 is a substrate of the PINK1 kinase and that TRAP1 phosphorylation is protective from mitochondrial stressors [2]. It is also well established that TRAP1 forms a complex with CypD [31], thereby inhibiting CypD's

ability to promote mtPTP opening, membrane depolarization, and subsequent cell death [30]. Using expertise gained in studying cytoplasmic Hsp90s and our recently solved TRAP1 structure, we will focus on understanding the molecular consequences of PINK1 phosphorylation on TRAP1 structure, conformational cycle, and how this translates to the chaperone's functional interactions using both our model substrate ( $\Delta 131\Delta$ ) as well as *in vivo* clients such as CypD. Further, the structural aspects of the TRAP1:CypD complex will be defined, other mitochondrial clients will be discovered and characterized, and the affects of TRAP1 phosphorylation on client-mediated downstream events will be investigated. Lastly, we will use the TRAP1 structure and our biophysical understanding of which surfaces and conformations of TRAP1 are involved in client interactions for the discovery and optimization of small molecules that preferentially modulate TRAP1 client interactions. The goal will be to avoid generic Hsp90 chaperone inhibitors directed against the ATP binding pocket in favor compounds that modulate specific client interactions by focusing on sites directly involved in TRAP1:client interactions or allosteric modulators.

### **Aim 1: Mechanistic consequences of TRAP1 phosphorylation by PINK1**

Here we propose to understand the mechanistic consequences of PINK1-mediated phosphorylation on the structure of TRAP1, its conformational cycle and function as assessed *in vitro* using a broad suite of biophysical methods and a model substrate that we previously used to characterize cytoplasmic Hsp90s.



## **FRET based elucidation of phospho-specific effects**

A unique property of TRAP1 is a remarkable temperature dependence on the interconversion between the open and closed “ATP” states (Figure 1, chapter 2), suggesting an extraordinary degree of kinetic regulation. Our work with other Hsp90s revealed that client proteins can significantly accelerate conformational interconversion [94]. As mentioned above, we have successfully extended our FRET based assay to report on conformational changes in TRAP1, and have shown that the acceleration of domain closure (the rate limiting conformational step) in response to temperature (Figure 4, chapter 2) can be readily measured, and that acceleration by the model client,  $\Delta 131\Delta$  is conserved (Figure S5, chapter 2). We now aim to use this assay to quantify TRAP1:client interactions and the effects of PINK1 mediated phosphorylation using *in vitro* phosphorylated TRAP1 (below), phosphomimetic and phospho-resistant TRAP1. Moreover, the very large kinetic barrier may well be responsive to determinants of mitochondrial physiology other than client proteins and temperature. With the goal of understanding key regulators of TRAP1 function, this FRET assay will allow the testing of mitochondria-relevant factors such as pH,  $\text{Ca}^{2+}$ , nucleotides, redox state, etc.

## **Structural and biochemical analysis of phospho-specific effects**

In collaboration with the Shokat Lab (UCSF) we will phosphorylate recombinant TRAP1 *in vitro* using PINK1 purified from baculovirus [82]. The sites of phosphorylation have been mapped as outlined above. Single particle EM will be used as an initial assessment of conformational state of phosphorylated TRAP1 under conditions of

different nucleotides (apo, AMPPNP, ATP $\gamma$ S, etc). If sufficient phosphorylated TRAP1 can be produced, SAXS will be used to quantify the equilibrium distribution of conformational states. Our new SAXS analytic methods allow us to determine not only the average conformation in solution, but also the equilibrium amongst up to 4 different species [41]. Regardless, the FRET assay is sufficiently sensitive to allow accurate quantification of kinetic changes in TRAP1 behavior in response to phosphorylation. It is also possible that phosphorylation might affect other steps of the nucleotide cycle, including the chemical step in ATP hydrolysis or ADP or phosphate release. Such effects can be readily assessed utilizing classical enzyme kinetic experiments previously used to characterize TRAP1 ATPase activity [43, 50], or when necessary single-turnover experiments. Because we have identified multiple PINK1 specific phosphosites, we will consider them in total as well as individually by combining phosphomimetic (Glu/Asp) and phosphomutant (Ala) mutations. Effects on both the intrinsic conformational cycle and its response to our model client  $\Delta$ 131 $\Delta$  can be investigated by ATPase stimulation and closure kinetics (Figure S9 chapter 1 and Figure S5 chapter 2, respectively). To assess if phosphorylation alters client protein affinity independent of kinetics, the affinity of TRAP1 for  $\Delta$ 131 $\Delta$  will be measured by polarization anisotropy using fluorescently labeled  $\Delta$ 131 $\Delta$  [94]. The proof of principal binding experiment for TRAP1:  $\Delta$ 131 $\Delta$  has been done, resulting in a  $\sim$ 25 $\mu$ M Kd (Figure S9, chapter 1.)

As outlined above, we have successfully constructed a phosphomimetic version of hTRAP1, which shows a 2-fold acceleration in ATPase. *In vivo* investigation is

currently underway (collaboration outlined above). Crystal structures of phosphomimic and phosphomutant TRAP1s will allow us to observe changes to the active closed state when compared to our full-length crystal structure of TRAP1 described in chapter 1. Therefore crystal trials with phosphomimetic and phospho-resistant TRAP1 will be pursued.

## **Aim 2: TRAP1:client interactions and consequences of TRAP1 phosphorylation by PINK1**

### **Identification and analysis of TRAP1 clients sensitive to phosphorylation by PINK1**

Biological effects of TRAP1 must necessarily be mediated through one or more of its client proteins. Unfortunately, few clients of TRAP1 have been identified. While CypD seems quite relevant and will be pursued in detail, it is likely that other TRAP1 clients may also be correlated with PD-relevant mitochondrial dysfunction and thus would also show sensitivity to the TRAP1 phosphorylation state. With this in mind, we propose to use a combination of in-cell SILAC labeling followed by pull downs and quantitative mass spectrometry to identify novel client proteins that are sensitive to PINK1 specific phosphorylation of TRAP1. Specifically, we will do paired experiments transfecting TRAP1 KO cells with TAP-tagged WT human TRAP1 and phosphomimetic TRAP1, non-phosphorylatable (phosphomutant) TRAP1, or empty vector. The WT control cells would be grown on heavy isotopes and the other cells on light, allowing

accurate quantification of ratios. Mitochondria will be isolated, proteins pulled down via the TRAP1 Tap-tag and analyzed by mass spectrometry [106]. This technology is well established in both the Krogan and Burlingame labs at UCSF.

With recent advances in SILAC protocols, it is possible to label whole organisms, specifically in *Drosophila melanogaster* [107]. Though our collaboration with L. Miguel Martins (outlined above), it should be possible to use this new protocol (with a similar strategy to the above) to isolate phospho-sensitive clients that are specific to PINK1 PTM. More specifically, post-labeling of the appropriated fly lines, mitochondria can be purified [108] in total or from a specific organ system of the different fly strains (with brains being the highest priority). This would then be followed by pull-down by a TRAP1 specific antibody (BD biosciences) or by affinity tag (if a tag is added to the pUAST vector construct used to make the fly lines- currently no tag) and analyzed by mass spectrometry as outlined above. In both the case of the cell and fly lines, interactions that quantitatively differ between the different cell/fly lines are indicative of clients whose binding to TRAP1 is modulated by PINK1-specific phosphorylation.

Potential phospho-sensitive client proteins will be prioritized for likely PD relevance and then assayed in tissue culture by siRNA knockdown looking for changes in PD phenotypes in the TRAP1 KO or fly lines described above. The most relevant hits as well as CypD (~10 to start) will recombinantly expressed and examined in detail using solution-based structural analysis described below. Based on these results, the most promising client proteins along with CypD will be subjected to further high-resolution structural investigation.

## **Structural analysis of TRAP1:client interactions**

Once identified, we will explore the physical interaction in increasing structural detail beginning with straightforward measures of binding affinity to WT, phosphomimetic and phospho-resistant TRAP1 mutants. This is readily quantified by fluorescence polarization anisotropy via the introduction of a LysCysLys motif into the client, activating the Cys for specific coupling of the fluorescent dye even in the presence of other Cys residues [109]. Binding affinities to TRAP1, phosphorylated TRAP1 and the phosphomimetic developed above (result section) will be measured under a variety of potentially relevant conditions of temperature, ions, redox state, etc. Now that we have a structure of TRAP1, we can exploit the  $\Delta 131\Delta$  binding site discovered near the MD:CTD junction [95] and immediately test by disruptive mutations or competitive inhibition with  $\Delta 131\Delta$  to assess whether the same site is utilized for these clients.

Determining the mode by which CypD and other high value clients bind to TRAP1 will be informative for all future mechanistic studies as well as for guiding efforts in small molecule discovery (Aim 3). Hsp90 clients could preferentially bind to one of the Hsp90 conformational states biasing the conformational ensemble or, as with some protein folding substrates (such as  $\Delta 131\Delta$ ), actually accelerate the interconversion between Hsp90 conformations. We will investigate these properties using both our FRET based assay, which allows rapid quantification (Figure 4, chapter 2) of closure kinetics and solution SAXS, which allows changes in the TRAP1 conformational ensemble to be

measured as discussed in Aim 1. Because the barrier separating TRAP1 conformational states has such a remarkable temperature dependence, all client interactions will be probed at 25° and 37°. These experiments will then be repeated in the context of the TRAP1 phosphomimetic and phospho-resistant mutants to assay for modulation of TRAP1:client interactions by PINK1 specific phosphorylation. As previously described for our model client,  $\Delta 131\Delta$ , the SAXS analysis provides a low-resolution map of the complex revealing where the client binds [94]. This may be useful to guide mutations or to facilitate higher resolution studies, below.

If conditions can be found where the TRAP1:client affinity is sufficiently high, then co-crystallization trials will be initiated. Our Mosquito drop setting robot permits rapid exploration of conditions with only ~ 1mg of protein required for every 1000 trials. While full-length structures are most desirable, depending on flexibility or conformational heterogeneity, it may also be useful to undertake crystal trials with either NTD:MD or CTD:MD fragments of TRAP1 as guided by the SAXS results. Depending on the client, it may also be necessary to make domain constructs from the client. If crystallization attempts are unsuccessful, we will focus on NMR to map the binding sites on the client and TRAP1, although the actual strategy will depend on the particular aspects of the client - ranging from relatively easy for  $\Delta 131\Delta$  to challenging for CypD, where the vast majority of peaks disappear upon addition of TRAP1 (Figure 5). CypD peaks could disappear because binding to the larger TRAP1 slows tumbling so much that the peaks broaden beyond visibility, or dynamic effects due to intermediate exchange between bound and free states.

While there are several possible strategies, including focusing on TRAP1 domains, a good starting place is to label the terminal methyl groups of aliphatic amino acids (Val, Ile, Leu) with  $^{13}\text{C}$  and  $^1\text{H}$ , while the remainder of the protein is deuterated. This provides a sensitive measure of local structure that can be monitored even in large protein complexes [110]. Complementary, or perhaps a preferred strategy to above, is to pursue client-binding interfaces utilizing the newly developed  $^{13}\text{C}$ -NMR assay for hTRAP1 with identified clients. Though not fully developed at the moment, (when properly assigned) it should be possible to directly identify client-binding interfaces. Similar strategies could be used reversing the labeling onto the client to assess binding and/or changes to client structure though function interaction with the chaperone. Further, hydrogen exchange on the client monitored either by NMR or mass spectrometry [94] should provide critical constraints for modeling even if detailed high-resolution structures are not forthcoming for a particular client.

Once the clients are identified and interacting regions determined and initially scored biochemically, mutations at identified client binding interfaces will be introduced and tested *in vivo* for modulation of PD phenotypes. Using the TRAP1 KO cells, this can be done with phosphomimetic and phospho-resistant mutations in combination with putative client binding site mutations. Alternatively, the mutations at identified binding sites could be explored in combination with PINK1 mutant flies. The expectation is that if phosphomimetic TRAP1 rescues PD phenotypes though modulating specific client interactions with the chaperone, specific mutation at the client-binding interface should

mitigate the rescue effect if the client is involved in downstream signaling of the PD relevant signaling pathway.

### **Aim 3: Identification of small molecules that enhance cytoprotective**

#### **TRAP1:client interactions**

Our goal will be to discover small molecules that mimic or enhance the cytoprotective effects of TRAP1 phosphorylation by PINK1 or otherwise stabilize beneficial TRAP1 conformations. While, such molecules could ideally serve as PD therapeutic leads, more likely they would act as proof-of-principle target validation tools for further *in vitro* and *in vivo* studies. Importantly, this will pioneer a new direction in Hsp90 modulators as all compounds currently in clinical trials act to inhibit rather than stabilize client interactions and most show little or no selectivity (ie. directed against the ATP binding pocket) [111]. Proof that such compounds can exist is provided by recent work on a class of cyclic peptides that bind Hsp90s near the NTD:MD interface, minimally impact ATP binding/hydrolysis, but show specificity in client inhibition [112, 113]. While the most desirable goals are clear, for validation purposes, it may also be useful to have destabilizing compounds.

Through the combination of the work above, we will have developed a thorough biophysical understanding of the conformational states and interactions that need to be stabilized/destabilized. This provides a remarkable amount of information to aid the discovery process. We will take two approaches: computational screening and physical



screening. Using the crystal structure as a guide and using information from the cytosolic Hsp90s and the solution SAXS and EM data we will model the three-dimensional structures of the most relevant conformational states of TRAP1 and refine these states by all atom MD using explicit solvent [114]. This will be used to computationally screen against available compounds and counter screen against alternative conformations. Additionally, TRAP1:client interfaces can be specifically targeted if high-resolution structural information proves successful. The top compounds will be purchased and screened below.

We have begun to develop robust screening assays for TRAP1 and cytosolic Hsp90s based on the FRET kinetic assay described above. This provides a sensitive monitor of conformational and kinetic modulation in Hsp90s, either in the presence or absence of client proteins. Importantly the FRET assay provides a way to bias against compounds that bind in the ATP binding pocket. While such compounds can be quite effective inhibitors of Hsp90 function, they tend to indiscriminately affect the majority of clients and signaling pathways, resulting in significant side effects. More importantly, as has been shown for the mitochondrially-directed geldanamycin analog [52], ATP-competitive inhibitors are pro-apoptotic. Since different clients seem to interact with different Hsp90 surfaces and prefer different conformational states, compounds that either directly modulate the client binding interaction or allosterically modulate via stabilizing particular conformational states seem more promising. From Aim 1 we know which TRAP1 conformational states are stabilized by PINK1 phosphorylation and which kinetic steps are most affected either in TRAP1 alone or in combination with our model

client  $\Delta 131\Delta$ . This information will be used to optimize the FRET assay to search for small molecules that mimic or enhance the effects of TRAP1 phosphorylation. Further, TRAP1:client interactions can be specifically targeted if there is a kinetic effect of the client using FRET (Aim 2), or by using the anisotropy direct binding assay as a readout of complex stabilization. We will start by undertaking a small pilot screen 200-1000 compounds using a set of known cytosolic Hsp90 inhibitors as well as a selected set of compounds from the computational screen to optimize the assay. Additionally cytosolic Hsp90 will be included as a control and for negative selection.

Based on the statistics and the most robust scenarios, we will scale up to ~50,000 compounds. All screening will be done using UCSF's Small Molecule Discovery Center (SMDC) run by Jim Wells. They have tremendous expertise in assay development and screening and will be invaluable to this effort. Interesting hits will be evaluated biochemically and biophysically for consistency with our desired modes of action and then optimized through screen of small libraries of commercially-available chemically-related compounds. The SMDC can provide further medicinal chemistry. We will try to crystallize the top 10 compounds with TRAP1 to better understand their specific mechanism of action. Promising compounds will be thoroughly evaluated in the cell models for improvement of PD phenotypes in WT, mutant TRAP1 and/or PINK1 mutant or KO backgrounds. CypD KO MEFS (ppif<sup>-/-</sup>) are also available (Eric Huang) and can be used to verify if the compounds are functioning in a CypD-dependent or independent manner.

## **Concluding thoughts**

This project represents a new avenue of research for TRAP1 biology, structure and function, as well as mitochondrial signaling pathways, and the etiology of PD. Provided the phosphomimetic and phospho-resistant mutants rescue or potentate PD phenotypes (respectively) in flies: our preliminary results, established collaborations, and promising new assay development (combined with the experiments outlined above) provide a platform for many exciting and important discoveries to come. My hope is that the progression of this project will afford a high-level mechanistic understanding of TRAP1/Hsp90 function, as well as novel intervention strategies for this devastating disease.

## References:

1. Deas, E., H. Plun-Favreau, and N.W. Wood, *PINK1 function in health and disease*. EMBO Mol Med, 2009. **1**(3): p. 152-65.
2. Pridgeon, J.W., et al., *PINK1 protects against oxidative stress by phosphorylating mitochondrial chaperone TRAP1*. PLoS Biol, 2007. **5**(7): p. e172.
3. Silvestri, L., et al., *Mitochondrial import and enzymatic activity of PINK1 mutants associated to recessive parkinsonism*. Hum Mol Genet, 2005. **14**(22): p. 3477-92.
4. Wang, H.L., et al., *PARK6 PINK1 mutants are defective in maintaining mitochondrial membrane potential and inhibiting ROS formation of substantia nigra dopaminergic neurons*. Biochim Biophys Acta, 2011. **1812**(6): p. 674-84.
5. Sim, C.H., et al., *C-terminal truncation and Parkinson's disease-associated mutations down-regulate the protein serine/threonine kinase activity of PTEN-induced kinase-1*. Hum Mol Genet, 2006. **15**(21): p. 3251-62.
6. Zhang, L., et al., *TRAP1 rescues PINK1 loss-of-function phenotypes*. Hum Mol Genet, 2013.
7. Costa, A.C., S.H. Loh, and L.M. Martins, *Drosophila Trap1 protects against mitochondrial dysfunction in a PINK1/parkin model of Parkinson's disease*. Cell Death Dis, 2013. **4**: p. e467.
8. Winklhofer, K.F. and C. Haass, *Mitochondrial dysfunction in Parkinson's disease*. Biochim Biophys Acta, 2010. **1802**(1): p. 29-44.
9. Henchcliffe, C. and M.F. Beal, *Mitochondrial biology and oxidative stress in Parkinson disease pathogenesis*. Nat Clin Pract Neurol, 2008. **4**(11): p. 600-9.
10. de Castro, I.P., L.M. Martins, and S.H. Loh, *Mitochondrial quality control and Parkinson's disease: a pathway unfolds*. Mol Neurobiol, 2011. **43**(2): p. 80-6.
11. Langston, J.W., et al., *Chronic Parkinsonism in humans due to a product of meperidine-analog synthesis*. Science, 1983. **219**(4587): p. 979-80.

12. LaVoie, M.J., et al., *Dopamine covalently modifies and functionally inactivates parkin*. Nature medicine, 2005. **11**(11): p. 1214-21.
13. Shin, J.H., et al., *PARIS (ZNF746) repression of PGC-1alpha contributes to neurodegeneration in Parkinson's disease*. Cell, 2011. **144**(5): p. 689-702.
14. Chung, K.K., et al., *S-nitrosylation of parkin regulates ubiquitination and compromises parkin's protective function*. Science, 2004. **304**(5675): p. 1328-31.
15. Zheng, B., et al., *PGC-1alpha, a potential therapeutic target for early intervention in Parkinson's disease*. Science translational medicine, 2010. **2**(52): p. 52ra73.
16. Kamp, F., et al., *Inhibition of mitochondrial fusion by alpha-synuclein is rescued by PINK1, Parkin and DJ-1*. EMBO J, 2010. **29**(20): p. 3571-89.
17. Nakamura, K., et al., *Direct membrane association drives mitochondrial fission by the Parkinson disease-associated protein alpha-synuclein*. The Journal of biological chemistry, 2011. **286**(23): p. 20710-26.
18. Panaretou, B., et al., *ATP binding and hydrolysis are essential to the function of the Hsp90 molecular chaperone in vivo*. The EMBO journal, 1998. **17**(16): p. 4829-36.
19. Butler, E.K., et al., *The Mitochondrial Chaperone Protein TRAP1 Mitigates alpha-Synuclein Toxicity*. PLoS genetics, 2012. **8**(2): p. e1002488.
20. Taipale, M., D.F. Jarosz, and S. Lindquist, *HSP90 at the hub of protein homeostasis: emerging mechanistic insights*. Nat Rev Mol Cell Biol, 2010. **11**(7): p. 515-28.
21. Johnson, J.L., *Evolution and function of diverse Hsp90 homologs and cochaperone proteins*. Biochim Biophys Acta, 2012. **1823**(3): p. 607-13.
22. Southworth, D.R. and D.A. Agard, *Species-dependent ensembles of conserved conformational states define the Hsp90 chaperone ATPase cycle*. Mol Cell, 2008. **32**(5): p. 631-40.

23. Chen, B., D. Zhong, and A. Monteiro, *Comparative genomics and evolution of the HSP90 family of genes across all kingdoms of organisms*. BMC Genomics, 2006. **7**: p. 156.
24. Zou, J., et al., *Repression of heat shock transcription factor HSF1 activation by HSP90 (HSP90 complex) that forms a stress-sensitive complex with HSF1*. Cell, 1998. **94**(4): p. 471-80.
25. Chakraborty, A., et al., *HSP90 regulates cell survival via inositol hexakisphosphate kinase-2*. Proc Natl Acad Sci U S A, 2008. **105**(4): p. 1134-9.
26. Edlich, F., et al., *The Bcl-2 regulator FKBP38-calmodulin-Ca<sup>2+</sup> is inhibited by Hsp90*. J Biol Chem, 2007. **282**(21): p. 15341-8.
27. Erdmann, F., et al., *Hsp90-mediated inhibition of FKBP38 regulates apoptosis in neuroblastoma cells*. FEBS Lett, 2007. **581**(29): p. 5709-14.
28. Haynes, C.M. and D. Ron, *The mitochondrial UPR - protecting organelle protein homeostasis*. J Cell Sci, 2010. **123**(Pt 22): p. 3849-55.
29. Youle, R.J. and D.P. Narendra, *Mechanisms of mitophagy*. Nat Rev Mol Cell Biol, 2011. **12**(1): p. 9-14.
30. Galluzzi, L., K. Blomgren, and G. Kroemer, *Mitochondrial membrane permeabilization in neuronal injury*. Nat Rev Neurosci, 2009. **10**(7): p. 481-94.
31. Kang, B.H., et al., *Regulation of tumor cell mitochondrial homeostasis by an organelle-specific Hsp90 chaperone network*. Cell, 2007. **131**(2): p. 257-70.
32. Whitesell, L. and S.L. Lindquist, *HSP90 and the chaperoning of cancer*. Nat Rev Cancer, 2005. **5**(10): p. 761-72.
33. Trepel, J., et al., *Targeting the dynamic HSP90 complex in cancer*. Nat Rev Cancer, 2010. **10**(8): p. 537-49.
34. Luo, W., et al., *Heat shock protein 90 in neurodegenerative diseases*. Mol Neurodegener, 2010. **5**: p. 24.

35. Jakob, U., et al., *Transient interaction of Hsp90 with early unfolding intermediates of citrate synthase. Implications for heat shock in vivo.* J Biol Chem, 1995. **270**(13): p. 7288-94.
36. Taipale, M., et al., *Quantitative analysis of HSP90-client interactions reveals principles of substrate recognition.* Cell, 2012. **150**(5): p. 987-1001.
37. Krukenberg, K.A., et al., *Conformational dynamics of the molecular chaperone Hsp90.* Quarterly reviews of biophysics, 2011. **44**(2): p. 229-55.
38. Dollins, D.E., et al., *Structures of GRP94-nucleotide complexes reveal mechanistic differences between the hsp90 chaperones.* Mol Cell, 2007. **28**(1): p. 41-56.
39. Ali, M.M., et al., *Crystal structure of an Hsp90-nucleotide-p23/Sba1 closed chaperone complex.* Nature, 2006. **440**(7087): p. 1013-7.
40. Shiau, A.K., et al., *Structural Analysis of E. coli hsp90 reveals dramatic nucleotide-dependent conformational rearrangements.* Cell, 2006. **127**(2): p. 329-40.
41. Krukenberg, K.A., et al., *Multiple conformations of E. coli Hsp90 in solution: insights into the conformational dynamics of Hsp90.* Structure, 2008. **16**(5): p. 755-65.
42. Krukenberg, K.A., et al., *pH-dependent conformational changes in bacterial Hsp90 reveal a Grp94-like conformation at pH 6 that is highly active in suppression of citrate synthase aggregation.* J Mol Biol, 2009. **390**(2): p. 278-91.
43. Lavery, L.A., et al., *Structural asymmetry in the closed state of mitochondrial Hsp90 (TRAP1) supports a two-step ATP hydrolysis mechanism* 2013.
44. Zuehlke, A. and J.L. Johnson, *Hsp90 and co-chaperones twist the functions of diverse client proteins.* Biopolymers, 2010. **93**(3): p. 211-7.
45. Liu, B., et al., *Folding of Toll-like receptors by the HSP90 paralogue gp96 requires a substrate-specific cochaperone.* Nat Commun, 2010. **1**: p. 79.

46. Mollapour, M. and L. Neckers, *Post-translational modifications of Hsp90 and their contributions to chaperone regulation*. Biochim Biophys Acta, 2012. **1823**(3): p. 648-55.
47. Song, H.Y., et al., *Identification of a protein with homology to hsp90 that binds the type 1 tumor necrosis factor receptor*. J Biol Chem, 1995. **270**(8): p. 3574-81.
48. Felts, S.J., et al., *The hsp90-related protein TRAP1 is a mitochondrial protein with distinct functional properties*. J Biol Chem, 2000. **275**(5): p. 3305-12.
49. Cechetto, J.D. and R.S. Gupta, *Immunoelectron microscopy provides evidence that tumor necrosis factor receptor-associated protein 1 (TRAP-1) is a mitochondrial protein which also localizes at specific extramitochondrial sites*. Exp Cell Res, 2000. **260**(1): p. 30-9.
50. Leskovar, A., et al., *The ATPase cycle of the mitochondrial Hsp90 analog Trap1*. J Biol Chem, 2008. **283**(17): p. 11677-88.
51. Kang, B.H. and D.C. Altieri, *Compartmentalized cancer drug discovery targeting mitochondrial Hsp90 chaperones*. Oncogene, 2009. **28**(42): p. 3681-8.
52. Kang, B.H., et al., *Preclinical characterization of mitochondria-targeted small molecule hsp90 inhibitors, gamitrinibs, in advanced prostate cancer*. Clin Cancer Res, 2010. **16**(19): p. 4779-88.
53. Kang, B.H., et al., *Combinatorial drug design targeting multiple cancer signaling networks controlled by mitochondrial Hsp90*. J Clin Invest, 2009. **119**(3): p. 454-64.
54. Altieri, D.C., et al., *TRAP-1, the mitochondrial Hsp90*. Biochim Biophys Acta, 2012. **1823**(3): p. 767-73.
55. Takamura, H., et al., *TRAP1 controls mitochondrial fusion/fission balance through Drp1 and Mff expression*. PLoS One, 2012. **7**(12): p. e51912.
56. Chae, Y.C., et al., *Control of tumor bioenergetics and survival stress signaling by mitochondrial HSP90s*. Cancer Cell, 2012. **22**(3): p. 331-44.



57. Amoroso, M.R., et al., *TRAP1 and the proteasome regulatory particle TBP7/Rpt3 interact in the endoplasmic reticulum and control cellular ubiquitination of specific mitochondrial proteins*. *Cell Death Differ*, 2012. **19**(4): p. 592-604.
58. Takemoto, K., et al., *Mitochondrial TRAP1 regulates the unfolded protein response in the endoplasmic reticulum*. *Neurochem Int*, 2011. **58**(8): p. 880-7.
59. Kornmann, B., et al., *An ER-mitochondria tethering complex revealed by a synthetic biology screen*. *Science*, 2009. **325**(5939): p. 477-81.
60. Chen, C.F., et al., *A new member of the hsp90 family of molecular chaperones interacts with the retinoblastoma protein during mitosis and after heat shock*. *Mol Cell Biol*, 1996. **16**(9): p. 4691-9.
61. Landriscina, M., et al., *Mitochondrial chaperone Trap1 and the calcium binding protein Sorcin interact and protect cells against apoptosis induced by antitubercular agents*. *Cancer Res*, 2010. **70**(16): p. 6577-86.
62. Simmons, A.D., et al., *A direct interaction between EXT proteins and glycosyltransferases is defective in hereditary multiple exostoses*. *Hum Mol Genet*, 1999. **8**(12): p. 2155-64.
63. Nakagawa, T., et al., *Cyclophilin D-dependent mitochondrial permeability transition regulates some necrotic but not apoptotic cell death*. *Nature*, 2005. **434**(7033): p. 652-8.
64. Baines, C.P., et al., *Loss of cyclophilin D reveals a critical role for mitochondrial permeability transition in cell death*. *Nature*, 2005. **434**(7033): p. 658-62.
65. Schinzel, A.C., et al., *Cyclophilin D is a component of mitochondrial permeability transition and mediates neuronal cell death after focal cerebral ischemia*. *Proc Natl Acad Sci U S A*, 2005. **102**(34): p. 12005-10.
66. Montesano Gesualdi, N., et al., *Tumor necrosis factor-associated protein 1 (TRAP-1) protects cells from oxidative stress and apoptosis*. *Stress*, 2007. **10**(4): p. 342-50.

67. Xiang, F., et al., *Mitochondrial chaperone tumour necrosis factor receptor-associated protein 1 protects cardiomyocytes from hypoxic injury by regulating mitochondrial permeability transition pore opening*. FEBS J, 2010. **277**(8): p. 1929-38.
68. Pogson, J.H., R.M. Ivatt, and A.J. Whitworth, *Molecular Mechanisms of PINK1-Related Neurodegeneration*. Curr Neurol Neurosci Rep, 2011. **11**(3): p. 283-90.
69. Westermann, B., *Mitochondrial fusion and fission in cell life and death*. Nat Rev Mol Cell Biol, 2010. **11**(12): p. 872-84.
70. Wang, X. and T.L. Schwarz, *The mechanism of Ca<sup>2+</sup> -dependent regulation of kinesin-mediated mitochondrial motility*. Cell, 2009. **136**(1): p. 163-74.
71. Vives-Bauza, C., et al., *PINK1-dependent recruitment of Parkin to mitochondria in mitophagy*. Proc Natl Acad Sci U S A, 2010. **107**(1): p. 378-83.
72. Matsuda, N., et al., *PINK1 stabilized by mitochondrial depolarization recruits Parkin to damaged mitochondria and activates latent Parkin for mitophagy*. J Cell Biol, 2010. **189**(2): p. 211-21.
73. Narendra, D.P., et al., *PINK1 is selectively stabilized on impaired mitochondria to activate Parkin*. PLoS Biol, 2010. **8**(1): p. e1000298.
74. Michiorri, S., et al., *The Parkinson-associated protein PINK1 interacts with Beclin1 and promotes autophagy*. Cell Death Differ, 2010. **17**(6): p. 962-74.
75. Narendra, D., et al., *Parkin is recruited selectively to impaired mitochondria and promotes their autophagy*. J Cell Biol, 2008. **183**(5): p. 795-803.
76. Gandhi, S., et al., *PINK1-associated Parkinson's disease is caused by neuronal vulnerability to calcium-induced cell death*. Molecular cell, 2009. **33**(5): p. 627-38.
77. Akundi, R.S., et al., *Increased mitochondrial calcium sensitivity and abnormal expression of innate immunity genes precede dopaminergic defects in Pink1-deficient mice*. PLoS One, 2011. **6**(1): p. e16038.

78. Gautier, C.A., T. Kitada, and J. Shen, *Loss of PINK1 causes mitochondrial functional defects and increased sensitivity to oxidative stress*. Proc Natl Acad Sci U S A, 2008. **105**(32): p. 11364-9.
79. Petit, A., et al., *Wild-type PINK1 prevents basal and induced neuronal apoptosis, a protective effect abrogated by Parkinson disease-related mutations*. J Biol Chem, 2005. **280**(40): p. 34025-32.
80. Deng, H., et al., *Small interfering RNA targeting the PINK1 induces apoptosis in dopaminergic cells SH-SY5Y*. Biochem Biophys Res Commun, 2005. **337**(4): p. 1133-8.
81. Wood-Kaczmar, A., et al., *PINK1 is necessary for long term survival and mitochondrial function in human dopaminergic neurons*. PLoS One, 2008. **3**(6): p. e2455.
82. Hertz, N.T., et al., *A Neo-Substrate that Amplifies Catalytic Activity of Parkinson's-Disease-Related Kinase PINK1*. Cell, 2013. **154**(4): p. 737-47.
83. Vives-Bauza, C., et al., *PINK1-dependent recruitment of Parkin to mitochondria in mitophagy*. Proceedings of the National Academy of Sciences of the United States of America, 2010. **107**(1): p. 378-83.
84. Cui, M., et al., *The organic cation transporter-3 is a pivotal modulator of neurodegeneration in the nigrostriatal dopaminergic pathway*. Proceedings of the National Academy of Sciences of the United States of America, 2009. **106**(19): p. 8043-8.
85. Morais, V.A., et al., *Parkinson's disease mutations in PINK1 result in decreased Complex I activity and deficient synaptic function*. EMBO molecular medicine, 2009. **1**(2): p. 99-111.
86. Porcelli, A.M., et al., *Respiratory complex I dysfunction due to mitochondrial DNA mutations shifts the voltage threshold for opening of the permeability transition pore toward resting levels*. The Journal of biological chemistry, 2009. **284**(4): p. 2045-52.

87. Shchepina, L.A., et al., *Oligomycin, inhibitor of the F<sub>0</sub> part of H<sup>+</sup>-ATP-synthase, suppresses the TNF-induced apoptosis*. *Oncogene*, 2002. **21**(53): p. 8149-57.
88. Yoshida, S., et al., *Molecular chaperone TRAP1 regulates a metabolic switch between mitochondrial respiration and aerobic glycolysis*. *Proceedings of the National Academy of Sciences of the United States of America*, 2013. **110**(17): p. E1604-12.
89. Sciacovelli, M., et al., *The Mitochondrial Chaperone TRAP1 Promotes Neoplastic Growth by Inhibiting Succinate Dehydrogenase*. *Cell metabolism*, 2013. **17**(6): p. 988-99.
90. Blethrow, J.D., et al., *Covalent capture of kinase-specific phosphopeptides reveals Cdk1-cyclin B substrates*. *Proceedings of the National Academy of Sciences of the United States of America*, 2008. **105**(5): p. 1442-1447.
91. Hertz, N.T., et al., *Chemical Genetic Approach for Kinase-Substrate Mapping by Covalent Capture of Thiophosphopeptides and Analysis by Mass Spectrometry*. *Current Protocols in Chemical Biology*, 2010.
92. Ultanir, S.K., et al., *Chemical genetic identification of NDR1/2 kinase substrates AAK1 and Rabin8 Uncovers their roles in dendrite arborization and spine development*. *Neuron*, 2012. **73**(6): p. 1127-42.
93. Genest, O., et al., *Uncovering a region of heat shock protein 90 important for client binding in E. coli and chaperone function in yeast*. *Mol Cell*, 2013. **49**(3): p. 464-73.
94. Street, T.O., L.A. Lavery, and D.A. Agard, *Substrate binding drives large-scale conformational changes in the Hsp90 molecular chaperone*. *Molecular cell*, 2011. **42**(1): p. 96-105.
95. Street, T.O., et al., *Cross-monomer substrate contacts reposition the Hsp90 N-terminal domain and prime the chaperone activity*. *Journal of molecular biology*, 2012. **415**(1): p. 3-15.

96. McLaughlin, S.H., H.W. Smith, and S.E. Jackson, *Stimulation of the weak ATPase activity of human hsp90 by a client protein*. J Mol Biol, 2002. **315**(4): p. 787-98.
97. Wang, Y. and D. Shortle, *The equilibrium folding pathway of staphylococcal nuclease: identification of the most stable chain-chain interactions by NMR and CD spectroscopy*. Biochemistry, 1995. **34**(49): p. 15895-905.
98. Alexandrescu, A.T., C. Abeygunawardana, and D. Shortle, *Structure and dynamics of a denatured 131-residue fragment of staphylococcal nuclease: a heteronuclear NMR study*. Biochemistry, 1994. **33**(5): p. 1063-72.
99. Alexandrescu, A.T. and D. Shortle, *Backbone dynamics of a highly disordered 131 residue fragment of staphylococcal nuclease*. J Mol Biol, 1994. **242**(4): p. 527-46.
100. Shortle, D. and A.K. Meeker, *Residual structure in large fragments of staphylococcal nuclease: effects of amino acid substitutions*. Biochemistry, 1989. **28**(3): p. 936-44.
101. Hessling, M., K. Richter, and J. Buchner, *Dissection of the ATP-induced conformational cycle of the molecular chaperone Hsp90*. Nat Struct Mol Biol, 2009. **16**(3): p. 287-93.
102. Motojima-Miyazaki, Y., M. Yoshida, and F. Motojima, *Ribosomal protein L2 associates with E. coli HtpG and activates its ATPase activity*. Biochem Biophys Res Commun, 2010. **400**(2): p. 241-5.
103. Reese, M.L. and V. Dotsch, *Fast mapping of protein-protein interfaces by NMR spectroscopy*. Journal of the American Chemical Society, 2003. **125**(47): p. 14250-1.
104. Schedlbauer, A., et al., *Automated backbone and side-chain assignment of mitochondrial matrix cyclophilin D*. J Biomol NMR, 2007. **38**(3): p. 267.
105. Godoy-Ruiz, R., C.Y. Guo, and V. Tugarinov, *Alanine Methyl Groups as NMR Probes of Molecular Structure and Dynamics in High-Molecular-Weight Proteins*. Journal of the American Chemical Society, 2010. **132**(51): p. 18340-18350.

106. Trester-Zedlitz, M., et al., *Mass spectrometric analysis of agonist effects on posttranslational modifications of the beta-2 adrenoceptor in mammalian cells*. *Biochemistry*, 2005. **44**(16): p. 6133-43.
107. Sury, M.D., J.X. Chen, and M. Selbach, *The SILAC Fly Allows for Accurate Protein Quantification in Vivo*. *Molecular & Cellular Proteomics*, 2010. **9**(10): p. 2173-2183.
108. Leister, D., et al., *Drosophila melanogaster as a Model System to Study Mitochondrial Biology*, in *Mitochondria*. 2007, Humana Press. p. 33-49.
109. Hansen, R.E., H. Ostergaard, and J.R. Winther, *Increasing the reactivity of an artificial dithiol-disulfide pair through modification of the electrostatic milieu*. *Biochemistry*, 2005. **44**(15): p. 5899-906.
110. Kay, L.E., *Solution NMR spectroscopy of supra-molecular systems, why bother? A methyl-TROSY view*. *Journal of magnetic resonance*, 2011. **210**(2): p. 159-70.
111. Kim, Y.S., et al., *Update on Hsp90 inhibitors in clinical trial*. *Curr Top Med Chem*, 2009. **9**(15): p. 1479-92.
112. Vasko, R.C., et al., *Mechanistic studies of Sansalvamide A-amide: an allosteric modulator of Hsp90*. *ACS Med Chem Lett*, 2010. **1**(1): p. 4-8.
113. Alexander, L.D., et al., *A small molecule that preferentially binds the closed conformation of Hsp90*. *Bioorganic & medicinal chemistry letters*, 2011. **21**(23): p. 7068-71.
114. Sellers, B.D., et al., *Toward better refinement of comparative models: predicting loops in inexact environments*. *Proteins*, 2008. **72**(3): p. 959-71.

## Chapter 4

Substrate binding drives large-scale conformational changes in the Hsp90 molecular chaperone

**Contributing Authors:** Timothy O. Street and David A. Agard.

*Citation: Substrate binding drives large-scale conformational changes in the Hsp90 molecular chaperone. Street TO, Lavery LA, and Agard DA. Mol Cell. 2011.*

## Preface

As echoed in the previous chapters of my thesis, the study of Hsp90 function centers around one major question: how does Hsp90 recognize and re-model a client proteins structure? Making this difficult to address directly are four main factors: 1) The recognition determinates are unclear as Hsp90 clients are divergent in size, structure and function with no known motif. 2) Hsp90 interacts with these clients in their near-native, or partially folded state. Thus, clients are aggregation prone and difficult to study *in vitro*. 3) If soluble client protein can be purified, known client affinities range 1-100 $\mu$ M resulting in short lived Hsp90:client complexes. 4) In the case of the cytosolic Hsp90s in eukaryotes, a large number of cochaperones are required for the chaperone to bind its clients, creating a system with many parts.

This chapter describes the development of a model substrate for the Hsp90 family of chaperones that overcomes many of these challenges and expose key mechanistic features of the chaperones function. Timothy Street, the lead author on this work saw the potential in a well-studied truncation mutant of Staphylococcal nuclease ( $\Delta$ 131 $\Delta$ ) that has many features well suited for studies with Hsp90 as it is partially folded, highly stable, and monomeric at high concentrations. Through investigation of  $\Delta$ 131 $\Delta$  in the context of bacterial Hsp90 (HtpG) (a 1:1, Hsp90: "client" system), we learn that Hsp90 recognizes regions of structure in a globally unfolded protein and that binding of the substrate activates the chaperone by stimulating the rate-limiting step to hydrolysis (closure). These findings tell us that ATP is reserved for when Hsp90 recognizes that it is engaged to a specific client.



I appear as second author on this work and contributed through the development of a FRET based assay for HtpG, which allowed us to couple hydrolysis rates to conformational rates of closure. Additionally, I am responsible for the steady-state kinetic experiments presented here in.

As discussed in previous chapters, I have shown that the  $\Delta 131\Delta$  model substrate system extends to the mitochondrial Hsp90 (TRAP1). Future investigation of  $\Delta 131\Delta$  with TRAP1 promises to further elucidate chaperone function in this system as it has for HtpG.

This work was published in the journal Molecular Cell and the reference information can be found on the title page to this chapter.

## Summary

Hsp90 is a ubiquitous molecular chaperone. Previous structural analysis demonstrated that Hsp90 can adopt a large number of structurally distinct conformations, however the functional role of this flexibility is not understood. Here we investigate the structural consequences of substrate binding with a model system in which Hsp90 interacts with a partially folded protein ( $\Delta 131\Delta$ ), a well-studied fragment of staphylococcal nuclease. SAXS measurements reveal that under apo conditions Hsp90 partially closes around  $\Delta 131\Delta$  and in the presence of AMPPNP  $\Delta 131\Delta$  binds with increased affinity to Hsp90's fully closed state. FRET measurement show that  $\Delta 131\Delta$  accelerates the nucleotide-driven open/closed transition and stimulates ATP hydrolysis by Hsp90. NMR measurements reveal that Hsp90 binds to a specific, highly structured, region of  $\Delta 131\Delta$ . These results suggest that Hsp90 preferentially binds a locally structured region in a globally unfolded protein and this binding drives functional changes in the chaperone by lowering a rate-limiting conformational barrier.

## Introduction

Hsp90 is a ubiquitous molecular chaperone. Originally identified in the heat shock response, Hsp90 plays important regulatory roles under non-stress conditions by its interactions with specific classes of substrates such as kinases and nuclear receptors [1]. Consistent with being upregulated upon heat shock, Hsp90 can suppress thermal aggregation [2, 3] and facilitate protein folding by reducing misfolding via interactions with aggregation-prone unfolding intermediates [4]. *In vivo*, Hsp90 receives unfolded proteins transferred from Hsp40/70 and receives specific classes of native or near-native substrates that are recruited by dedicated cochaperones. In eukaryotes, Hsp90's substrate interactions are highly regulated by cochaperones that modulate the Hsp90 ATPase activity, aid in substrate recruitment, maturation or release, and target substrates for degradation or intracellular trafficking. These important and multifaceted roles are reflected in Hsp90's high cellular abundance (2-5% of cytosolic protein under non-stressed conditions). The *in vivo* characterized substrates (see <http://www.picard.ch/>) have not been found to share a common sequence or structure motif and span an exceptionally wide range of sizes from  $\alpha$ -synuclein to telomerase (14-290 kD [5, 6]).

Recent structural work demonstrated that while Hsp90 is a dimer where each monomer has three well-folded and stable domains (N-terminal, middle, C-terminal), the overall molecule can adopt radically different conformations (Figure 1) in response to nucleotide and conditions. For example, under apo conditions the Hsp90 from *E. coli*, HtpG, crystallized in a 'V'-shaped conformation [7] (ribbon structure, left panel Figure 1)

while in solution a highly open conformation (blue surface structure) and a more closed conformation (red surface) are populated in a pH-dependent manner [8, 9]. The more closed state is similar to a crystal structure of the Hsp90 homolog specific to the endoplasmic reticulum, Grp94 [10]. The apo conformations largely differ by rigid-body rotation at the interface between the middle domain (MD) and C-terminal domain (CTD), creating a variable sized cleft between the monomer arms; there is also NTD-MD rotation, changing the NTD orientation. Addition of non-hydrolysable ATP analogs such as AMPPNP results in closure to an N-terminal domain (NTD) dimerized conformation [11] (Figure 1, central panel), while ADP transiently stabilizes a very compact state (Figure 1, right panel)[7] (Southworth and Agard, 2008). Small angle x-ray scattering (SAXS) and single particle electron microscopy measurements have shown that multiple Hsp90 conformations coexist in a delicate equilibrium that can be shifted not only by nucleotide binding, but also by osmolyte and pH conditions [9, 12, 13]. SAXS has been a powerful tool for characterizing the Hsp90 conformational ensemble [8, 9, 14-17], and has shown that the apo-state flexibility is universal in all homologs that have been examined (HtpG, Hsc82, hHsp90 $\alpha$ , Grp94 and TRAP, [14] and unpublished observations). However, the functional role of Hsp90 flexibility and conformational dynamics is not understood.

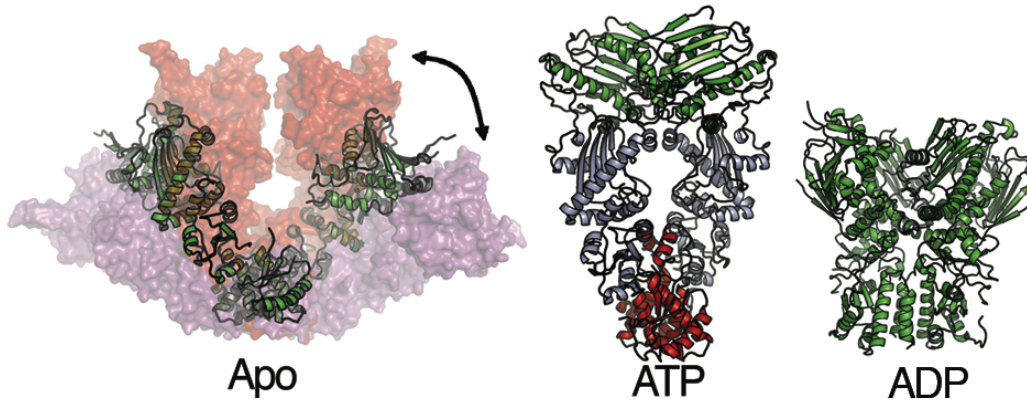


**Figure 1. Conformational flexibility of the Hsp90 molecular chaperone.** The bacterial Hsp90 homolog, HtpG, crystallized in a ‘V’-shaped conformation (cartoon, left panel). SAXS measurements have demonstrated that in solution more extended and compact conformations are primarily populated, differing by rigid-body rotation at the junction between the middle and C-terminal domains. The closed ‘ATP’ state (central panel) involves rigid rotation at the MC interface and additional rotation of the N-terminal domain (green) resulting in secondary dimer contacts. ADP transiently stabilizes a very compact state (right panel).

Indeed, despite the ubiquity of Hsp90 and the long list of *in-vivo* identified substrates (known as client proteins) little is known about how Hsp90 makes these interactions. There is some evidence suggesting that substrate folding stability is linked to Hsp90 binding. Hsp90 has a much stronger *in-vivo* interaction with the highly destabilized v-Src versus c-Src (otherwise having 98% sequence identity) [18], NMR studies of p53 indicate that human Hsp90 only binds after substrate unfolding[19], and HtpG has been found to bind an unfolded ribosomal protein L2 [20]. Indeed, the ability of Hsp90 to interact with and shift the equilibrium between metastable conformations is thought to play a role in Hsp90 in transitioning the glucocorticoid receptor between apo and ligand-bound states, which requires a large conformational change. These observations suggest that Hsp90/substrate interactions may be enhanced by reducing substrate stability to favor partially structured or metastable conformations. This

approach is technically challenging because for most proteins partially folded states are difficult to populate and are prone to misfolding and aggregation.

One protein system that is amenable to this approach is the well-characterized staphylococcal nuclease (SN). Extensive studies have shown that a 131-residue fragment of SN ( $\Delta 131\Delta$ ; full length is 149 residues) is globally unfolded but remains compact with residual structured regions [21] [22-24]. Indeed,  $\Delta 131\Delta$  and other similarly destabilized SN variants are close in free energy to the native state, as indicated by the fact they can be effectively refolded with tight binding inhibitors and stabilizing osmolytes [25, 26].  $\Delta 131\Delta$  is monomeric at high concentrations, stable under a wide variety of conditions, and amenable to NMR, all of which has made it an ideal model system to investigate structural properties of unfolded proteins [21]. Here we test  $\Delta 131\Delta$  as a model system to investigate Hsp90/substrate interactions. Using a combination of SAXS, FRET, binding anisotropy and NMR, we find that Hsp90 binds a structured region of  $\Delta 131\Delta$ , which results in conformational and functional changes in the chaperone.

## Results

To determine Hsp90's binding affinity for  $\Delta 131\Delta$ , we labeled a cysteine variant of  $\Delta 131\Delta$  with the IAEDANS fluorophore to measure fluorescence polarization anisotropy. The Perrin equation estimates of the rotational correlation times for  $\Delta 131\Delta$  and HtpG (5 and 55 ns) span the IAEDANS excited state lifetime (10-15 ns), suggesting that binding will significantly increase polarization anisotropy. Indeed, upon addition of the bacterial

Hsp90, HtpG, the fluorescence anisotropy of IAEDANS-labeled  $\Delta 131\Delta$  increases substantially (Figure 2a). The concentration series is well-fit by single-site non-cooperative binding (solid lines), resulting in a  $K_d$  of 9  $\mu\text{M}$ . Similar binding curves were measured for the yeast Hsp90 homolog ( $K_d$  of 6  $\mu\text{M}$ ) whereas addition of BSA resulted in minimal anisotropy changes (not shown). Anisotropy titration measurements show saturation near a 1:1 stoichiometry (Hsp90 dimer: $\Delta 131\Delta$ , Figure S1).

Previous studies have shown that unfolded SN fragments can be refolded in the presence of  $\text{CaCl}_2$  and a tight binding inhibitor, thymidine 3',5'-bisphosphate (pdTp) [27]. We used these stabilizers to refold IAEDANS-labeled  $\Delta 131\Delta$  and found that HtpG no longer significantly increases fluorescence anisotropy, demonstrating that HtpG is binding a globally unfolded state. However, as discussed later HtpG selectively interacts with a highly structured region within the unfolded protein.

The micromolar concentration range for binding precludes structural analysis by electron microscopy, which for Hsp90 is performed at  $\sim 100$  nM, whereas SAXS measurements are ideally suited for this concentration regime. Previous studies have shown that SAXS measurements can be used to determine the multi-state conformational equilibrium of Hsp90. For these experiments, X-ray scattering intensity was measured between Q values ( $4\pi\sin\theta/\lambda$ , where  $2\theta$  is the scattering angle) of 0.01 to  $0.3\text{\AA}^{-1}$ , radially averaged and buffer subtracted. The resulting data were transformed to an interatomic distance distribution,  $P(r)$ , using the GNOM program [28]. The  $P(r)$  distribution of HtpG alone has significant magnitude at large distances (Figure 2b), indicative of a substantial open state population, very similar to other measurements of

HtpG at pH 7.5 [9]. Subsequent addition of  $\Delta 131\Delta$  shows a conformational change; a concentration series with increasing  $\Delta 131\Delta$  results in a systematic contraction in the  $P(r)$  distribution (Figure 2b). These changes reflect a transition to more compact Hsp90 conformations that saturates near a 1:1 stoichiometry (Hsp90 dimer: $\Delta 131\Delta$ ). The Guinier analysis of low-Q scattering is linear for all concentrations measured (data not shown), indicating no significant aggregation.

Similar  $\Delta 131\Delta$ -induced contractions are observed in the  $P(r)$  distributions for the yeast and human Hsp90 homologs (Figure S2). Their contractions are smaller than for HtpG, which is consistent with previous SAXS and electron microscopy measurements that show the yeast and human homologs more strongly favor the open state relative to HtpG in the absence of nucleotide [13]. The substrate-induced conformational change is specific to unfolded staphylococcal nuclease (SN), addition of folded wild-type SN results in no significant conformational change and the scattering of SN and HtpG are independent and additive (Figure S3a).



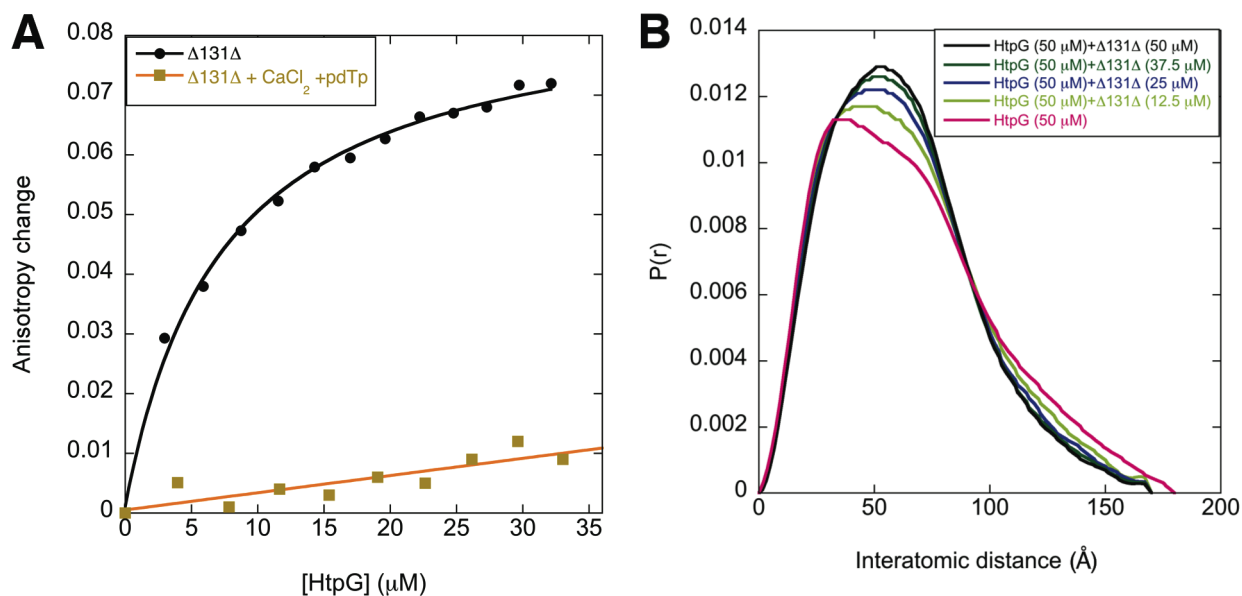


**Figure 2. HtpG binds  $\Delta 131\Delta$ , resulting in a conformational change.** (a) IAEDANS-labeled  $\Delta 131\Delta$  undergoes a significant increase in anisotropy upon addition of HtpG. In contrast, in the presence of 10 mM  $\text{CaCl}_2$  and 5 mM pdTp binding is negligible. The curve is fit with non-cooperative hyperbolic binding (solid lines). (b) Scattering curves are shown for HtpG with increasing concentration of  $\Delta 131\Delta$ . The  $P(r)$  curve, which summarizes the relative probability of interatomic scattering distances, contracts with increasing  $\Delta 131\Delta$ . Conditions: 25 mM TRIS pH 7.5, 25 mM KCl, 10 mM  $\text{MgCl}_2$ .

### Apo Hsp90 partially closes around $\Delta 131\Delta$

The measured SAXS change in response to  $\Delta 131\Delta$  (Figure 2b) has two contributions: (1) additional scattering from bound  $\Delta 131\Delta$  and (2) altered scattering from chaperone contraction. As discussed below, we separated out these contributions by first determining the location of  $\Delta 131\Delta$  on HtpG subdomains using *ab-initio* reconstructions and then applying structure-based fitting and rigid-body analysis to determine the chaperone conformation.

To locate  $\Delta 131\Delta$  on HtpG we first examined a subdomain containing the N-terminal and middle domains (NM, residues 1-495). This monomeric fragment behaves as a rigid object and is significantly smaller than the HtpG dimer, increasing the relative signal from  $\Delta 131\Delta$  scattering in the complex. We used the DAMMIN and MONSA

programs[29] to generate *ab-initio* molecular envelopes from the NM/ $\Delta$ 131 $\Delta$  scattering curve (Figure S3c), for use as a starting point for modeling scattering from the full length HtpG dimer. DAMMIN determines an envelope from exhaustive rearrangement and Monte-Carlo minimization of dummy atoms to match the experimentally-determined distance distribution. MONSA simultaneously fits scattering data of complexes and individual sub-components to determine the location of members within a complex. No initial model was used and yet the resulting DAMMIN volume for the NM domain alone matches well with the expected structure (upper left panel, Figure 3a).

The MONSA reconstruction shows that  $\Delta$ 131 $\Delta$  (cyan volume, Figure 3a upper right) binds predominantly at the middle domain. Multiple repeated MONSA runs were very similar (Figure S4a). The DAMMIN and MONSA envelopes for the NM/ $\Delta$ 131 $\Delta$  complex are broadly consistent with small local differences (Figure S4b); the additional information from simultaneous fitting used in MONSA provides higher resolution information versus DAMMIN. The conclusion that  $\Delta$ 131 $\Delta$  binds at a terminal region of the NM domain is evident from the primary scattering data, which shows that the addition of  $\Delta$ 131 $\Delta$  results in a relative increase in long range scattering distances (Figure S3c). When the MONSA reconstruction is mapped back on the full-length HtpG structure,  $\Delta$ 131 $\Delta$  is found to project between the monomer arms (Figure 3a). Although these reconstructions provide a starting point for analyzing the SAXS data from the full-length HtpG/ $\Delta$ 131 $\Delta$  complex, it should be noted that the reconstructions are too low resolution to conclude whether  $\Delta$ 131 $\Delta$  binding is restricted to the MD or whether additional contacts are made to the NTD.

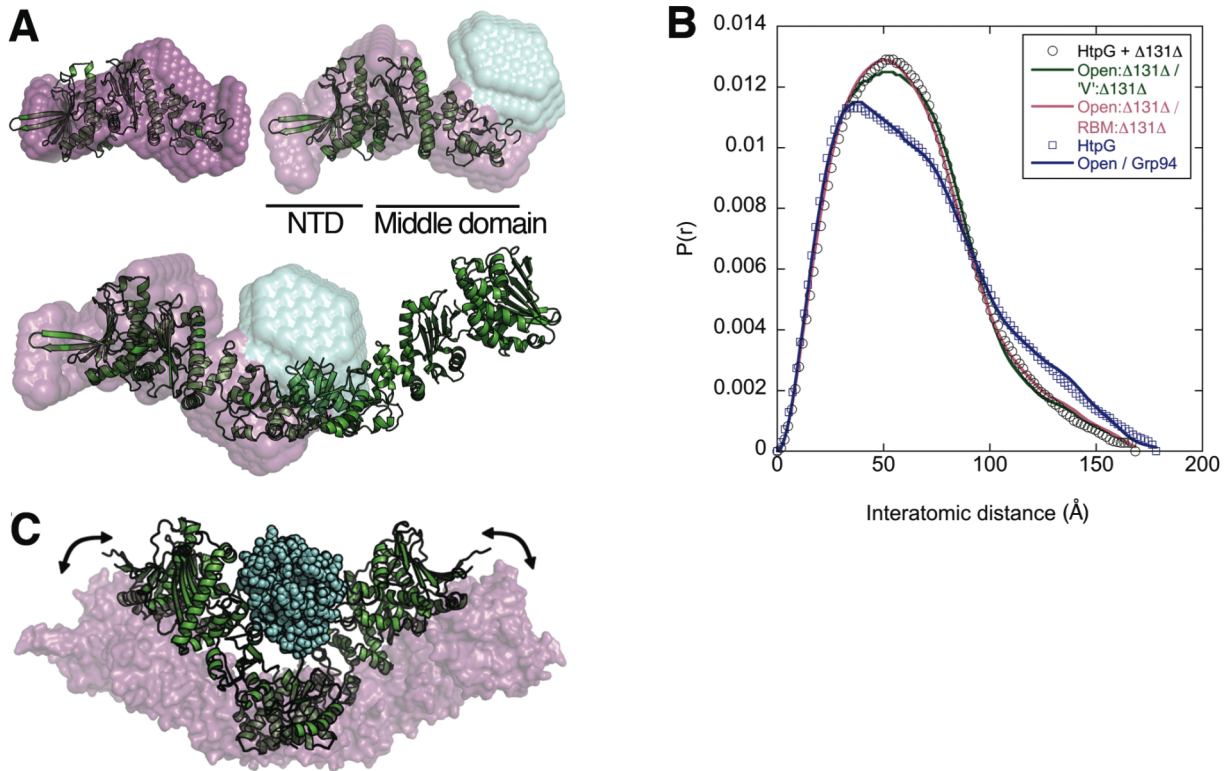


**Figure 3. Contraction of HtpG upon binding  $\Delta 131\Delta$ .** (a) The NM domain DAMMIN reconstruction (upper left panel, magenta surface) matches well with the expected structure (cartoon). The MONSA reconstruction of the NM/ $\Delta 131\Delta$  complex shows that  $\Delta 131\Delta$  (right panel, cyan surface) binds on the middle domain towards the C-terminus. This reconstruction allows the  $\Delta 131\Delta$  volume to be mapped back on full-length HtpG, revealing that  $\Delta 131\Delta$  projects towards the dimer cleft. (b) Scattering for HtpG alone (blue squares) is well fit with a simple two-state model involving the open/Grp94 states (blue line). Scattering from HtpG/ $\Delta 131\Delta$  (black circles) was fit by the open/'V'-shaped states and the open/rigid-body model (RBM), which both fit the data well. (c) This analysis shows that HtpG contracts to a 'V'-shaped conformation with  $\Delta 131\Delta$  (cyan spheres) projecting between the monomer arms. This conformation remains in equilibrium with the open state (magenta surface).

To analyze the SAXS data from the full-length HtpG/ $\Delta 131\Delta$ , we first examined whether any of the four dominant HtpG conformations (open, ATP, Grp94, and 'V'-shaped) could satisfactorily describe the chaperone conformation upon binding  $\Delta 131\Delta$ . For reference, previous studies showed that HtpG's conformational ensemble could be determined by linear combination fitting of SAXS data with different structural states [14]. In the absence of  $\Delta 131\Delta$  and at pH7.5, HtpG adopts an 81/19% open/Grp94

equilibrium resulting in a good fit to the chaperone alone data (blue squares, Figure 3b) and is quantified by a low R-factor of 2.2% (see equation in Methods). Single HtpG conformations fit the HtpG/ $\Delta 131\Delta$  scattering poorly (Figure S5a), with R-factors of 23, 24, 17, and 17% for the open, ATP, Grp94, and 'V'-shaped conformations, respectively. Inspection of Figure S5a shows that combining only ATP, Grp94, and 'V'-shaped conformations would fit the experimental data poorly due to the lack of long-range scattering distances above 120 Å. By contrast a 58%:42% linear combination of open:'V'-shape provides a better description of the SAXS data (Figure S5a) indicating that HtpG remains in a conformational equilibrium upon  $\Delta 131\Delta$  binding, but now with the V-shaped conformer.

To account for scattering from bound  $\Delta 131\Delta$  we generated structural models of HtpG: $\Delta 131\Delta$  complexes with 131 residues of SN attached to the HtpG middle domain, based on the MONSA reconstruction (see Methods). For the open and crystallographic 'V'-shaped conformations this addition significantly decreased R-factors (from 23 to 13% for the open state and from 17 to 11% for the 'V'-shaped conformation), whereas for the Grp94 and ATP conformations this addition resulted in higher R-factors. Indeed, a 51/49 linear combination of the open: $\Delta 131\Delta$ /'V': $\Delta 131\Delta$  states fit the scattering data well (Figure 3b, R-factor of 3.8%). The relative contributions from the open and 'V'-shaped states to the P(r) fit are shown in Figure S5b. All SAXS fitting statistics are summarized in Table S1. Although the MONSA analysis suggests  $\Delta 131\Delta$  binds predominantly at the MD, as an additional check we generated structural models with  $\Delta 131\Delta$  located at

different NTD positions and confirmed with linear combination fitting with the open state that this positioning resulted in a poorer fit to the data (Figure S5c).

The above results indicate that HtpG adapts its conformation by partially closing around  $\Delta 131\Delta$ . To best determine the chaperone conformation in this state, we performed rigid-body analysis. Since the open/'V'-shaped/Grp94 conformations of HtpG differ primarily by the opening angle between the middle and C-terminal (MC) domains (Figure 1), the Grp94 conformation can be used as a starting point in a rigid-body minimization where the MC angle is systematically explored for an optimal fit to the scattering data. To ensure robustness we performed this analysis by simultaneously fitting four data sets with varying ratios of open and  $\Delta 131\Delta$ -induced closure (see Methods). This analysis confirms that a 'V'-shaped structure is favored, very similar in opening angle to the crystallographically-determined structure (comparison shown in Figure S6c). The rigid-body model (RBM) in equilibrium with the open state (Figure 3c) results in a good fit with an R-factor of 3.4% (Figure 3b). The remaining three data sets used in the simultaneous fitting have similarly low R-factors (Table S1; 1.9, 1.9, and 3.3%). Since the RBM does not allow for the NTD rotation observed in the ATP conformation, we also confirmed that an ATP: $\Delta 131\Delta$ /open: $\Delta 131\Delta$  combination does not fit the data (R-factor of 7.3%).

### **Influence of $\Delta 131\Delta$ on the Hsp90 nucleotide cycle**

In the presence of AMPPNP Hsp90 undergoes a dramatic closure involving N-terminal dimerization (Figure 1). For HtpG at pH 7.5 previous studies showed that

saturating AMPPNP only drives a partial population shift to the ATP conformation [14]. Since the ATP conformation is marginally populated it is sensitive to whether  $\Delta 131\Delta$  binds favorably; if  $\Delta 131\Delta$  favors/disfavors binding the closed state then an increase/decrease in closure is expected. Indeed, in the presence of 10 mM AMPPNP we find that  $\Delta 131\Delta$  increases closure, which results in a  $P(r)$  distribution very different from that observed under apo conditions (Figure 4a). To quantify the relative populations of different states, we again used linear combination fitting, utilizing the structural models based on the previous MONSA analysis (Figure 4b). This fitting shows an approximately two-fold increase in the ATP state population (from 39% to 70%, Table S1).

Consistent with the above observations we find the binding affinity between HtpG and  $\Delta 131\Delta$  is enhanced two-fold by AMPPNP (Figure 4c). This enhancement is blocked by a competitive inhibitor geldanamycin (GE); the small increase in  $K_d$  from GE is from the DMSO storage buffer, which alone increases the  $K_d$ . These results predict that the effect of AMPPNP on the binding affinity for  $\Delta 131\Delta$  should be most pronounced at pH 9, where HtpG undergoes a full population shift from the most open state to the ATP conformation [14]. Indeed, at pH 9 there is a 5-fold increase in binding affinity for  $\Delta 131\Delta$  upon addition of AMPPNP. Under both apo and AMPPNP conditions binding is pH dependent over the neutral range (pH 6-9) suggesting the involvement of a histidine. There is a strong salt dependence to  $\Delta 131\Delta$  binding  $K_d$  and the resulting conformational equilibrium in HtpG: $\Delta 131\Delta$  (Figure S6a and b), suggesting an electrostatic contribution.

This conformational variation was useful in performing the rigid body minimization of multiple data sets as discussed earlier (see Methods).

In contrast to AMPPNP, there is a negligible influence of ADP on binding. Previous electron microscopy measurements have identified a compact HtpG conformation in the presence of ADP [7, 13], yet this state is only transiently populated under SAXS experimental conditions [8]. Our results therefore suggest that under our experimental conditions, the ADP state is insufficiently populated to affect the bulk binding of  $\Delta 131\Delta$ .

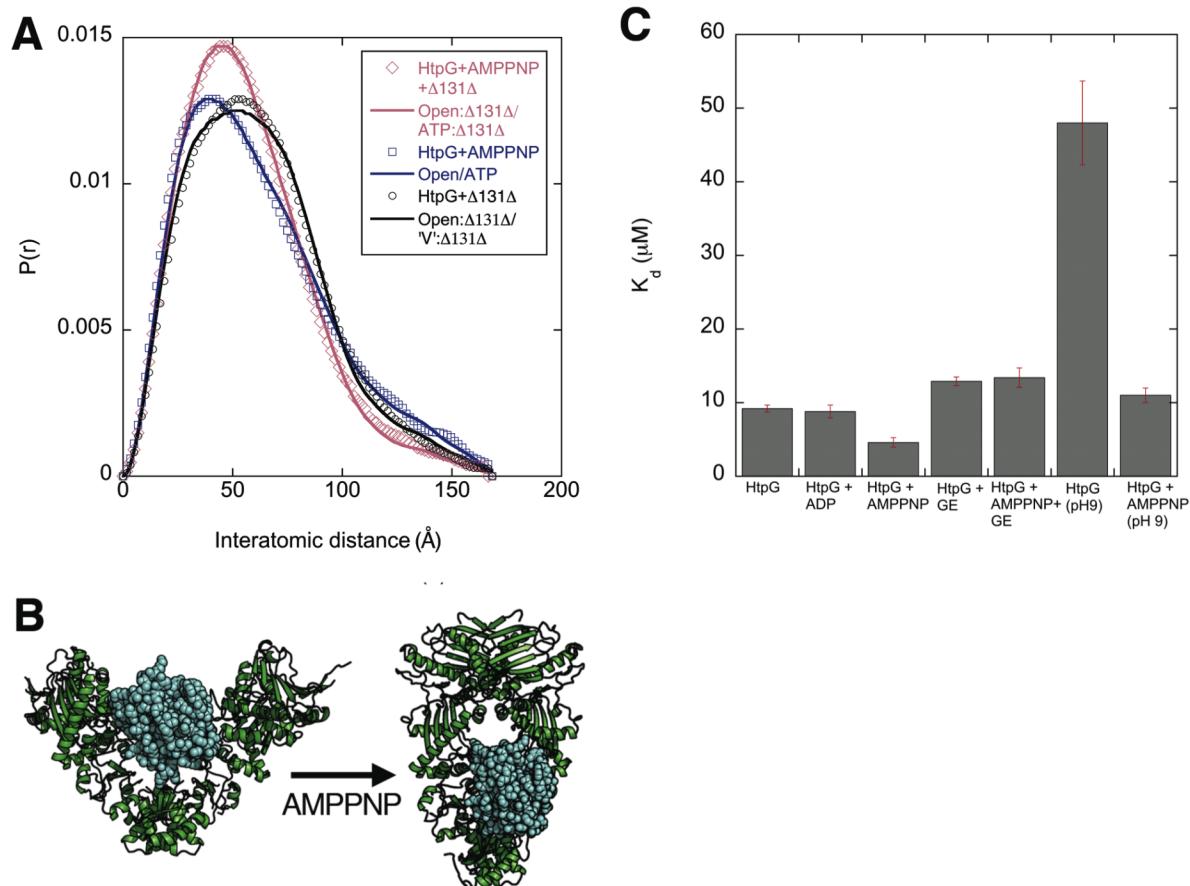


**Figure 4. Nucleotide dependence of  $\Delta 131\Delta$  binding.** (a) In the presence of 10 mM AMPPNP, HtpG's  $P(r)$  distribution is shifted towards smaller distances reflecting an increase in the population of the ATP conformation (blue squares). The subsequent addition of  $\Delta 131\Delta$  (grey diamonds) increases the ATP conformation from 39 to 70% (fits shown in solids lines). The influence of  $\Delta 131\Delta$  on HtpG under AMPPNP conditions differs significantly from apo conditions (black circles). (b) The open/ATP structural transition differs by a significant change in chaperone conformation. (c) Fluorescence anisotropy measurements show an increase in binding affinity under AMPPNP conditions. Bars represent the standard error on the mean. Geldanamycin (GE) and nucleotide concentrations were 250  $\mu\text{M}$  and 5 mM, other buffer conditions are same as Figure 2.

Since  $\Delta 131\Delta$  affects the apo/ATP equilibrium it either accelerates closure or slows reopening. We tested this prediction with FRET since the Buchner and Hugel labs have showed that the open/ATP kinetics can be monitored this way [30, 31]. Following their work, we generated heterodimers of HtpG labeled with Alexafluor 647 and Alexafluor 555 at positions 62 and 341 on opposite monomers (see Methods). FRET



measurements were performed at pH 9 because under these condition HtpG undergoes a complete open/ATP population shift [14]. Indeed, under apo conditions there is minimal FRET whereas after an extended incubation with AMPPNP, there is significant FRET as indicated by an increase/decrease in acceptor/donor fluorescence (Figure 5a).

The large change in acceptor fluorescence at 664 nm provides a sensitive assay for closure kinetics. As shown in Figure 5b (red circles), upon addition of AMPPNP there is a slow increase in acceptor fluorescence, with single exponential kinetics similar to those measured with the yeast Hsp90 homolog [30]. When  $\Delta 131\Delta$  is incubated with HtpG prior to addition of AMPPNP, nucleotide-driven closure is accelerated five-fold (Figure 5b, green squares), similar to the affinity enhancement measured by anisotropy at pH 9. As a control, we tested the influence of BSA and the folded wild-type SN (both at 50  $\mu\text{M}$ , the same concentration that was used with  $\Delta 131\Delta$ ) on closure kinetics and found no significant change (not shown). In contrast to closure kinetics,  $\Delta 131\Delta$  has no effect on reopening from the closed state (Figure S7a). The closure acceleration by  $\Delta 131\Delta$  implies that hydrolysis should also be accelerated, which we tested with a previously described assay (see Methods). At 50  $\mu\text{M}$   $\Delta 131\Delta$  the hydrolysis rate is increased four-fold (Figure S7b). The increase in hydrolysis is specific to  $\Delta 131\Delta$ 's influence on HtpG, as this increase can be abolished by 200  $\mu\text{M}$  radicicol.

The SAXS modeling and anisotropy data suggest a single bound  $\Delta 131\Delta$  per HtpG dimer. This predicts a non-cooperative concentration dependence of the  $\Delta 131\Delta$ -induced closure acceleration, in contrast to a two-site cooperative model in which an initial quadratic dependence on  $\Delta 131\Delta$  concentration would be expected. Indeed, the

$\Delta 131\Delta$ -induced closure acceleration (Figure 5c) has a simple rectangular hyperbolic concentration dependence (solid line).

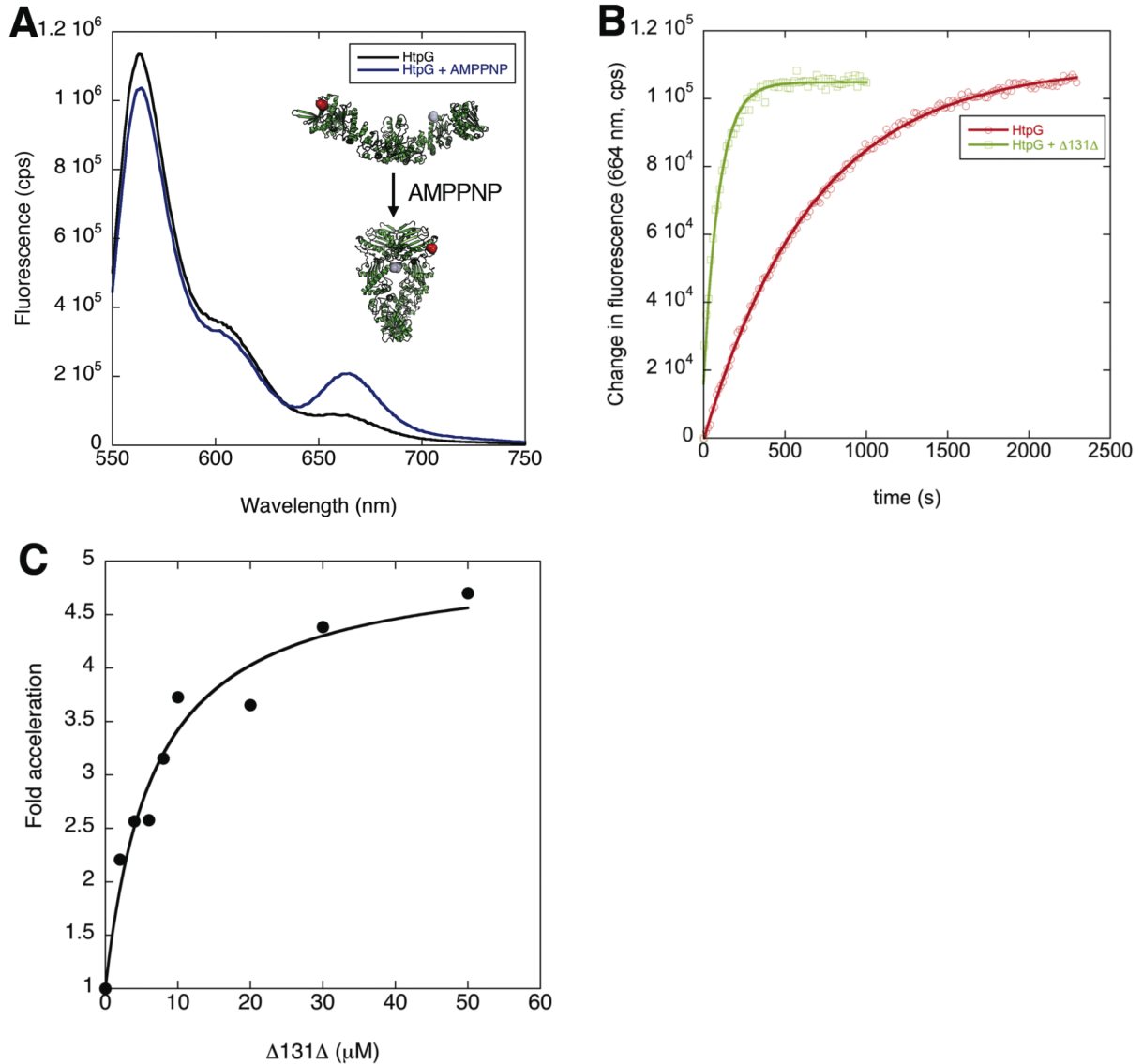


**Figure 5. Substrate binding accelerates nucleotide-driven closure.** (a) FRET measurements of apo (black) and AMPPNP (blue) HtpG show an increase/decrease in acceptor/donor fluorescence at 664 and 563 nm, respectively. These changes reflect the dramatic change in fluorophore distance between the open and ATP states (cartoon, red and blue spheres show the fluorophore locations at residues 62 and 341). (b) Closure is five-fold accelerated by  $\Delta 131\Delta$ , single exponential fits are shown in solid lines. (c) The  $\Delta 131\Delta$  concentration dependence on closure acceleration shows a non-cooperative relationship between  $\Delta 131\Delta$  binding and closure.

## HtpG binds a locally structured region on $\Delta 131\Delta$

A significant advantage of using  $\Delta 131\Delta$  as a model system is that it is amenable to NMR measurements. To gain a higher resolution picture of the interaction site on  $\Delta 131\Delta$ , we measured the  $\Delta 131\Delta$  HSQC with and without HtpG. The original assignment of  $\Delta 131\Delta$  was performed at low pH, high temperature and the absence of buffer, salt and magnesium chloride [24], under which conditions HtpG is not stable. However, the majority of the peaks remain and at similar chemical shifts at pH 6.0, 25 mM MES, 25 mM KCl and 5 mM  $MgCl_2$  (Figure 6a, left panel). The transferred  $\Delta 131\Delta$  assignments under these conditions were confirmed with HNCA and CBCA(CO)NH measurements on double labeled sample. Of the 131 residues of  $\Delta 131\Delta$ , 41 residues could be unambiguously assigned allowing us to monitor their response to HtpG.

A non-specific binding interaction between to the entire  $\Delta 131\Delta$  and HtpG would result in a loss of signal uniformly across the molecule, however at stoichiometric concentrations of HtpG and  $\Delta 131\Delta$  we observe that a subset of peaks disappear while others have reduced intensity (Figure 6a, right panel). The fractional loss of peak height across different positions of the  $\Delta 131\Delta$  sequence is HtpG concentration dependent and shows a clear trend where locations near  $\Delta 131\Delta$  residue 100 are highly impacted by the addition of HtpG whereas more distant positions are less affected (Figure 6b). The region from residues 85-110 is completely broadened at stoichiometric concentrations of Hsp90. There is a roughly monotonic increase in peak height at increasing sequence distance away from the region that loses complete peak intensity, which suggests that chain mobility restricted by HtpG binding is relieved with increasing chain length from

the binding site due to lack of structure in  $\Delta 131\Delta$ . No new peaks were observed upon addition of HtpG, as expected for their complete broadening due to the slow tumbling of the interface region of  $\Delta 131\Delta$  in complex with HtpG.

Significantly, the region with maximal peak loss (residues 85-110) has been identified as the most structured region within the globally unfolded protein. In particular, the helix between residues 97-107 has been shown to have significant structure as well as two turns located at residues 83-86 and 94-97 [22-24]. Relaxation measurements have shown that this region has high order parameters and positive NOEs again indicative of significant structure [24, 32].

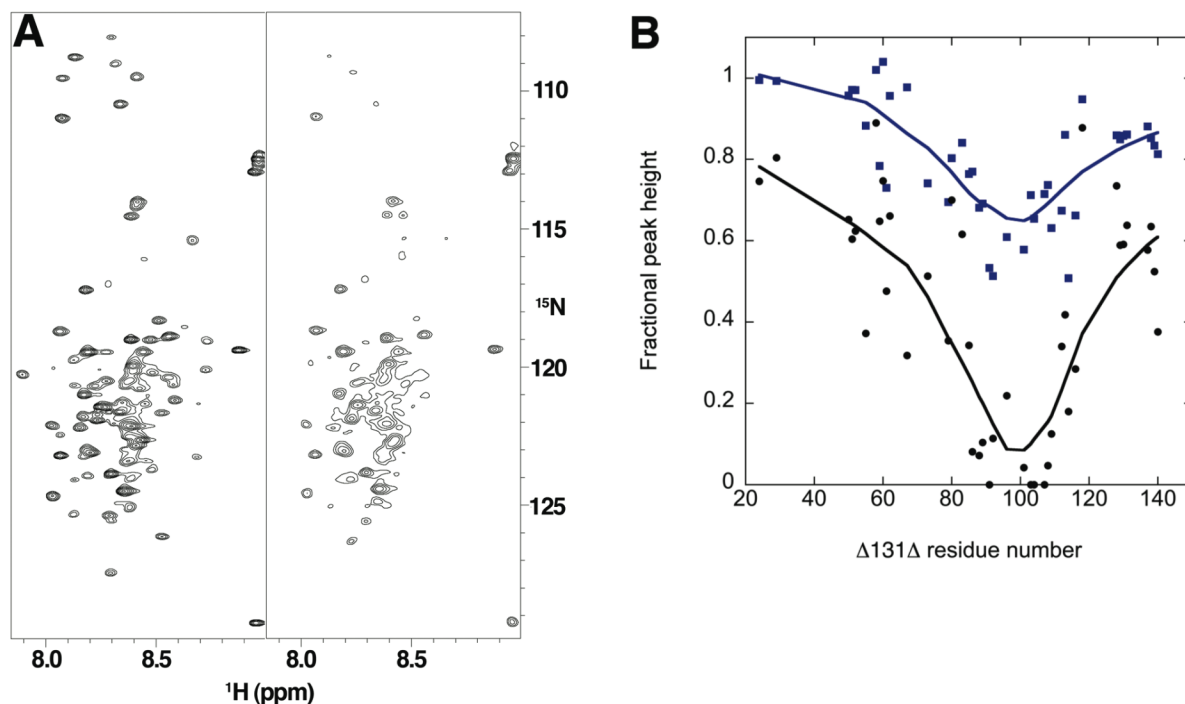


**Figure 6. HtpG binds a specific region on  $\Delta 131\Delta$ .** (a) The HSQC of  $\Delta 131\Delta$  has 41 peaks that can be unambiguously assigned. Addition of an equimolar concentration of HtpG results in peak height reduction for many but not all of the  $\Delta 131\Delta$  residues. (b) Peak for different  $\Delta 131\Delta$  residues are differentially affected by HtpG. At a 1:10 and 1:1 concentration ratios (HtpG: $\Delta 131\Delta$ , blue squares and black circles) in a loss of peak intensity is observed from residues 85-110, whereas the other residues are progressively less affected away from this region. Solid lines are interpolations.

## Discussion

Hsp90:client interactions have proven difficult to study *in-vitro* likely because the chaperone favors interactions with partially folded or metastable client states that are only transiently populated. Here our aim has been to test the use of a model system of non-native states for probing Hsp90:substrate interactions. Our choice of system was guided by the fact that although globally unfolded,  $\Delta 131\Delta$  has significant residual structure, is only marginally unstable, but is soluble and non-aggregating even at high concentrations. Using a combination of SAXS, FRET, fluorescence anisotropy and NMR, we have found that HtpG binds a specific region of  $\Delta 131\Delta$  and this binding results in large-scale conformational and functional changes to the chaperone. These findings reveal basic steps in the Hsp90: $\Delta 131\Delta$  nucleotide cycle (Figure 7).

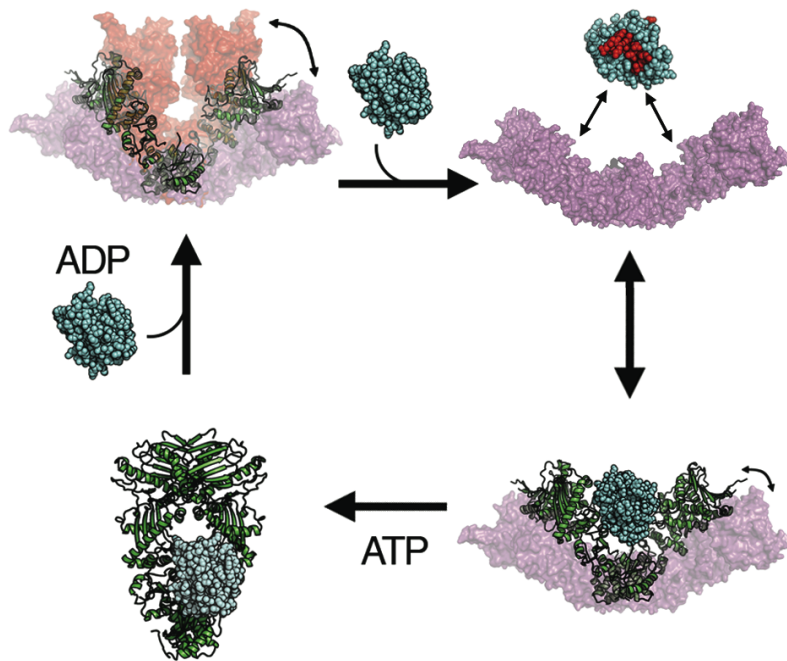


**Figure 7. Hsp90 chaperone cycle for  $\Delta 131\Delta$ .** Under apo conditions, Hsp90's flexibility allows for efficient substrate loading by structural accommodation. This substrate-loaded state accelerates closure to the ATP conformation and subsequent hydrolysis.

Our SAXS measurements and modeling suggest that under apo conditions HtpG adapts its conformation to  $\Delta 131\Delta$  by a partial closure (Figure 3c). This structural analysis was aided by localizing  $\Delta 131\Delta$  with *ab-initio* reconstructions prior to structure-based fitting and rigid-body analysis. The SAXS fitting on full-length HtpG shows that upon binding  $\Delta 131\Delta$  the chaperone adopts an equilibrium between a ‘V’-shaped conformation and a fully open state (Figure 3c, Table S1), indicating that Hsp90 maintains significant flexibility even after substrate loading. The residual flexibility suggests that Hsp90 could accommodate other cochaperones or binding partners within the loaded conformation. Also, to advance through the nucleotide cycle, Hsp90 must undergo large conformational changes requiring significant structural plasticity to reach the ATP state. While our SAXS modeling suggests that  $\Delta 131\Delta$  remains bound to roughly the same region on HtpG, it is likely that concomitant with HtpG closure, there is some alteration in  $\Delta 131\Delta$ :HtpG interactions and perhaps in  $\Delta 131\Delta$  structure.

The apo, substrate-bound conformation of Hsp90 has a significant impact on the kinetics of the nucleotide cycle. Following previous work [30, 31], we used kinetic FRET measurements to show that closure to the ATP state is significantly accelerated by  $\Delta 131\Delta$  (Figure 5). This closure acceleration is paralleled by an ATPase acceleration (Figure S7b), similar to reports of ATPase stimulation of human Hsp90 by the ligand binding domain of the glucocorticoid receptor [33]. Our findings suggest that closure is rate limiting in ATP hydrolysis by Hsp90, and that client binding activates the chaperone by lowering this rate-limiting conformational barrier. The coupling between client

binding, Hsp90 conformational changes and subsequent ATP hydrolysis, suggests a simple mechanism by which Hsp90 restricts unnecessary ATP utilization while maximizing efficiency of client activation.

The ATP state transition involves numerous structural changes: (i) ATP binding restructures an N-terminal helical region that makes cross-monomer contacts, (ii) dramatically changes the NTD/MD orientation leading to an interaction between a highly conserved arginine (residue 336 in HtpG) and the ATP  $\gamma$ -phosphate, and (iii) is associated with the release of a  $\beta$ -strand that is swapped across monomers stabilizing N-terminal dimerization, however it is not known which of these processes (or others) are rate-limiting. Indeed, our SAXS measurements are too low resolution to conclude whether  $\Delta 131\Delta$  contacts are restricted to a single monomer or whether  $\Delta 131\Delta$ -induced closure is driven by cross monomer contacts. A detailed study is needed to address these points.

The results with  $\Delta 131\Delta$  suggest that Hsp90's conformational plasticity is functionally important and may allow it to adapt to structurally diverse substrates, which catalyze further structural changes that lead to ATP hydrolysis. This implies that Hsp90's flexibility should be conserved, which is indeed true for the homologs investigated by SAXS (HtpG, Hsc82, hHsp90a, Grp94 and TRAP, [14] and unpublished observations). For bacterial, yeast and human Hsp90, detailed electron microscopy measurements have shown that a three-state apo-ATP-ADP conformational cycle is conserved but that the equilibria between states is species-specific [13]. This result suggested that the Hsp90 conformational equilibrium is tuned to the specific

substrate/cochaperone requirements of each organism. Indeed,  $\Delta 131\Delta$  binds to the bacterial, yeast, and human Hsp90 homologs and affects their conformations however the relative magnitude of these structural changes are species-specific (Figure S2).

The conformational diversity and large structure of Hsp90 suggests that it can provide a combinatorial set of binding surfaces and conformations for interacting with structurally diverse substrates. An electron microscopy reconstruction of an Hsp90-Cdc37-Cdk4 complex [34] shows that Hsp90 adopts a more closed conformation in complex with the kinase-cochaperone complex than we observe with  $\Delta 131\Delta$ . This observation suggests that different substrates and cochaperone complexes can be accommodated by different Hsp90 conformations and possibly have different nucleotide cycle dependences.

Our NMR measurements suggest that Hsp90 selectively interacts with a region of  $\Delta 131\Delta$  (residues  $\sim 85-110$ ) that has been shown to have significant structure despite the fact that  $\Delta 131\Delta$  is globally unfolded [22-24, 32]. Hsp90 is often referred to as operating in later stages of client folding, consistent with this finding. Future studies will be required to reveal whether binding changes the structure within this region, which specific elements of Hsp90 are involved in binding, and the impact of nucleotide-induced conformational changes in Hsp90. Inspection of the fractional peak height distribution in Figure 6b also shows decreased peak heights towards the C-terminus of  $\Delta 131\Delta$ , possibly indicating a second binding site. Clearly, although SAXS measurements are ideal for characterizing the flexible Hsp90 conformation and the



influence of  $\Delta^{131}\Delta$ , high-resolution measurements are needed to elucidate these molecular details.

### **Acknowledgements**

We thank David Shortle for kindly providing the  $\Delta^{131}\Delta$  construct and Greg Hura for help with SAXS data collection and Mark Kelly for help with NMR. Funding for this project was provided by the Howard Hughes Medical Institute. TOS was supported by a Damon Runyon Cancer Research Foundation fellowship. Many thanks to members of the Agard lab for helpful discussions.

## Supplemental Information

### Supplemental Figures and Legends

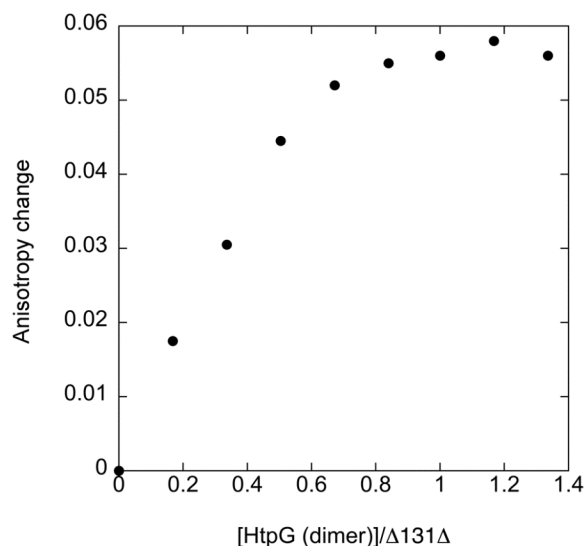


**Figure S1. Binding saturation measurements.** To determine binding stoichiometry we measured the HtpG associated change in anisotropy of a 50  $\mu$ M  $\Delta$ 131 $\Delta$  sample containing 500 nM IAEDANS -labeled  $\Delta$ 131 $\Delta$ . By increasing molar ratios of HtpG: $\Delta$ 131 $\Delta$  anisotropy saturation was achieved close to a 1:1 stoichiometry of HtpG (dimer): $\Delta$ 131 $\Delta$ . Conditions same as Figure 2.

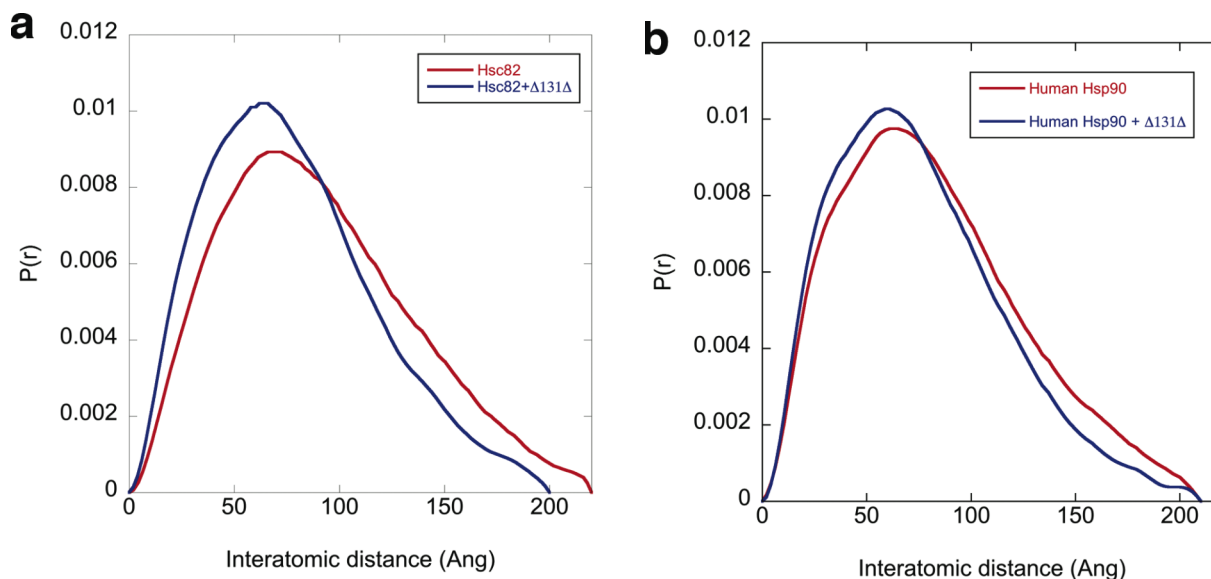


**Figure S2. Substrate-induced conformational changes in the yeast and human Hsp90 homologs.** Similar to the behavior of HtpG,  $\Delta$ 131 $\Delta$  induces a structural contraction in the (a) yeast and (b) human Hsp90 homologs. The structural contractions are smaller than for HtpG, which is consistent with electron microscopy studies that show the yeast and human Hsp90 homologs favor the open state in absence of nucleotide, relative to HtpG.

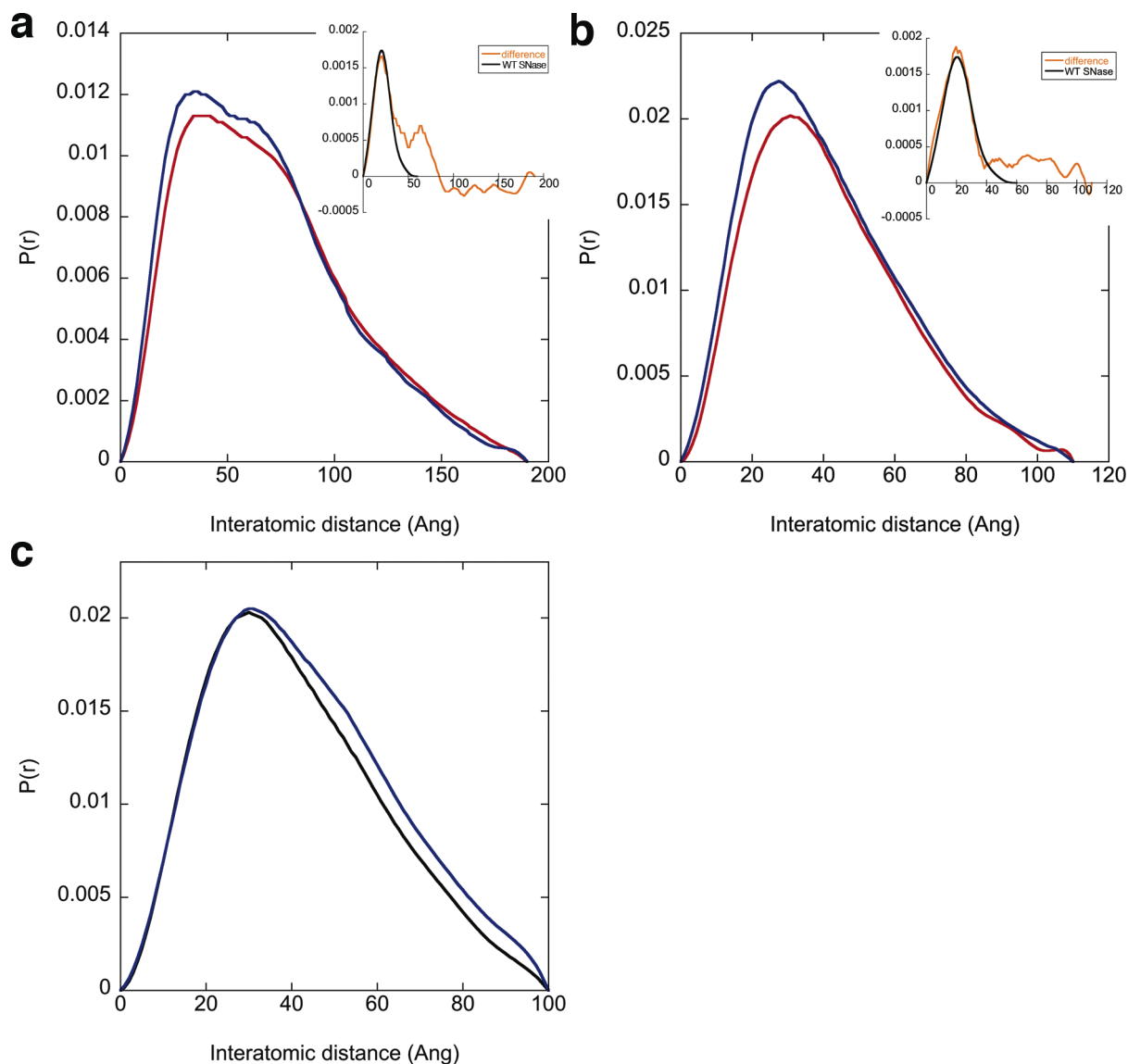


**Figure S3. The Hsp90 conformational changes are specific to unfolded SN.** (a) The SAXS distance distributions for HtpG alone (red curve) and with folded, wild-type SN (blue) are very similar with the exception of additional magnitude around 20 Å. The difference distribution is shown in the inset (orange) and compares well with the scattering from the wild-type SN alone (black). This shows that HtpG and SN are scattering as two independent units, and not inducing any significant conformational change. (b) Similar results are observed for the scattering of the NM domain from HtpG (residues 1-495, red), and with mixture with wild-type SN (blue). (c) In contrast, the NM domain with a stoichiometric concentration of  $\Delta 131\Delta$  (blue) has increased scattering at long distances.

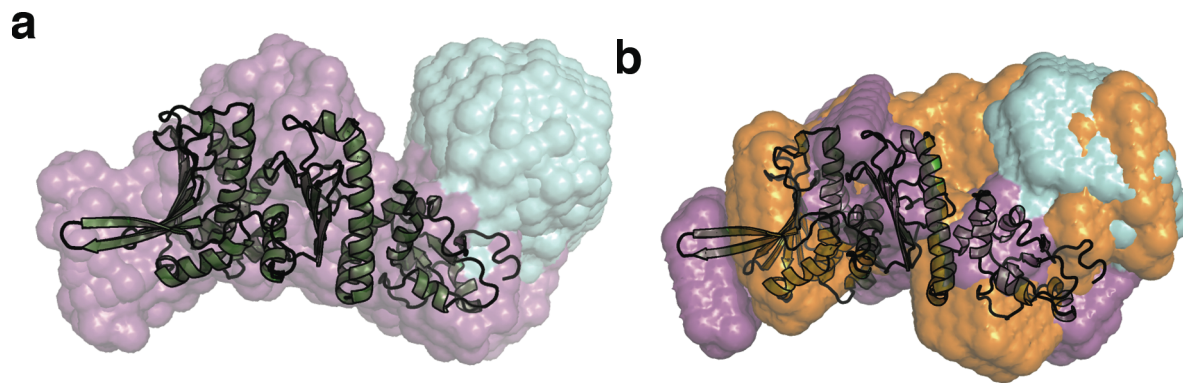


**Figure S4. DAMMIN and MONSA reconstructions with the NM domain and  $\Delta 131\Delta$ .** (a) Five independent MONSA runs were aligned and overlaid to show that independent reconstructions are highly consistent. (b) The volume envelope for the MONSA reconstruction and DAMMIN (orange) largely agree, although there are local discrepancies. The additional information from simultaneous fitting exploited in MONSA provides higher resolution information versus DAMMIN.

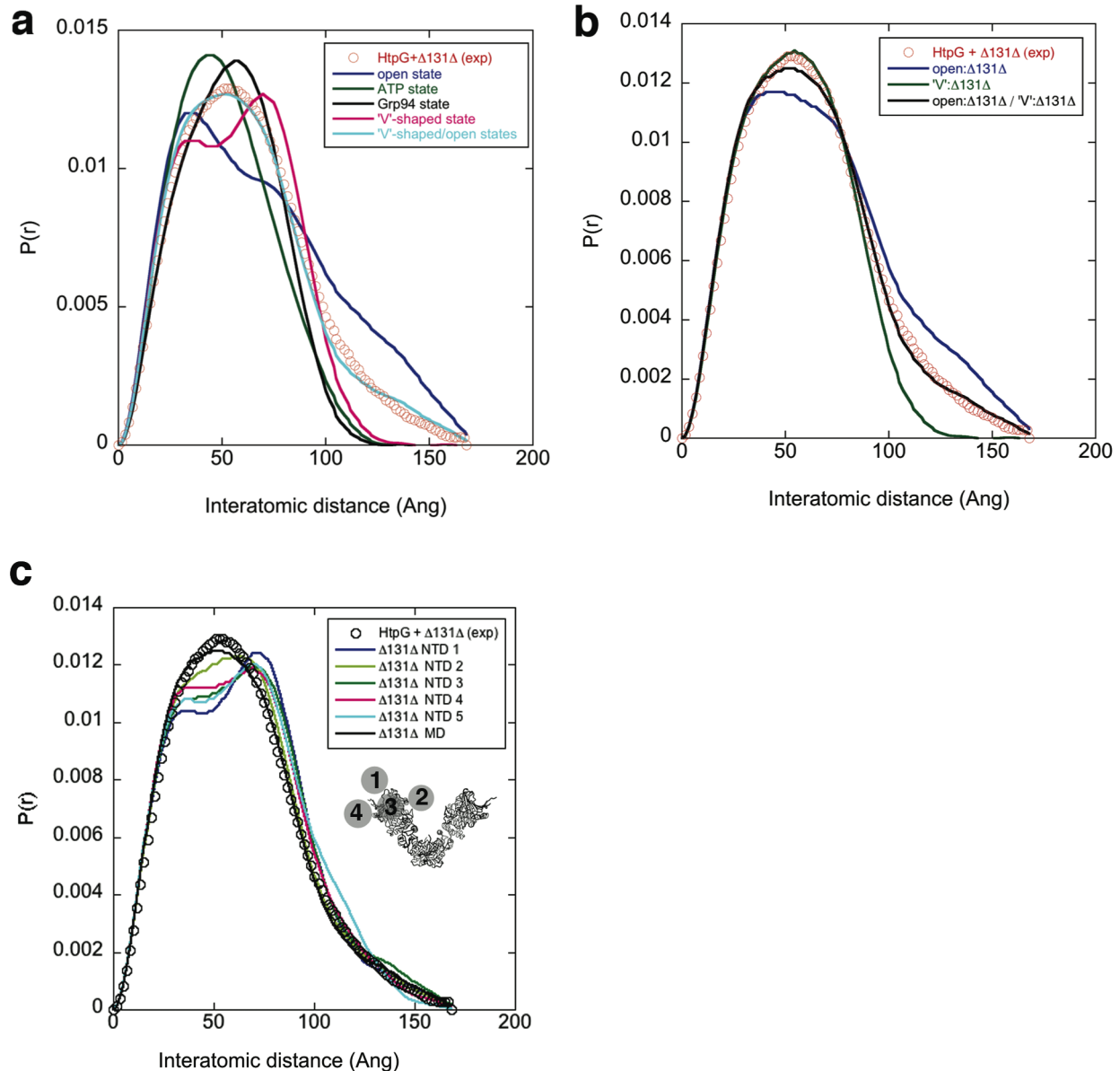


**Figure S5. Structure-based fitting of SAXS data.** (a) The structure-based fitting shows that a combination of states is required to fit the experimental data (circles), which is clear by a comparison with  $P(r)$  distributions for individual HtpG conformations (solid lines). A 62/38 linear combination of the 'V'-shaped/open states fits with an R-factor of 9.3 %. (b) Upon addition of  $\Delta 131\Delta$  to the open and 'V'-shaped conformations, the resulting single state  $P(r)$  distributions better match the experimental distribution. A 49/51 linear combination of these states results in a good fit (black line) that is quantified by a low R-factor of 3.8%. (c) To examine whether  $\Delta 131\Delta$  located at the NTD could satisfactorily fit the scattering data, we generated structural models with  $\Delta 131\Delta$  located at 5 positions on the NTD in both the 'V'-shaped and open state. These positions are shown below the legend with position 5 opposite position 3. The original  $\Delta 131\Delta$  MD location is shown with a black sphere. Linear combination fitting was performed and the R-factors for  $\Delta 131\Delta$  at positions 1-5: 13.0, 4.8, 11.5, 9.2, and 12.8 % are greater than the MD value 3.8%.

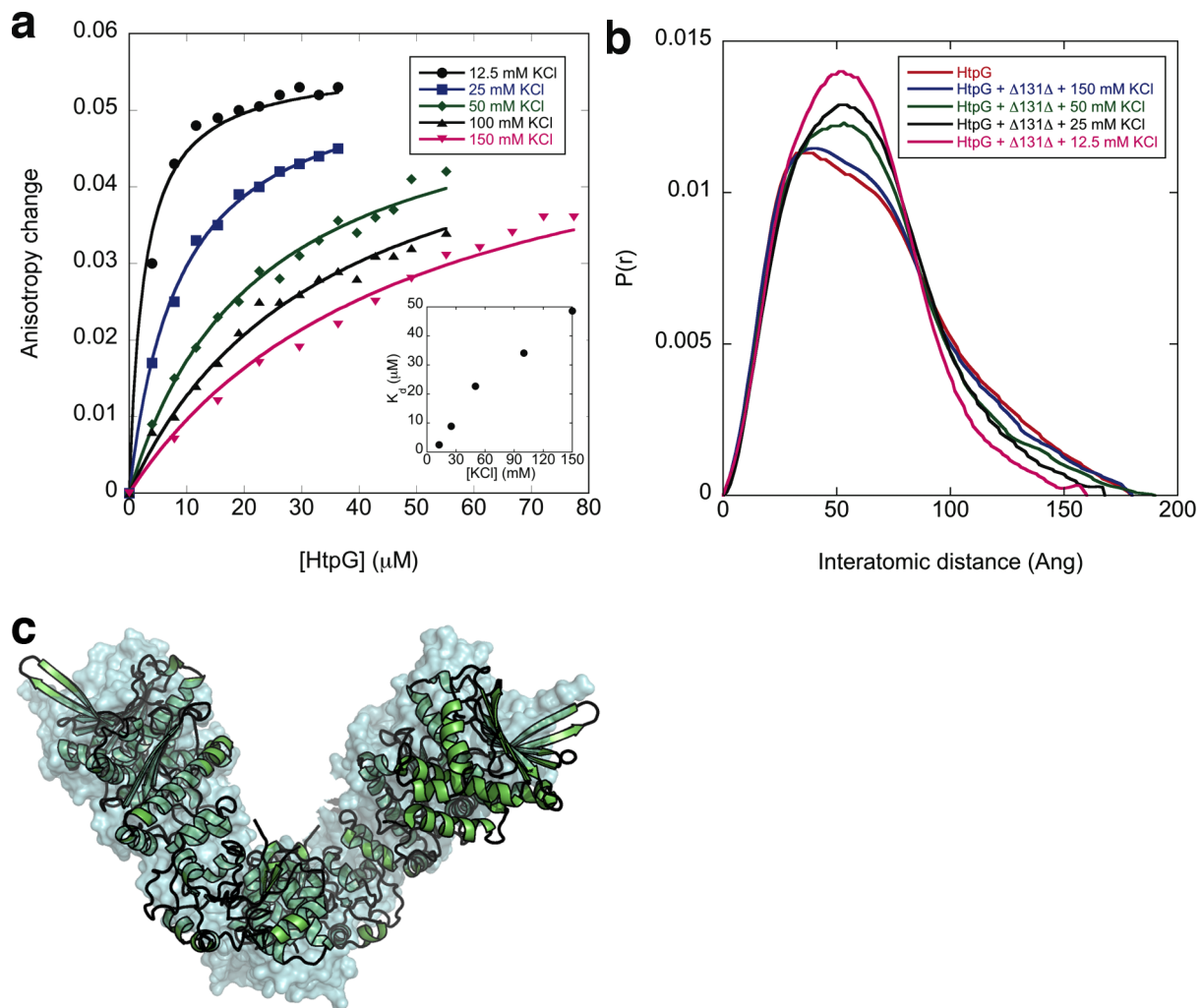


**Figure S6. Salt-dependent binding affinity.** (a) The anisotropy binding assay shows a strong KCl dependence in  $\Delta 131\Delta$  affinity. The  $K_d$  values from fitting with standard noncooperative binding is shown in the inset. (b) SAXS measurements made at varying KCl concentrations mirrors the salt trend; decreasing the salt results in a larger substrate-induced conformational change. (c) The structure-based fitting of HtpG/ $\Delta 131\Delta$  scattering data showed that the crystallographically-solved conformation (surface, pdb: 2IOQ) matches well with the conformation determined by rigid-body modeling (cartoon).

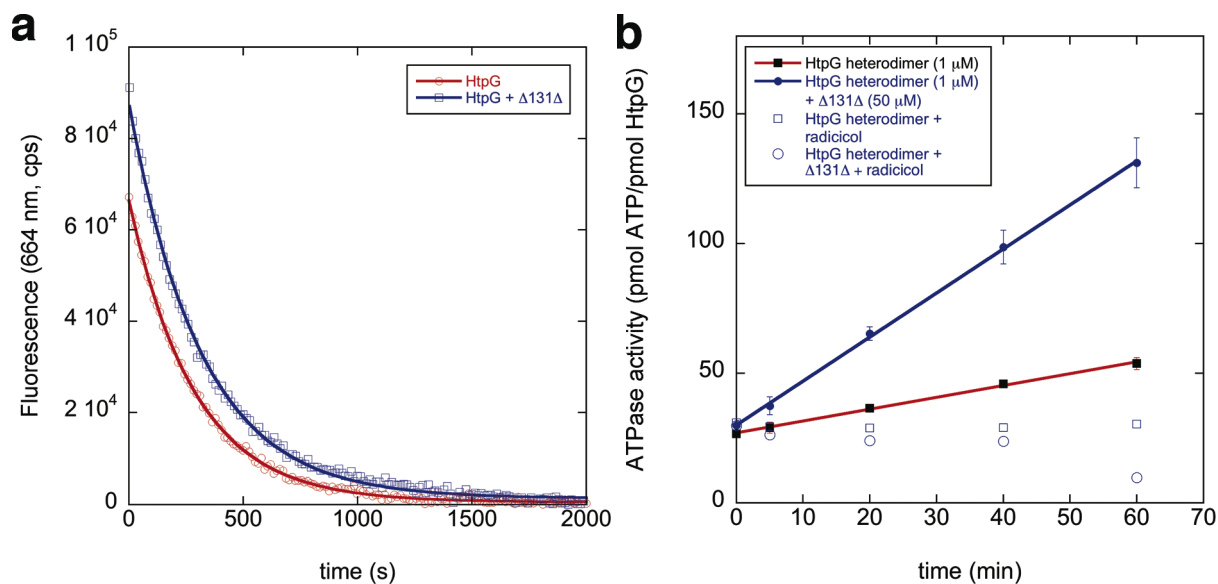


**Figure S7.  $\Delta 131\Delta$  does not affect the reopening rate from the ATP state.** (a) The reopening rate for the ATP/open transition was determined by preincubating hetero-labeled HtpG with AMPPNP (5 mM) until acceptor saturation was achieved. Then upon addition of excess of ADP (50 mM) the loss of FRET was monitored by acceptor fluorescence decrease. As opposed to closure where  $\Delta 131\Delta$  significantly affects the kinetics, reopening is not significantly changed. (b) ATP hydrolysis was measured by a previously described radiolabeled ATP assay. Similar to the  $\Delta 131\Delta$  acceleration of closure, there is a significant acceleration of ATP hydrolysis by HtpG. For a direct comparison to the FRET, we used the same heterodimer (E62C/D341C) used in that assay.

**Table S1. Conformational equilibrium of HtpG while bound to  $\Delta 131\Delta$ .**

	State population (%)		R-factor (%)
	Open: $\Delta 131\Delta^a$	'V': $\Delta 131\Delta^a$	
HtpG+ $\Delta 131\Delta$	58 [41, 58]	42 [42, 59]	3.1
	Open: $\Delta 131\Delta^a$	RBM: $\Delta 131\Delta^a$	
HtpG+ $\Delta 131\Delta$	58 [48, 64]	42 [32, 52]	3.4
+12 mM KCl	29 [25, 30]	71 [70, 75]	1.9
+50 mM KCl	66 [57, 70]	34 [30, 43]	1.9
H446K+ $\Delta 131\Delta$	29 [26, 29]	71 [71, 74]	3.3
	Open: $\Delta 131\Delta^a$	ATP: $\Delta 131\Delta^a$	
HtpG+ $\Delta 131\Delta$ + AMPPNP	26 [26, 31]	74 [69, 74]	3.4

Buffer conditions: 25 mM TRIS pH 7.5, 25 mM KCl, 10 mM MgCl<sub>2</sub>, unless other KCl conditions are noted, AMPPNP was 10 mM. <sup>a</sup>131 residues of SN were attached to HtpG conformations (open, ATP and the 'V'-shaped). RBM refers to the conformation determined by rigid-body modeling. H446K refers to an HtpG variant. The variability in fitted parameters with different open state models is shown in brackets.

## Experimental Procedures

The expression and purification of Hsp90 homologs and variants as well as  $\Delta 131\Delta$  has been described previously [8, 13, 23, 35]. SAXS measurements were performed at the SIBYLS beamline (12.3.1) at the Advanced Light Source in Berkeley. Scattering was measured with 0.5, 2, and 5 second integrations and buffer subtracted. The radial intensity was converted to the  $P(r)$  representation with the GNOM program [28].  $D_{max}$  cut-off values were selected manually to achieve smooth tails at high distance values.

## SAXS analysis

DAMMIN [29] reconstructions used spherical starting models with no symmetry constraints. MONSA [29] reconstructions used simultaneous fitting on multiple data sets (the NM domain and the NM/ $\Delta 131\Delta$  complex) keeping the  $\Delta 131\Delta R_g$  fixed at 18 Å. The SUBCOMP program was used to align structures into DAMMIN and MONSA reconstructions. 131 residues of an SN crystal structure (1STN) was used to approximate scattering from  $\Delta 131\Delta$  by appending it to the middle domains of the crystallographically solved 'V'-shaped conformation (2IOQ) as well as the open, Grp94, and ATP conformations. This was achieved by aligning HtpG conformations to the NM/ $\Delta 131\Delta$  MONSA envelope and positioning SN to avoid steric clash with HtpG. All HtpG conformations are available for download (<http://www.msg.ucsf.edu/agard/>).



Structure-based fitting and rigid-body analysis of SAXS data was performed with the PRFIT program, described previously [9]. The quality of fit is quantified by an R-factor

$$R = \sum \left| \frac{I_{\text{obs}}(s) - I_{\text{fit}}(s)}{I_{\text{obs}}(s)} \right|$$

For rigid-body analysis, the N-terminal and middle domains of HtpG were allowed to pivot against the C-terminal domain at residue 500 using rigid-body analysis described previously [8, 9, 14]. General three-axis rotational motion around this pivot started with a course step size of 10° and then was refined with 1° steps. The attached 131 residues of SN were included on a single monomer arm. The rigid-body fitting was simultaneously performed on multiple data sets with varying levels of  $\Delta 131\Delta$ -induced closure. Specifically, we used a salt series that titrates the binding affinity and degree of closure (Figures S6a and b) and a previously characterized HtpG variant (H446K) that favors the Grp94 conformation [14]. If the 'V'-shaped conformation is a robust solution, then the rigid-body search will independently identify this state in these diverse data sets. To determine the robustness of the SAXS modeling, limiting cases with zero or two bound  $\Delta 131\Delta$  were investigated and indeed only modestly affect fitted parameters (range shown in brackets in Table S1) as expected given the small size of  $\Delta 131\Delta$  relative to HtpG.

### Fluorescence measurements

Fluorescence anisotropy was measured on a Jobin Yvon fluorometer with excitation and emission monochromator slits both set to 5 nm, an integration time of 2

seconds, and excitation/emission wavelengths of 340/480 nm. A five-fold molar excess of IAEDANS (Invitrogen) was used to label a cysteine variant of  $\Delta 131\Delta$ , K16C, at room temperature for one hour and free dye was removed by extensive dialysis. Measurements with nucleotides and geldanamycin were pre-equilibrated for at least 20 minutes. Binding stoichiometry measurements were performed at 50  $\mu\text{M}$   $\Delta 131\Delta$  with only a small concentration, 500 nM, labeled with IAEDANS.

FRET measurements were performed on the same fluorometer. A five-fold molar excess of dye (Alexafluor 647 and Alexafluor 555, Invitrogen) was incubated with HtpG variants E62C and D341C for three hours at room temperature. HtpG has no native cysteines. The reaction was quenched with 2-fold excess of BME over dye. Free dye was separated by extensive dialysis and G50 size exclusion chromatography (Roche). HtpG heterodimers (250 nM at a 1:1 stoichiometry) were formed by incubation for 30 minutes at 30 °C. FRET measurements had 250 nM of heterodimer at a 1:1 stoichiometry. Closure was initiated by manual mixing of 5 mM AMPPNP and reopening was initiated by subsequent addition of 50 mM ADP. The excitation and emission slits were 2 and 3 nm, with an integration time of 0.3 s. To control for photobleaching and burst phase fluorescence, separate reactions without nucleotide were monitored and subtracted from nucleotide-containing samples.

### **ATPase measurements**

ATP hydrolysis was measured by a phosphate release assay described previously [35]. Briefly, 1  $\mu\text{M}$  of HtpG dimer was incubated with 50  $\mu\text{M}$   $\Delta 131\Delta$  at pH 9,

50 mM KCl, 5 mM MgCl<sub>2</sub> at 22 °C and assayed for radiolabeled <sup>32</sup>P<sub>i</sub> release. 5mM ATP was used with 0.8 pM of radiolabeled ATP. Negligible background ATPase was confirmed by addition of 200 μM radicicol. Free P<sub>i</sub> was separated from ATP and ADP by thin layer chromatography. Spot imaging was performed on a Typhoon Imager (GE Healthcare) and was quantified with the ImageQuant program (GE Healthcare).

### **NMR analysis**

Isotopically labeled Δ131Δ was produced by a 10 mL overnight starter culture, which was spun down and washed in M9 minimal growth medium, and then resuspended in 1 L of M9 media supplemented with 1 g/L <sup>15</sup>N ammonium chloride and 0.5 g/L isogrow growth supplement (Sigma). Uniformly labeled <sup>13</sup>C, <sup>15</sup>N samples were derived similarly with 1 g of <sup>13</sup>C glucose per liter of media. HSQC measurements were performed on a Bruker Avance800 with Δ131Δ concentration of 200 μM. HNCA and CBCA(CO)NH measurements were performed on an Avance500. Data was processed with NMRPipe [36] and peak height analysis was performed with the ccpn analysis software (<http://www.ccpn.ac.uk>). The Δ131Δ assignment was transferred from a previously published study of Δ131Δ [24] and confirmed with the HNCA and CBCA(CO)NH experiments.

## References:

1. Young, J.C., I. Moarefi, and F.U. Hartl, *Hsp90: a specialized but essential protein-folding tool*. J Cell Biol, 2001. 154(2): p. 267-73.
2. Jakob, U., et al., *Transient interaction of Hsp90 with early unfolding intermediates of citrate synthase. Implications for heat shock in vivo*. J Biol Chem, 1995. 270(13): p. 7288-94.
3. Wiech, H., et al., *Hsp90 chaperones protein folding in vitro*. Nature, 1992. 358(6382): p. 169-70.
4. Schneider, C., et al., *Pharmacologic shifting of a balance between protein refolding and degradation mediated by Hsp90*. Proc Natl Acad Sci U S A, 1996. 93(25): p. 14536-41.
5. Falsone, S.F., et al., *The molecular chaperone Hsp90 modulates intermediate steps of amyloid assembly of the Parkinson-related protein alpha-synuclein*. J Biol Chem, 2009. 284(45): p. 31190-9.
6. Forsythe, H.L., et al., *Stable association of hsp90 and p23, but Not hsp70, with active human telomerase*. J Biol Chem, 2001. 276(19): p. 15571-4.
7. Shiau, A.K., et al., *Structural Analysis of E. coli hsp90 reveals dramatic nucleotide-dependent conformational rearrangements*. Cell, 2006. 127(2): p. 329-40.
8. Krukenberg, K.A., et al., *Multiple conformations of E. coli Hsp90 in solution: insights into the conformational dynamics of Hsp90*. Structure, 2008. 16(5): p. 755-65.
9. Krukenberg, K.A., et al., *pH-Dependent Conformational Changes in Bacterial Hsp90 Reveal a Grp94-Like Conformation at pH 6 That Is Highly Active in Suppression of Citrate Synthase Aggregation*. J Mol Biol, 2009.
10. Dollins, D.E., et al., *Structures of GRP94-nucleotide complexes reveal mechanistic differences between the hsp90 chaperones*. Mol Cell, 2007. 28(1): p. 41-56.

11. Ali, M.M., et al., *Crystal structure of an Hsp90-nucleotide-p23/Sba1 closed chaperone complex*. *Nature*, 2006. 440(7087): p. 1013-7.
12. Street, T.O., et al., *Osmolyte-induced conformational changes in the Hsp90 molecular chaperone*. *Protein Sci*, 2009.
13. Southworth, D.R. and D.A. Agard, *Species-dependent ensembles of conserved conformational states define the Hsp90 chaperone ATPase cycle*. *Mol Cell*, 2008. 32(5): p. 631-40.
14. Krukenberg, K.A., et al., *Grp94, the endoplasmic reticulum Hsp90, has a similar solution conformation to cytosolic Hsp90 in the absence of nucleotide*. *Protein Sci*, 2009. 18(9): p. 1815-27.
15. Bron, P., et al., *Apo-Hsp90 coexists in two open conformational states in solution*. *Biol Cell*, 2008. 100(7): p. 413-25.
16. Onuoha, S.C., et al., *Structural studies on the co-chaperone Hop and its complexes with Hsp90*. *J Mol Biol*, 2008. 379(4): p. 732-44.
17. Zhang, W., et al., *Biochemical and structural studies of the interaction of Cdc37 with Hsp90*. *J Mol Biol*, 2004. 340(4): p. 891-907.
18. Taipale, M., D.F. Jarosz, and S. Lindquist, *HSP90 at the hub of protein homeostasis: emerging mechanistic insights*. *Nat Rev Mol Cell Biol*, 2010. 11(7): p. 515-28.
19. Rudiger, S., et al., *CRINEPT-TROSY NMR reveals p53 core domain bound in an unfolded form to the chaperone Hsp90*. *Proc Natl Acad Sci U S A*, 2002. 99(17): p. 11085-90.
20. Motojima-Miyazaki, Y., M. Yoshida, and F. Motojima, *Ribosomal protein L2 associates with E. coli HtpG and activates its ATPase activity*. *Biochem Biophys Res Commun*, 2010.
21. Shortle, D., *The expanded denatured state: an ensemble of conformations trapped in a locally encoded topological space*. *Adv Protein Chem*, 2002. 62: p. 1-23.

22. Wang, Y. and D. Shortle, *The equilibrium folding pathway of staphylococcal nuclease: identification of the most stable chain-chain interactions by NMR and CD spectroscopy*. *Biochemistry*, 1995. 34(49): p. 15895-905.
23. Alexandrescu, A.T., C. Abeygunawardana, and D. Shortle, *Structure and dynamics of a denatured 131-residue fragment of staphylococcal nuclease: a heteronuclear NMR study*. *Biochemistry*, 1994. 33(5): p. 1063-72.
24. Alexandrescu, A.T. and D. Shortle, *Backbone dynamics of a highly disordered 131 residue fragment of staphylococcal nuclease*. *J Mol Biol*, 1994. 242(4): p. 527-46.
25. Wang, Y., A.T. Alexandrescu, and D. Shortle, *Initial studies of the equilibrium folding pathway of staphylococcal nuclease*. *Philos Trans R Soc Lond B Biol Sci*, 1995. 348(1323): p. 27-34.
26. Baskakov, I. and D.W. Bolen, *Forcing thermodynamically unfolded proteins to fold*. *J Biol Chem*, 1998. 273(9): p. 4831-4.
27. Shortle, D. and A.K. Meeker, *Residual structure in large fragments of staphylococcal nuclease: effects of amino acid substitutions*. *Biochemistry*, 1989. 28(3): p. 936-44.
28. Svergun, D., *Mathematical models in small-angle scattering data analysis*. *J.Appl.Cryst.*, 1991. 24: p. 485-492.
29. Svergun, D.I., *Restoring low resolution structure of biological macromolecules from solution scattering using simulated annealing*. *Biophys J*, 1999. 76(6): p. 2879-86.
30. Hessling, M., K. Richter, and J. Buchner, *Dissection of the ATP-induced conformational cycle of the molecular chaperone Hsp90*. *Nat Struct Mol Biol*, 2009. 16(3): p. 287-93.
31. Mickler, M., et al., *The large conformational changes of Hsp90 are only weakly coupled to ATP hydrolysis*. *Nat Struct Mol Biol*, 2009. 16(3): p. 281-6.

32. Ohnishi, S. and D. Shortle, *Effects of denaturants and substitutions of hydrophobic residues on backbone dynamics of denatured staphylococcal nuclease*. Protein Sci, 2003. 12(7): p. 1530-7.
33. McLaughlin, S.H., H.W. Smith, and S.E. Jackson, *Stimulation of the weak ATPase activity of human hsp90 by a client protein*. J Mol Biol, 2002. 315(4): p. 787-98.
34. Vaughan, C.K., et al., *Structure of an Hsp90-Cdc37-Cdk4 complex*. Mol Cell, 2006. 23(5): p. 697-707.
35. Cunningham, C.N., K.A. Krukenberg, and D.A. Agard, *Intra- and intermonomer interactions are required to synergistically facilitate ATP hydrolysis in Hsp90*. J Biol Chem, 2008. 283(30): p. 21170-8.
36. Delaglio, F., et al., *NMRPipe: a multidimensional spectral processing system based on UNIX pipes*. J Biomol NMR, 1995. 6(3): p. 277-93.

## Chapter 5

Cross monomer substrate contacts reposition the Hsp90

N-terminal domain and prime the chaperone activity

**Contributing Authors:** Timothy O. Street, Kliment Verba, Chung-Tien Lee, Matthias P. Mayer and David A. Agard.

*Citation: Cross-Monomer Substrate Contacts Reposition the Hsp90 N-Terminal Domain and Prime the Chaperone Activity. Street TO, Lavery LA, Verba KA, Lee CT, Mayer MP, Agard DA. J Mol Biol. 2012.*



## Preface

Hsp90 undergoes large nucleotide dependant conformational changes where previous studies have shown that the rate-limiting step to hydrolysis is closure. We had shown that a model substrate ( $\Delta 131\Delta$ ) could accelerate this transition preserving ATP expenditure for times of functional use. In support of this being a conserved feature of Hsp90:client interactions, the glucocorticoid receptor and ribosomal protein L2 (verified *in vivo* client proteins) also accelerate the chaperone's ATPase rate. However the mechanism by which this occurs was unknown.

The work presented in this chapter is a continuation of collaborative work with Timothy Street (the lead author on this paper). My new contribution to what follows was the development of a FRET pair that could measure the rotation of the N-terminal domain (NTD) relative to the middle domain (MD) in an effort to dissect the conformational changes on pathway to the closed state. Combined with the work of Timothy and the other authors on this paper (for reference information see title page to this chapter) we learn that  $\Delta 131\Delta$  accelerates the rate-limiting transition via an asymmetric mechanism. Here the model substrate engages a patch of residues that span the MD and c-terminal domain (CTD) and cross-monomer contacts to induce a rotation of the NTD on-pathway to the closed state.

Applying knowledge gained from the work below (and a recent follow up study elucidating more of the client binding interface) to the newly discovered asymmetric active closed state discovered in TRAP1 (chapter 1) we proposed a mechanism for the Hsp90 family of chaperones that directly couples ATP hydrolysis to client re-modeling.

## **Summary**

The ubiquitous molecular chaperone Hsp90 plays a critical role in substrate protein folding and maintenance, but the functional mechanism has been difficult to elucidate. In previous work a model Hsp90 substrate revealed an activation process in which substrate binding accelerates a large open/closed conformational change required for ATP hydrolysis by Hsp90. While this could serve as an elegant mechanism for conserving ATP usage for productive interactions on the substrate, the structural origin of substrate catalyzed Hsp90 conformational changes are unknown. Here we find that substrate binding affects an intrinsically unfavorable rotation of the Hsp90 N-terminal domain (NTD) relative to the middle domain (MD) that is required for closure. We identify an MD substrate binding region on the interior cleft of the Hsp90 dimer and show that a secondary set of substrate contacts drive an NTD orientation change on the opposite monomer. These results suggest an Hsp90 activation mechanism in which cross-monomer contacts mediated by a partially structured substrate prime the chaperone for its functional activity.

## **Introduction**

Molecular chaperones confer stress resistance critical for survival under harsh environmental conditions and maintain protein homeostasis under normal conditions. Beyond their role in protein folding, chaperones affect protein activation and trafficking, facilitating the degradation of terminally misfolded proteins, and the formation and disassembly of macromolecular complexes. Hsp90 is a highly conserved member of the

chaperone family, and plays a unique role by its regulatory influence in eukaryotes via the activation of specific classes of substrates (also known as clients), such as nuclear receptors and kinases <sup>1</sup>. This broad regulatory influence is thought to underlie the potent influence of Hsp90 inhibitors on the growth of diverse cancer types <sup>2</sup>. Despite its fundamental cell biological and clinical importance, the mechanism by which Hsp90 stabilizes and remodels client proteins is not understood.

One confounding problem is that Hsp90 is large, conformationally dynamic, and undergoes dramatic structural changes upon ATP binding and hydrolysis (Figure 1A)<sup>3; 4; 5</sup>. Small-angle x-ray scattering (SAXS) and electron microscopy measurements (EM) have revealed an underlying complexity of Hsp90's conformational dynamics <sup>6; 7; 8; 9; 10; 11</sup>. The Hsp90 monomer is composed of three stable domains (N-terminal domain, NTD; middle, MD; C-terminal, CTD), and conformational flexibility results from their rigid body-like rearrangement. Under apo conditions a weak MD/CTD interface allows for a wide range of arm-arm geometries that can be influenced by pH and osmolyte conditions <sup>8; 12</sup>. This striking flexibility has been observed for highly diverse Hsp90 homologs <sup>6; 9</sup> and is postulated to be critically important to Hsp90's ability to recognize a remarkably diverse set of client proteins.

Unlike other molecular chaperones, Hsp90 appears to prefer largely folded but non-native states. This poses an additional practical challenge as such states can be difficult to populate and are prone to aggregation. Previous work introduced a well-behaved model client protein, the partially folded, but non-aggregating protein,  $\Delta 131\Delta$ , a fragment of Staphylococcal Nuclease that has been studied extensively by the protein

folding community<sup>13</sup>. Using this model client revealed that (i) under apo conditions Hsp90 partially closes around  $\Delta 131\Delta$ ; (ii) Hsp90 binds a highly structured region of  $\Delta 131\Delta$ ; (iii)  $\Delta 131\Delta$  accelerates a nucleotide-driven open/closed transition and stimulates ATP hydrolysis by Hsp90, effectively activating the chaperone by lowering a rate-limiting conformational barrier. Taken in the context that the ligand-binding domain of GR enhances the ATPase of the human Hsp90<sup>14</sup> and that the ribosomal subunit L2 enhances the ATPase of the bacterial Hsp90<sup>15</sup>, this suggests that activation of the rate-limiting Hsp90 conformational transition is a conserved feature of *bone fide* Hsp90 clients, similar to Hsp70 activation by peptide substrates. However, the mechanism by which substrate binding can drive the dramatic Hsp90 open-closed transition is unknown. Indeed, a previous low resolution SAXS analysis<sup>13</sup> could not determine whether  $\Delta 131\Delta$  makes cross-monomer contacts as has been observed for the activating cochaperone aha1<sup>16</sup>, or solely intramonomer contacts as observed for an Hsp90-cdc37-cdk4 (chaperone-cochaperone-kinase substrate) EM reconstruction<sup>17</sup>.

The Hsp90 ATPase is slow, on the order of 0.1-1 hydrolysis events per minute depending on the homolog and conditions<sup>18; 19; 20</sup>, and mirrors a slow conformational change from the open apo state to the closed ATP conformation<sup>13; 21</sup>. This dramatic transition involves a large change in arm-arm proximity, a domain-level change in the NTD orientation, and local structural changes within the NTD (lid closure over the nucleotide binding pocket, strand exchange between NTDs) and the MD (restructuring of the catalytic loop)<sup>3; 5; 19; 22</sup>. Although the relative importance of these structural changes to the closure rate is not known, the structures of the AMPPNP-bound canine

Grp94 (the Hsp90 homolog specific to the ER) and the apo bacterial Hsp90 (HtpG) suggest that the NTD rotational state plays an important role. Both structures exhibit an open resting state in which the NTDs are diametrically opposed, requiring a significant conformational change to come into a closure-competent alignment<sup>4; 5; 23</sup>. As illustrated in Figure 1A, the required movement involves a 90° rotation and a 25 Å translation of the NTD center of mass, rearranging ~2000 Å<sup>2</sup> at the MD interface. This aligns closed-state contacts (Figure 1A, red and blue spheres) and also repositions ATP by ~20 Å allowing the  $\gamma$ -phosphate to contact a highly conserved arginine on the MD (R336 in HtpG) that is essential for both closure and the bound ATP hydrolysis<sup>3; 20; 24</sup> (Figure 1B). Importantly, a full lid closure over the nucleotide pocket, which appears to be necessary for closure<sup>25</sup>, cannot occur in the NTD resting state due to a significant steric clash with the middle domain<sup>4</sup>. These observations suggest that an NTD rotation may be involved in the timing and order of many critical steps in closure and subsequent ATP hydrolysis.

Here we use our HtpG activating substrate to interrogate the open/closed transition and how this process is substrate-catalyzed. Key questions include (i) whether substrate contacts are within a single monomer or across monomers, (ii) defining the substrate binding region on HtpG in greater detail than could be achieved from our previous SAXS analysis, (iii) establishing whether a single set or multiple substrate contacts are utilized, (iv) determining how substrate binding affects HtpG structural dynamics, particularly at the NTD, and how this is related to the large energetic barrier to closure.

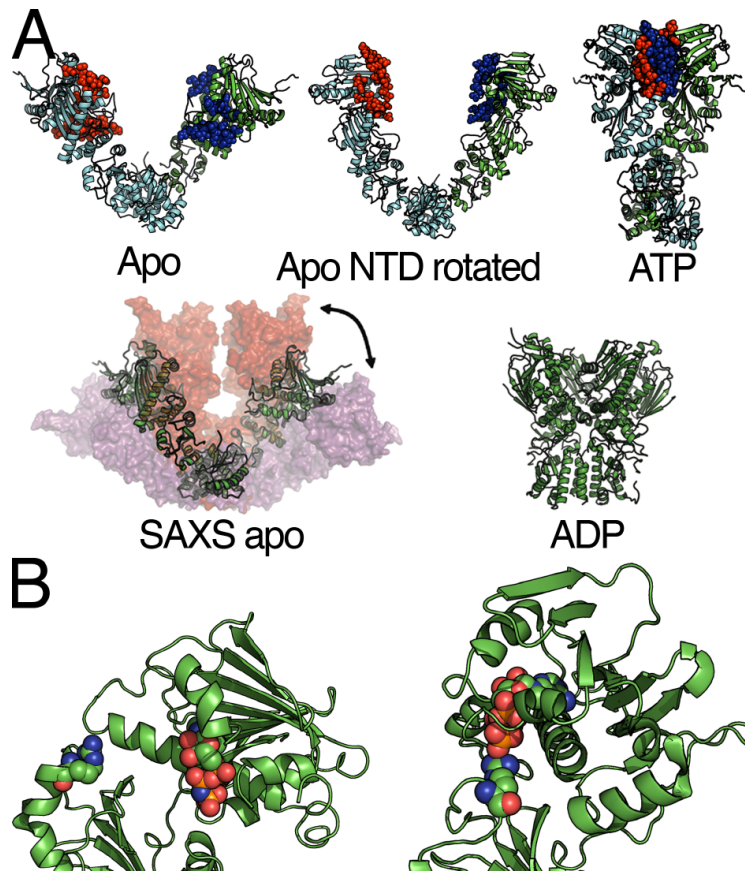


**Figure 1. Hsp90 conformational flexibility.** (A) The HtpG apo crystal structure (left <sup>5</sup>) requires significant structural plasticity to reach the closed ATP state (right <sup>3</sup>). The contacts formed in the closed conformation (red and blue spheres) are significantly out of alignment in the apo structure, prior to NTD rotation (middle). Shown below are the apo solution conformations of HtpG determined by SAXS <sup>7,8</sup>, and the compact ADP state <sup>9</sup>. (B) The NTD orientation in the Grp94 crystal structure <sup>4</sup> shows the nucleotide positioned far from the highly conserved arginine (spheres), whereas in the closed conformation the ATP  $\gamma$ -phosphate makes a direct contact <sup>3</sup>.

## Results

### Monitoring NTD movement by FRET

HtpG can be substrate-activated by accelerating the kinetics of a slow open/closed structural transition required for maximal ATP hydrolysis. Previously, closure kinetics were measured by FRET, in which opposite monomers were labeled

with donor and acceptor pairs <sup>13</sup>. To monitor NTD/MD rotation, we designed a FRET pair within a single monomer. We identified residues S52/D341 on the NTD/MD that significantly change distance (22 to 39 Å) in the open/closed conformations, yet remain solvent exposed. These sites were mutated to cysteine and labeled with Alexafluor 647 and Alexafluor 555. Since this pair is on the same monomer, a 20x excess of unlabeled wild-type HtpG was added to ensure only one labeled monomer per dimer.

Figure 2A shows the apo and AMPPNP fluorescence spectrum for this FRET pair. There is significant acceptor signal in the apo state, and after a prolonged incubation with AMPPNP there is a decrease/increase in acceptor/donor signal. Similar to previous studies, these measurements were performed at pH 9 because for HtpG at this pH there is a complete conversion between the open/closed state <sup>8</sup>. Upon adding AMPPNP there is a slow time-dependent loss in acceptor signal with single exponential kinetics (Figure 2B) and a rate ( $k=0.002\text{ s}^{-1}$ ) that is the same as the arm-arm closure rate measured previously <sup>13</sup>. As a control, we designed a fixed-point FRET pair within the MD (residues 350 and 362), which does not change distance in the open/closed transition and confirmed that closure did not affect this FRET signal (Figure S1A).

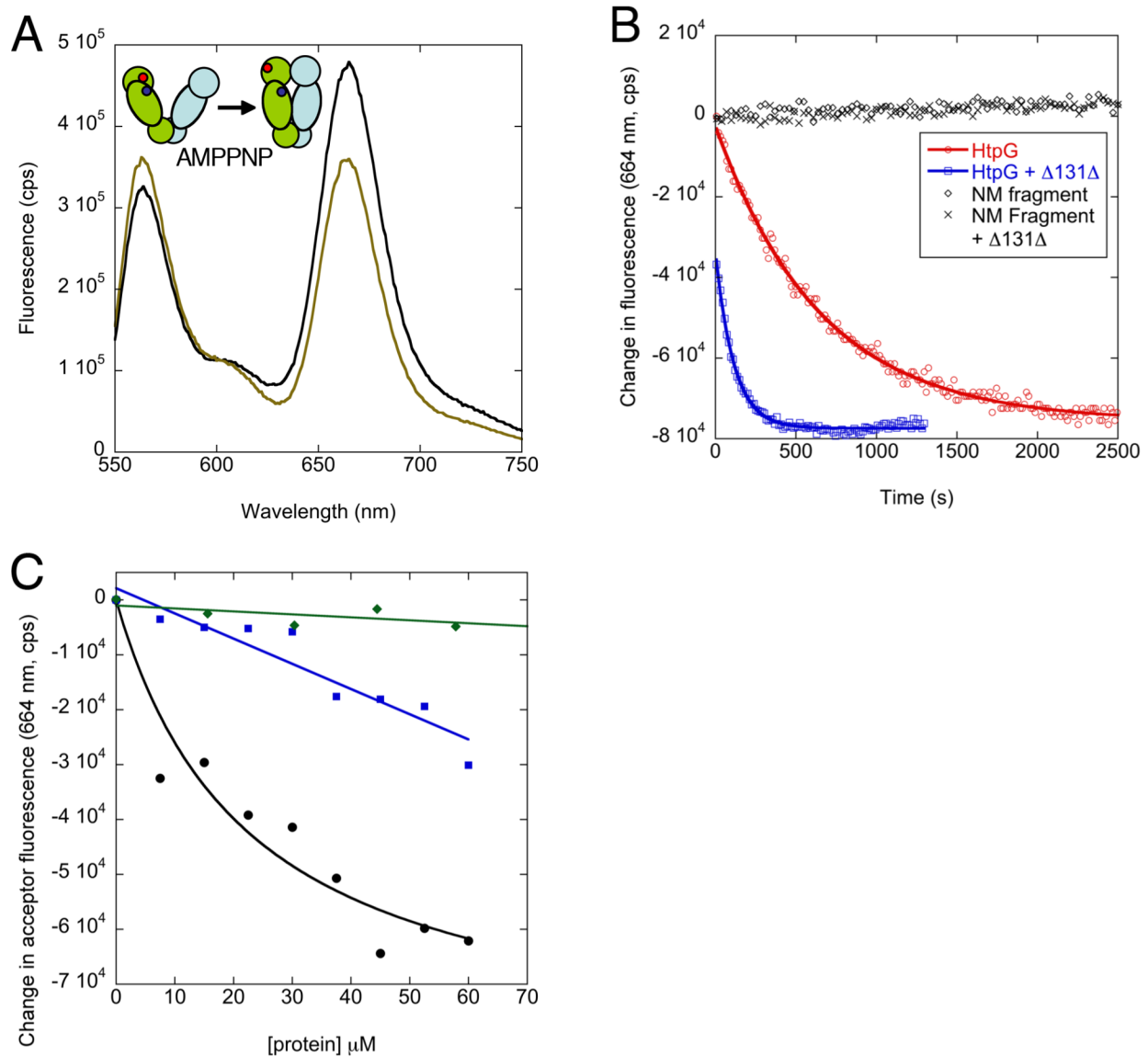


**Figure 2. Substrate binding affects an intrinsically unfavorable NTD rotation required for closure.** (A) FRET measurements within a single HtpG monomer track the NTD rotation associated with closure. This rotation is reflected in the apo (black) and AMPPNP (green) fluorescence spectrum. (B) Closure kinetics are monitored by the decrease in acceptor fluorescence and are significantly accelerated by  $\Delta 131\Delta$ , single exponential fits are shown in solid lines. The same FRET pair on the NM fragment shows no change in FRET from AMPPNP. (C) Heterodimers consisting of unlabeled HtpG on one arm and the NM FRET pair on the opposite arm allow for NTD rotation to be monitored under apo conditions.  $\Delta 131\Delta$  binding changes the NTD orientation, as reflected by a loss in acceptor signal (black circles). The 30 residue peptide corresponding to the dominant binding region on  $\Delta 131\Delta$  does not affect the NTD orientation (green diamonds). The W467A heterodimer (one arm NM FRET and second arm W467A, blue squares) shows minimal impact from  $\Delta 131\Delta$ .

The similar rates for NTD rotation and arm-arm closure suggests simple two-state cooperativity, however, given the large number of structural motions that can occur



in Hsp90 this observation does not rule out other intermediates. Cooperativity can only be established by the coincidence of a large number of structural probes. To examine this possibility we measured closure kinetics by SAXS. Previous work demonstrated that SAXS measurements can determine the conformational equilibrium of HtpG by linear combination fitting of the scattering spectra<sup>7,8</sup>. Given that closure is slow, it is possible to simultaneously initiate closure on multiple samples and sequentially measure scattering at different timepoints. The robotic sample loading system at the SIBYLS beamline at the Advanced Light Source (Berkeley, CA) allows for each measurement to take only ~2 minutes. An advantage of this method is that SAXS reports on all scattering positions, as opposed to the limited sites measured by FRET. Here we find that the kinetics of closure by SAXS match well with the arm-arm closure and NTD rotation measured by FRET (Figure S1B). Although these measurements do not indicate whether local sequential conformational changes occur prior to the rate-limiting step, they do indicate that the gross conformational changes associated with HtpG closure obey simple two-state cooperativity.

Given this cooperativity, we wanted to know if NTD rotation was contributing to the high-energy barrier separating the open/closed states. In other words, we wanted to know whether NTD rotation could be significantly populated in isolation on a single monomer or whether this rotation is intrinsically unfavorable and requires stabilization from NTD dimerization contacts with the opposite monomer. To test this question we made the same NTD/MD FRET pair in the monomeric NM fragment of HtpG (residues 1-495). The acceptor/donor fluorescence spectrum on the NM fragment is similar to the

corresponding spectrum on the full-length dimer (not shown). We find that the acceptor fluorescence on the NM fragment does not undergo any net change upon addition of AMPPNP even in the presence of  $\Delta 131\Delta$  (Figure 2B), demonstrating that the NTD rotation required for closure requires stabilization from the opposite monomer. These results reveal a major energetic mismatch in the local and global energetics associated with Hsp90 closure. NTD rotation creates highly stabilizing dimer contacts in the closed state at the expense of a locally disfavored NTD/MD interface. This suggests that substrate binding could activate HtpG by relieving this rotational penalty.

To investigate this possibility, we tested whether substrate binding is linked to NTD rotation in the HtpG dimer. We first investigated how  $\Delta 131\Delta$  affects AMPPNP-driven closure kinetics as monitored by NTD rotation. Previously we observed that  $\Delta 131\Delta$  binding accelerated arm-arm closure kinetics five-fold<sup>13</sup>, and here a similar acceleration of the NTD rotation is observed (Figure 2B). The acceptor fluorescence for HtpG: $\Delta 131\Delta$  starts at a lower value than for HtpG, suggesting that substrate binding alone could affect an NTD rotation. Indeed under apo conditions  $\Delta 131\Delta$  affects the NTD orientation, indicated by a loss of acceptor fluorescence (black circles, Figure 2C) directly coupled to an increase in donor fluorescence (not shown). These results support the idea that substrate binding in the chaperone apo state could prime Hsp90 for ATP driven closure by affecting an NTD rotation.

Given the large surface that would be rearranged by a substrate-driven NTD rotation, we reasoned that  $\Delta 131\Delta$  could affect HtpG hydrogen exchange patterns. In particular, our results suggest that substrate binding may be altering the NTD/MD

interface and potentially exposing previously buried surfaces, which should show increased hydrogen exchange. Also, substrate binding itself has the potential to protect regions of HtpG from exchange. To test these predictions we performed HX-MS measurements on HtpG and HtpG/ $\Delta 131\Delta$ . The methodology, described previously for HtpG alone <sup>26</sup>, involves rapid dilution into D<sub>2</sub>O and allowing exchange for 30 s. H-D exchange is quenched by lowering temperature and pH, and proteolytically digested fragments are then separated and analyzed by a combined HPLC-MS setup.

The effect of  $\Delta 131\Delta$  on HtpG H-D exchange shows a striking pattern (Figure 3A). Regions at the MD/CTD become protected (blue spheres, Figure 3B), while regions at the NTD/MD interface, as well a patch at the MD/CTD interface, show increased exchange (red spheres). Two regions at the NTD/MD that become deprotected undergo large rearrangements and become significantly more exposed upon NTD rotation (residues 246-277 and 191-206). These results further support a model in which substrate binding results in an NTD rotation.  $\Delta 131\Delta$ -induced HtpG protection (blue spheres, Figure 3B) is observed in both the CTD and MD, centered at the base of the dimer cleft. This area contains residues 543-565, which are disordered in the apo crystal structure (dashed lines, Figure 3B). In the isolated CTD structure this region adopts an amphipathic helix, postulated to be involved in substrate interactions <sup>27</sup>. Although these results may suggest  $\Delta 131\Delta$  binding extends to the CTD dimer cleft, it is not known whether the dominant source of  $\Delta 131\Delta$ -induced protection is from an increase in structure of the amphipathic helices or by a direct interaction.

To distinguish between these scenarios we measured an  $^{15}\text{N}$  HSQC of the isolated CTD alone and with  $\Delta 131\Delta$  and observed a small number of binding-induced chemical shifts, suggesting the hydrogen exchange protection has a contribution from a direct interaction (Figure S2). As described below we also identify a  $\Delta 131\Delta$  binding region on the interior of the dimer cleft on the MD, which suggests that  $\Delta 131\Delta$  binding may span both the MD and CTD.

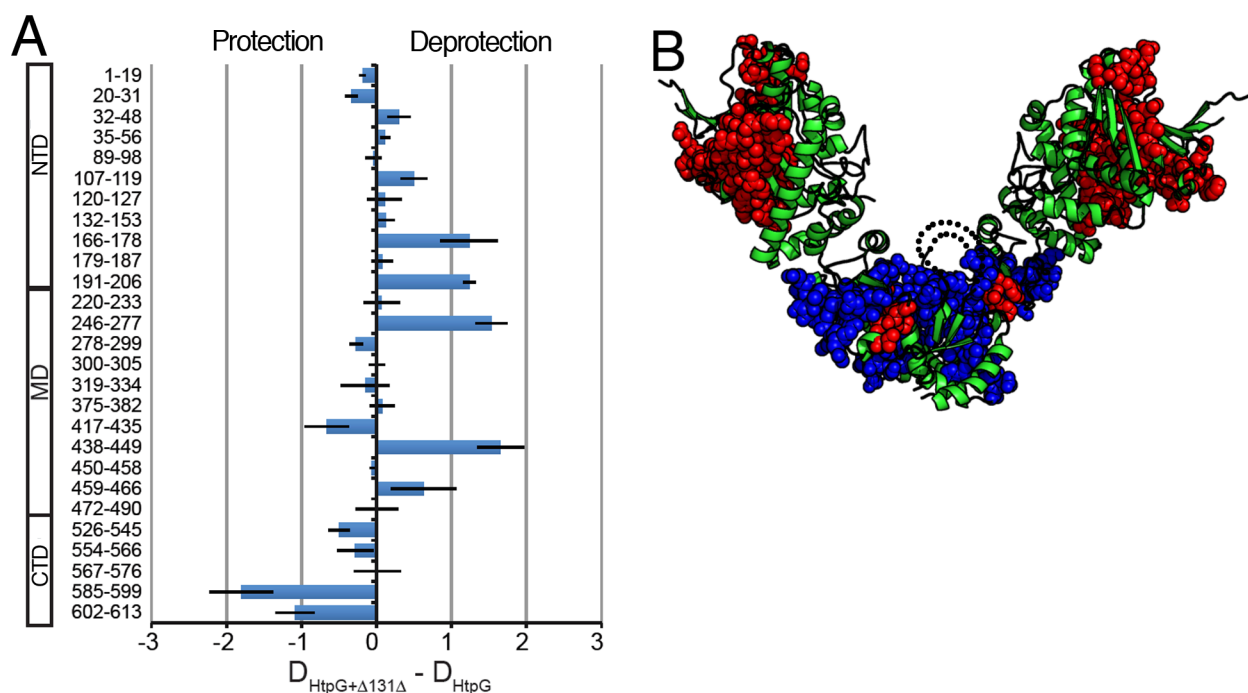


**Figure 3. Substrate binding affects hydrogen-exchange patterns across the HtpG structure.** (A) Difference values of deuterons incorporated into HtpG after 30 s of exchange in  $\text{D}_2\text{O}$  reflect the structural impact of  $\Delta 131\Delta$  binding. Black bars represent the standard error on the mean of three independent measurements. (B) The influence of  $\Delta 131\Delta$  on HtpG exchange show protected regions at the MD/CTD (blue spheres), whereas regions at the MD/NTD interface show increased exchange (red spheres). The  $\Delta 131\Delta$ -induced protection at the base of the dimer cleft lies near a region that is disordered in the crystal structure (dashed lines).

### Identifying a substrate-binding region on the middle domain

Previous SAXS measurements suggested an MD binding region, however the measurements were too low resolution to determine a residue-level surface. To gain this

insight we next used NMR and mutagenesis. The HtpG middle domain (residues 231-495, 31 kDa) can be purified and  $^{15}\text{N}$  labeled for NMR studies, but the HSQC spectrum is rather crowded (Figure S3A) and the residue assignments are unknown. Given that the structure of the middle domain is known we explored an approach utilizing selective amino-acid labeling to simplify the process of identifying a  $\Delta 131\Delta$  binding location. Specifically, the Volker Doetsch lab introduced a method whereby multiple HSQC spectra are collected each one corresponding to a single type of amino acid being  $^{15}\text{N}$  labeled. By counting the number of peaks that are affected by the substrate it is possible to identify one or more patches on the structure that have the correct number of affected residues. Iterating this process with different labeled amino acids can identify a unique region that has correct surface residue composition of the binding site <sup>28</sup>. Although this method is advantageous because single amino-acid labeling greatly simplifies the HSQC spectra, it only provides a predicted binding region so the results must be independently tested.

We produced four variants of the HtpG MD specifically  $^{15}\text{N}$  labeled on Asp, Phe, Tyr, and Gly residues. These residues have an asymmetric distribution over the MD suggesting the potential to uniquely identify a binding region.  $\Delta 131\Delta$  affects both the chemical shifts and intensities for a subset of the labeled residues on the middle domain, an example with Asp is shown in Figure 4A-C. We measured chemical shifts and intensity changes, normalized them and defined their mean and standard deviation. The peaks that were significantly impacted were counted by defining a significance threshold for each amino-acid type (see Methods).

This process identified 2 Phe, 3 Tyr, 2 Asp, and 1 Gly, in the predicted binding region (Figure S3 B-I). Inspection of the MD shows a patch facing into the HtpG dimer cleft in the apo state with this surface residue distribution (Figure 4D), whereas the opposite face shows no such site (Figure S3J). As a test, we mutated three residues within this patch (positive predictions: W467A, F390A, D476K) and three analogous mutations outside of this patch (negative predictions: W224A, F257A, E369K). We included charge reversal mutations because the strong salt dependence of  $\Delta 131\Delta$  binding suggested an electrostatic contribution.

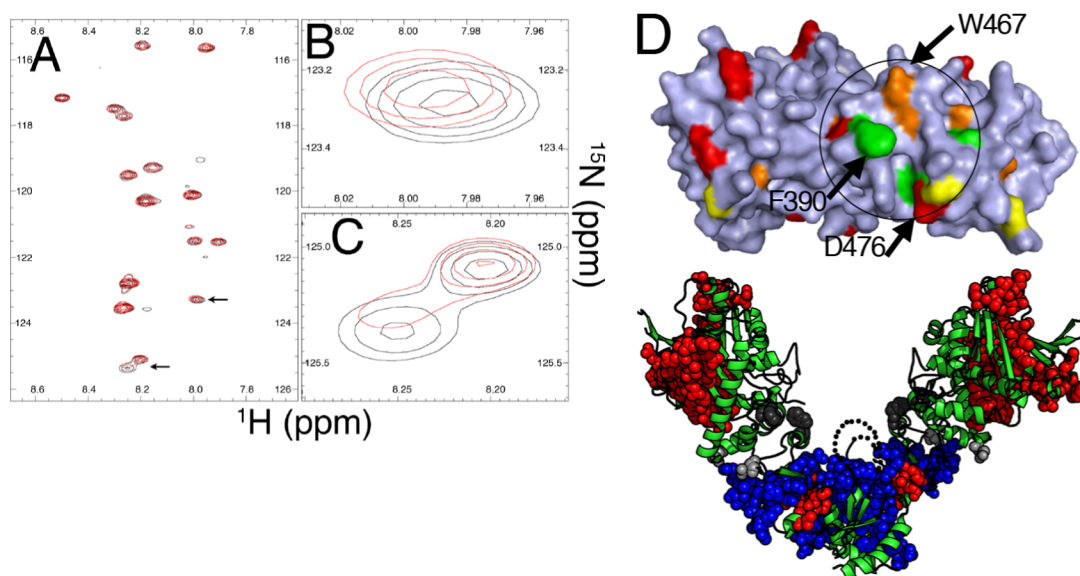


**Figure 4. Mapping a substrate binding location on the HtpG middle domain.** (A) The HtpG MD with  $^{15}\text{N}$ -labeled Asp residues shows a dramatic simplification in the HSQC spectrum. (B-C) Both peak intensity and chemical shift changes are observed from  $\Delta 131\Delta$ . (D) The middle domain in surface representation with a patch that contains Phe (yellow), Tyr (orange), Asp (red), and Gly (pink). Mutation sites to test this proposed substrate-binding region are shown on the apo state HtpG structure (W467, F390, D476). The mutations that strongly affect substrate binding (dark grey: W467, F390) lie within the dimer cleft close the regions that show HX protection from  $\Delta 131\Delta$  (blue spheres). The charge-reversal mutations that make a marginal impact on binding are shown in light grey (D476K, E369K).

Using a previously described fluorescence polarization binding assay with IAEDANS-labeled  $\Delta 131\Delta$  we measured the binding  $K_d$  of these variants (wild-type HtpG

has a  $K_d$  of 9  $\mu\text{M}$ ). The hydrophobic truncations have significantly reduced binding (W467A: 42  $\mu\text{M}$ , F390A: 38  $\mu\text{M}$ ) while the negative predictions are minimally affected (W224A: 11  $\mu\text{M}$ , F257A: 10  $\mu\text{M}$ ), which confirms that  $\Delta 131\Delta$  binds to the HtpG interior cleft at the MD. Both the positive and negative prediction charge reversal mutations show an intermediate reduction in binding (D476K: 19  $\mu\text{M}$ , E369K: 21  $\mu\text{M}$ ), one explanation may be that long-range electrostatic interactions between HtpG and  $\Delta 131\Delta$  contribute to binding. This would be consistent with the significant difference in  $pI$  between HtpG (5.1) and  $\Delta 131\Delta$  (9.5) and also consistent with recent studies of unfolded citrate synthase binding to Hsp90<sup>29</sup>. However, if long-range electrostatics are playing a role, then neither mutation (D476K and D369K) is a reliable test for direct binding. Therefore we used the W467A and F390A variants to investigate the relationship between substrate binding and HtpG conformational changes.

First, as a control, we tested the impact of these mutations on  $\Delta 131\Delta$ -induced conformational changes in HtpG. For reference, our previous SAXS measurements revealed that substrate binding is coupled to large-scale conformational changes of HtpG both under apo and AMPPNP conditions<sup>13</sup>, therefore we expected that by disrupting substrate binding these large conformational changes should be reduced. The  $\Delta 131\Delta$ -induced conformational changes in HtpG are visibly evident in the contracted SAXS  $P(r)$  spectrum, which reflects the combined set of scattering distances within the complex. In contrast to wild-type HtpG, the W467A mutant has a significantly reduced conformational change from  $\Delta 131\Delta$  under both apo (Figure 5A) and nucleotide conditions (inset), confirming that the reduction in substrate binding is directly translated

in a reduction in the chaperone conformational response. The W467A mutation itself does not affect the HtpG conformation (Figure S4A). Similar results were observed for the F390A mutation, although the mutation itself resulted in a change to the conformational state of HtpG (not shown).

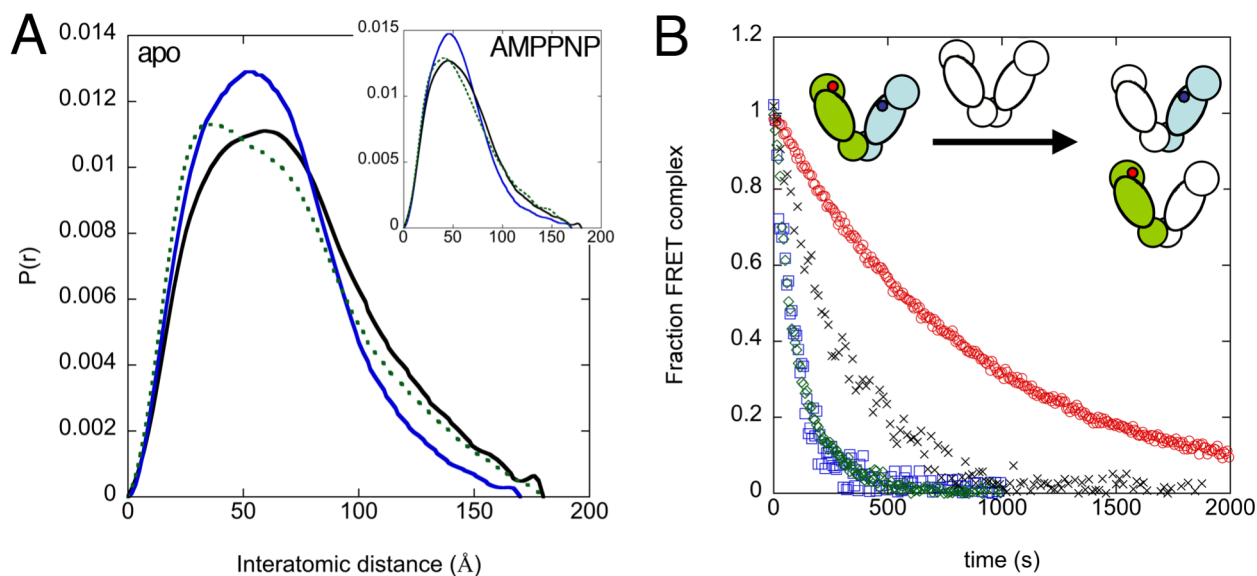


**Figure 5. Cross-monomer substrate contacts are coupled to HtpG conformational changes.** (A) The W467A mutation reduces substrate-induced conformational changes of HtpG under apo conditions as measured by SAXS. Here the wild-type/ $\Delta 131\Delta$  scattering distribution (blue) is significantly more contracted than W467A/ $\Delta 131\Delta$  (black). For reference, the HtpG spectrum in the absence of  $\Delta 131\Delta$  is shown in dashed lines. Similarly, the W467A mutation reduces substrate-induced conformational changes of HtpG under AMPPNP conditions (inset). Both HtpG and  $\Delta 131\Delta$  are at 50  $\mu\text{M}$ . (B) Monomer exchange kinetics were measured by the loss of FRET that results from adding an excess of unlabeled HtpG.  $\Delta 131\Delta$  clearly slows exchange (red circles), whereas the peptide (green diamonds) is similar to the HtpG monomer exchange rate in the absence of substrate (blue squares). The  $\Delta 131\Delta$  construct that lacks the C-terminal 30 residues has only a modest effect on exchange (black crosses).

### A secondary set of cross-monomer substrate contacts activate HtpG

A crucial mechanistic distinction concerning  $\Delta 131\Delta$  activation of HtpG is whether the substrate activates from within a monomer or across monomers and whether there are single or multiple contacting regions of the substrate. As discussed below, we addressed these questions in three ways, (i) a heterodimer analysis with the W467A



variant and NM FRET measurements (*ii*) HtpG monomer exchange measurements and (*iii*) by studying different fragments of  $\Delta 131\Delta$ .

Beyond identifying a substrate binding region in greater detail, the W467A mutation provides an opportunity to form heterodimers of HtpG where one arm contains the NM FRET pair, and the opposite arm is either wild-type HtpG or the W467A mutant. This type of heterodimer experiment has been used previously to identify cross-monomer determinants of Hsp90 hydrolysis rate<sup>20; 25</sup> and cochaperone activation<sup>16</sup>. As discussed earlier, under apo conditions  $\Delta 131\Delta$  affects an NTD rotation in the wild-type heterodimer (one arm NM FRET, second arm wild-type HtpG) as seen from a concentration-dependent loss of acceptor fluorescence (black circles, Figure 2C). In contrast, for the W467A heterodimer (one arm NM FRET, second arm W467A),  $\Delta 131\Delta$  only has a modest impact on the NM FRET (blue squares, Figure 2C). This result shows that substrate binding at the MD of one arm is directly coupled to the NTD rotation on the opposite arm. Since the heterodimer has a wild-type MD on the FRET labeled monomer,  $\Delta 131\Delta$  should make a modest acceleration of closure by its impact on the opposing NTD. Indeed, in contrast to the five-fold acceleration of AMPPNP-mediated closure observed for wild-type HtpG,  $\Delta 131\Delta$  only accelerates the W467A heterodimer by a factor of two (Figure S4B). W467A heterodimers have a similar intrinsic closure rate as the wild-type heterodimers (not shown).

A second test for cross-monomer contacts is that  $\Delta 131\Delta$  should slow the rate of HtpG monomer exchange. Here we used a FRET-based assay developed in the Buchner lab<sup>16; 21</sup>. In this experiment Hsp90 heterodimers are labeled with donor and

acceptor fluorophores on opposite arms, with a resulting FRET signal that can be extinguished by adding an excess of unlabeled wild-type Hsp90 (shown schematically in Figure 5B). Here the loss of acceptor fluorescence occurs because monomer exchange randomizes fluorescently labeled monomers with unlabeled monomers. We observe a striking slowdown of monomer exchange kinetics in the presence of  $\Delta 131\Delta$  (red circles, Figure 5B), corroborating that cross-monomer substrate contacts are formed.

There are two models that could explain cross-monomer substrate contacts. The first model is that there is a single dominant substrate-binding region that spans the Hsp90 monomers. The second model is that binding is predominantly contained within a monomer with secondary substrate contacts that span the monomers. To discriminate between these models we investigated a limited construct that only contains the dominant binding region of the substrate. For reference, previous measurements with  $\Delta 131\Delta$  suggested that there was a dominant binding region of  $\sim 25$  residues around position 100 in  $\Delta 131\Delta$ , therefore we synthesized a 30 residue peptide corresponding to residues 87-116 in  $\Delta 131\Delta$ . If cross-monomer contacts are due to secondary substrate contacts, then this limited construct will not rotate the NTD or slow monomer exchange. Indeed, although the peptide binds ( $K_d$  of  $40 \mu\text{M}$ ) it is unable to rotate the NTD (green diamonds, Figure 2C), does not change the monomer exchange rate (Figure 5C) and has a minimal impact on the closure kinetics (not shown). SAXS measurements under apo conditions show that HtpG still contracts upon binding the peptide (Figure S4C), indicating an alteration of the MD/CTD interface.

Although these results strongly suggest that multiple regions of the substrate are required to make cross monomer contacts, rotate the NTD, accelerate closure, and subsequently activate HtpG, a potential confounding factor could be that the peptide is either misfolded or does not have a sufficient level of structure to activate the chaperone. Given that previous studies on  $\Delta 131\Delta$  demonstrated that the region around residue 100 has significant structure<sup>30; 31; 32</sup>, this was a possibility we wanted to explore in detail. Therefore we performed NOESY measurements (Figure S5A) on the peptide alone. We assigned the peptide using standard methods involving TOCSY and NOESY comparisons and a natural abundance  $^{13}\text{C}$ - $^1\text{H}$  HSQC (see Methods). Inspection of the pattern of non-local NOEs shows many  $i$ - $i+3$  and  $i$ - $i+4$  NOEs in the peptide region of the native  $\alpha$ -helix in the wild-type structure (residues 98-107, Figure S5B). Weak long-range NOEs suggest modest tertiary organization. Using NOE distance constraints and dihedral constraints based on  $C_\alpha/C_\beta$  chemical shifts with the DANGLE program<sup>33</sup>, we determined an ensemble of compatible structures with the ARIA program<sup>34</sup> (Figure S5C). The peptide structure ensemble reveals a helical region centered on the native  $\alpha$ -helix and adjacent N- and C-terminal loops that loosely interact. The central helical region is not present in all members of the ensemble, indicating that the helix is a folding equilibrium, consistent with early  $\Delta 131\Delta$  studies<sup>30</sup>. This result shows that the dominant substrate region recognized by Hsp90 has a moderate level of structure and that the peptide is not misfolded.

Finally, we wanted to investigate the location of the secondary contacts on the substrate. As shown here Hsp90 binds to a locally structured region of  $\Delta 131\Delta$  around

residue 100, and our results show that secondary contacts from this region are required for cross-monomer contacts that affect an NTD rotation, which primes the chaperone for ATP-driven closure. These findings are consistent with our previous NMR measurements that suggested a secondary binding site at the  $\Delta 131\Delta$  C-terminus<sup>13</sup>. To test whether the C-terminal region indeed makes secondary contacts, we investigated a  $\Delta 131\Delta$  variant in which the C-terminal 30 residues are removed (residues 111-141). Indeed, this construct only results in a modest slowdown of HtpG monomer exchange (Figure 5B), and has a minimal impact on the closure kinetics (not shown). Although these results do not exclude a synergistic contribution from the  $\Delta 131\Delta$  N-terminal region, secondary contacts from C-terminal region of  $\Delta 131\Delta$  clearly play a central role in Hsp90 activation.

## Discussion

The Hsp90 ATPase is required for *in-vivo* function<sup>35; 36</sup> and is regulated by numerous co-chaperones in eukaryotes<sup>37</sup>. Previous work with the model client  $\Delta 131\Delta$  demonstrated that substrate binding can also regulate the activity of HtpG<sup>13</sup>, similar to reports of human Hsp90 activation by the ligand binding domain of the glucocorticoid receptor<sup>14</sup> and an *E. coli* ribosomal protein L2 that activates HtpG<sup>15</sup>. Elucidating the Hsp90 functional mechanism requires an understanding of how the chaperone can be activated by substrates. Here we have focused on NTD structural motions in the HtpG conformational cycle, identifying a client binding region on the MD, and establishing that

multiple regions of the substrate make cross-monomer contacts required for HtpG activation (Figure 6).

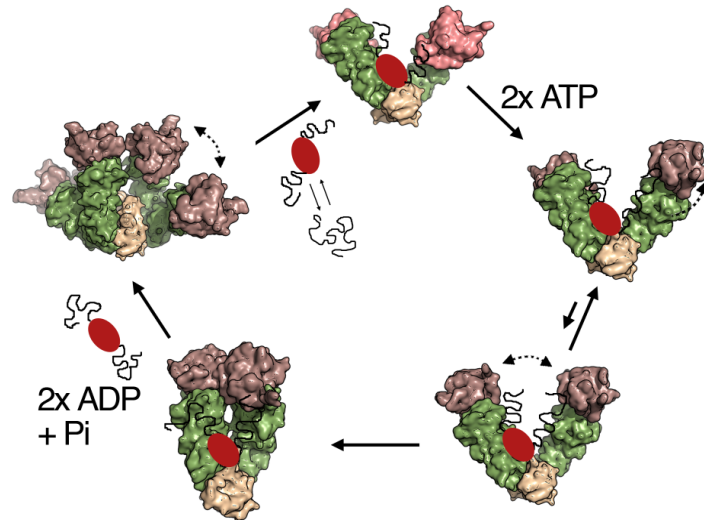


**Figure 6. Model of NTD rotation in substrate activation of Hsp90 ATP hydrolysis cycle.** Substrate binding activates Hsp90 by an asymmetric mechanism in which NTD domain rotation makes a significant contribution to the rate-limiting step in Hsp90 closure and ATP hydrolysis. The dominant unit of structure recognized by Hsp90 is a locally structured region (green oval) and is in a local folding equilibrium. However secondary contacts outside this structured region are required for NTD rotation and acceleration of closure. Although the substrate is shown bound for the entire cycle, given the low affinity of  $\Delta 131\Delta$  and the Hsp90 long closure time, many bind and release steps are likely occurring during the course of the cycle.

This proposed activation of HtpG by  $\Delta 131\Delta$  has a parallel with the mechanism of the activating cochaperone Aha1 on the yeast Hsp90<sup>16</sup>. Those authors demonstrate that cross-monomer Aha1 contacts prime Hsp90 for closure and subsequent hydrolysis, while FRET measurements suggested that Aha1 could affect NTD orientation<sup>21</sup>. There is a second interesting parallel between our HtpG/ $\Delta 131\Delta$  findings and cochaperone-stabilized Hsp90 conformations. Recent electron microscopy measurements of human Hsp90 demonstrated that the cochaperone Hop (involved in substrate loading from Hsp70) induces a partial closure of Hsp90 and fully rotates both NTDs into a closure-

competent orientation <sup>38</sup>. Previous measurements on  $\Delta 131\Delta$  showed that substrate binding induces a partial closure of HtpG in the apo state <sup>13</sup>, similar to the Hop-stabilized conformation. These similarities suggest that Hop stabilizes an Hsp90 conformation that is naturally predisposed for substrate binding, subsequent chaperone closure, and ATP hydrolysis.

Comparison of our results with an electron microscopy reconstruction of an Hsp90-cdc37-cdk4 complex <sup>17</sup>, reveals differences between these substrates. Modeling suggested the kinase substrate, cdk4, binding both the NTD and MD on a single monomer, in contrast to the cross-monomer contacts we observe. In the Hsp90-cdc37-cdk4 complex the substrate-bound NTD is in a closure-competent conformation while the other monomer, bound to cdc37, is hinged away. While the primary  $\Delta 131\Delta$  interaction is with the MD, one possibility is that secondary substrate contacts are made to the NTD. This would be consistent with early studies indicating that Hsp90 has two substrate binding sites with different specificities <sup>39</sup>, an NTD site that can bind short unstructured peptides and a CTD/MD site that can bind partially folded substrates <sup>40</sup>. Given that our HX-MS measurements do not show significant  $\Delta 131\Delta$ -induced protection at the NTD, if  $\Delta 131\Delta$  is contacting the NTD these contacts are likely transient.

Recent studies have identified that the ribosomal subunit L2 activates HtpG, similar to the effect from  $\Delta 131\Delta$ , however L2 is unable to activate the yeast Hsp90 homolog <sup>15</sup>. Interestingly, we find that  $\Delta 131\Delta$  does not accelerate closure for the yeast Hsp90 but does accelerate closure for human TRAP1, the mitochondria-specific Hsp90 homolog (TOS and LAL unpublished observations). Although there is very strong

evidence that the conformational states of Hsp90 are highly conserved, the degree to which substrates accelerate conformational transitions for Hsp90 homologs appears to be variable.

Numerous studies have established a conserved Hsp90 mechanism in which structural rearrangements resulting in NTD dimerization organizes the catalytic machinery required for ATP hydrolysis<sup>3; 9; 21; 25; 41</sup>. SAXS and EM studies have shown that rigid-body motions between the NTD/MD and the MD/CTD can account for the wide range of Hsp90 conformational states<sup>7; 8; 9</sup>. The extreme apo state flexibility arises from a weak coupling between the MD/CTD, allowing for a wide range of arm-arm geometries. In contrast, here we find that the NTD/MD rotation required for closure is a high-energy state. The closed conformation, although stable, comes with a cost of adopting an unfavorable NTD/MD interface. However, our measurements do not indicate whether the NM rotation has a large kinetic barrier in addition to an unfavorable equilibrium constant, nor do our measurements assess the degree to which the NM rotation is unfavorable, in terms of kcal/mol. Also, it is not known whether  $\Delta 131\Delta$  affects a discrete NTD rotation or whether substrate binding weakens the NTD/MD interface resulting in an ensemble of domain orientations. Further studies are needed to address these questions.

## Supplemental Information

### Supplemental Figures and Legends

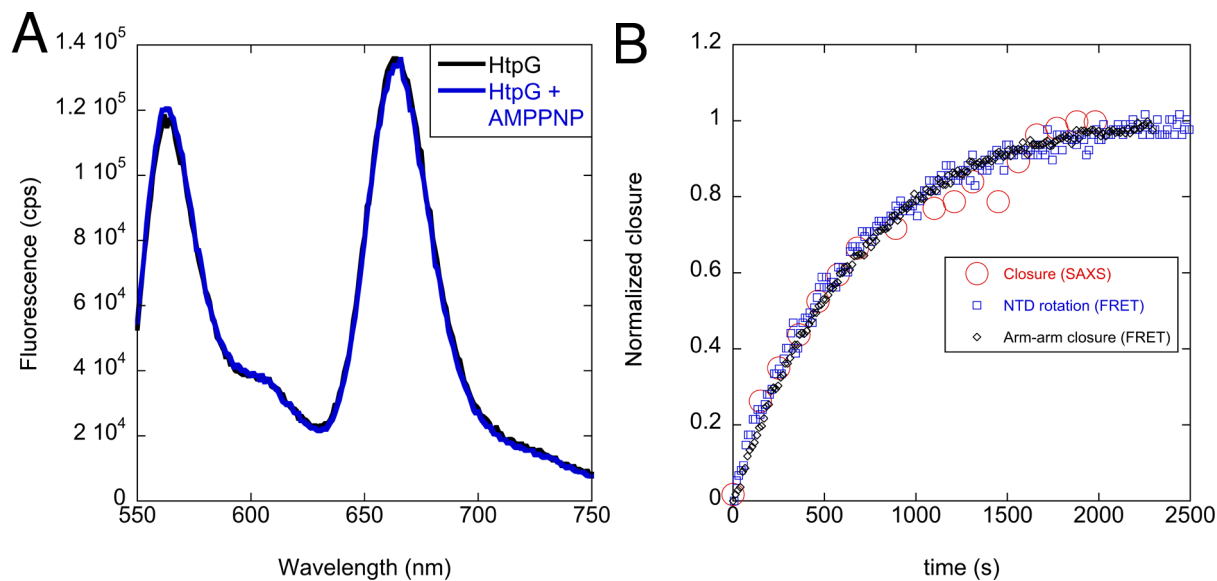


**Figure S1. Control FRET pair on the middle domain.** (A) A fixed-point FRET pair, residues 350 and 362, showed a fluorescence spectrum that was unchanged by the addition of 5 mM AMPPNP. (B) The kinetics of arm-arm closure, NTD rotation, and closure as measured by SAXS are similar. Normalized closure is defined by the plateau value for each measurement type determined from single exponential fitting.

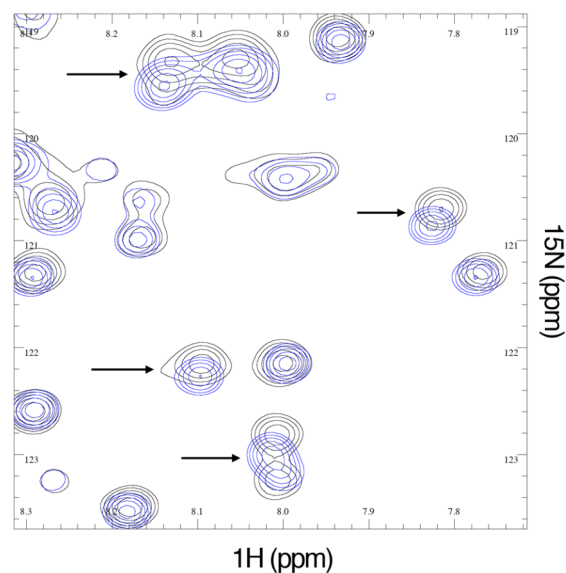


**Figure S2.** An  $^{15}\text{N}$  HSQC of the isolated HtpG CTD (residues 511-624) shows particular peaks (black) that undergo chemical shifts from  $\Delta 131\Delta$  (blue). Buffer conditions 25 mM MES pH 6.0, 25 mM KCl, 5 mM  $\text{MgCl}_2$ .



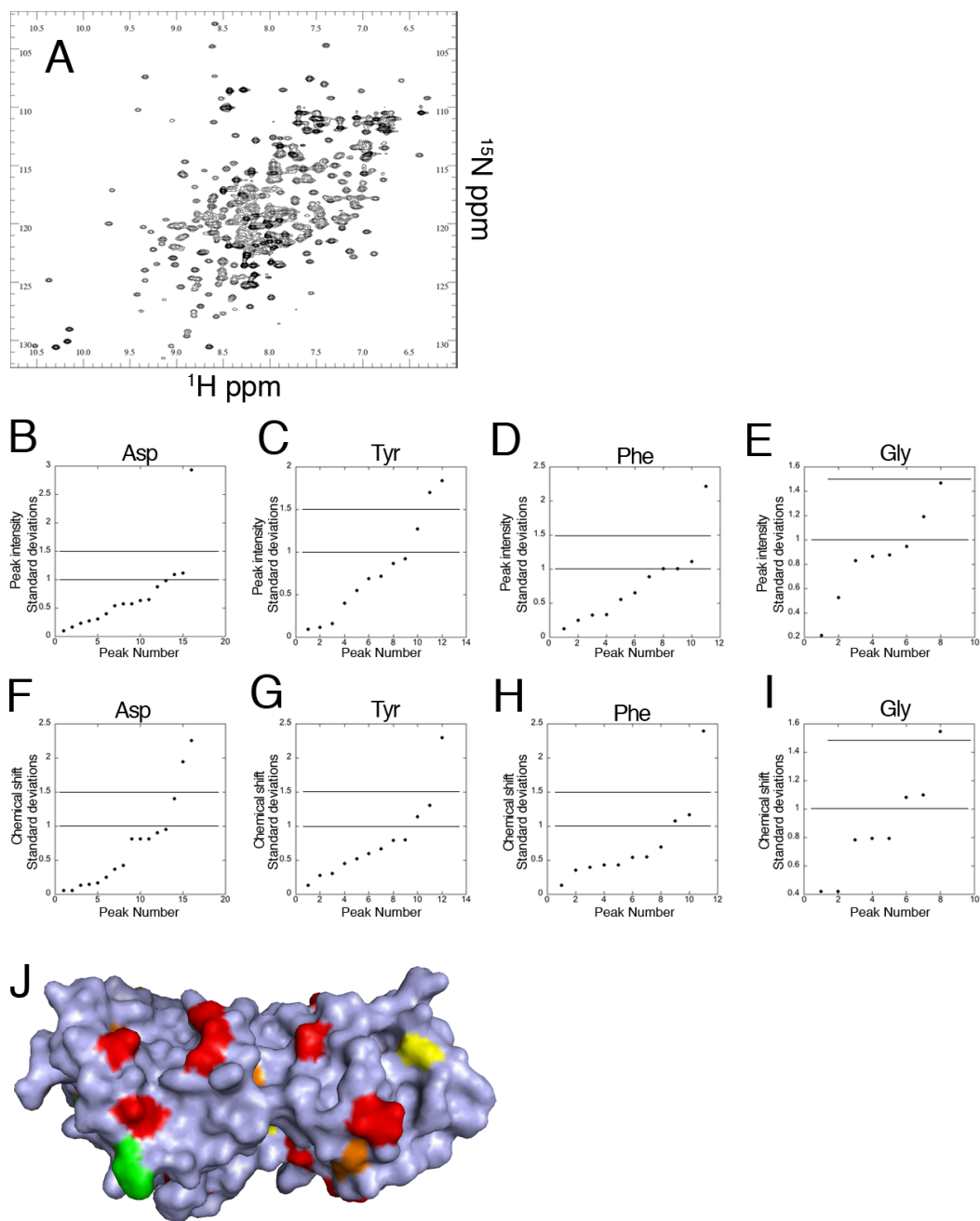


**Figure S3. Selective amino-acid labeling of the middle domain to determine a  $\Delta 131\Delta$  binding region on the HtpG MD.** (A) The HtpG HSQC spectrum is crowded, which complicates a full assignment and chemical shift mapping. The selective labeling method described in the main text was aimed at simplifying this spectra to rapidly generate a hypothesis about the substrate binding region. Buffer conditions 25 mM MES pH 6.0, 25 mM KCl, 5 mM  $MgCl_2$ . Four labeled MD samples (Asp: B, F; Tyr: C, G; Phe: D, H; Gly: E, I) were prepared and the effect of  $\Delta 131\Delta$  on peak intensities (upper row) and chemical shifts (lower row) was determined as described in Methods. Solid lines show the  $1\sigma$  and  $1.5\sigma$  significance thresholds. (J) The opposite face of the middle domain of HtpG in surface representation with Phe (yellow), Tyr (orange), Asp (red), and Gly (pink). The opposite face shows no such region that can satisfy the surface residue composition affected by  $\Delta 131\Delta$  binding.

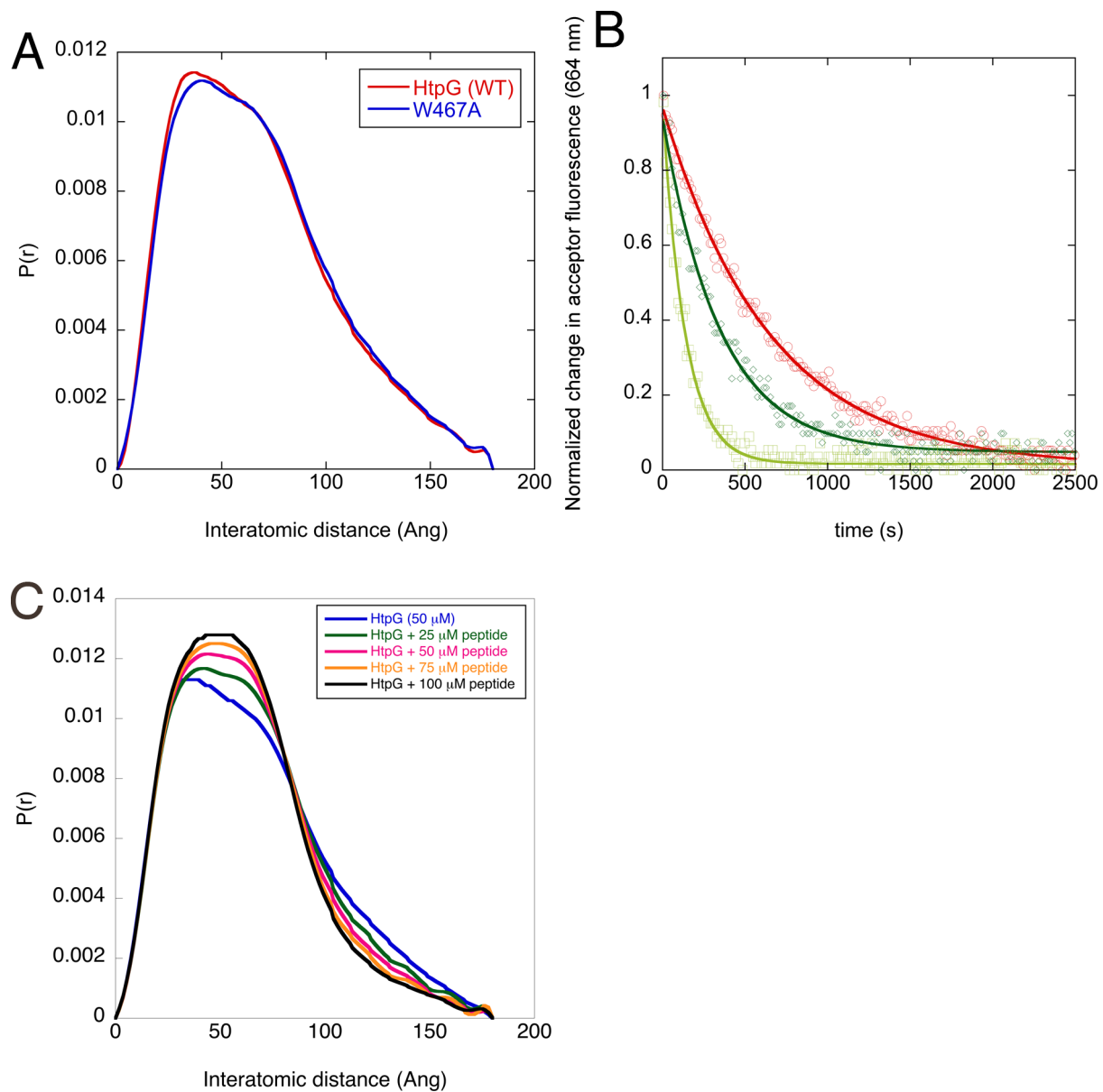


**Figure S4.** (A) The W467A substitution does not affect HtpG conformation. SAXS measurements on the W467A variant show that the  $P(r)$  curve for wild-type HtpG is very similar to the W467A variant. (B) The NM FRET pair was mixed with a 10x excess of wild-type HtpG or the W467A variant. Closure kinetics were measured by the loss of acceptor fluorescence. The HtpG closure without  $\Delta 131\Delta$  (red circles) is five-fold accelerated by  $\Delta 131\Delta$  (green squares), however the wt:W467A heterodimer is only accelerated two-fold. The  $\Delta 131\Delta$  concentration used was 50  $\mu\text{M}$ . Solid lines show single exponential fits. (C) A 30 residue peptide from  $\Delta 131\Delta$  induces partial closure of HtpG under apo conditions. SAXS measurements of HtpG in increasing concentrations of peptide show a contraction under apo conditions.

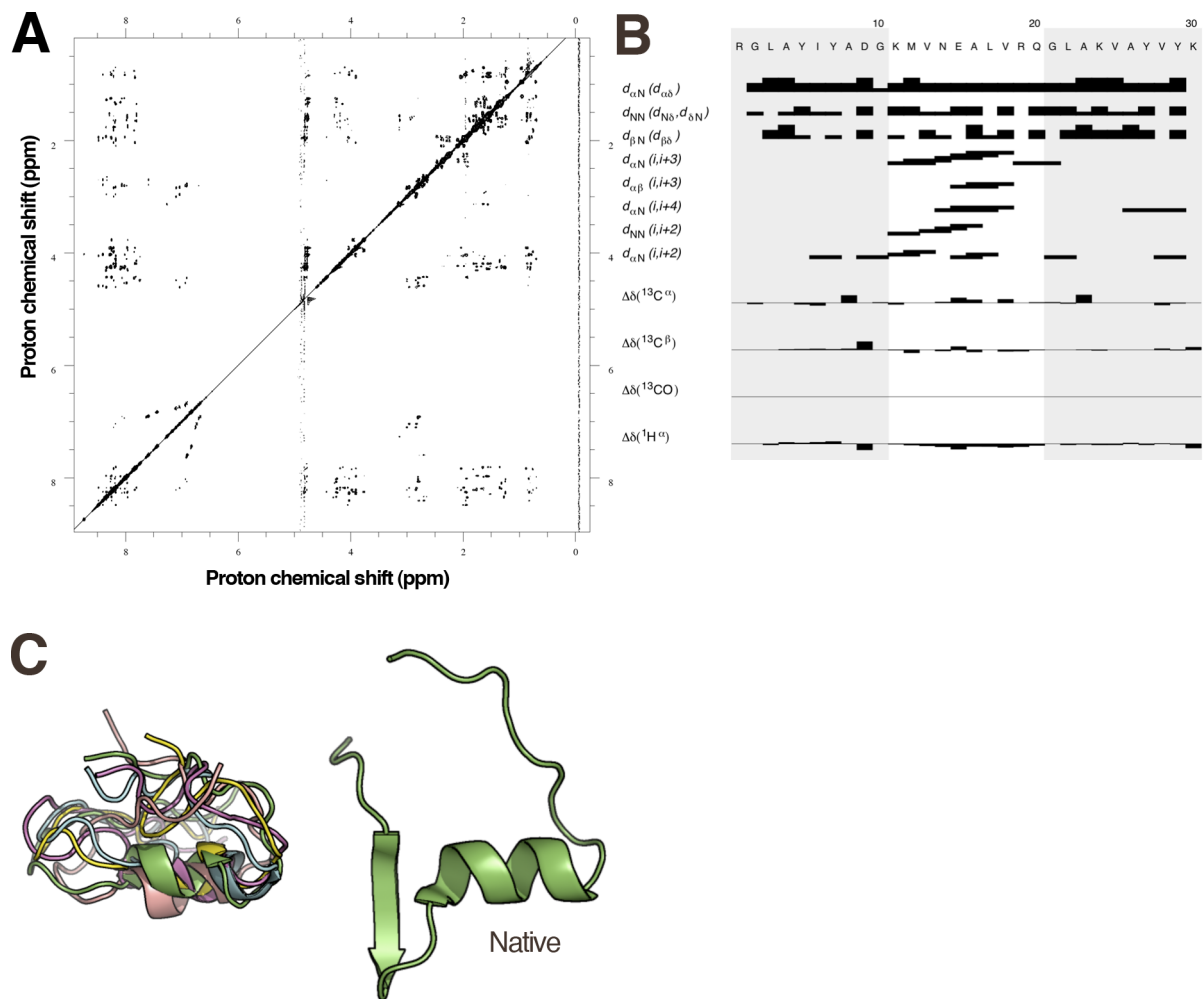


**Figure S5. The 30 residue peptide from  $\Delta 131\Delta$  has significant structure.** (A) The NOESY spectrum of this peptide at pH 6.0, 25 mM  $\text{KH}_2\text{PO}_4$ , 25 mM KCl, 5 mM  $\text{MgCl}_2$ . (B) An assignment chart shows many  $i$ - $i+3$  and  $i$ - $i+4$  NOEs, indicative of helical structure. (C) The structural ensemble from ARIA shows a helical region centered on the native SN helix and adjacent N- and C-terminal loops that loosely interact. The helical region is not present in all members of the ensemble suggesting that it remains in a folding equilibrium.

## Experimental Procedures

HtpG, variants of HtpG, and  $\Delta 131\Delta$  were purified as described previously<sup>7; 30</sup>. A peptide corresponding to residues 87-116 in  $\Delta 131\Delta$  was synthesized (Genemed Synthesis), HPLC purified and confirmed by mass-spectrometry. A similar peptide was synthesized with a C-terminal cysteine and labeled with IAEDANS for fluorescence

anisotropy measurements. Hydrogen exchange mass-spectrometry measurements<sup>26</sup> were performed at pH 7.5, 25 mM TRIS, 25 mM KCl, 5 mM MgCl<sub>2</sub>. The closure, monomer exchange, and NM FRET measurements, were performed at pH 9.0, 25 mM TRIS, 50 mM KCl, 5 mM MgCl<sub>2</sub>, 25 C.

### **Fluorescence measurements**

Fluorescence anisotropy on IAEDANS-labeled  $\Delta 131\Delta$  was measured on a Jobin Yvon fluorometer. Excitation and emission monochromator slits were both set to 5 nm, an integration time of 2 seconds, and excitation/emission wavelengths of 340/480 nm. The NTD/MD FRET pair (S52C/D341C) was labeled with a five-fold molar excess of Alexafluor 647 and Alexafluor 555 (Invitrogen) for three hours at room temperature and quenched with BME. Measurements were performed with the resulting mixture of labeled species with FRET occurring between HtpG labeled with both fluorophores. HtpG heterodimers with 250 nM labeled monomer and 5  $\mu$ M wild-type HtpG were formed by incubation for 30 minutes at 30 °C. Closure was initiated by 5 mM AMPPNP, either in isolation or with 50  $\mu$ M  $\Delta 131\Delta$ . Excitation and emission monochromator slits were set at 2 and 3 nm, respectively. Monomer exchange measurements were performed with a previously described FRET pair at positions 62 and 341 on HtpG<sup>13</sup>. Cross-monomer FRET was measured by forming heterodimers (250 nM of each monomer) by incubation for 30 minutes at 30 °C. A 20x excess of unlabeled HtpG was added and the loss of acceptor fluorescence was measured at 664 nm. Addition of 25  $\mu$ M  $\Delta 131\Delta$  resulted in slower monomer exchange kinetics.

## **SAXS measurements**

SAXS measurements, as described previously, were performed at the Advanced Light Source in Berkeley<sup>7; 8; 20</sup>. The concentrations of HtpG, variants of HtpG, and  $\Delta 131\Delta$  were 50  $\mu\text{M}$ . To measure closure kinetics by SAXS, closure was initiated by simultaneously adding 10 mM AMMPNP to multiple samples with a multichannel pipette. SAXS measurements were taken at varying timepoints on different samples to avoid radiation damage. The linear combination fitting used to determine the population of closed state has been described previously<sup>7; 8</sup>.

## **NMR measurements**

HSQC measurements were performed on a Bruker Avance800. Fully  $^{15}\text{N}$  labeled HtpG MD was produced by a 10 mL overnight starter culture, washed in M9 minimal medium, and resuspended in M9 with 1 g/L  $^{15}\text{N}$  ammonium chloride and 0.5 g/L isogrow supplement (Sigma). Selectively labeled MD samples were produced by supplying all  $^{14}\text{N}$  amino-acids except the labeled  $^{15}\text{N}$  amino-acid. These were added in the following quantities in each liter of minimal media (A:500 mg, R:400 mg, D:400 mg, C:50 mg, Q:400 mg, E:650 mg, G:550 mg, H:100 mg, I:230 mg, L:230 mg, K:420 mg, M:250 mg, F:130 mg, P:100 mg, S:210 mg, T:230 mg, Y:170 mg, V:230 mg, N:300 mg, 500 mg of tryptophan was added after autoclaving the media). NMR buffer conditions were 25 mM MES pH 6.0, 25 mM KCl, 5 mM  $\text{MgCl}_2$ .

For each labeled MD sample, chemical shifts and peak intensities were measured in ccpNMR (<http://www.ccpn.ac.uk>). For changes in the chemical shifts, shifts in the  $^1\text{H}$  dimension were normalized in magnitude to the shifts in  $^{15}\text{N}$  dimension by multiplying each shift in  $^1\text{H}$  dimension by a ratio of mean shift changes in  $^{15}\text{N}$  over mean shift changes in  $^1\text{H}$ . After this an overall change in chemical shifts was determined in 2 dimensions, and an overall mean change was found for each spectrum. This mean was subtracted from the chemical shift change for each particular peak, divided by the standard deviation and plotted to generate Figure S2, E-H. For changes in the peak intensities, a ratio of intensities of bound versus unbound for each peak were calculated, a mean and standard deviation of all ratios for a pair of spectra were found. To generate Figure S2 A-D, the mean ratio was subtracted from the ratio for each particular residue, and then divided by the standard deviation. Residues over a  $1.5 \sigma$  threshold from the mean for either chemical shift or intensity changes were counted. Although the choice of  $1.5 \sigma$  was an adjustable parameter, values significantly above and below yielded surface residue compositions for the  $\Delta 131\Delta$  binding site that were incompatible with the MD surface.

NOESY measurements on 800  $\mu\text{M}$  peptide were performed on a Bruker Avance800 with a 120 ms mixing time. The spectra were processed with NMRpipe<sup>42</sup> and analyzed using ccpNMR. Structural ensembles were calculated using ARIA<sup>34</sup>.

## **Acknowledgements**

We thank Mark Kelly for help with NMR. Funding for this project was provided by the Howard Hughes Medical Institute. TOS was supported by a Damon Runyon Cancer Research Foundation fellowship. Many thanks to members of the Agard lab for helpful discussions.

## References:

1. Young, J. C., Moarefi, I. & Hartl, F. U. (2001). Hsp90: a specialized but essential protein-folding tool. *J Cell Biol* **154**, 267-73.
2. Workman, P. (2004). Combinatorial attack on multistep oncogenesis by inhibiting the Hsp90 molecular chaperone. *Cancer Lett* **206**, 149-57.
3. Ali, M. M., Roe, S. M., Vaughan, C. K., Meyer, P., Panaretou, B., Piper, P. W., Prodromou, C. & Pearl, L. H. (2006). Crystal structure of an Hsp90-nucleotide-p23/Sba1 closed chaperone complex. *Nature* **440**, 1013-7.
4. Dollins, D. E., Warren, J. J., Immormino, R. M. & Gewirth, D. T. (2007). Structures of GRP94-nucleotide complexes reveal mechanistic differences between the hsp90 chaperones. *Mol Cell* **28**, 41-56.
5. Shiau, A. K., Harris, S. F., Southworth, D. R. & Agard, D. A. (2006). Structural Analysis of E. coli hsp90 reveals dramatic nucleotide-dependent conformational rearrangements. *Cell* **127**, 329-40.
6. Krukenberg, K. A., Bottcher, U. M., Southworth, D. R. & Agard, D. A. (2009). Grp94, the endoplasmic reticulum Hsp90, has a similar solution conformation to cytosolic Hsp90 in the absence of nucleotide. *Protein Sci* **18**, 1815-27.
7. Krukenberg, K. A., Forster, F., Rice, L. M., Sali, A. & Agard, D. A. (2008). Multiple conformations of E. coli Hsp90 in solution: insights into the conformational dynamics of Hsp90. *Structure* **16**, 755-65.
8. Krukenberg, K. A., Southworth, D. R., Street, T. O. & Agard, D. A. (2009). pH-Dependent Conformational Changes in Bacterial Hsp90 Reveal a Grp94-Like Conformation at pH 6 That Is Highly Active in Suppression of Citrate Synthase Aggregation. *J Mol Biol.*
9. Southworth, D. R. & Agard, D. A. (2008). Species-dependent ensembles of conserved conformational states define the Hsp90 chaperone ATPase cycle. *Mol Cell* **32**, 631-40.
10. Bron, P., Giudice, E., Rolland, J. P., Buey, R. M., Barbier, P., Diaz, J. F., Peyrot, V., Thomas, D. & Garnier, C. (2008). Apo-Hsp90 coexists in two open conformational states in solution. *Biol Cell* **100**, 413-25.
11. Onuoha, S. C., Coulstock, E. T., Grossmann, J. G. & Jackson, S. E. (2008). Structural studies on the co-chaperone Hop and its complexes with Hsp90. *J Mol Biol* **379**, 732-44.



12. Street, T. O., Krukenberg, K. A., Rosgen, J., Bolen, D. W. & Agard, D. A. (2010). Osmolyte-induced conformational changes in the Hsp90 molecular chaperone. *Protein Sci* **19**, 57-65.
13. Street, T. O., Lavery, L. A. & Agard, D. A. (2011). Substrate binding drives large-scale conformational changes in the hsp90 molecular chaperone. *Mol Cell* **42**, 96-105.
14. McLaughlin, S. H., Smith, H. W. & Jackson, S. E. (2002). Stimulation of the weak ATPase activity of human hsp90 by a client protein. *J Mol Biol* **315**, 787-98.
15. Motojima-Miyazaki, Y., Yoshida, M. & Motojima, F. (2010). Ribosomal protein L2 associates with E. coli HtpG and activates its ATPase activity. *Biochem Biophys Res Commun*.
16. Retzlaff, M., Hagn, F., Mitschke, L., Hessling, M., Gugel, F., Kessler, H., Richter, K. & Buchner, J. (2010). Asymmetric activation of the hsp90 dimer by its cochaperone aha1. *Mol Cell* **37**, 344-54.
17. Vaughan, C. K., Gohlke, U., Sobott, F., Good, V. M., Ali, M. M., Prodromou, C., Robinson, C. V., Saibil, H. R. & Pearl, L. H. (2006). Structure of an Hsp90-Cdc37-Cdk4 complex. *Mol Cell* **23**, 697-707.
18. Prodromou, C., Panaretou, B., Chohan, S., Siligardi, G., O'Brien, R., Ladbury, J. E., Roe, S. M., Piper, P. W. & Pearl, L. H. (2000). The ATPase cycle of Hsp90 drives a molecular 'clamp' via transient dimerization of the N-terminal domains. *Embo J* **19**, 4383-92.
19. Richter, K., Muschler, P., Hainzl, O. & Buchner, J. (2001). Coordinated ATP hydrolysis by the Hsp90 dimer. *J Biol Chem* **276**, 33689-96.
20. Cunningham, C. N., Krukenberg, K. A. & Agard, D. A. (2008). Intra- and intermonomer interactions are required to synergistically facilitate ATP hydrolysis in Hsp90. *J Biol Chem* **283**, 21170-8.
21. Hessling, M., Richter, K. & Buchner, J. (2009). Dissection of the ATP-induced conformational cycle of the molecular chaperone Hsp90. *Nat Struct Mol Biol* **16**, 287-93.
22. Richter, K., Moser, S., Hagn, F., Friedrich, R., Hainzl, O., Heller, M., Schlee, S., Kessler, H., Reinstein, J. & Buchner, J. (2006). Intrinsic inhibition of the Hsp90 ATPase activity. *J Biol Chem* **281**, 11301-11.

23. Huai, Q., Wang, H., Liu, Y., Kim, H. Y., Toft, D. & Ke, H. (2005). Structures of the N-terminal and middle domains of *E. coli* Hsp90 and conformation changes upon ADP binding. *Structure* **13**, 579-90.
24. Meyer, P., Prodromou, C., Hu, B., Vaughan, C., Roe, S. M., Panaretou, B., Piper, P. W. & Pearl, L. H. (2003). Structural and functional analysis of the middle segment of hsp90: implications for ATP hydrolysis and client protein and cochaperone interactions. *Mol Cell* **11**, 647-58.
25. Vaughan, C. K., Piper, P. W., Pearl, L. H. & Prodromou, C. (2009). A common conformationally coupled ATPase mechanism for yeast and human cytoplasmic HSP90s. *Febs J* **276**, 199-209.
26. Graf, C., Stankiewicz, M., Kramer, G. & Mayer, M. P. (2009). Spatially and kinetically resolved changes in the conformational dynamics of the Hsp90 chaperone machine. *Embo J* **28**, 602-13.
27. Harris, S. F., Shiau, A. K. & Agard, D. A. (2004). The crystal structure of the carboxy-terminal dimerization domain of htpG, the *Escherichia coli* Hsp90, reveals a potential substrate binding site. *Structure* **12**, 1087-97.
28. Reese, M. L. & Dotsch, V. (2003). Fast mapping of protein-protein interfaces by NMR spectroscopy. *J Am Chem Soc* **125**, 14250-1.
29. Wayne, N. & Bolon, D. N. (2010). Charge-rich regions modulate the anti-aggregation activity of Hsp90. *J Mol Biol* **401**, 931-9.
30. Alexandrescu, A. T., Abeygunawardana, C. & Shortle, D. (1994). Structure and dynamics of a denatured 131-residue fragment of staphylococcal nuclease: a heteronuclear NMR study. *Biochemistry* **33**, 1063-72.
31. Alexandrescu, A. T. & Shortle, D. (1994). Backbone dynamics of a highly disordered 131 residue fragment of staphylococcal nuclease. *J Mol Biol* **242**, 527-46.
32. Wang, Y. & Shortle, D. (1995). The equilibrium folding pathway of staphylococcal nuclease: identification of the most stable chain-chain interactions by NMR and CD spectroscopy. *Biochemistry* **34**, 15895-905.
33. Cheung, M. S., Maguire, M. L., Stevens, T. J. & Broadhurst, R. W. (2010). DANGLE: A Bayesian inferential method for predicting protein backbone dihedral angles and secondary structure. *J Magn Reson* **202**, 223-33.

34. Linge, J. P., Habeck, M., Rieping, W. & Nilges, M. (2003). ARIA: automated NOE assignment and NMR structure calculation. *Bioinformatics* **19**, 315-6.
35. Obermann, W. M., Sondermann, H., Russo, A. A., Pavletich, N. P. & Hartl, F. U. (1998). In vivo function of Hsp90 is dependent on ATP binding and ATP hydrolysis. *J Cell Biol* **143**, 901-10.
36. Panaretou, B., Prodromou, C., Roe, S. M., O'Brien, R., Ladbury, J. E., Piper, P. W. & Pearl, L. H. (1998). ATP binding and hydrolysis are essential to the function of the Hsp90 molecular chaperone in vivo. *Embo J* **17**, 4829-36.
37. Pearl, L. H. & Prodromou, C. (2006). Structure and mechanism of the Hsp90 molecular chaperone machinery. *Annu Rev Biochem* **75**, 271-94.
38. Southworth, D. R. & Agard, D. A. (2011). Client-Loading Conformation of the Hsp90 Molecular Chaperone Revealed in the Cryo-EM Structure of the Human Hsp90:Hop Complex. *Mol Cell* **42**, 771-81.
39. Young, J. C., Schneider, C. & Hartl, F. U. (1997). In vitro evidence that hsp90 contains two independent chaperone sites. *FEBS Lett* **418**, 139-43.
40. Scheibel, T., Weikl, T. & Buchner, J. (1998). Two chaperone sites in Hsp90 differing in substrate specificity and ATP dependence. *Proc Natl Acad Sci U S A* **95**, 1495-9.
41. Richter, K., Soroka, J., Skalniak, L., Leskovar, A., Hessling, M., Reinstein, J. & Buchner, J. (2008). Conserved conformational changes in the ATPase cycle of human Hsp90. *J Biol Chem* **283**, 17757-65.
42. Delaglio, F., Grzesiek, S., Vuister, G. W., Zhu, G., Pfeifer, J. & Bax, A. (1995). NMRPipe: a multidimensional spectral processing system based on UNIX pipes. *J Biomol NMR* **6**, 277-93.

## Conclusions and Future directions

Through the work presented above we have a new working model for the mechanism of Hsp90. Though I outlined several future experiments and directions in the postscripts for previous chapters, I wanted to give a few general comments and prospects for the future with the TRAP1 system.

In my mind the most important next step is to gain traction on a bonafide TRAP1 client. CypD provides a good starting place and is potentially ideal, though if the “make or break” experiments outlined in the postscript for chapter 1 show that the structure of CypD is not modulated by TRAP1 then this client is not the right one for future investigations aimed at probing client re-modeling. While  $\Delta 131\Delta$  can provide some mechanistic clues, the need for client discovery for the TRAP1 system is of highest importance. As a bonus the investigator has the opportunity to uncover novel signaling pathways in the mitochondria that are linked to the chaperone. From a basic biology stand point this is quite exciting and interesting, but the larger implications for this work lie in the fact that TRAP1 signaling through its clients is uniquely linked to several disease pathways (see previous chapters). With the elucidation of these pathways and studies of specific clients *in vitro* there is the potential for novel therapeutic strategies with heightened specificity and potentially efficacy (please see chapter 3 for an outline of drug discovery experiments).

Finally, through investigating an Hsp90 homolog that was poorly studied at the time I learned that there is great potential in the many homologs that evolution has provided to us. There are likely advantages and new concepts to discover in the diverse

homologs, where future investigations would allow us to learn both shared and unique mechanistic properties and biological function of the Hsp90 system.

## **Appendix: Select Protocols**

### **Preface**

In this appendix I have included a select number of protocol that are not specifically outlines in the chapters above, or that I believe a more detailed protocol will be of benefit to future investigations. For full protocols and experimental detail see lab notebooks 1-13.

## Human TRAP1 His-tagged protein Purification

(L. Lavery, Agard Lab UCSF. Spring 2013)

(certain specifics may need to be adjusted for other proteins)

---

### Expression:

- 1) Grow an overnight starter culture from a freshly transformed colony (10mL per L culture in step 2) \*BL21 DE3 or RIL cells (RIL cells work a bit better)
- 2) Inoculate 1L of TB media with 10mL of the ON culture
- 3) Grow cells at 37C to OD = .5 and then induce with 1mL of 1M IPTG
- 4) reduce temp to 16C and grow ON

### Purification:

- 1) Pellet cells @ 5,000 xG for 15 minutes
- 2) Resuspend pellet in 50mL of Lysis buffer plus one protease inhibitor tablet

If you want to pellet the cells and store them in the -80°C freezer to prep at a later time, resuspend the pellet in 150mM NaCl, spin down in a conical for 15min at 5,000 xG, and flash freeze in liquid nitrogen.

**Lysis Buffer:** 50mM Hepes pH 7.5

.5M KCl

20mM Imidizol (pH 7.5)

10% Glycrol

1% Tween-20

(+ 6mM added fresh)

3) Homogonize resuspended pellet in a beaker with a stir bar in the cold room until no chunks of cells are left. (~10min)

4) Use Emulsaflux to lyse the cells (~ 40psi should give a resulting pressure of 15,000 psi. If you don't have an Emulsaflux- substitute sonication here)

5) Spin the lysed cells in high speed round bottom tubes @ 35,000 xG for 30 min

6) While waiting for step 5 to finish prepare 10mL of Ni-NTA resin in 50% ETOH by putting it in a 50mL conical and filling it up the rest of the way with sterile H2O. Spin down for 5 min.

7) Aspirate off H2O/ETOH



8) Once the spin from step 5 is finished add the supernadant to the freshly washed resin. Either put this mixture in a 50mL conical (if it fits) and rotate in the cold room, or put the mixture in a beaker and a stir bar and mix in the cold room. Let this go for at least 1hr (I do 2hrs).

9) pour incubated resin mixture into a disposable column of appropriate size for resin volume (~ 9cm in length by 2cm in width is what I use) with a reservoir attached to the top of the column to accommodate the extract that will flow through during packing.

10) Pack column at 4mL/min on bioRad (or do all by gravity if pump is not available)

11) once column is packed wash with lysis buffer @ 2mL/min for 20min (or 10CV)

12) Wash the column with Wash Buffer @ 2mL/min for at least 20min (or 10CV)

**Wash Buffer:** 50mM Hepes pH 7.5

.5M KCl

20mM Imidizol (pH 7.5)

(+ 6mM added fresh)

13) Once wash steps are complete and the Absorbance reading is close to zero, Elute the protein at 2mL/min with Elution buffer.

**Elution Buffer:** 50mM Hepes pH 7.5

100mM KCl

250 mM Imidizol (pH 7.5)

(+ 6mM added fresh)

- Fill fraction collector with 2mL tubes
- This takes approximately 20 tubes and usually comes off at frac. ~6-8

**Note:** if doing by gravity: protein typically elutes after 8mLs of Elution buffer (flow through), after that peak is ~10mLs, typical for WT protein (collect).

14) MonoQ purification step: Take the elution peak of ~ 10mL and dilute in Buffer A to 50mL. (1/5)

15) wash and fill the 50mL super-loop with the sample

Note: If you do not use dilution/superloop, simply dialyze into a buffer with lower salt so the protein will bind the column.

16) run MonoQ with gradient of salt- 10% – 60%

**Buffer A:** 20mM Hepes pH 7.5

1mM DTT

**Buffer B:** 20mM Hepes pH 7.5

**.5M KCl (depends on pI)**

1mM DTT

17) Take 10-12 mL of correct MonoQ peak and add 10ug of TEV per 1mg protein

18) dialyze protein + TEV (20:1 molar ratio protein:TEV) in buffer with low salt overnight

to cleave His tag

**Dialysis Buffer:** 50mM Hepes pH 7.5

100mM KCl

1mM DTT

19) Extract dialysis and fill a syringe with 5mL for injection for gel filtration run (S200)

20) Wash 5mL loop with buffer once or twice with buffer (for the 16/60 S200 on Akta)

-inject multiple times if enough sample is obtained

21) Prepare Purification Buffer to be used for S200 FPLC column run

**Storage Buffer** (depends on application):

**WT storage (“xtal buffer”)**

20mM Hepes pH 7.5

50mM KCl

2mM MgCl<sub>2</sub>

1mM DTT

**For maleimide labeling:**

50mM Hepes pH 7.5

100mM KCl

**500uM TCEP**

22) Fill fraction collector with 2mL tubes

23) Inject Sample

24) Run the S200 program (includes column equilibration step prior to run if equilibration isn't done over night)

**Evaluating and Concentrating the protein:**

1) Collect the most concentrated and clean fractions

- 2) Run a 4-12% protein gel with standard
  
- 3) Stain gel with simply blue by microwave for 20sec (don't let it boil too long) and then let gel plus stain incubate on a rotator for ~5min
  
- 4) Destain with miliQ water on rotator
  
- 5) Choose the most concentrated and clean fraction (as chosen by looking at the gel) and concentrate with a Milipore 50mL conical (MW C/O 10,000) *See below*
  
- 6) Wash membrane with purification buffer; spin down at 5,000 xG for 15min -20min.
  
- 7) Take fractions and fill newly washed Milipore conical. Spin down at 5,000 xG for 25-30min.
  
- 8) Spec on Diode Array in Edelhoch buffer (50uL buffer **blank** and 1/10 or 1/100 dilution of protein in buffer)

Edelhoch buffer (**more accurate protein conc- see reference**):

20mM Phosphate buffer pH 6.5

6M Guanidinium HCl

**Storage:**

1) Once desired concentration is reached aliquote out into tubes on ice.

mg/mL = dilution corrected A280/ Extinction coeff

2) Flash freeze in liquid nitrogen

3) Store at -80°C

**Numbers:****WT human TRAP1 (residues 60-704)****pre-TEV**

Extinction coeff. = 62020

MW= 77230

**post-TEV**

Extinction coeff. = 60280

MW= 74077

## **<sup>13</sup>C-Alanine <sup>15</sup>N TRAP1 His-tagged protein Purification**

(L. Lavery, Agard Lab UCSF. Spring 2013)

(certain specifics may need to be adjusted for other proteins)

---

**Expression protocol credit:** Stephen N. Floor

Adapted from Floor et al., “Interdomain dynamics and coactivation of the mRNA decapping enzyme Dcp2 are mediated by a gatekeeper tryptophan.” PNAS 2012.

**Note:** This protocol is for <sup>13</sup>C-Alanine, <sup>15</sup>N labeled protein. Expression, final buffers and optional labeling are the sections of this protocol that differ from typical TRAP1 purification (see WT protocol for comparison).

Additionally, this protocol calls for overnight growth in D20, so for reasonable hours of work you will want to resuspend the cells in 1L of M9 D20 by ~6pm or so. That way the cells can grow overnight. You will have to come in early the next day to make sure they don't grow too far though.

### ***Purification #1 Notes:***

.6 mg/L from first trial

75uL of 110uM (monomer) run to obtain first HSQC experiment by J. Prestegard group

Changes to initial protocol incorporated in this protocol: adding precursor at higher OD and transferring cells to 1L culture faster so growth isn't slowed. Higher salt in final NMR buffer left at an option and noted below. Note that for buffer optimization both protein stability as well as effect of changes to NMR spectrum should be considered and cost/benefit weighed.

---

### **Expression:**

#### **Day1:**

1) Grow an overnight starter culture from a freshly transformed colony (BL21 RIL cells or equivalent expression strain)

#### **Day2:**

2) In the morning start a new 10mL LB culture by inoculating with 100uL of the overnight

3) @ OD ~0.1 (~2 hours) make **M9 H<sub>2</sub>O** media

#### **5x M9 Salts (1L)**

<b>Reagent</b>	<b>Amount</b>
KH <sub>2</sub> PO <sub>4</sub>	15g
Na <sub>2</sub> HPO <sub>4</sub>	30g
NaCl	2.5g

Sterile filter and autoclave!



### **100mL M9 H<sub>2</sub>O**

Add ~70mL of ddH<sub>2</sub>O to a graduated cylinder and then add these:

<b>Reagent</b>	<b>Amount</b>
5x M9 Salts	20mL
Antibiotic	100uL
CaCl <sub>2</sub>	100uL (0.1M, autoclaved stock)
MgSO <sub>4</sub>	150uL (1M, autoclaved stock)
<sup>15</sup> NH <sub>4</sub> Cl ( <b>Sigma 299251-10G</b> )	1.87mL (1M)
Glucose	1mL (20%)

Raise volume in graduated cylinder to 100mL.

Sterile filter using a sterile 0.45um filter.

4) @ OD ~0.5 add 500uL directly to 50mL of M9 H<sub>2</sub>O

5) @ OD of culture from step 4 is ~0.2 make the **M9 D<sub>2</sub>O** media

### **1L M9 D<sub>2</sub>O**

Add ~300mL D<sub>2</sub>O to a graduated cylinder with stir bar (~3 inch recommended). **Ensure all reagent are anhydrous**, except for the stock solutions made in water. **DO NOT heat.**

<b>Reagent</b>	<b>Amount</b>
----------------	---------------

KH <sub>2</sub> PO <sub>4</sub>	3g
Na <sub>2</sub> HPO <sub>4</sub>	6g
NaCl	0.5g
<b>-wait for these to dissolve-</b>	-
Antibiotic	1mL
CaCl <sub>2</sub>	1mL (0.1M, autoclaved stock)
MgSO <sub>4</sub>	1.5mL (1M, autoclaved stock)
<sup>15</sup> NH <sub>4</sub> Cl	1g
<sup>2</sup> H <sup>12</sup> C Glucose ( <b>Sigma 552003-1g</b> )	2g

Raise the volume to 1L with D<sub>2</sub>O. Sterile filter using a sterile 0.45um filter.

6) @ OD ~0.8 pellet cells by centrifuge at 2000g for 10 minutes

7) Gently resuspend the cells in **M9 D<sub>2</sub>O** media (1L media made above)

8) Grow at 37°C overnight

### Day 3:

9) come in early (~8am assuming you inculcated at ~6pm) to check the OD of the cells.

10) Monitor OD until it reaches ~0.8 (*this high because in my experience the cells will stop growing once the precursor is added*), and add 200mg/L <sup>13</sup>C-Alanine precursor (L-ALANINE-3-113C,2-D, **Sigma 740055-1g**)

11) induce with 1mL of 1M IPTG after 40 minutes

12) drop temperature and grow at 16°C for 18 hours (up to 24 is ok)

### **Purification**

#### **Day 4:**

12) Pellet cells @ 5,000 xG for 15 minutes

13) Resuspend pellet in 50mL of Lysis buffer plus one protease inhibitor tablet (Roche 11873580001)

**Lysis Buffer:** 50mM HEPES pH 7.5

.5M KCl

20mM Imidazole (pH 7.5)

10% Glycerol

1% Tween-20

(+ 6mM BME added fresh)

14) Homogenize resuspended pellet (dounce homogenizer or in beaker with a stir bar in the cold room) until no chunks of cells are left. (~10-15min)

15) Use EmulsiFlex-C3 (Avestin) to lyse the cells (~ 40psi should give a resulting pressure of 15,000 psi. If you don't have an Emulsaflux- substitute sonication or analogs methods here)

16) Pellet lysed cells by centrifugation in high speed round bottom tubes @ 35,000 xG for 30 min

17) While waiting for step 5, wash 10mL of Ni-NTA resin stored in 50% ETOH in a 50mL conical by filling it up the rest of the way with sterile H<sub>2</sub>O. Spin down for 5 min at 4000G. (5mL final bead volume)

18) Aspirate off H<sub>2</sub>O/ETOH

19) Once the spin from step 5 is finished add the supernatant to the freshly washed resin. Either put this mixture in a 50mL conical (if it fits) and rotate in the cold room, or put the mixture in a beaker and a stir bar and slowly mix in the cold room. Incubate for 2 hours in the cold room.

20) pour incubated resin mixture into a disposable column of appropriate size for resin volume (~ 9cm in length by 2cm in width is what I use) with a reservoir attached to the top of the column to accommodate the extract that will flow through during packing. (if you don't have a reservoir use a bigger column or add slowly)

21) Pack column at 4mL/min on bioRad (or do all by gravity if pump is not available)

22) once column is packed wash with lysis buffer @ 2mL/min for 20min (or 10CV)

23) Wash the column with Wash Buffer @ 2mL/min for at least 20min (10CV)

**Wash Buffer:** 50mM Hepes pH 7.5

.5M KCl

20mM Imidazole (pH 7.5)

(+ 6mM BME added fresh)

24) Once wash steps are complete and/or the Absorbance reading is close to zero,

Elute the protein at 2mL/min with Elution buffer. Collect Peak

**Note:** if doing by gravity: protein typically elutes after 8mLs of Elution buffer (flow through), after that peak is ~10mLs, typical for WT protein (collect).

**Elution Buffer:** 50mM Hepes pH 7.5

100mM KCl

250 mM Imidazole (pH 7.5)

(+ 6mM added fresh)

25) MonoQ purification step: Take the elution peak and dilute 1/5 with Buffer A (below)

26) wash and fill the 50mL super-loop with the diluted sample

27) run MonoQ with gradient of salt- 10% – 60% Buffer B

**Buffer A:** 20mM Hepes pH 7.5

1mM DTT

**Buffer B:** 20mM Hepes pH 7.5

**.5M KCl (depends on pI)**

1mM DTT

28) Take 10-12 mL of correct MonoQ peak and add 10ug of TEV per 1mg protein

29) dialyze protein + TEV (20:1 molar ratio protein:TEV) in dialysis buffer overnight to cleave His tag

**Dialysis Buffer:** 50mM Hepes pH 7.5

100mM KCl

1mM DTT

30) Prepare Purification Buffer to be used for S200 FPLC column run

**IMPORTANT NOTE:** For Cys Free proteins to be labeled via maleimide chemistry  
**exclude DTT**

**S200 Buffer (depends on application):**

20mM Sodium Phosphate pH6.5

50mM NaCl

2mM MgCl<sub>2</sub>

1mM DTT (**Use for WT protein only**)

(in H<sub>2</sub>O)

(note: buffer could be optimized with pH and higher salt to increase stability. This would also extend to the D<sub>2</sub>O buffer.)

31) Equilibrate S200 for next day size exclusion (S200 buffer below)

**Day 5:**

32) Extract dialysis and fill a syringe to injection for gel filtration run

(S200- 16/60 typical. Smaller or bigger column can be used depending on yield)

33) Wash loop with buffer once or twice with buffer

-inject multiple times if enough sample is obtained

34) Run S200

**Evaluating and concentrating the protein:**

35) Collect the most concentrated and clean fractions

36) Run a 4-12% protein gel with standard

37) Stain gel with simply blue by microwave for 20sec (don't let it boil too long) and then let gel plus stain incubate on a rotator for ~5min

38) Destain with milliQ water on rotator

39) Choose the most concentrated and clean fraction (as chosen by looking at the gel) and concentrate with a Millipore 50mL conical (MW C/O 10,000) *See below*

40) Wash membrane with purification buffer; spin down at 5,000 xG for 15min -20min.

41) Take fractions and fill newly washed Millipore conical. Spin down at 5,000 xG for 25-30min.



42) Spec (on Diode Array if available) in Edelhoch buffer (50uL buffer **blank** and 1/10 or 1/100 dilution of protein in buffer)

**Edelhoch buffer (more accurate protein conc- see reference):**

20mM Phosphate buffer pH 6.5

6M Guanidinium HCl

Reference: Gill, S.C., and von Hippel, P.H. (1989). Calculation of protein extinction coefficients from amino acid sequence data. *Anal Biochem* 182, 319-326.

43) Collect peak and pool pure protein

**\*\*\*\*If maleimide based labeling is desired proceed to steps 44 below. For other samples proceed to step 47 \*\*\*\***

44) Suspend spin probe in DMSO

45) For protein to be labeled with maleimide reactive spin probe (**you should NOT have DTT around at this point**) - concentrate down to a reasonable volume/concentration (1-1.5mls/100-200uM) and add 2:1 probe: protein (2:1 for each cysteine site. Thus for double cysteine mutants add 4:1) Shake/nutate at 4°C overnight. (*Note that depending on the type of maleimide probe a different ration may be optimal*)

### **Day 6:**

46) To get rid of excess label- Dialyze protein at 4°C in 500mL of the S200 buffer.

Change dialysis buffer after ~4 hours or until you leave for the day. Dialyze in this fresh 500mL ON.

### **Day 7:**

47) Concentrate protein 15/50mL (depending on volume) concentrator (10000 MW/co Centricon, Millipore) to a small volume (~500uL)

48) Dilute concentrated protein with D20 buffer (**see below**) to top of the concentrator and re-concentrate to a small volume

49) Repeat step 48 2X to get rid of H<sub>2</sub>O in the sample.

50) Concentrate proteins to high enough concentration for application

51) spec as above

### **Making D<sub>2</sub>O buffer:**

**IMPORTANT NOTE:** For proteins labeled with redox sensitive probes (ie MSL or equilivent) **exclude DTT**

Use D2O and all **anhydrous** components to make:

20mM Sodium Phosphate pH6.5

50mM NaCl (**\*\*potential to optimize. Higher salt should stabilize. 100-150mM**

**suggested)**

2mM MgCl<sub>2</sub>

1mM Deuterated DTT (Sigma 485535-500MG) (**Use for WT protein only**)

**(in D<sub>2</sub>O)**

\*check pH

**(Note:** if pH adjustment is needed you will only need to dip a glass pipette into the base/acid and then dip into the D2O buffer. Do not add a drop or you will most likely go over as the solution is a weak buffer. You can also use less concentrated NaOH, but here you will be adding more H2O back to the reactions, which is not optimal.)

**Storage:**

52) Once desired concentration is reached aliquot out into tubes on ice.

mg/mL = dilution corrected A280/ Extinction coeff

53) Flash freeze in liquid nitrogen

54) Store at -80°C

**Numbers:**

**WT human TRAP1** (mature form- i.e. without mitochondrial localization sequence)

pre-TEV

Extinction coeff. = 62020

MW= 77230 g/mol

post-TEV

Extinction coeff. = 60280 g/mol

MW= 74077 g/mol

## AlexaFluor Labeling Protocol Hsp90 homolog Cys mutants

(L. Lavery, Agard Lab UCSF)

---

**Note:** Labeling protocol assumes that protein to be labeled is stored without DTT. If DTT or other cysteine-containing reagent is present it must be removed prior to labeling reaction. Also note that buffers throughout may need to be changed for specific protein of interest.

### **Storage buffer for Cys mutants:**

50mM Hepes pH 7.5

100mM KCl

500uM TCEP

### **Specific Reagents:**

#### Dyes

AlexaFluor 555 C2-maleimide (Invitrogen A-20346) **or** Atto 550 (Atto-Tec AD 550-41)

Alexa Fluor 647 C2-maleimide (Invitrogen A-20347) **or** Atto 647N (Atto-Tec AD 647N-41)

#### Columns

Slide-A-Lyzer Mini Dialysis Units (250 units) (Thermo Scientific 69572)

(or regular dialysis depending on the volume)

Nick Columns Sephadex G-50 DNA Grade (GE Helthcare 17-0855-02)

## Labeling

1) Add 5-fold molar excess dye to Cys mutant

**Note:** Ratios of protein:dye may need to be optimized for other dyes/reagents

2) Incubate at 25C in the dark for 3 hours with shaking (350rpm) in tabletop incubator.

**Note:** alternatively ON at 4°C

3) Quench reaction with 2X BME over dye and allow 10 min incubation

4) Soak dialysis columns in DI H2O for 15min

5) Dialyze reactions into 1L buffer below ON at 4C wrapping the beaker in foil to protect the fluorophore

### Dialysis Buffer:

50mM Hepes pH 7.5

50mM KCl

1mM DTT

**Note:** dialysis can be skipped if using multiple Nick Columns. Dialysis doesn't work that well with the FRET dyes typically.

6) Using the same buffer above, remove the remaining dye with G-50 NICK column (see NICK protocol for details)

7) Concentrate the cleaned reaction back to desired volume (I usually aim for about half the original volume)

### **Protein concentration and % label calculation**

1) Make a 1/100 (or 1/10, but this wastes more protein) dilution of labeled protein and read 280nm, 555nm, 650nm and 750nm on diode array

2) Correct readings for dilution factor

2) Subtract the 750nm reading from all wavelengths

3) Correct the 280nm value using the equation below (***this is only accurate for single labeled mutants***)

**280nm (CF) = 280nm - (CF\*max dye absorbance)**

**CF AF 555 = .08**

**CF AF 647 = .03**

*Max dye absorbance's are 555nm and 650nm for AF555 and 647, respectively.*

4) Calculate mg/mL of protein with new 280 readings

5) Calculate %label using equation below

**%label** = (max dye absorbance/extinction coefficient) \* (MW protein/ mg/mL protein)

**e (AF555) = 158,000**

**e (AF647) = 265,000**

**For Double Cys Mutants:**

**Pre-mix dyes!! Otherwise one of them will over label. If you premix (40:60 AF 555:647) you should get 50/50 labeling.**

**Calculation for double mutants:**

**280nm (CF) = 280nm - (CF\*max dye absorbance 555) - (CF\*max dye absorbance 647)**



Calculate mg/mL of protein with new 280 readings

Calculate %label for each dye using equation below

**%label** = (max dye absorbance/extinction coefficient) \* (MW protein/ mg/mL protein)

**e (AF555)** = 158,000

**e (AF647)** = 265,000

**Note:** your %label expected here is 200%. (ie 1 per site)

Store protein in small aliquots (I do 5uL) in -80C

FRET away!

## TRAP1 Mouse Fibroblast Cell Lines

(Protocols and Notes L. Lavery, Agard Lab UCSF)

*(A gift from Dr. Didier Picard, University of Geneva)*

---

Email Correspondence with Guillaume Mühlebach (Graduate student in Didier Picard's lab who generated the TRAP1 KO mice)

### **Culturing: (Guillaume Notes)**

*"Fibroblasts from the 4 different cell lines have been shipped today. They are 2 flasks per cell line, with 2 different dilutions.*

### **Cells are grown in:**

DMEM, high glucose, w/ phenol red, w/ Glutamax (invitrogen, 11880036)

10% NCS (newborn calf serum, Sigma, N4637)

100U penicillin / 0.1mg streptomycin (Sigma, P4333)

2mM L-Glutamine (Sigma, G7513)

at 37°C in 5% CO<sub>2</sub>

### **Flasks are labeled as followed:**

**W1:** *Fibroblast from adult WT mouse, immortalized*

**N1:** *Fibroblast from adult NULL mouse, immortalized*

**W1T:** *W1 cells infected with lentiviral vector coding for Trap1 (without any tag) under the EF1a promoter and ZsGreen (like GFP but brighter) after an IRES sequence. It is NOT a fusion protein.*

**W1G:** *W1 cells infected with lentiviral EMPTY vector coding only for ZsGreen after an IRES sequence.*

“

**Notes from first passage (LL):**

I replaced the DMEM from invitrogen with one from sigma (sigma D5790) and FBS (invitrogen 11880036) instead of NCS. Guillaume said that these substitutions should be fine, and the cells seemed to grow equally well in FBS or NCS.

Also, N1 cells seem to grow slower than the other cell lines. In addition they are harder to detach from the cell culture plate with the same concentration of Trypsin used for the other cell lines. Of note is that the slower growth could be due to a higher dilution of the N1 cells during passaging, and that because the media passed to the next flask might have been less concentrated than intended, it took the cells longer to recover. This might manifest as a slower growth rate. Guillaume also noted in one of his emails that:

**Guillaume:** *“It's true that the KO cells (N1) detach less well than the WT ones. As mentioned before, we use Trypsin from Sigma, which when diluted corresponds to 0.5g*

*porcin trypsin, 0.2g EDTA. We use Trypsin from Sigma, which arrives in 10x solution (T4174). We use 1x, that corresponds to 0.5g porcin trypsin, 0.2g EDTA.*

*To freeze them, I use standard protocol, that means:*

- Trypsinize until cell detach (less than 5')*
- Harvest cells with medium*
- spin 5' to pellet cells*
- resuspend in cold freezing medium (DMEM + 30% serum + 10% DMSO)*
- slowly bring them to freezing temperature. We use freezing boxes.*

*Usually I freeze 2 vials from a fully confluent 10cm plate.*

*I never had problem when defreezing these cells, but maybe it comes from the fact that I use a 100% confluent plate to prepare 2 vials (so 50% in each). I use the same freezing medium as you, same technique.”*

**Notes on above (LL):** I froze with NCS (FBS can be used as well) in freezing media as in the original protocol. Also, I chose to freeze 3 X 2mL vials per 300cm round disk at ~100% confluent for all cell types except the knockout cells (N1), which I froze twice as dense to match the density Guillaume says he thaws each time he starts a fresh culture. Upon rapid thaw (37°C water bath till thawed) all cells survived except the N1 cells. The second time I froze the N1 cells I froze at the same density, but froze at a lower

confluence (~85-90%), which worked. The N1 cells were probably over confluent the first time around. Notes on final freeze/thaw protocol are below.

### **Final Protocol four TRAP1 KO Mouse Fibroblasts (LL)**

#### **Cell Culture Media and Growth conditions:**

DMEM (sigma D5790)

10% FBS (invitrogen 11880036)

100U penicillin / 0.1mg streptomycin (Sigma, P4333)

2mM L-Glutamine (Sigma, G7513)

at 37°C in 5% CO<sub>2</sub>

#### **Passaging and Freezing conditions:**

- Trypsinize (0.5g porcine trypsin, 0.2g EDTA. *Note that half as much is sufficient to lift all cell lines except N1*) until cell detach in 37C incubator (less than 5')

- Harvest cells by washing with medium and tap on the lip of the hood to detach (*note: it is necessary to wash several times and to tap especially in the case of the N1 cell line*)

Passage or freeze from here.

#### **To Freeze:**

- spin 5' to pellet cells at 500-1000g
- resuspend in cold (4C) freezing medium (DMEM + 30% serum + 10% DMSO)
- slowly bring them to freezing temperature in freezing boxes (24hrs in -80C).
- Store in liquid nitrogen dewar

### **To Thaw:**

- thaw cells rapidly in water bath
- dilute in fresh media (I did 2mL in 10mL new media)
- pellet cells at 500-1000g and remove media
- resuspend in 12mL fresh media and grown in S75 flask
- let attach and grow till the next day
- remove old media and replace the next day
- passage cells as before and freeze more as needed for stocks

**Final Notes:** cells should attach in an hour if they are happy. N1 cells take a bit of time to recover. Also, note that the time the N1 cells recovered well Mariano (our faithful lab manager) thawed them by just putting the 2mL stock in 10mL fresh media, letting the cells grow for 1/2hour and then replaced the media. The cells were then allowed to grow ON and the media was replaced again the next day. However, I think the success of the recovery was due to freezing the cells at a lower/healthier density. This still should be noted.

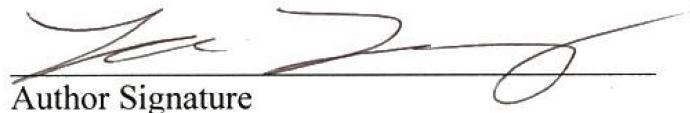
**6 X 2mL vials** of each cell line have been frozen and one thawed successfully. (Note: check for # of remaining stocks and replenish as needed. The Nakamura lab (Gladstone UCSF) has a select number of these cell lines as well.)

**Publishing Agreement**

*It is the policy of the University to encourage the distribution of all theses, dissertations, and manuscripts. Copies of all UCSF theses, dissertations, and manuscripts will be routed to the library via the Graduate Division. The library will make all theses, dissertations, and manuscripts accessible to the public and will preserve these to the best of their abilities, in perpetuity.*

***Please sign the following statement:***

*I hereby grant permission to the Graduate Division of the University of California, San Francisco to release copies of my thesis, dissertation, or manuscript to the Campus Library to provide access and preservation, in whole or in part, in perpetuity.*

  
\_\_\_\_\_

Author Signature

09/10/2013  
Date